MULTIDISCIPLINARY CENTER FOR EARTHQUAKE ENGINEERING RESEARCH
A National Center of Excellence in Advanced Technology Applications

ISSN 1520-295X

# IDARC-BRIDGE: A Computational Platform for Seismic Damage Assessment of Bridge Structures

by

A.M. Reinhorn, V. Simeonov, G. Mylonakis and Y. Reichman
University at Buffalo, State University of New York
Department of Civil, Structural and Environmental Engineering
Ketter Hall
Buffalo, New York 14260

Technical Report MCEER-98-0011

October 2, 1998

This research was conducted at the University at Buffalo, State University of New York and was supported by the Federal Highway Administration under contract number DTFH61-92-C-00106.

# NOTICE

This report was prepared by the University at Buffalo, State University of New York as a result of research sponsored by the Multidisciplinary Center for Earthquake Engineering Research (MCEER) through a contract from the Federal Highway Administration. Neither MCEER, associates of MCEER, its sponsors, the University at Buffalo, State University of New York, nor any person acting on their behalf:

a. makes any warranty, express or implied, with respect to the use of any information, apparatus, method, or process disclosed in this report or that such use may not infringe upon privately owned rights; or

b. assumes any liabilities of whatsoever kind with respect to the use of, or the damage resulting from the use of, any information, apparatus, method, or process disclosed in this report.

Any opinions, findings, and conclusions or recommendations expressed in this publication are those of the author(s) and do not necessarily reflect the views of MCEER or the Federal Highway Administration.

MULTIDISCIPLINARY CENTER FOR EARTHQUAKE ENGINEERING RESEARCH
A National Center of Excellence in Advanced Technology Applications

# IDARC-BRIDGE: A Computational Platform for Seismic Damage Assessment of Bridge Structures

by

A.M. Reinhorn[1], V. Simeonov[2], G. Mylonakis[3] and Y. Reichman[4]

Publication Date: October 2, 1998
Submittal Date: November 4, 1997

Technical Report MCEER-98-0011

Task Numbers 106-E-7.2.2 and 106-E-7.2.3

FHWA Contract Number DTFH61-92-C-00106

1 Professor and Chairman, Department of Civil, Structural and Environmental Engineering, University at Buffalo, State University of New York
2 Ph.D. Candidate, Department of Civil, Structural and Environmental Engineering, University at Buffalo, State University of New York
3. Assistant Professor, Department of Civil Engineering, City College of New York, City University of New York; formerly of the Department of Civil, Structural and Environmental Engineering, University at Buffalo, State University of New York
4. R&D Engineer, Israeli Electric Power Co., Haifa, Israel; formerly of the Department of Civil, Structural and Environmental Engineering, University at Buffalo, State University of New York

MULTIDISCIPLINARY CENTER FOR EARTHQUAKE ENGINEERING RESEARCH
University at Buffalo, State University of New York
Red Jacket Quadrangle, Buffalo, NY 14261

# Preface

The Multidisciplinary Center for Earthquake Engineering Research (MCEER) is a national center of excellence in advanced technology applications that is dedicated to the reduction of earthquake losses nationwide. Headquartered at the University at Buffalo, State University of New York, the Center was originally established by the National Science Foundation in 1986, as the National Center for Earthquake Engineering Research (NCEER).

Comprising a consortium of researchers from numerous disciplines and institutions throughout the United States, the Center's mission is to reduce earthquake losses through research and the application of advanced technologies that improve engineering, pre-earthquake planning and post-earthquake recovery strategies. Toward this end, the Center coordinates a nationwide program of multidisciplinary team research, education and outreach activities.

MCEER's research is conducted under the sponsorship of two major federal agencies, the National Science Foundation (NSF) and the Federal Highway Administration (FHWA), and the State of New York. Significant support is also derived from the Federal Emergency Management Agency (FEMA), other state governments, academic institutions, foreign governments and private industry.

The Center's FHWA-sponsored Highway Project develops retrofit and evaluation methodologies for existing bridges and other highway structures (including tunnels, retaining structures, slopes, culverts, and pavements), and improved seismic design criteria and procedures for bridges and other highway structures. Specifically, tasks are being conducted to:

- assess the vulnerability of highway systems, structures and components;
- develop concepts for retrofitting vulnerable highway structures and components;
- develop improved design and analysis methodologies for bridges, tunnels, and retaining structures, which include consideration of soil-structure interaction mechanisms and their influence on structural response;
- review and recommend improved seismic design and performance criteria for new highway systems and structures.

Highway Project research focuses on two distinct areas: the development of improved design criteria and philosophies for new or future highway construction, and the development of improved analysis and retrofitting methodologies for existing highway systems and structures. The research discussed in this report is a result of work conducted under the existing highway structures project, and was performed within Task 106-E-7.2.2, "Structure Analysis and Response—Develop a Comprehensive Method of Analysis for Bridge Assessment" and Task 106-E-7.2.3, "Development of a Standardized Computer Platform for Bridge Analysis" of that project as shown in the flowchart on the following page.

*The overall objectives of these tasks were to develop a computer software package to assist in the analysis of bridges for seismic response, and to develop an integrated software platform for damage evaluation of bridges which could be used as a research tool and for practical*

*engineering applications. This report describes the newest edition to the IDARC series of computer programs, IDARC-BRIDGE, which was developed to determine the seismic response of bridges. IDARC-BRIDGE offers methods to investigate the demand on bridges imposed by various types of excitation, and includes static and dynamic pushover options for assessing available capacity and possible collapse modes. Some of the component and damage models in the original IDARC program, for the two dimensional analysis of buildings, have been adapted and extended in this version. A user's guide is provided as an appendix to the report.*

*The IDARC-BRIDGE software can be obtained by downloading it from the World Wide Web page of the Research Group for Nonlinear Structural Dynamics and Control of the Department of Civil, Environmental and Structural Engineering at the University at Buffalo. The address is http://civil.eng.buffalo.edu or http://civil.eng.buffalo.edu/idarc-bridge. A link has also been provided from MCEER's web site at http://mceer.buffalo.edu, under "Publications/Software." If problems are encountered when downloading the software, send an email message to reinhorn@buffalo.edu.*

## SEISMIC VULNERABILITY OF EXISTING HIGHWAY CONSTRUCTION
## FHWA Contract DTFH61-92-C-00106

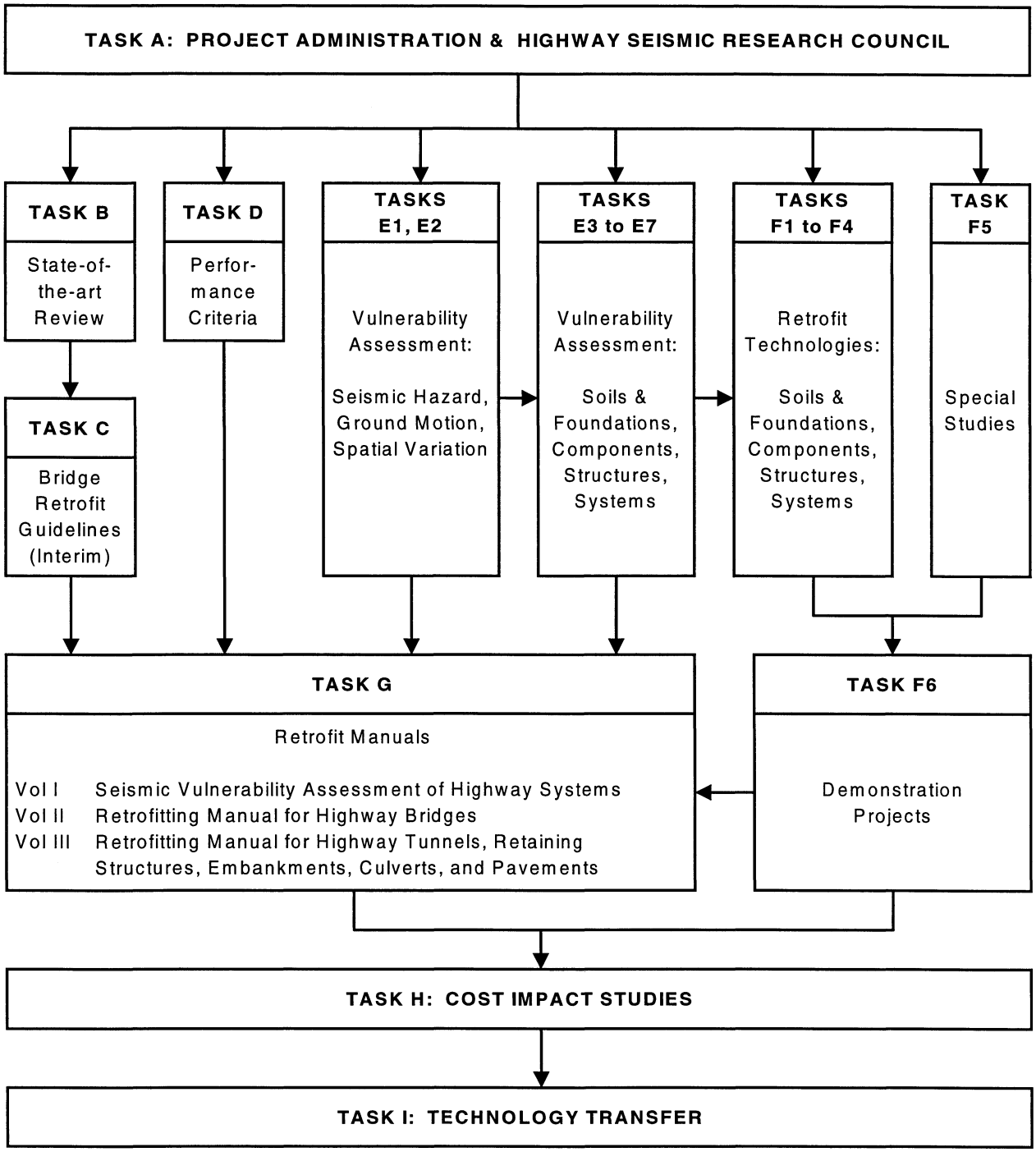

# ABSTRACT

This report presents the theoretical background of a computer platform for three-dimensional inelastic analysis of bridge structures. IDARC-BRIDGE utilizes recent developments by the authors and other researchers involved in the current and related NCEER projects. The program adapts and extends some of the component and damage models of the existing platform for two-dimensional analysis of buildings IDARC-2D (Kunnath et. al, 1987, Valles et. al, 1996). A number of unique features, however, expand its range of applicability to include bridge structures, which often present unusual and uncommon modeling problems. Two distinct goals define the scope of IDARC-BRIDGE: 1) to serve as an efficient and user-friendly analytical tool for investigating the behavior of bridge structures by engineers and researchers, and 2) to provide a framework for future software development by allowing the user to incorporate new modules, element types and component models or replace the existing ones. The platform is intended for inelastic analysis of structures. It offers methods for investigating the demand imposed by various types of excitation, as well as static and dynamic pushover options for assessing the available capacity and possible collapse modes. These two aspects of structural behavior are compared, using the concept of cumulative damage indexing, to provide information on the amount and location of damage in the system. The platform employs a macro-modeling approach to component modeling, which requires a good knowledge of the force-deformation properties of the member elements – information, which can be derived by experiment or analysis of rigorous micro-models.

# TABLE OF CONTENTS

# TABLE OF CONTENTS (Cont'd)

# TABLE OF CONTENTS (Cont'd)

# TABLE OF CONTENTS (Cont'd)

# LIST OF ILLUSTRATIONS

**FIGURE** **TITLE** **PAGE**

## LIST OF ILLUSTRATIONS (Cont'd)

**FIGURE** **TITLE** **PAGE**

## LIST OF ILLUSTRATIONS (Cont'd)

**FIGURE** **TITLE** **PAGE**

## LIST OF ILLUSTRATIONS (Cont'd)

**FIGURE** **TITLE** **PAGE**

## LIST OF ILLUSTRATIONS (Cont'd)

**FIGURE TITLE** **PAGE**

## LIST OF ILLUSTRATIONS (Cont'd)

**FIGURE TITLE** **PAGE**

# LIST OF TABLES

# SECTION 1
# INTRODUCTION

## 1.1 Introduction

Bridges are vital elements of the economic functioning of modern urban societies. In the event of an earthquake, failure or even damage of a bridge can pose a significant life hazard, and cause difficulties in the emergency response to the earthquake as well as in subsequent recovery activities. It is therefore important to develop reliable methods for predicting the performance of new bridge designs and for evaluating the existing structures.

Damage of bridge structures in earthquakes has been reviewed by Iwasaki (1972), Okamoto (1983), Imbsen and Penzien (1986), Housner et al. (1990), Buckle (1994), Priestley et al. (1996), and others. These studies highlight common failure mechanisms of bridges, namely: (i) tilting of the substructure, (ii) relative displacement of supports, (iii) settlement of abutments, and (iv) loss of capacity of elements of the superstructure. Examples of these types of failure have been observed in all recent major earthquakes --- even in relatively new bridge designs --- showing that much is yet to be learned before full understanding can develop on the seismic behavior of these structures.

Until 1971 design codes had put little emphasis on provisions regarding the dynamic response of bridges. Designs were based exclusively on elastic theory using equivalent horizontal static forces limited to about 10% of the weight of the structure. The San Fernando Earthquake of 1971 initiated a series of changes in the approach to seismic design of bridges. A significant amount of damage was attributed to dynamic inertia effects and the design methodology evolved to account for these effects. Moreover, capacity design considerations (Pauley and Priestley, 1992) started also evolving.

Since 1971, many destructive earthquakes occurred in densely populated areas in California and Japan. The 1989 Loma Prieta (Housner et al., 1990), 1994 Northridge (Buckle, 1994; EERI, 1995), and 1995 Kobe (Aydinoglu et al., 1995) earthquakes caused severe damage to bridges and highlighted the need to improve the design and retrofit provisions for new and existing bridges structures. The extensive damage and the surprisingly high levels of ground and spectral accelerations measured in those events emphasize the urgency for development of more accurate methods for analyzing bridges.

The structural behavior of bridges is different from that of most other types of structures. It is characterized by a number of distinctive features, which require special attention in analysis and design. The most important of these features are:

1) The unequal heights of bridge columns which lead to uneven distribution of horizontal stiffness along the axis of the structure. This, in turn, may cause a highly unbalanced distribution of damage during the earthquake shaking.

2) The large number of loosely connected parts the bridge may involve. The dynamic properties of the bridge change abruptly during an earthquake due to the separation or contact of adjacent superstructure segments at the two sides of expansion joints.

3) The large number of amply spaced supports the bridge may have. The supports (which are typically not interconnected) may be founded on different types of soil. Differences in amplitude and phase in the incoming seismic waves at the various supports may alter the amplitude and the distribution of seismic demand along the bridge.

4) The different stiffness and redundancy of the bridge in the longitudinal and transversal directions. As a result, the elastic vibrational characteristics and the seismic capacity of the system may be profoundly different in the two horizontal axes. Moreover, the bridge may be curved in plan, which makes the dynamic response three dimensional, even in the ideal case of uniaxial ground excitation and linear elastic structural behavior.

## 1.2 The IDARC Computer Program Series

The computer program IDARC was conceived as a platform for nonlinear static and seismic analysis of reinforced concrete structures, in which various aspects of concrete behavior can be modeled, tested and improved. Program development and enhancements have been focused primarily into linking experimental research and analytical developments.

IDARC was introduced in 1987 as a two-dimensional analysis program for studying the non-linear response of multi-story reinforced concrete buildings. The original version of the program (Park et al., 1987) included a set of structural elements for modeling columns, beams, and shear walls. Also a damage model was included to provide a measure of the accumulated damage on the structure and its components.

One of the key features incorporated in the IDARC program is the two-dimensional beam-column macromodel that calculates the inelastic stiffness of reinforced concrete beams by considering the plasticity of the material to be spread along the axis of the member --- as opposed to earlier formulations (Kaanan and Powell, 1973; Tseng and Penzien, 1973) that were based on concentrated plasticity considerations. To trace the hysteretic loops (in the moment-curvature plane) of the two outer sections of the member, a three-parameter model was developed. Through the combination of three basic parameters and a trilinear skeleton curve, stiffness degradation, strength deterioration, and pinching response were modeled. Later editions of the program (Kunnath et al., 1992; Valles et al., 1996) included, among other options, various types of static and dynamic "push-over" analyses; P-Delta effects; automatic calculation of the moment-curvature curves for beam-column elements; viscoelastic, friction, and hysteretic elements; various types of structural damping; new damage indicators.

## 1.3 Objectives and Organization of the Report

The objective of this report is to review some of the recent advances in bridge modeling and to present a new edition of the computer series IDARC, IDARC-BRIDGE, developed to calculate

the seismic response of bridge structures. Specific advances are presented towards the development and implementation of: (i) three-dimensional formulations of component models, (ii) new structural elements, and (iii) new procedures for evaluating the seismic performance of bridge structures through pertinent "capacity" vs. "demand" calculations. All these features were incorporated into a computational platform, which provides the user with the capability to analyze the static and dynamic response of bridges and their supporting systems in three dimensions and which can be used for other structural systems as well. The program offers computational tools for analysis, as well as for design of bridges by integrating non-linear dynamic damage analysis and push-over analysis procedures developed specifically for such structures.

### 1.3.1 Organization of the Report

In Section 1, a brief introduction on the importance of the subject and the objectives of this study are presented

In Section 2, the structure of computer program IDARC-BRIDGE is presented. New features pertaining to the programming of the computer platform are briefly discussed. The types of elements and dynamic analyses provided in IDARC-BRIDGE are outlined.

In Section 3, procedures for estimating the "demand" imposed on bridge structures by strong earthquakes, and the corresponding (available) "capacities" of the bridge systems, are presented. Some damage indicators are also presented.

In Section 4, techniques for the solution of the set of simultaneous differential equations governing the response of the structural system, are outlined.

Section 5 presents the component models incorporated in IDARC-BRIDGE. Among the element types currently available are: (1) elastic beam-column element; (2) hysteretic beam-column element with elastic shear deformations; (3) hysteretic beam-column element with inelastic shear

deformations; (4) triaxial sliding isolator element; (5) bearing element; (6) unidirectional gap/ restrainer element (7) three-dimensional linear spring element; (8) three-dimensional linear viscous dashpot element; (9) pile group foundation element.
Some special boundary conditions and connectivity option such as end springs, end releases, and rigid arms are also presented.

In Section 6, results of analysis runs versus results from the available literature, are conferred. A number of case studies based on data from actual bridges, are also reported.

In Appendix I, a manual of the computer program is provided.

# SECTION 2
# STRUCTURE OF COMPUTATIONAL PLATFORM IDARC-BRIDGE

## 2.1 Programming Features

The computational platform for seismic damage assessment of bridge structures IDARC-BRIDGE is written in Sun™ FORTRAN - a development system for Sun workstations that utilizes the FORTRAN 77 standard but also offers some FORTRAN 90 enhancements such as dynamic allocation of memory through integer pointers, recursion, long variable names, and extended line format. Subroutines or functions written in other Sun languages (C, Pascal and Modula-2) may be combined with those coded in FORTRAN, since these languages have common calling routines. A PC-version of the program is under development.

The design of the platform is dictated by considerations of its projected use: 1) to serve as a reliable and user-friendly analytical tool for evaluation of bridge structures by engineers, and 2) to provide a framework for future software development by allowing the user to incorporate new functions, elements and models or replace the existing ones. The platform is built in a modular manner in terms of: (i) design and translation of the analysis algorithm into a high-level language, and (ii) physical organization of the source code. The latter is contained in 182 files arranged in a hierarchical five-level directory tree and consists of more than 250 separate modules - functions and subroutines. The readability of the source code, however, is not affected by the large number of programming units. "Top-down", action-oriented design is implemented to facilitate the future developer in understanding and following the flow of the program. The function or subroutine in which any given operation is performed can be located by the source code file name, which typically prompts the utility of the procedure contained in the file. Long variable names provide reference to the specific use of the stored information, while most functions and subroutines contain a summary of the theoretical basis of the implementation. The programming effort to achieve a highly modular and manageable development is well justified since it grants the user the opportunity to easily extend the code by including new element types

or replacing the existing ones (see Appendix A for complete procedure). The authors have also devoted a lot of effort in the direction of creating a user-friendly computational platform for researchers and practicing engineers. The input to the program uses free format, which is rare among research programs of similar intent. The nonlinear elements require information on the generalized forces (stresses) and displacements (strains) at yield and the post-yield stiffness. Both can be obtained by hand computations or simple computer programs, which require only knowledge of the material stress-strain relationships. Deterioration phenomena in nonlinear bending elements are modeled by controlling the shape, slope and area of the predefined hysteretic rules. Typical ranges of the parameters are available in other publications on the IDARC program series (Valles et al., 1996). The experience of the authors is that users become accustomed to the features of the program with very little effort, however, understanding the fundamentals of nonlinear analyses is needed to make full use of its capabilities. This report provides most of the background information needed to provide meaningful input to the program and interpret its results.

### 2.2 Analysis Types

The computational platform IDARC-BRIDGE offers several dynamic, quasi-static and pushover analysis options applicable in both analysis and design situations:

1) Non-linear dynamic time-history analysis using uniform ground acceleration input.
2) Non-linear dynamic time-history analysis using ground displacement input. The displacement input may be different at each support to account for the spatial variability of seismic excitation.
3) Non-linear dynamic time-history analysis using specified forces as input.
4) Non-linear quasi-static analysis using incremental displacements as input.
5) Non-linear quasi-static analysis using incremental forces as input.
6) Eigenvalue analysis.
7) Monotonic pushover (collapse mode) analysis with user-specified distribution of lateral forces. Prescribed displacement or base shear limits terminate the analysis.

8) Monotonic adaptive pushover analysis in which the distribution of lateral forces acting on the structure is adjusted to the instantaneous mode shapes. The stopping criteria are analogous to those of option 7.
9) Dynamic pushover analysis for a linearly increasing ("ramped") acceleration input. The analysis ends when a prescribed displacement limit is reached.

In dynamic pushover analyses, the critical component can be identified by monitoring the response maxima to a series of accelerograms having the same time history but progressively increasing peak ground acceleration. Impulsive acceleration records of varying duration or ramped acceleration records with different rates of application may be used to identify a set of members where the structural collapse may possibly originate.

Three-dimensional nonlinear or linear analysis is performed, depending on the stiffness and damping properties of the elements used in the structural model. The damage of all components exhibiting hysteretic behavior is monitored at the end of each loading increment through cumulative indexing (Park and Ang, 1985; Williams and Sexsmith, 1994; Reinhorn et al., 1996).

## 2.3 Element Types

IDARC BRIDGE provides an element library for modeling the stiffness and damping properties of structural components, damping and isolation devices, expansion joints and foundation systems commonly encountered in bridge structures:

1) Three-dimensional beam-column element with linear elastic moment-rotation, shear and axial force-displacement relations at each end. This basic stick element of the matrix analysis theory is particularly useful for modeling deck and column segments in which the cracking moment capacity (of components made of reinforced concrete) or yielding moment capacity (of components of steel structures) is not likely to be exceeded during the analysis.

2) Three-dimensional beam-column element with: (i) nonlinear inelastic moment-curvature, (ii) linear elastic shear force-displacement, and (iii) linear elastic axial force-displacement laws. The element is an extension of the spread-plasticity model of IDARC family, and is typically used to model the hysteretic behavior of the bridge deck and columns.

3) Three-dimensional beam-column element with: (i) nonlinear inelastic moment-curvature, (ii) nonlinear inelastic shear force-displacement, and (iii) linear elastic axial force-displacement laws. Testing and calibration of the parameters controlling the hysteresis of this element is under way and although it is already implemented, directions for its use will appear in the next release.

4) Three-dimensional sliding isolator element with nonlinear inelastic force-displacement curves in each (global) horizontal direction. The effect of the variation of the vertical force on friction is considered explicitly in the model. The element is specifically developed to represent a class of bridge friction bearings.

5) Three-dimensional isolator element with (i) nonlinear inelastic force-displacement relations in each of the horizontal global directions, (ii) linear elastic bending moment-rotation, and (iii) axial force-displacement laws. The element can be used to model bridge elastomeric bearings.

6) Unidirectional bilinear element capable of modeling: (i) initial tension and compression gaps ($F \approx 0$, $\delta \neq 0$), (ii) nonlinear inelastic axial force-displacement relation in tension, and (iii) nonlinear elastic axial force-displacement relation in compression. The element is developed to represent the interaction between adjacent deck element in a typical expansion joint characterized by minimal stiffness in the gap, possible yielding of the restrainers, and load transfer upon impact.

7) Three-dimensional spring element. Apart from the diagonal terms, the element includes the coupling terms between rotation and translation along the two horizontal axes, providing means for modeling flexible connections and soil-structure interaction.

8) Three-dimensional viscous damping element. The structure of the element is analogous to that of the three-dimensional spring element described above. The influence of sources of concentrated damping/energy dissipation is added directly to the global damping matrix.

9) Three-dimensional pile-group element with nonlinear inelastic moment-rotation, shear and axial force-displacement relations. The element has been developed to represent inelastic soil-structure-interaction effects. The theory and computer implementation of this model will be published in a separate MCEER report.

The shear wall element, available in other programs of the IDARC series, will be implemented in a future version of IDARC-BRIDGE.

## 2.4 General Algorithm of IDARC-BRIDGE

# SECTION 3
# METHODS FOR EVALUATING THE SEISMIC PERFORMANCE OF BRIDGES

## 3.1 Introduction

Modern seismic design philosophy is based on the ability of structures to undergo inelastic deformations in a "ductile" manner that permits them to deform inelastically without significant loss of strength and capability for hysteretic energy dissipation. By allowing inelastic response, the forces on the structural elements become smaller which leads to smaller energy input into the structural system. This beneficial effect, however, may be limited by the damage inflicted to the members in terms of excessive deformations that may result to degradation in the functionality of the structure after the earthquake, and deterioration of its subsequent ductility capacity.

The quantification of damage is part of the seismic evaluation process and most modern analytical tools need to provide such capability. This can be done by monitoring the response of structural components, substructures, or the entire system during the dynamic excitation, and compare it to the respective capacities. Time history analysis can trace simultaneously the response parameters and the ultimate capacities, both of which are changing throughout the earthquake. Strictly speaking, damage analysis can be performed only in the course of time history analyses. Approximations, however, can be utilized to simulate and obtain damage information through quasi-static push-over analyses at the expense of accuracy. The subject of evaluation of seismic performance of bridges is briefly addressed in the following paragraphs.

## 3.2 Multi-Step Methodology for Evaluating the Seismic Performance of Bridges

The evaluation of the performance of a bridge during a seismic event is critical in the design or retrofit of its structure. The evaluation procedure can be put on a rational basis by comparing, at the same instant, the "demand" imposed by the earthquake to the corresponding "capacity" of the

structure. The "demand" is usually expressed in terms of maximum deformations the structure will be subjected to during the event, while "capacity" stands for the maximum deformation the structure and its components can sustain corresponding to a specified collapse or serviceability limit.

A rational evaluation of structural behavior can be performed to the level of detail required by the problem at hand or by the purpose of the evaluation. If the structure can be proven safe by a simple method, no further analysis is usually required. Some cases, however, can not be assessed without resorting to more elaborate methodology.

A multi-step evaluation procedure based on various levels of sophistication is outlined below.

Step 1: Define the seismic loading in the form of either spectra or time histories. In some cases both are required. Determine the geometry of the structure, behavior of connections, kinematic restrictions, behavior of the foundation etc.

Step 2: Build a model that fits the physical geometry of the structure and its mechanical characteristics. Define the yield capacity of the various structural components. Perform a quasi-static analysis using a spectral approach. If the elastic demand is smaller than the yield capacity for all critical elements, the evaluation may be considered to be complete and the structure may assumed to be safe.

Step 3: In case the yield capacity of critical elements is exceeded by the demand, identify potential collapse mechanisms based on the elastic forces calculated in Step 2. This technique requires a good estimate of the yield and ultimate strength of the components but not of their ultimate deformations. If a complete plastic mechanism is not formed (or close to be formed --- see Bracci et al., 1992), further analysis may not be necessary.

Step 4: If Steps 2 and 3 do not provide conclusive results, plastic analysis (which is based on a presumably known force distribution) is required to determine the critical failure mechanism and the corresponding collapse load of the structure. Although such analysis may be quite complicated, it can be done (even if approximately) using hand

calculations. The overall capacity of the structure can then be compared to the force demand calculated in Step 1.

Step 5: If more rigorous investigation is considered necessary, a "push-over" analysis can be performed. The latter may require a more detailed representation of the structural geometry and explicit modeling of the nonlinear behavior of the structural components. Moreover, a good definition of local failure is needed to allow for accurate monitoring of damage. The method also requires an adequate definition of loading that varies with the progression of damage (this subject is addressed later in the report). The demand can then be established using an inelastic spectrum approach (Reinhorn, 1997). The method provides information on local and global strength variation with increasing deformation. A comparison of inelastic spectrum demand to the corresponding capacity will allow evaluation of the structural performance. This type of analysis, however, only approximates the interaction between seismic demand and structural capacity. Still, it may be deemed sufficient if large margins exist between these quantities.

Step 6: If higher accuracy is desired or the margins mentioned above are narrow, a non-linear time history analysis is usually required. The description of structural behavior may incorporate three-dimensional modeling, stiffness degradation and strength deterioration, while a family of time-histories should be used to define the loading. The non-linear time history analysis will produce information on damage progression, which can be compared to the performance targets. Such evaluation is accurate but time consuming and sensitive to modeling and load uncertainties. One the goals of this project is to develop a three-dimensional analytical tool capable of effectively performing such analyses.

Step 7: Risk and fragility analysis is a further step in the evaluation process which typically encompasses transportation systems and bridges. The analysis compares the probability of reaching a performance limit during a series of earthquakes. Fragility curves are developed using either time-history analysis (Step 5) or simplified "push-over" methods (Step 4), that summarize the demand-capacity relations in terms of the aforementioned probabilities (Reinhorn and Barron, 1998). This last approach, however, is beyond the scope of this report.

In summary, one of the goals of this project is to develop a computational tool capable of effectively performing the analysis types of steps 5 through 7.

## 3.3 Methods for Calculating the Seismic Demand on Bridges

### 3.3.1 Introduction

The response of bridges to seismic loading can be obtained by a variety of methods the most popular of which are the ***modal superposition*** and the ***direct integration methods*** (Chopra, 1995). Though more efficient numerically, the mode superposition procedure is, at least in principle[1], limited to linear elastic analysis; it is therefore only briefly reviewed in paragraph 3.3.2. Direct integration of the equations of motion is the method of choice in IDARC-BRIDGE, due to its ability to handle nonlinear structural response and to the availability of efficient numerical algorithms.

Three distinct time history analysis procedures are currently implemented in IDARC-BRIDGE: (i) dynamic analysis with base acceleration input (hereafter termed "***dynamic acceleration***" type of analysis), which is restricted for the case of uniform ground motion; (ii) dynamic analysis with base displacement input ("***dynamic displacements***") which can be used for both uniform and spatially varying ground motions; (iii) dynamic analysis with force input ("***dynamic force***").

### 3.3.2 Modal Analysis Using a Response Spectrum Approach

Consider the structure to be modeled as an elastic multi-degree-of-freedom system with each degree of freedom representing the displacement (or rotation) along (or about) an axis of a given coordinate system. Stiffness, damping and lumped mass matrices (hereafter denoted as [M], [C],

[1] If instantaneous modal information is available, modal superposition can be used for the analysis of inelastic response (Reinhorn, 1997).

and [K], respectively) are used to introduce the properties of the structure into the governing equilibrium equations:

$$[M]\{\ddot{u}(t)\} + [C]\{\dot{u}(t)\} + [K]\{u(t)\} = -[M]\{r\}\ddot{u}_g(t) \tag{3-1}$$

where:

$\{u(t)\}$ = Nodal displacements

$\{\dot{u}(t)\}$ = Nodal velocities

$\{\ddot{u}(t)\}$ = Nodal accelerations

$[M]\{r\}\ddot{u}_g$ = Loading vector in the case of uniform ground motion

$\{\ddot{u}_g(t)\}$ = Ground acceleration

Upon applying the modal transformation:

$$\{u(t)\} = [\Phi]\{y(t)\} \tag{3-2}$$

where, $[\Phi]$ = matrix of undamped mass-normalized mode shapes

$\{y(t)\}$ = modal amplitude vector

Multiplying (3-1) on the left by $[\Phi]^T$, introducing (3-2) into (3-1), and using the orthogonality conditions (Chopra, 1995) gives:

$$m_i^*\ddot{y}_i(t) + 2\xi_i\omega_i m_i^*\dot{y}_i(t) + \omega_i^2 m_i^* y_i(t) = -\{\phi_i\}^T[M]\{r\}\ddot{u}_g(t) \tag{3-3}$$

where, $m_i^*$ = $\{\phi_I\}^T[M]\{\phi_i\}$ [ = 1 for mass-normalized mode shapes]

$y_i$ = amplitude of mode i

$2\xi_i\omega_i m_i^*$ = $\{\phi_I\}^T[C]\{\phi_i\}$ [ = $2\xi_i\omega_i$ for mass-normalized mode shapes]

$\omega_i^2 m_i^*$ = $\{\phi_I\}^T[K]\{\phi_i\}$ [ = $\omega_i^2$ for mass-normalized mode shapes]

$\{\phi_i\}$ = mode shape of mode

Equation (3-3) is a second-order linear differential equation and can be integrated in time by, say, a convolution integral approach to provide $y_i(t)$ for each mode. The displacements along the structural degrees of freedom can then be calculated using (3-2). The equation for the modal amplitudes will change if mass-normalized mode shapes are used, but not the final solution. The elastic restoring forces can be obtained from the relation:

$$\{f(t)\} = [K]\{u(t)\} = [K][\Phi]\{y(t)\} \approx \omega_i^2 [M][\Phi]\{y_i(t)\} \tag{3-4}$$

A simplified form of the modal analysis procedure outlined above is the modal response spectrum analysis in which response spectra are used to obtain the maxima of the modal amplitudes (i.e., instead of their complete time-histories). The maximum deformations $u_{max}$ and restoring forces $f_{max}$ can be statistically approximated from the following equations:

$$u_{max} \approx SRSS_{i=1}^{n} [\{\phi_i\} \Gamma_i S_d(\omega_i, \xi_i)] \tag{3-5}$$

$$f_{max} \approx SRSS_{i=1}^{n} [\omega_i^2 [M]\{\phi_i\} \Gamma_i \, S_v(\omega_i, \xi_i)] \tag{3-6}$$

$$\Gamma_i = \{\phi_i\}^T [M]\{r\} \tag{3-7}$$

where:

$\Gamma_i$ = modal participation factor

$S_d(\omega_i,\xi_i)$ = spectral displacement response

$SRSS_{i=1}^{n}(x_i)$ = "Square Root of Sum of Squares" algebraic operator: $SRSS_{i=1}^{n}(x_i) = \left( \sum_{i=1}^{n} x_i^2 \right)^2$.

The spectral displacement $S_d$, velocity $S_v$ and acceleration $S_a$ are joined, for each natural mode, by the relations:

$$S_v = \omega \, S_d \tag{3-8}$$

$$S_a = \omega^2 S_v \tag{3-9}$$

The response spectra may be obtained by averaging multiple spectra from a large number of earthquakes. This type of approach may be helpful for predicting the structural response during future events. Response spectrum analysis, however, gives a limited insight into the dynamic behavior of the bridge since the required values of forces and deformations are derived by simply combining the modal maximum response through, say, the SRSS rule. The use of the latter is based on the presumption of well-separated modes which may or may not hold for a bridge structure. The SRSS (Chopra, 1995) superposition can be replaced by the CQC (Smeby and Der Kiureghian, 1985) or CQC3 (Menun, 1996) combination rules for more accurate and efficient computation. The SRSS operator, however, will be carried throughout this presentation for the familiarity of the engineering community with it.

Since modal analysis is inherently linear, nonlinear effects can be assessed only approximately, say by modifying the maximum deformations and forces according to expected "ductility" levels (Newmark and Hall, 1981). There is, however, no direct influence of the nonlinear inelastic behavior of the structural components on the response of the system. The effects of additional protective systems (e.g., isolation systems) on the response can be approximated by linearization of their properties leading to "equivalent" stiffness and damping moduli. The "equivalent" properties may be applied at specific locations of the structure (which correspond to the actual locations of those elements), or may be "smeared". Also, positive tie and impact in the expansion joints cannot be modeled directly. To compensate for this shortcoming an approximate procedure based on interpolation between analysis with open and with closed gaps is suggested by Caltrans (Caltrans, 1992). The effect of differential ground motions cannot be facilely modeled using this type of analysis.

### 3.4 Nonlinear Inelastic Analysis

The limitations of linear time history analysis, such as the response spectrum approach based on elastic mode shapes outlined in the previous section, in accounting for the nonlinear behavior of structural elements can be overcome through the use of non-linear time history analysis. In such a case, the governing equation of motion of a structure subjected to earthquake excitation can be written as:

$$[M]\{\ddot{u}(t)\}+[C(t)]\{\dot{u}(t)\}+[K(t)]\{u(t)\}=\{F(t)\} \qquad (3\text{-}10)$$

where the stiffness and damping matrices,[K(u)] and [C(u)], respectively, depend on the level of the structural response, while the forcing vector in the right-hand of (3-10), {F(t)}, depends on the type of seismic input (i.e., displacement/velocity or acceleration --- see Chapter 4)

Given an earthquake motion, (3-10) can be integrated in a step-by-step manner to provide the time histories of the response along the various degrees of freedom. The structural deformations can be compared, at each analysis step, with predefined limits of response (i.e., ultimate displacements, curvatures, seat capacities etc.), at the section, component, substructure, or global level. To this end, a damage index indicator (Park and Ang, 1985; Valles et al., 1996) may be used to evaluate the accumulation of damage into the structure and its components. The procedure is very comprehensive since it provides means to monitor local damage and/or partial/full collapse of the structure under any type of dynamic loading. Details on damage indices are given in section 3.6.

To take advantage of the capabilities of non-linear analyses, the hysteretic behavior of structural elements must be modeled as accurate as possible. Because of the direct interaction in time between the various structural components, the influence of the protective systems (such as base isolation and damping devices) on the bridge system is direct and no approximations on the mechanical characteristics of the devices are required. Also, the influence of the non-uniform ground excitation, at the various supports of the bridge can be directly accounted for, although today's knowledge on this type of seismic input is rather limited.

Despite the fact that, with non-linear inelastic analyses the amount of damage to a single element can, at least in principle, be calculated in a straightforward way, the reliability of the overall system is still difficult to be assessed. This is because, the response of each element depends on the nonlinear properties of all the other elements of the system. To assess the actual capacity of the bridge, a series of analysis should be performed with gradually increasing intensity of ground motion, until failure conditions are reached. Relating the level of intensity of ground motion required to cause collapse in the system to its actual "design" intensity will provide an estimate of the reliability of the design. It is clear, however, that this type of procedure has some drawbacks; specifically: (i) it requires a huge amount of computations; (ii) the response of the bridge system is sensitive to the details of the ground excitation and the modeling of structural components; (iii) the analysis can be performed only with a limited number of ground motions which might not be enough to represent accurately the "design" earthquake. Methods for evaluating the capacity of bridges are discussed in the following paragraph.

### 3.5 Methods for Evaluating the Seismic Capacity of Bridges

The "capacity" of a bridge is usually defined in terms of ultimate displacements a component, or the structure as a whole, can sustain before reaching a certain serviceability or failure limit (figure 3-1).

The capacity of the entire structure may be derived from the capacities of its individual components in a procedure that is conceptually similar to the reliability methods of probabilistic analyses ("fault tree"). Alternatively, the overall structural capacity can be estimated by applying one of thew following methods: (1) a plastic mechanism (limit) analysis; (2) an incremental "push-over" analysis; (3) a certain type of seismic loading (i.e., impulse, ramp, or general time history). The latter method usually requires multiple solutions with increasing levels of excitation until failure conditions are reached. In the following paragraphs each different method will be briefly reviewed.

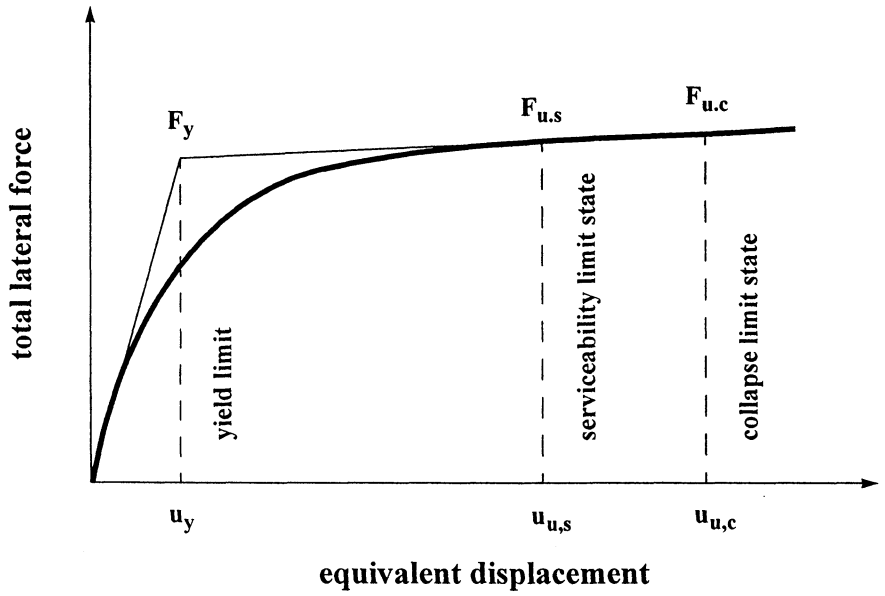


**FIGURE 3-1 Typical Structure Capacity Curve**

### 3.5.1 Plastic Mechanism Analysis

Three fundamental assumptions characterize this approach: (i) the (frame) structure is transformed into a mechanism through the formation of a sufficient number of plastic hinges; (ii) the idealized moment-curvature relation at any section is elastic-plastic; (iii) buckling or instability are not considered as possible mechanisms of failure. Once formed, the plastic mechanism will collapse under any further load increase (the strain hardening effect is typically neglected). The collapse load of the structure can be calculated by equating the external and internal work during a virtual movement of the collapse mechanism; the collapse load determined in this way is an upper bound on the correct static load capacity.

Although such analysis may be quite complicated, it can be done, even if approximately, using hand calculations. The resulting ultimate force capacity obtained with this method can be compared to force demands obtained from spectral analyses. This method can show if the structure is safe, say, if its ultimate force capacity is significantly larger than the corresponding force demand. In the case of earthquake loading, however, the converse is not true. The structure may survive a strong earthquake --- even if its ultimate force resistance is smaller than any specific force level. Its survival will depend on its post-yielding displacement capacity versus the corresponding seismic demand, an information that the simplistic plastic mechanism analysis cannot provide. Additional discussion on this method can be found in Bracci et al. (1992).

### 3.5.2 Pushover Analysis

Monotonic incremental static or dynamic analysis can be used to determine the capacity of a complete bridge structure or some of its parts. Assuming that the structural geometry and the load-deformation relations of the individual components are well defined, useful information on the inelastic behavior of the bridge can be obtained by applying lateral forces (i.e., in force control) or displacements (in displacement control) on the bridge until a failure criterion is reached. This will provide information on the distribution and progression of damage within the structure, as well as on the relation between damage and global displacements. In the displacement-control option, the bridge is subjected to a displacement profile, and the lateral forces needed to generate that deformation are calculated. Since the inelastic deformation profile of the structure is not known -- whereas an estimate of the lateral distribution of forces is easier to be made, force-controlled analyses are usually preferred. The force distribution should be representative of the pattern most likely to occur during an actual event.

Considering a discrete model of a structural system subjected to a (pseudo-static) inertial load, the spatial distribution of the load can be expressed in the following general form:

$$F_i = V \xi_i \qquad (3\text{-}11)$$

where: $F_i$ is the force along the degree of freedom i; V is the total base shear; $\xi_i$ is a dimensionless distribution function. It is important to recognize that in buildings the distribution of structural mass is typically a function of height whereas in extended bridge structures the scatter of mass is more pronounced (especially in the horizontal direction), which may result in complicated spatial distribution of load.

Appropriate selection the distribution function $\xi_i$ is crucial in order to obtain a realistic picture of the inelastic behavior of the system. To determine $\xi_i$, it is useful to examine the force distributions along the structure in the realm of elastic modal analysis. To this end, the maximum inertia force acting along the degree of freedom i, in a mode of vibration $\rho$ of the aforementioned discrete system subjected to an ***arbitrary*** earthquake time history, can be written as:

$$F_{i\rho} = m_i \, \phi_{i\rho} \, \Gamma_\rho \, S_a(\omega_\rho, \xi_\rho) \tag{3-12}$$

in which $m_i$ is the lumped mass belonging to the degree of freedom i; $\phi_{i\rho}$ is the value of the (mass-normalized) mode shape $\rho$ along that degree-of-freedom; $S_a(\omega_\rho, \xi_\rho)$ and $\Gamma_\rho$ are the spectral acceleration response and participation factor of mode $\rho$, respectively. For mass-normalized mode shapes $\Gamma_\rho$ is given by:

$$\Gamma_\rho = \{\phi_\rho\}^T [m] \{r\} \tag{3-13}$$

where $\{r\}$ is a vector that depends on the direction of excitation (Chopra, 1995).

The sum of the inertial forces (i.e., the "base shear") acting on the structure along the direction of loading corresponding to mode $\rho$ is calculated as:

$$V_\rho = \{F_{i\rho}\}^T \{r\} = \Gamma_\rho^2 \, S_a(\omega_\rho, \xi_\rho) \tag{3-14}$$

If more than one mode is considered, the maximum lateral inertial forces can be approximated by:

$$F_{i,\,max} = m_i \, \phi_{i\rho} \, \Gamma_\rho \, S_a(\omega_\rho, \xi_\rho) \; SRSS_{j=1}^{n}(f_{ij} \gamma_j S_{a_j}) \tag{3-15}$$

in which, n is the number of selected modes; $SRSS^{n}_{j=1}()$ denotes the "Square Root of Sum of Squares" operator; the non-dimensional coefficients in (3-15) are defined as ratios between the properties of the various modes and those of a "dominant" mode ρ, i.e.:

$$f_{ij} = \frac{\phi_{ij}}{\phi_{i\rho}} \tag{3-16a}$$

$$\gamma_j = \frac{\Gamma_j}{\Gamma_\rho} \tag{3-16b}$$

$$s_{a_j} = \frac{S_a(\omega_j, \xi_j)}{S_a(\omega_\rho, \xi_\rho)} \tag{3-16c}$$

The maximum base shear obtained by the combination of n modes can be written in a form analogous to (3-15):

$$V_{max} = \Gamma_\rho{}^2 \, S_a(\omega_\rho, \xi_\rho) SRSS^{n}_{j=1}(\gamma_j s_{a_j}) \tag{3-17}$$

Combining (3-15) and (3-17), the distribution function of the lateral load $\xi_i$ can be expressed as:

$$\xi_i = \frac{m_i \varphi_{i\rho}}{\Gamma_\rho} B_i \tag{3-18}$$

Note that, the above expression is independent of the time characteristics of the seismic excitation. The rational expression at the right-hand side of (3-18) stands for the effect of the dominant mode ρ , while the function $B_i$ stands for the contribution of the higher modes:

$$B_i = \frac{SRSS^{n}_{j=1}(f_{ij} \gamma_j s_{a_j})}{SRSS^{n}_{j=1}(\gamma_j s_{a_j})} \tag{3-19}$$

Consider an ***inelastic*** structure subjected to a progressively increasing base shear distributed over the structure in the form given by (3-11) and (3-18). It is apparent that after the structure yields,

its modal characteristics will start changing with increasing load. To capture the effect of structural yielding on the distribution of inertial forces, the modal characteristics of the system have to be adjusted with each increment of load. Accordingly, an eigenvalue analysis should be performed at each loading step and equations 3-18 and 3-19 be adjusted correspondingly. This will keep the pseudo-static monotonic load compatible with the instantaneous modal characteristics of the structure until failure takes place.

In the case of incremental analysis (see Chapter 4), the incremental load along the degree-of-freedom *i* is calculated as:

$$\Delta F_{i,k} = \frac{m_i \varphi_{i\rho}(u_{k-1})}{\Gamma_\rho(u_{k-1})} B_i(u_{k-1}) V_k - F_{k-1} \qquad (3\text{-}20)$$

where:

$\Delta F_{i,k}$ = increment of lateral load along the degree of freedom i over the interval $\Delta t = t_k - t_{k-1}$.

$\varphi_{i\rho}(u_{k-1})$ = ordinate of the instantaneous shape of the fundamental mode $\rho$ along the degree of freedom i at time $t_{k-1}$.

$\Gamma_\rho(u_{k-1})$ = participation factor of mode $\rho$ at time $t_{k-1}$.

$B_i(u_{k-1})$ = value of the function at time $t_{k-1}$.

$V_k$ = total base shear at time $t_k$ (known a priori).

$F_{k-1}$ = total lateral load along degree of freedom i at time $t_{k-1}$.

The above formula was developed by the senior author of this report (Reinhorn, 1997; Bracci et al., 1997), and has been incorporated into the programs IDARC2D-4.0 (Valles et al., 1996) and IDARC-BRIDGE.

Equation (3-20) is the most general force distribution and probably the most "accurate", but it requires significant computational effort which in the case of large structures may reach unmanageable proportions. Two more economic alternatives of (3-20) with increasing level of approximation are outlined below:

*First*, neglecting the higher modes in (3-18) --- which corresponds to setting $B_i$ equal to 1 in equations (3-18) and (3-19), equations (3-18) and (3-20) will reduce to an adaptable first mode approximation. This approach, however, may produce erroneous results for long or irregular bridges, especially in cases where the direction of the lateral load is transverse to the deck centerline (Priestley and Calvi, 1997; Fischinger et al., 1997).

*Second*, in addition to neglecting the higher modes, one may approximate the shape of the first mode by the simple formulas described in seismic codes. One such expression is the so-called generalized power distribution given by:

$$\Delta F_i = \frac{W_i h_i^{\,k}}{\sum_{m=1}^{n} W_m h_m^{\,k}} \Delta F \qquad (3\text{-}21)$$

where k is a parameter controlling the shape of the distribution/mode (Reinhorn, 1997). Equation (3-21) has been developed for buildings. For bridge structures, approximate mode shapes can be developed by calculating the elastic deflection of the bridge to a distributed static load, applied over its length in a uniform or mass-proportional way (AASHTO, 1996).

### 3.5.3 Capacity Analysis Using Dynamic Loads

In the previous sections the capacity of the bridge structure was evaluated using limit analyses or push-over procedures of various degrees of sophistication. All these methods are essentially ***pseudostatic*** since cyclic and damping effects cannot be (at least explicitly) accounted for.

As an extension to the pseudostatic methods, dynamic time histories can be used to extract information on the seismic capacity of the bridges. The idea is to apply a dynamic load on the bridge and calculate its response using a non-linear dynamic analysis technique. This analysis will provide quantitative information on the inelastic behavior of the structure corresponding to a specific level of intensity of the excitation. For example, if seismic excitation is applied to the base of a bridge, the maximum displacement, $u_m$, say, at the top of a column can be calculated as

a function of the effective ground acceleration $a_g$. Then, the intensity of excitation can be increased by scaling the time history and the analysis repeated to provide a new pair ($u_m$, $a_g$).

The resulting function $u_m(a_g)$ defines a dynamic push-over curve which can be considered an extension of the pseudostatic push-over curves. This is because, by applying a slowly increasing acceleration function, $a_g = a*t$, to the supports of the bridge, the pushover curve calculated using the most rigorous pseudostatic procedure (i.e., equation 3-20) can be reproduced. The dynamic pushover analysis, however, is much more general since: (i) dynamic, cyclic, and damping effects are explicitly accounted for; (ii) any function of dynamic loading (i.e., of both space and time) can be incorporated in the analysis.

Three types of dynamic loading can be used in IDARC-BRIDGE for analysis of structural capacity: (i) earthquake time histories (***"dynamic acceleration"***); (ii) loads increasing linearly with time (***"push ramp"***); (iii) impulsive (short duration) loads. It is worth mentioning that despite the fact that both (ii) and (iii) are special cases of (i), loading option (ii) is implemented as a separate analysis type in the program.

### 3.6 Quantification of Damage

The need for assessment the performance of structures during earthquakes and their condition afterwards has led to the development of indicators for quantification of seismic damage sustained by individual members, substructures or the complete structural assemblies (see pertinent reviews by Chung et al. (1987), Manfredi (1993), Williams and Sexsmith (1994). Although such indicators (or indices) incorporate many uncertainties stemming from modeling assumptions, incomplete knowledge of actual and current material properties and loading history, they can provide information on the envelope of design requirements for new or serviceability of existing structures. Damage indices are typically defined as ratios of demand versus capacity in terms of displacements (curvatures), displacement ranges, or cumulative displacements. The deterioration of capacity during cyclic loading is incorporated in the "cumulative damage theory" (Chung et al. 1987; Powel and Allahabadi 1988; Cosenza and Manfredi 1992).

The current release of the computational platform IDARC-BRIDGE employs a fatigue based model (Reinhorn and Valles, 1996) for damage quantification. The damage index is automatically calculated for elements responding in the plastic range during the execution of all time-history, quasistatic or pushover analysis types.

### 3.6.1 Park and Ang Damage Model

The Park and Ang (1985) formulation is an integral part of the three-parameter hysteretic rule used by the program (the rate of strength degradation is directly related to the coefficient β) and will be presented in brief. The damage index for a structural element is defined as:

$$DI = \frac{\delta_m}{\delta_u} + \frac{\beta}{\delta_u P_y} \int dE_h \qquad (3\text{-}22)$$

where:

$\delta_m$ = Maximum experienced deformation at the current state of analysis

$\delta_u$ = Ultimate deformation capacity of the element

$P_y$ = Yield strength of the element

$\int dE_h$ = Hysteretic energy absorbed by the element during the response history

$\beta$ = Model parameter. Suggested values between 0.1 and 0.3 (Park et al., 1987)

The damage due to the maximum deformation is linearly combined with the contribution from the history of deformation. This index was modified by Kunnath et al., (1997), to reflect the influence of the inelastic excursions, rather than total deformations, on component damage.

For element end sections the original model can be expressed in terms of rotations (Kunnath et al., 1992):

$$DI = \frac{\theta_m - \theta_r}{\theta_u - \theta_r} + \frac{\beta}{M_y \theta_u} E_h \tag{3-23}$$

where:

$\theta_m$ = Maximum rotation attained during the loading history

$\theta_u$ = Ultimate rotation capacity

$\theta_r$ = Recoverable rotation (upon unloading)

$M_y$ = Yield moment

$E_h$ = Energy dissipated in the section

### 3.6.2 Fatigue Based Damage Model

The development (Reinhorn and Valles, 1996) of the formulation currently used in IDARC-BRIDGE for damage quantification is based on considerations similar to the Park and Ang model and a low-cycle fatigue rule:

$$DI = \frac{\delta_a - \delta_y}{\delta_u - \delta_y} \frac{1}{\left(1 - \frac{E_h}{4Q_y(\delta_u - \delta_y)}\right)} \tag{3-24a}$$

where:

$\delta_a$ = Maximum experienced deformation

$\delta_y$ = Yield deformation capacity

$\delta_u$ = Ultimate deformation capacity

$Q_y$ = Yield force capacity

$E_h$ = Cumulative dissipated energy

For cases when the maximum deformations are close to the ultimate deformation capacity of the element, the ratio $(\delta_a - \delta_y)/(\delta_u - \delta_y)$ approaches 1.0, and (3-23) simplifies to the modified Park and Ang formula (equation 3-22) for $\beta = 0.25$:

$$DI = \frac{\delta_a - \delta_y}{\delta_u - \delta_y} + \frac{E_h}{4Q_y(\delta_u - \delta_y)} \qquad (3\text{-}24b)$$

In the context of nonlinear time history analysis, the numerator ($\delta_a$ - $\delta_y$) of (3-24a) is the "permanent" displacement or curvature *demand*, while the denominator:

$$(\delta_u - \delta_y)\left(1 - \frac{E_h(t)}{4Q_y(\delta_u - \delta_y)}\right) \qquad (3\text{-}25)$$

is the permanent displacement or curvature *capacity* reduced as the hysteretic energy dissipation $E_h(t)$ increases during inelastic excursions.

The damage characterization is derived at the local and global levels.

A. Local damage indices (DI)

1) Section damage is typically characterized in terms of curvature.

2) Element or component damage is characterized in terms of the element deformation calculated as the difference between the displacements of the one end relative to the other. This should account for all deformations, flexural and shear.

B. Global structural damage indices

1) Substructure damage is characterized in terms of the overall substructure drift. It accounts for element deformations as well as for element-to-element interaction.

2) Global damage is characterized by the structural maximum drift, whichever place it occurs. It account for the interaction between all the substructures. This index may be of lesser value for the structural engineer, it is valuable, however, for global vulnerability analysis and regional decisions.

# SECTION 4
# NUMERICAL PROCEDURES AND SOLUTION TECHNIQUES IN IDARC-BRIDGE

## 4.1 Introduction

The response of bridges to seismic loading can be obtained by a variety of methods the most popular of which are the modal superposition and the direct integration methods (Chopra, 1995). Though more efficient numerically, the mode superposition procedure is, at least in principle, limited to linear elastic analysis. Direct integration of the equations of motion is the method of choice in IDARC-BRIDGE for its ability to handle nonlinear structural response in an efficient way, and due to availability of efficient numerical algorithms in the literature (Hilber et al., 1977; Imbsen and Penzien, 1986; Carr, 1994).

Three different time history analysis procedures are currently implemented in IDARC-BRIDGE: (i) dynamic analysis with base acceleration input (called "***dynamic acceleration***" analysis option) for the case of uniform ground motion, (ii) dynamic analysis with base displacement input ("***dynamic displacement***" option) useful for both uniform and spatially varying ground motion and (iii) dynamic analysis with force input at non-restrained degrees of freedom ("***dynamic force***" option).

## 4.2 Dynamic Analysis for Ground Acceleration Input

The governing equation of motion of a multi-degree-of-freedom nonlinear system under dynamic loading can be expressed in the following incremental form (Chopra, 1995):

$$[M]\{\Delta\ddot{u}\} + [C(u)]\{\Delta\dot{u}\} + [K(u)]\{\Delta u\} = \{\Delta F\} \qquad (4\text{-}1)$$

where:

$\{\Delta u\}$ = Incremental nodal displacements over the time interval $\Delta t = t_{i+1} - t_i$.

$\{\Delta\dot{u}\}$ = Incremental velocities.

$\{\Delta\ddot{u}\}$ = Incremental accelerations.

$\{\Delta F\} = -[M]\{\Delta\ddot{u}_g\}$ = Loading vector in the case of uniform ground motion.

$\{\Delta\ddot{u}_g\}$ = Ground acceleration increment.

The stiffness and damping matrices, [K(u)] and [C(u)], are assumed constant during the time interval $\Delta t = t_{i+1}-t_i$ Dynamic equilibrium of a nonlinear system at time instant $t_{i+1}$ will be achieved only if the incremental stiffness and damping matrices are calculated from the response at the two end of the time interval (i.e., $t_i$ and $t_{i+1}$). Since this is not possible (the response at the end of the time interval is not known a priori), the stiffness and damping matrices are usually approximated by the corresponding tangent values at the previous time step, i.e. $[C] = [C_T]_i$ and $[K] = [K_T]_i$.

The equation of motion is integrated directly using Newmark's Beta method (Newmark, 1959). According to this method, the acceleration response of the system is assumed to follow a certain pattern within the range $\Delta t = t_{i+1}-t_i$ The velocity and displacement at $t = t_{i+1}$ are computed by integrating the (assumed) acceleration function:

$$\{\dot{u}_{i+1}\} = \{\dot{u}_i\} + (1-\delta)\Delta t\{\ddot{u}_i\} + \delta\Delta t\{\ddot{u}_{i+1}\} \tag{4-2}$$

$$\{u_{i+1}\} = \{u_i\} + \Delta t\{\dot{u}_i\} + \left(\frac{1}{2}-\alpha\right)(\Delta t)^2\{\ddot{u}_i\} + \alpha(\Delta t)^2\{\ddot{u}_{i+1}\} \tag{4-3}$$

where $\alpha$ and $\delta$ are parameters defining the variation of acceleration over the time step.
The velocity and acceleration increments over the time interval $\Delta t$ are obtained by rewriting (4-2) and (4-3) and solving the second equation for $\Delta\ddot{u}$ :

$$\{\Delta\dot{u}\} = \left(\frac{\delta}{\alpha\Delta t}\right)\{\Delta u\} - \left(\frac{\delta}{\alpha}\right)\{\dot{u}_i\} + \left(1-\frac{\delta}{2\alpha}\right)\Delta t\{\ddot{u}_i\} \tag{4-4}$$

$$\{\Delta\ddot{u}\} = \frac{1}{\alpha(\Delta t)^2}\{\Delta u\} - \frac{1}{\alpha\Delta t}\{\dot{u}_i\} - \frac{1}{2\beta}\{\ddot{u}_i\} \tag{4-5}$$

Introducing (4-4) and (4-5) into (4-1) will result in a algebraic form of the equations of motion:

$$[\tilde{K}]\{\Delta u\} = \{\Delta\tilde{F}\} \tag{4-6}$$

where the equivalent (effective) stiffness matrix $[\tilde{K}]$ and load vector $\{\Delta\tilde{F}\}$ are equal to:

$$[\tilde{K}] = \frac{1}{\alpha(\Delta t)^2}[M] + \frac{\delta}{\alpha\Delta t}[C] + [K] \tag{4-7}$$

$$\{\Delta\tilde{F}\} = \{\Delta F\} + \left(\frac{\delta}{\alpha\Delta t}[M] + \frac{\delta}{\alpha}[C]\right)\{\dot{u}_i\} + \left(\frac{1}{2\alpha}[M] + \frac{\delta}{2\alpha}\Delta t[C] - \Delta t[C]\right)\{\ddot{u}_i\} \tag{4-8}$$

Once the solution of (4-6) is obtained, $\{\Delta\dot{u}\}$ and $\{\Delta\ddot{u}\}$ are computed from (4-4) and (4-5). Adding the incremental quantities to the response of the system at time $t_i$ gives the desired response at time $t_{i+1}$.

The above method has been shown to be unconditionally stable (Bathe and Wilson, 1976) for:

$$\delta \geq \frac{1}{2} \quad , \quad \alpha \geq \frac{1}{4}\left(\frac{1}{2} + \delta\right)^2 \quad , \quad \frac{1}{2} + \delta + \alpha > 0 \tag{4-9}$$

The parameter values selected for implementation in IDARC-BRIDGE are:

$$\delta \geq \frac{1}{2} + \gamma \qquad \alpha = \frac{1}{4}(1+\gamma)^2 \qquad \gamma \geq 0 \tag{4-10}$$

where $\gamma$ is the amplitude decay factor which typically takes on values between 0 and 0.005. This source of numerical damping is desirable to filter out the response contributions of some of the higher modes of vibration which may be quite inaccurate since they have been calculated from a finite-element idealization of the structure, and have been shown to produce unacceptable levels

of numerical noise in cases when other sources of damping are not present (Zienkiewicz, 1977). Newmark's constant average acceleration method is retrieved for $\gamma$ equal zero.

### 4.3 Dynamic Analysis for Ground Displacement Input

The equation of motion of the structural system can be written in the following general form:

$$\begin{bmatrix} [M_{f-f}] & 0 \\ 0 & [M_{c-c}] \end{bmatrix} \begin{Bmatrix} \{\ddot{u}_f\} \\ \{\ddot{u}_c\} \end{Bmatrix} + \begin{bmatrix} [C_{f-f}] & [C_{f-c}] \\ [C_{c-f}] & [C_{c-c}] \end{bmatrix} \begin{Bmatrix} \{\dot{u}_f\} \\ \{\dot{u}_c\} \end{Bmatrix} + \begin{bmatrix} [K_{f-f}] & [K_{f-c}] \\ [K_{c-f}] & [K_{c-c}] \end{bmatrix} \begin{Bmatrix} \{u_f\} \\ \{u_c\} \end{Bmatrix} = \begin{Bmatrix} \{0\} \\ \{R\} \end{Bmatrix} \quad (4\text{-}11)$$

where $\{u_f\}$ and $\{u_c\}$ denote the free and restricted degrees of freedom, respectively; $\{R\}$ stands for the support reactions. The first sub-matrix equation in (4-11) represents the response of the superstructure and can be written as:

$$[M_{f-f}]\{\ddot{u}_f\} + [C_{f-f}]\{\dot{u}_f\} + [K_{f-f}]\{u_f\} = -[C_{f-c}]\{\dot{u}_g\} - [K_{f-c}]\{u_g\} \quad (4\text{-}12)$$

where the response of the "restricted" degrees of freedom has been set equal to the seismic motion $\{\dot{u}_g\}$ and $\{u_g\}$. The solution is similar to that for the ground acceleration input with proper adjustment of the forcing vector.

### 4.4 Modeling of Damping

The global damping matrix can be expressed as a combination of: (i) distributed "inherent" damping in the structure; (ii) damping of concentrated or localized sources of energy dissipation:

$$[C] = [C]_d + [C]_c \quad (4\text{-}13)$$

Since the inherent damping is difficult to define, it is usually expressed as a function of the mass and stiffness matrices of the structure. The common model of Rayleigh damping (Chopra, 1995) has been implemented in IDARC-BRIDGE:

$$[C]_d = \alpha[M] + \beta[K] \quad (4\text{-}14a)$$

where [M] is the global mass matrix, [K] is the global stiffness matrix, $\alpha$ and $\beta$ are determined so that specific damping ratios are obtained for two selected frequencies, say those of two elastic modes $\omega_n$ and $\omega_k$:

$$\alpha = \frac{2\omega_n\omega_k}{\omega_n{}^2 - \omega_k{}^2}(\omega_n\xi_k - \omega_k\xi_n) \tag{4-15a}$$

$$b = \frac{2\omega_n\omega_k}{\omega_n{}^2 - \omega_k{}^2}\left(\frac{\xi_k}{\omega_n} - \frac{\xi_n}{\omega_k}\right) \tag{4-15b}$$

In the case of an inelastic structure, the stiffness matrix [K] and, thus, the frequencies $\omega_n$ and $\omega_k$ are changing with time. Several options are available to update the damping matrix (Fajfar et al., 1994), some of which are: (i) keep the initial damping matrix constant for the whole time of analysis; (ii) update the damping matrix such that $[C] = \alpha[M] + \beta[K(t)]$, where [K(t)] is the tangent stiffness; (iii) update the damping matrix considering the change of natural frequencies with level of response. The latter option requires calculation of at least two natural frequencies at every time step, as well as estimation of the corresponding damping ratios (which also increase with increasing level of response). Since such a procedure may become very cumbersome for large structures, options (i) and (ii) are currently implemented in IDARC-BRIDGE.

The damping from concentrated sources has the form:

$$[C]_c = [C(t)]_d + [C(t)]_i + [C(t)]_{SSI} \tag{4-14b}$$

where $[C(t)]_d$ denotes the contribution of dampers, $[C(t)]_i$ – contribution of isolators. Both of them are derived from the "constitutive" relations of the respective protective systems. The coefficients of $[C(t)]_{SSI}$, damping concentrated to the supports of the structure due to soil-structure interaction effects, are calculated from geotechnical considerations (Wolf, 1985; Mylonakis et al., 1997).

## 4.5 Coupled Motions

The efficiency of the solution of a structural analysis problem can be improved by coupling the motions of degrees of freedom in rigid zones, leading to significant reduction on the total number of degrees of freedom. This may be useful in modeling complicated deck-pier connections as well as the action of isolators and restrainers in expansion joints, located away from the deck centerline.

The coupling procedure in IDARC-BRIDGE is based on the Lagrange multiplier method (Bathe, 1992). The conditions to be satisfied between the solution variables (i.e. between displacements of certain degrees of freedom) are specified using a variational formulation of the structural system operated on (the formulation) by the Lagrange multiplier method:

$$\prod = \frac{1}{2} u^T K u - u^T f + \lambda(cu + c^*) \tag{4-16}$$

where:

$\prod$ = Total potential of the system

u = Displacement solution vector

K = Global stiffness matrix

f = Load vector

$\lambda$ = Lagrange multiplier

c and c* = Coefficients of the coupling equations

Taking the variation of (4-16) and equating it to zero leads to:

$$\delta \prod = \delta u^T K u - \delta u^T f + \delta\lambda(cu + c^*) + \lambda c \delta u = 0 \tag{4-17}$$

Since $\delta u$ and $\delta\lambda$ are arbitrary, a set of linear equations is obtained:

$$\begin{vmatrix} Ku - f = 0 \\ cu + c^* = 0 \end{vmatrix} \tag{4-18}$$

Substituting the second equation of (4-18) into the first and taking c* as zero shows that the number of equations needed to obtain a solution is equal to the initial number of degrees of freedom minus the number of coupling equations. The coupled (slaved) degrees of freedom are eliminated from the global property matrices and load vector. The terms in the stiffness matrix are modified as follows:

$$K_{ij}^{coupled} = K_{ij} - \sum_{L_1=C_i} c_{iL_1} K_{L_1 j} - \sum_{L_2=C_j} c_{jL_2} K_{iL_2} + \sum_{L_1=C_i} \sum_{L_2=C_j} c_{iL_1} c_{jL_2} K_{L_1 L_2} \qquad (4\text{-}19)$$

where:

$C_i$ = Indices of the degrees of freedom coupled to the $i^{th}$ (master) degree of freedom

$c_{iL}$ = Coefficients of the constraint equation (see later) relating the motions of the slaved degrees of freedom and the motion of the $i^{th}$ (master) degree of freedom

$C_j$ = Indices of the degrees of freedom coupled to the $j^{th}$ degree of freedom

$c_{jL}$ = Coefficients of the constraint equation (see later) relating the motions of the slaved degrees of freedom and the motion of the $j^{th}$ (master) degree of freedom

The terms in the modified load vector are obtained from original load vector:

$$f_i^{coupled} = f_i - \sum_{L=C_i} c_{iL} f_L \qquad (4\text{-}20)$$

### 4.6 Numerical Solution of the System of Equilibrium Equations

The set of equations of dynamic equilibrium has been shown to reduce (Newmark β integration method) to a system of linear algebraic equations:

$$\tilde{K}\, \Delta u = \{\tilde{f}\} \qquad (4\text{-}21)$$

where:

$\tilde{K}$ = Equivalent (effective) stiffness matrix

$\Delta u$ = Vector of incremental displacements

$\tilde{f}$ = Equivalent (effective) load vector

The stiffness matrix is typically stored as a rectangular matrix with dimensions determined by the band width and the length of diagonal. To enhance the efficiency of this type of storage, most of the commonly used solution procedures perform reordering of elements to achieve a smaller band width - a costly operation both in terms of computer time and memory. This issue may be particularly important in the presence of coupled motions, since degrees of freedom with no interaction influence coefficients in the initial assembly, may interact after modifications related to coupled motions and the band width of the property matrices may actually increase.

Most matrix or finite element analysis programs employ exact elimination (Gauss, Gauss-Jordan) or decomposition methods (LU, Crout, Cholesky) for solving the set of linear algebraic equations. These procedures are typically accompanied by a variety of pivoting, scaling and partitioning techniques to mitigate the problems they are particularly prone to: round-off, division by zero, ill-conditioning. The latter may become very pronounced in property matrices of bridge structures for a number of reasons: (i) uneven distribution of stiffness typically caused by columns with different strength, (ii) geometric discontinuities due to the presence of expansion joints or isolation and (iii) sudden changes of stiffness of columns and abutments upon exceeding their cracking or yielding capacity.

To overcome the aforementioned difficulties, a sparse matrix storage format (Yale) combined with an iterative solution method (Conjugate Gradient Iterative Solver) are used in the present development.

### 4.6.1 Sparse Matrix Storage

The computational platform IDARC-BRIDGE utilizes the sparse matrix storage format described by Kincaid et al., (1990).

A symmetric matrix [K] can be represented by three vectors {A}, {JA} and {IA}. All nonzero elements of the upper triangular portion of [K] are stored in {A}. The $j^{th}$ element of vector {JA}

contains the number of the column where the $j^{th}$ element of {A} is located in the upper part of [K]. Vector {IA} holds the index of each diagonal element of [K] resulting from counting only the nonzero entities in each row of its upper triangular portion.

An example on the application of Yale sparse matrix storage format is given below:

$$[K] = \begin{bmatrix} 11. & 0. & 0. & 14. & 15. \\ 0. & 22. & 0. & 0. & 0. \\ 0. & 0. & 33. & 0. & 0. \\ 14. & 0. & 0. & 44. & 45. \\ 15. & 0. & 0. & 45. & 55. \end{bmatrix}$$

The three vectors representing matrix [K] are:

A = [11. 14. 15. 22. 33. 44. 45. 55.]

JA = [1 4 5 2 3 4 5 5]

IA = [1 4 5 6 8 9]

The length of vectors {A} and {JA} is equal to the number of nonzero elements in the upper triangular portion of [K]. The dimension of {IA} is always equal the number of rows of [K] plus one. The number of nonzero elements in the $i^{th}$ row of the upper part of K can be obtained by subtracting the $i^{th}$ from the $(i+1)^{st}$ element of {IA}.

### 4.6.2 Conjugate Gradient Iterative Method

Iterative solution techniques have utility in structural dynamics problems for a variety of reasons: (i) large differences between terms of the influence matrix do not affect the accuracy of the solution; (ii) the solution from the previous analysis step can be used as an initial guess at the next step which is particularly useful in incremental analyses; (iii) iterative methods are suitable for problems involving sparse matrices, since they typically employ matrix-vector and vector-vector multiplication operations.

### 4.6.2.1 Conjugate Gradient Method

The Conjugate Gradient Method has been proven to be one of the most effective iterative procedures for solving large systems of linear algebraic equations of the form:

$$Ax = b \tag{4-22}$$

where:

A = Symmetric, positive definite matrix of coefficients

x = Solution vector

b = Right-hand-side vector

The basic quadratic form is a quadratic function of vector x:

$$f(x) = \frac{1}{2} x^T Ax - b^T x + c \tag{4-23}$$

where c is a scalar.

The gradient of f(x) is obtained by differentiating (4-23):

$$f'(x) = \frac{1}{2} A^T x + \frac{1}{2} Ax - b \tag{4-23}$$

Since matrix A is symmetric:

$$f'(x) = Ax - b \tag{4-24}$$

Setting the gradient to zero retrieves (4-22). Therefore, if the coefficient matrix is positive-definite and symmetric, the solution of the set of linear algebraic equations is the minimum of the quadratic form (4-23).

### 4.6.2.2 Steepest Descent and Conjugate Directions Convergence Techniques

The solution by the method of ***steepest descent*** starts with an initial guess $x_0$ for vector x and proceeds by taking a series of steps ($x_1$, $x_2$, ...) toward x until a convergence criterion is satisfied. The direction of each step is that of the gradient of function f(x):

$$-f'(x_i) = b - Ax_i = r_i \tag{4-25}$$

where $r_i$ is the vector of residuals.

The latter can also be defined as,

$$r_i = -A(x_i - x) = -Ae_i \tag{4-26}$$

where $e_i$ is the error term.

The solution vector $x_i$ and the residual $r_i$ from the $i^{th}$ convergence iteration are used in the subsequent step:

$$x_{i+1} = x_i + \alpha r_i \tag{4-27}$$

where $\alpha_i$ is a direction scalar which characterizes the length of the search vector and minimizes the quadratic form f(x) such that:

$$\frac{df(x_{i+1})}{d\alpha} = f'^{T}(x_{i+1})\frac{dx_{i+1}}{d\alpha} = f'^{T}(x_{i+1})\frac{d(x_i + \alpha r_i)}{d\alpha} = f'^{T}(x_{i+1})r_i = r^{T}_{i+1}r_i = 0 \tag{4-28}$$

Using the last equality in (4-27), (4-26) and (4-25):

$$\alpha = \frac{r_i^{T} r_i}{r_i^{T} A r_i} \tag{4-29}$$

The reduction of the error between consecutive steps is calculated from:

$$\|e_{i+1}\|_A^2 = \|e_i\|_A^2 \omega^2 \tag{4-30}$$

$$\omega^2 = 1 - \frac{(k^2 + \mu^2)^2}{(k + \mu^2)(k^3 + \mu^2)} \tag{4-31}$$

$$k = \frac{\lambda_1}{\lambda_2} \tag{4-32}$$

$$\mu = \frac{\zeta_1}{\zeta_2} \tag{4-33}$$

where:

$\lambda_1, \lambda_2$ = Eigenvectors (first two) of matrix A

$\xi_1; \xi_2$ = Lengths of projection of the error term $e_i$ on the eigenvectors of A

The drawback of steepest descent is that steps are taken in the same direction several times and the number of iterations might be large.

The method of ***conjugate directions*** is based on the idea of choosing the search directions so that they are orthogonal to the matrix of coefficients A.

In general the length $\alpha_i$ of each search vector $u_i$ is found from:

$$\alpha_i = \frac{d_i^T d_i}{d_i^T A d_i} \tag{4-34}$$

The Gram-Schmidt orthogonalization process is used to make the search vector $d_i$ orthogonal to A:

$$d_i = u_i + \sum_{j=0}^{i-1} \beta_{ik} d_k \tag{4-35}$$

$$\beta_{ij} = \frac{-u_i^T A d_j}{d_j^T A d_j} \tag{4-36}$$

where $u_j$ is a set of independent vectors (j = i - 1).

To derive the search vector of the $i^{th}$ iteration, the vectors from the previous i-1 iterations must be stored - a possible drawback. However, instead of an arbitrary set of vectors $u_j$, the set of residuals $r_j$ may be used to improve the performance of the method and simplify the solution. The final procedure in algorithmic form is:

$$x_{i+1} = x_i + \alpha_i d_i \tag{4-37}$$

$$\alpha_i = \frac{r_i^T r_i}{d_i^T A d_i} \tag{4-38}$$

$$d_{i+1} = r_{i+1} + \beta_{i+1} d_i \tag{4-39}$$

$$\beta_{i+1} = \frac{r_{i+1}^T r_{i+1}}{r_i^T r_i} \tag{4-40}$$

$$r_{i+1} = r_i - \alpha_i A d_i \tag{4-41}$$

The initial searching vector is:

$$d_0 = r_0 = b - Ax_0 \tag{4-42}$$

The rate of convergence of the method of conjugate directions (or decrease of the error norm) is a function of the condition of matrix A:

$$\|e_i\|_A \leq 2\left(\frac{\sqrt{k-1}}{\sqrt{k+1}}\right)^i \|e_0\|_A \tag{4-43}$$

where:

$k = \frac{\lambda_{min}}{\lambda_{max}}$ = Condition number

$\lambda_{min}$ and $\lambda_{max}$ = Minimum and maximum eigenvalue of matrix A.

#### 4.6.2.3 Jacobi Preconditioning Technique

A preconditioning technique is used to decrease the condition number of A. The system of linear algebraic equations is premultiplied by a symmetric, positive definite matrix $M^{-1}$:

$$M^{-1}Ax = M^{-1}b \tag{4-44}$$

where M is equal to the diagonal of A (Jacobi preconditioning).
The complete solution algorithm is:

$$r_0 = b - Ax_0 \tag{4-45}$$

$$d_0 = M^{-1}r_0 \tag{4-46}$$

$$\alpha_i = \frac{r_i^T M^{-1} r_i}{d_i^T A d_i} \tag{4-47}$$

$$x_{i+1} = x_i + \alpha_i d_i \tag{4-48}$$

$$r_{i+1} = r_i - \alpha_i d_i \tag{4-49}$$

$$\beta_{i+1} = \frac{r_{i+1} M^{-1} r_{i+1}}{r_i^T M^{-1} r_i} \tag{4-50}$$

$$d_{i+1} = M^{-1} r_{i+1} + \beta_{i+1} d_i \tag{4-51}$$

The solver of IDARC-BRIDGE employs a gradient method utilizing the conjugate directions convergence and Jacobi preconditioning techniques for solving the set of algebraic equations

resulting from the incremental formulation of Newmark's method for numerical integration of the system of linearized differential equations of dynamic equilibrium.

# SECTION 5

# COMPONENT MODELING AND ELEMENT TYPES

## 5.1 Description of Bridge Components

The computational platform IDARC-BRIDGE offers an exhaustive element library for modeling the stiffness and damping properties of commonly encountered constituents of bridge structures. The element force-displacement rules reflect the distinctive features of behavior of the major components of a typical bridge assembly such as: deck, bents, foundations, abutments, preventive systems, and expansion joints (figure 5-1). A brief description of each component is given herein.

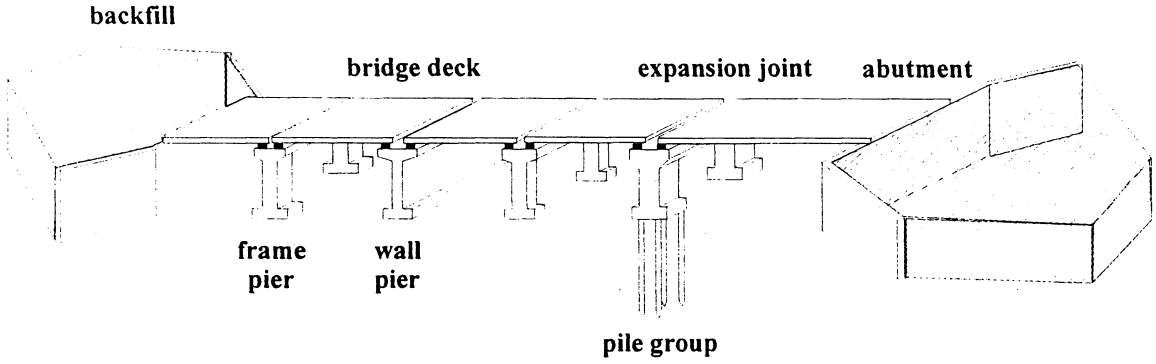


**FIGURE 5-1 Typical Bridge Assembly and Major Components**

The deck is the surface on which the traffic moves. Several structural arrangements of the deck are used: prestressed box girders, monolithically cast beams and slabs, concrete or steel slabs supported on steel beams etc. The deck is supported on vertical elements ("bents") which

typically resist both vertical (gravity, traffic) and lateral (wind, earthquake) loads. A variety of configurations are used: single and multiple-column bents, wall piers, etc.

Expansion joints are used to divide the deck of long bridges into segments for the sake of preventing undesirable forces due to thermal expansion. Expansion bearings are also placed between the deck and the bent to prevent such thermal distress. Various kinds of bearings are used for this purpose, including elastomeric bearings, teflon steel sliders, steel bearings etc.

Restrainers are used in the intermediate (or abutment) expansion joints of some of the more recent bridge designs and retrofits to prevent unseating of the deck at the supports. The restrainers are typically made of steel rods or cables anchored in each of the neighboring deck segments to limit the longitudinal or vertical relative displacements. More modern solutions utilize nonlinear damping devices with energy or shock absorption characteristics.
Shear keys, which restrain transverse movement but allow longitudinal movement, are provided between the different sections of the bridge. This is to ensure that the bridge sections move together in the transverse direction.

The bridge foundation transfers the gravity load of the bridge to the soil. It also transfers horizontal forces and overturning moments due to wind and earthquake loading. Three major types of foundations systems are used: spread footings, piles and pile groups, and caissons.

The abutments are substructures located at the two ends of the bridge. They sustain vertical and lateral forces from the deck, and retain the soil behind them. The abutments are usually made of a central wall and two wing walls. The deck is supported vertically on the central wall through a joint, while the wing walls provide horizontal support to the soil behind them.

Modern protective systems such as base isolation, dampers, and active control devices are also used to reduce the forces transmitted to bridges structure during earthquakes. These mechanisms are usually placed in the expansion joints between deck sections or between the deck and the bent.

The subsequent paragraphs discuss the properties of macro-models of various bridge components and the corresponding element types of the computational platform.

## 5.2 Elastic Beam-Column Element

The basic space-frame element of three-dimensional matrix analysis of structures (Weaver and Gere, 1990) is incorporated in IDARC-BRIDGE under the name "elastic 3d beam" and has utility in modeling beam-column members which are likely to remain elastic throughout the analysis. The element is defined by two nodes with 3 translational and 3 rotational degrees of freedom each, area of the cross section, torsional constant, moments of inertia about the weak and the strong axes of the section, modulus of elasticity, shear modulus, angle of rotation of the local coordinate system about the longitudinal axis of the element and two shape factors for shearing in the direction of principal axis. For member-oriented axes, the force-displacement relation can be written as:

$$[K]\{u\} = \{F\} \tag{5-1}$$

where:

$[K] = \begin{bmatrix} [k_{i-i}] & [k_{i-j}] \\ [k_{j-i}] & [k_{j-j}] \end{bmatrix}$ = Stiffness matrix (figure 5-3), partitioned to delineate the sub-matrices associated with the ends of the element at nodes "i" and "j".

$\{u\} = \begin{Bmatrix} \{u_i\} \\ \{u_j\} \end{Bmatrix}$ = Vector of displacements (translations and rotations) of the local degrees of freedom.

$\{F\} = \begin{Bmatrix} \{F_i\} \\ \{F_j\} \end{Bmatrix}$ = Vector of element actions (forces and moments).

The effect of the shear forces on the displacements of the member is included in the analysis by modifying the direct and cross stiffness coefficients associated with the translational degrees of

freedom (figure 5-4). The non-dimensional constants $g_y$ and $g_z$ have no physical meaning and are used for simplicity of notation:

$$g_y = \frac{f_y 6EI_z}{GA_x L^2} \qquad g_z = \frac{f_z 6EI_y}{GA_x L^2}$$

The shape factors $f_y$ and $f_z$ reflect the need to distinguish the shear areas $A_y = A_x/f_y$ and $A_z = A_x/f_z$ in the principal directions of the cross section. Being a part of the user input, these factors provide a way to neglect the effect of shear deformations.

The element stiffness matrix is obtained with respect to the local coordinate system and then transformed to the structural axes. The global stiffness matrix is constructed by summing contributions from the individual member matrices. In dynamic analysis, the mass of the element must be lumped in the end nodes. Special end conditions, discussed in depth later in this section, such as "rigid arms", "end releases" and "end springs" may be specified for the elastic beam element.

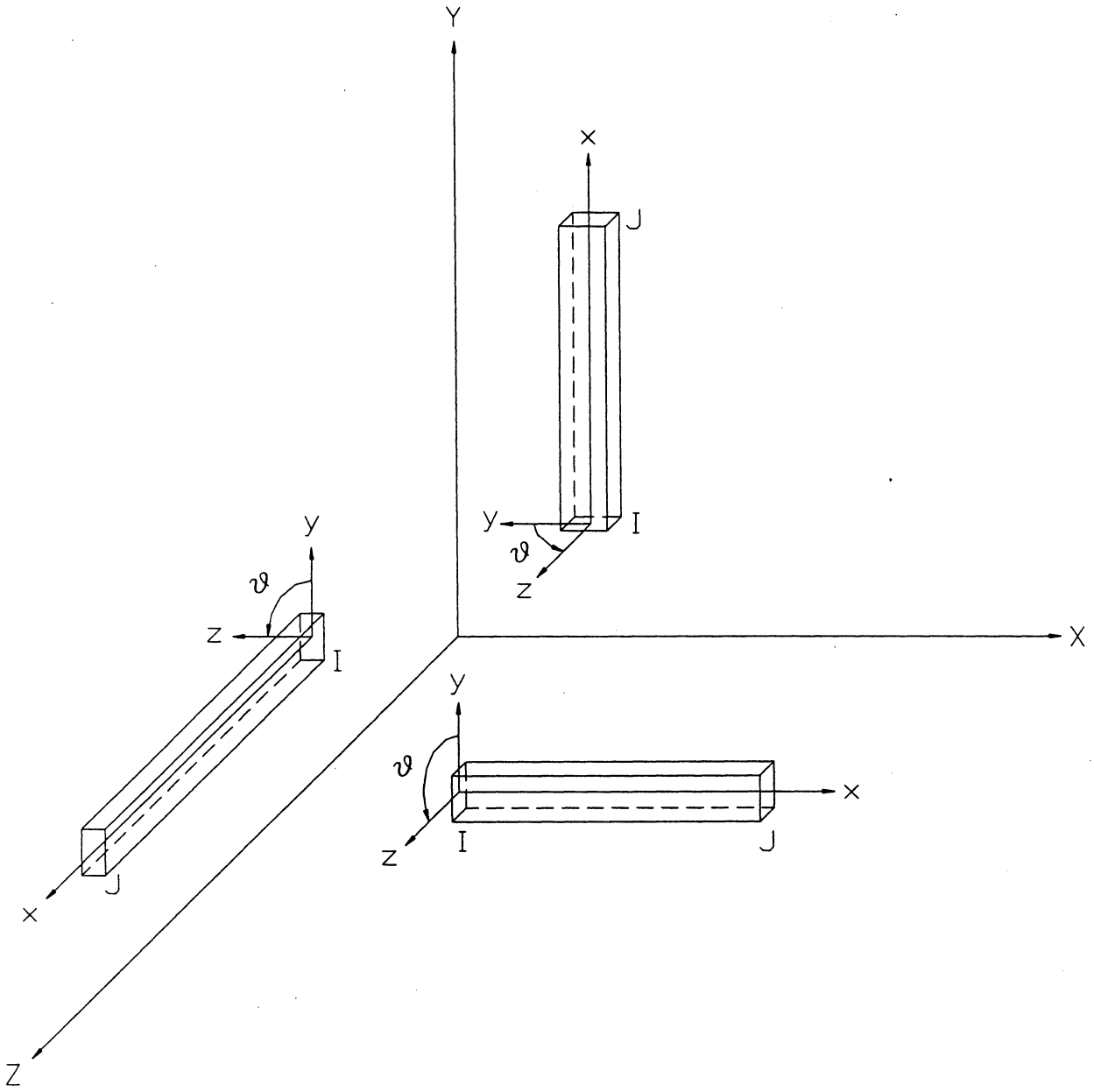


**FIGURE 5-2 Rotation of the Local Coordinate System of Elastic Beam-Column Element**

$$[K] = \begin{bmatrix}
\frac{EA_x}{L} & 0 & 0 & 0 & 0 & 0 & -\frac{EA_x}{L} & 0 & 0 & 0 & 0 & 0 \\
 & \frac{12EI_z}{L^3} & 0 & 0 & 0 & \frac{6EI_z}{L^2} & 0 & -\frac{12EI_z}{L^3} & 0 & 0 & 0 & \frac{6EI_z}{L^2} \\
 & & \frac{12EI_y}{L^3} & 0 & -\frac{6EI_y}{L^2} & 0 & 0 & 0 & -\frac{12EI_y}{L^3} & 0 & -\frac{6EI_y}{L^2} & 0 \\
 & & & \frac{GI_x}{L} & 0 & 0 & 0 & 0 & 0 & -\frac{GI_x}{L} & 0 & 0 \\
 & & & & \frac{4EI_y}{L} & 0 & 0 & 0 & \frac{6EI_y}{L^2} & 0 & \frac{2EI_y}{L} & 0 \\
 & & & & & \frac{4EI_z}{L} & 0 & -\frac{6EI_z}{L^2} & 0 & 0 & 0 & \frac{2EI_z}{L} \\
 & & & & & & \frac{EA_x}{L} & 0 & 0 & 0 & 0 & 0 \\
 & & & & & & & \frac{12EI_z}{L^3} & 0 & 0 & 0 & -\frac{6EI_z}{L^2} \\
 & & \text{symm} & & & & & & \frac{12EI_y}{L^3} & 0 & \frac{6EI_y}{L^2} & 0 \\
 & & & & & & & & & \frac{GI_x}{L} & 0 & 0 \\
 & & & & & & & & & & \frac{4EI_y}{L} & 0 \\
 & & & & & & & & & & & \frac{4EI_z}{L}
\end{bmatrix}$$

**FIGURE 5-3 Stiffness Matrix of Elastic Beam-Column Element**

$$[K_{i-i}]=\begin{bmatrix} \frac{EA_x}{L} & 0 & 0 & 0 & 0 & 0 \\ & \frac{12EI_z}{L^3(1+2g_y)} & 0 & 0 & 0 & \frac{6EI_z}{L^2(1+2g_y)} \\ & & \frac{12EI_y}{L^3(1+2g_z)} & 0 & -\frac{6EI_y}{L^2(1+2g_z)} & 0 \\ & & & \frac{GI_x}{L} & 0 & 0 \\ & \text{symm.} & & & \frac{(4+2g_z)EI_y}{(1+2g_z)L} & 0 \\ & & & & & \frac{(4+2g_y)EI_z}{(1+2g_y)L} \end{bmatrix}$$

$$[K_{i-j}]=\begin{bmatrix} -\frac{EA_x}{L} & 0 & 0 & 0 & 0 & 0 \\ 0 & -\frac{12EI_z}{L^3(1+2g_y)} & 0 & 0 & 0 & \frac{6EI_z}{L^2(1+2g_y)} \\ 0 & 0 & -\frac{12EI_y}{L^3(1+2g_z)} & 0 & -\frac{6EI_y}{L^2(1+2g_z)} & 0 \\ 0 & 0 & 0 & -\frac{GI_x}{L} & 0 & 0 \\ 0 & 0 & \frac{6EI_y}{L^2(1+2g_z)} & 0 & \frac{(2-2g_z)EI_y}{(1+2g_z)L} & 0 \\ 0 & -\frac{6EI_z}{L^2(1+2g_y)} & 0 & 0 & 0 & \frac{(2-2g_y)EI_z}{(1+2g_y)L} \end{bmatrix}$$

$$[K_{j-j}]=\begin{bmatrix} \frac{EA_x}{L} & 0 & 0 & 0 & 0 & 0 \\ & \frac{12EI_z}{L^3(1+2g_y)} & 0 & 0 & 0 & -\frac{6EI_z}{L^2(1+2g_y)} \\ & & \frac{12EI_y}{L^3(1+2g_z)} & 0 & \frac{6EI_y}{L^2(1+2g_z)} & 0 \\ & & & \frac{GI_x}{L} & 0 & 0 \\ & \text{symm.} & & & \frac{(4+2g_z)EI_y}{(1+2g_z)L} & 0 \\ & & & & & \frac{(4+2g_y)EI_z}{(1+2g_y)L} \end{bmatrix}$$

**FIGURE 5-4 Element Sub-Matrices Including the Effect of Shear Deformations**

## 5.3 Hysteretic Beam-Column Element

In nonlinear analyses (time history analysis, incremental static analysis, push-over analysis), the coefficients of the element stiffness matrix depend on the displacements (or forces) at the end nodes as well as on the history of loading. The stiffness matrix of a nonlinear concrete element in bending is derived using a flexibility formulation similar to that proposed by Lobo (1994). The moment distribution along a member, subjected to lateral loads, is linear, as shown in figure 5-5a. The presence of gravity loads will alter the distribution, and in cases of significant gravity moments, the structural elements should be subdivided to capture the variation. When the member experiences inelastic deformations, cracks tend to spread from the joint interface resulting in the curvature distribution shown in figure 5-5b. Sections along the element will also exhibit different flexibility characteristics, depending on the corresponding degree of inelasticity. The spread plasticity concept is employed to define the flexural load-deformation rules of the "hysteretic 3d beam" element in IDARC-BRIDGE, capture the variation of flexibility and combine the contribution of various regions along the member to the element stiffness matrix. Currently, the interaction of bending of the element in the two principal directions is ignored.

### 5.3.1 Spread Plasticity Formulation

The flexibility of a hysteretic beam-column element is assumed to follow the distribution shown in figure 5-5b, where: $EI_A$ and $EI_B$ are the current flexural stiffness of the sections at end "A" and "B", respectively; $EI_0$ is the stiffness at the center of the element; $GA_Z$ is the shear stiffness assumed constant along the element; $\alpha_A$ and $\alpha_B$ are the yield penetration coefficients; L is the length of the element. The flexural stiffness $EI_A$ and $EI_B$ are determined from the hysteretic model. The stiffness $EI_0$ and the yield penetration coefficients $\alpha_A$ and $\alpha_B$ are determined as described later in Section 5.3.2, depending on the moment distribution and the previous yield penetration history.

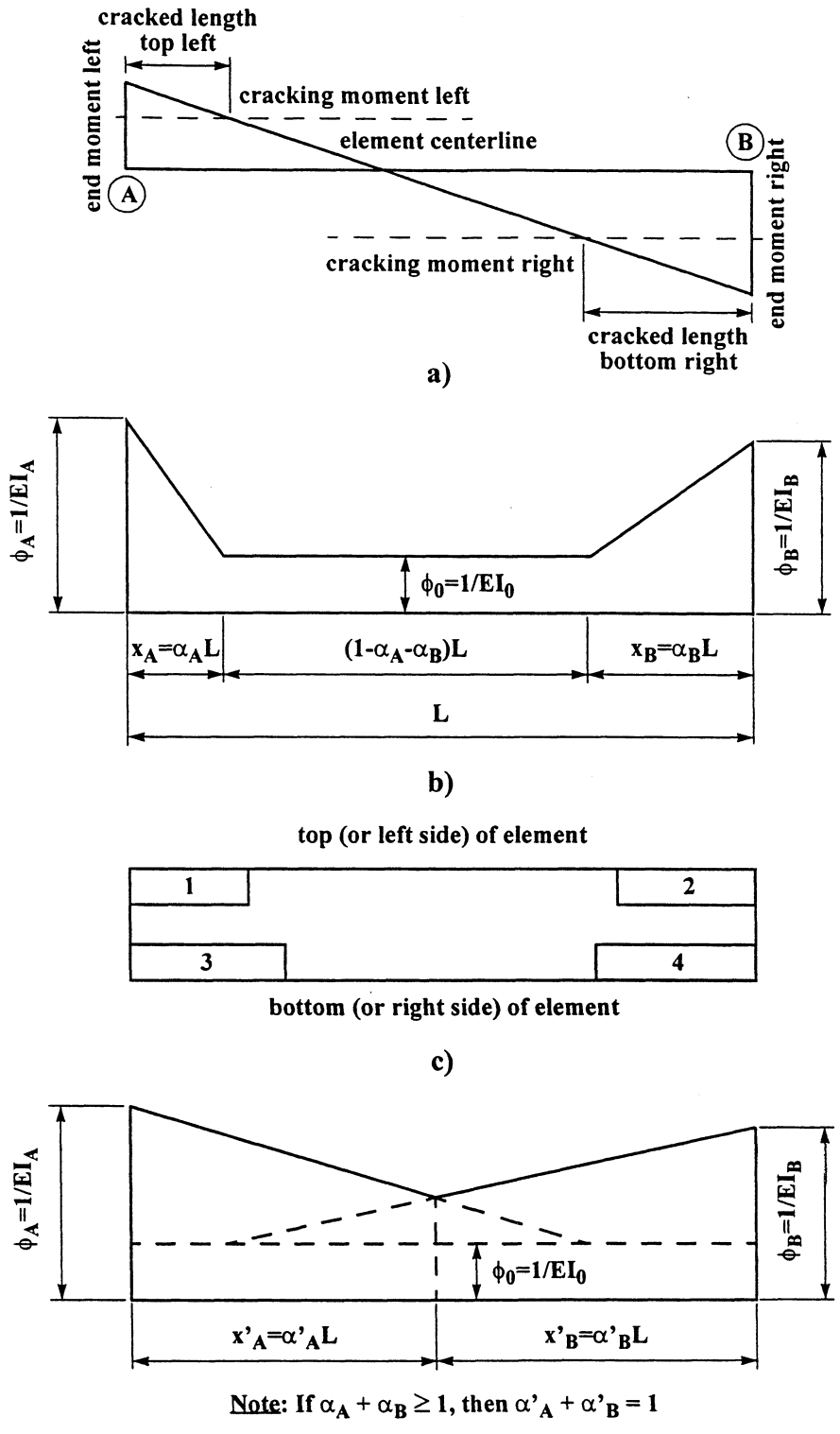


**FIGURE 5-5 Calculation of Stiffness of Damaged Beam-Column Elements: a) Distribution of Moment, b) Distribution of Flexibility, c) Damaged Zones, d) Yield Penetration Lengths for Fully Inelastic Elements**

The flexibility matrix of the element is:

$$\begin{Bmatrix}\theta_A\\ \theta_B\end{Bmatrix}=\begin{bmatrix}f_{AA} & f_{AB}\\ f_{BA} & f_{BB}\end{bmatrix}\begin{Bmatrix}M_A\\ M_B\end{Bmatrix} \tag{5-2}$$

where:

$\theta_A$ and $\theta_B$ = Rotations at ends "A" and "B".

$M_A$ and $M_B$ = End moments.

The flexibility coefficients are calculated from the following relationship:

$$f_{ij}=\int_0^L \frac{m_i(x)m_j(x)}{EI(x)}dx+\int_0^L \frac{v_i(x)v_j(x)}{GA_Z}dx \tag{5-3}$$

where:

$m_i(x)$ and $m_j(x)$ = Moment distributions due to a virtual unit moment at end "i" or "j", respectively.

$v_i(x)$ and $v_j(x)$ = Corresponding shear distributions.

The flexibility coefficients are determined by integration of the equation above (Lobo, 1994; Valles et al., 1996):

$$f_{AA}=\frac{L}{12}\left[\frac{4}{EI_0}+\left(\frac{1}{EI_A}-\frac{1}{EI_0}\right)\left(6\alpha_A-4\alpha_A^2+\alpha_A^3\right)+\left(\frac{1}{EI_B}-\frac{1}{EI_0}\right)\alpha_B^3\right]+\frac{1}{GA_ZL} \tag{5-4a}$$

$$f_{AB}=\frac{L}{12}\left[\frac{-2}{EI_0}-\left(\frac{1}{EI_A}-\frac{1}{EI_0}\right)\left(2\alpha_A^2-\alpha_A^3\right)-\left(\frac{1}{EI_B}-\frac{1}{EI_0}\right)\left(2\alpha_B^2-\alpha_B^3\right)\right]+\frac{1}{GA_ZL} \tag{5-4b}$$

$$f_{BA}=f_{AB} \tag{5-4c}$$

$$f_{BB} = \frac{L}{12}\left[\frac{4}{EI_0} + \left(\frac{1}{EI_B} - \frac{1}{EI_0}\right)\left(6\alpha_B - 4\alpha_B^2 + \alpha_B^3\right) + \left(\frac{1}{EI_A} - \frac{1}{EI_0}\right)\alpha_A^3\right] + \frac{1}{GA_Z L} \tag{5-4d}$$

In the current release of IDARC-BRIDGE, the above formulation was rewritten, and closed form solutions were derived for the element stiffness matrix to avoid numerical instabilities if close to failure conditions are observed in flexure or shear.

$$f_{AA} = \frac{L}{12EI_0EI_AEI_B} f'_{AA} + \frac{1}{GA_Z L} \tag{5-5a}$$

$$f_{AB} = f_{BA} = \frac{L}{12EI_0EI_AEI_B} f'_{AB} + \frac{1}{GA_Z L} \tag{5-5b}$$

$$f_{BB} = \frac{L}{12EI_0EI_AEI_B} f'_{BB} + \frac{1}{GA_Z L} \tag{5-5c}$$

where:

$$f'_{AA} = 4EI_AEI_B + (EI_0 - EI_A)EI_B\left(6\alpha_A - 4\alpha_A^2 + \alpha_A^3\right) + (EI_0 - EI_B)EI_A\alpha_B^3 \tag{5-6a}$$

$$f'_{AB} = -2EI_AEI_B - (EI_0 - EI_A)EI_B\left(2\alpha_A^2 - \alpha_A^3\right) - (EI_0 - EI_B)EI_A\left(2\alpha_B^2 - \alpha_B^3\right) \tag{5-6b}$$

$$f'_{BB} = 4EI_AEI_B + (EI_0 - EI_A)EI_B\alpha_{AB}^3 + (EI_0 - EI_B)EI_A\left(6\alpha_B - 4\alpha_B^2 + \alpha_B^3\right) \tag{5-6c}$$

The total flexibility of the element is the sum of the flexural and shear contributions. The element stiffness matrix, including shear deformations, relating moments and rotations at the element ends is found by inverting the flexibility matrix:

$$\begin{Bmatrix} M_A \\ M_B \end{Bmatrix} = \begin{bmatrix} k_{AA} & k_{AB} \\ k_{BA} & k_{BB} \end{bmatrix} \begin{Bmatrix} \theta_A \\ \theta_B \end{Bmatrix} = [K] \begin{Bmatrix} \theta_A \\ \theta_B \end{Bmatrix} \tag{5-7}$$

where:

$$k_{AA} = \frac{12EI_0EI_AEI_B}{D_{et}L}\left(f'_{BB}GA_ZL^2 + 12EI_0EI_AEI_B\right) \tag{5-8a}$$

$$k_{AB} = k_{BA} = \frac{-12EI_0EI_AEI_B}{D_{et}L}\left(f'_{AB}GA_ZL^2 + 12EI_0EI_AEI_B\right) \tag{5-8b}$$

$$k_{BB} = \frac{12EI_0EI_AEI_B}{D_{et}L}\left(f'_{AA}GA_ZL^2 + 12EI_0EI_AEI_B\right) \tag{5-8c}$$

$$D_{et} = GA_ZL^2\left(f'_{AA}f'_{BB} - f'^2_{AB}\right) + 12EI_0EI_AEI_B\left(f'_{AA} + f'_{BB} - 2f'_{AB}\right) \tag{5-8d}$$

In the present formulation, shear or flexural failure of the element can be incorporated. The remaining stiffness coefficients (i.e. those relating forces and displacements, moments and displacements, and forces and rotations) are calculated from (5-8) using equilibrium considerations.

### 5.3.2 Yield Penetration Model

The yield penetration model combined with the spread plasticity formulation captures the variation of flexural rigidity along the structural element. The spread plasticity formulation described in Section 5.3.1 is dependent on the yield penetration parameters $\alpha_A$ and $\alpha_B$, and on the rigidity $EI_0$ of the uncracked portion of the member. The rules for the variation of these parameters, as the moment diagram changes in the element, are described below. The yield penetration parameters, $\alpha_A$ and $\alpha_B$, specify the proportion of the element where the acting moment is greater than the section cracking moment, $M_{Acr}$ or $M_{Bcr}$. These parameters are first calculated for the current moment distribution, and then compared with the previous maximum penetration lengths $\alpha_{Amax}$ and $\alpha_{Bmax}$. The yield penetration parameters cannot be smaller than the previous maximum values regardless of the current moment distribution. Two cases for the moment distribution are identified: (i) single curvature and (ii) double curvature moment diagrams. A set of rules is specified for each of these cases.

### 5.3.2.1 Single-Curvature Moment Diagram ($M_A M_B \geq 0$)

1) End moments smaller than the corresponding cracking moments ($|M_A| \leq |M_{Acr}|$ and $|M_B| \leq |M_{Bcr}|$):

$$\alpha_A = 0 \quad \text{but} \quad \alpha_A \geq \alpha_{A\,max} \tag{5-9a}$$

$$\alpha_B = 0 \quad \text{but} \quad \alpha_B \geq \alpha_{B\,max} \tag{5-9b}$$

$$EI_0 = \frac{2EI_{A0}EI_{B0}}{EI_{A0} + EI_{B0}} \tag{5-9c}$$

2) Moment at end "A" greater than the cracking moment ($|M_A| > |M_{Acr}|$ and $|M_B| \leq |M_{Bcr}|$):

$$\alpha_A = \frac{M_A - M_{Acr}}{M_A - M_B} \leq 1 \quad \text{but} \quad \alpha_A \geq \alpha_{A\,max} \tag{5-10a}$$

$$\alpha_B = 0 \quad \text{but} \quad \alpha_B \geq \alpha_{B\,max} \tag{5-10b}$$

$$EI_0 = \frac{2EI_{A0}EI_{B0}}{EI_{A0} + EI_{B0}} \tag{5-10c}$$

3) Moment at end "B" greater than the cracking moment ($|M_A| \leq |M_{Acr}|$ and $|M_B| > |M_{Bcr}|$):

$$\alpha_A = 0 \quad \text{but} \quad \alpha_A \geq \alpha_{A\,max} \tag{5-11a}$$

$$\alpha_B = \frac{M_B - M_{Bcr}}{M_B - M_A} \leq 1 \quad \text{but} \quad \alpha_B \geq \alpha_{B\,max} \tag{5-11b}$$

$$EI_0 = \frac{2EI_{A0}EI_{B0}}{EI_{A0} + EI_{B0}} \tag{5-11c}$$

4) Moment at both ends greater than the cracking moments ($|M_A| > |M_{Acr}|$ and $|M_B| > |M_{Bcr}|$):

$$\alpha_A = 0.5 \tag{5-12a}$$

$$\alpha_B = 0.5 \tag{5-12b}$$

$$EI_0 = \frac{2EI_AEI_B}{EI_A + EI_B} \tag{5-12c}$$

where:

$M_{Acr}$ and $M_{Bcr}$ = Cracking moments of the section corresponding to the sign of the applied moments.

$EI_{A0}$ and $EI_{B0}$ = Elastic flexural rigidity based on the geometric properties of the end sections.

### 5.3.2.2 Double-Curvature Moment Diagram ($M_AM_B < 0$)

In the double curvature moment diagram the moments at the end of the element have different signs. Depending on the moment distribution four cases can be identified:

1) End moments smaller than the corresponding cracking moments ($|M_A| \le |M_{Acr}|$ and $|M_B| \le |M_{Bcr}|$):

$$\alpha_A = 0 \quad \text{but} \quad \alpha_A \ge \alpha_{A\,max} \tag{5-13a}$$

$$\alpha_B = 0 \quad \text{but} \quad \alpha_B \ge \alpha_{B\,max} \tag{5-13b}$$

$$EI_0 = \frac{2EI_{A0}EI_{B0}}{EI_{A0} + EI_{B0}} \tag{5-13c}$$

2) Moment at end "A" greater than the cracking moment ($|M_A| > |M_{Acr}|$ and $|M_B| \le |M_{Bcr}|$):

$$\alpha_A = \frac{M_A - M_{Acr}}{M_A - M_B} \le 1 \quad \text{but} \quad \alpha_A \ge \alpha_{A\,max} \tag{5-14a}$$

$$\alpha_B = 0 \quad \text{but} \quad \alpha_B \ge \alpha_{B\,max} \tag{5-14b}$$

$$EI_0 = \frac{2EI_{A0}EI_{B0}}{EI_{A0} + EI_{B0}} \tag{5-14c}$$

3) Moment at end "B" greater than the cracking moment ($|M_A| \le |M_{Acr}|$ and $|M_B| > |M_{Bcr}|$):

$$\alpha_A = 0 \quad \text{but} \quad \alpha_A \ge \alpha_{A\,max} \tag{5-15a}$$

$$\alpha_B = \frac{M_B - M_{Bcr}}{M_B - M_A} \le 1 \quad \text{but} \quad \alpha_B \ge \alpha_{B\,max} \tag{5-15b}$$

$$EI_0 = \frac{2EI_{A0}EI_{B0}}{EI_{A0} + EI_{B0}} \tag{5-15c}$$

4) Moment at both ends greater than the cracking moments ($|M_A| > |M_{Acr}|$ and $|M_B| > |M_{Bcr}|$):

$$\alpha_A = \frac{M_A - M_{Acr}}{M_A - M_B} \quad \text{but} \quad \alpha_A \ge \alpha_{A\,max} \tag{5-16a}$$

$$\alpha_B = \frac{M_B - M_{Bcr}}{M_A - M_B} \quad \text{but} \quad \alpha_B \ge \alpha_{B\,max} \tag{5-16b}$$

$$EI_0 = \frac{2EI_A EI_B}{EI_A + EI_B} \qquad (5\text{-}16c)$$

where the symbols $M_{Acr}$, $M_{Bcr}$, $EI_{A0}$ and $EI_{B0}$ have meaning similar to the single-curvature case.

In the foregoing formulation, the cracking moments are dependent on the sign of the applied moments. Special provisions are made in the program to adjust the flexibility distribution of members where yield penetration has taken place along the whole length of the element, i.e. when $\alpha_A + \alpha_B \geq 1$. In such cases, the stiffness $EI_0$ is modified to capture the actual distribution considering a new set of yield penetration coefficients that will satisfy $\alpha_A + \alpha_B \leq 1$ (see figure 5-5d).

In general, the lateral load in bridge columns is resisted by a combined flexure and shear mechanism. The shear contribution is dominant when the aspect ratio is less than about 4.

### 5.3.3 Hysteretic Rules

Two models of nonlinear inelastic behavior of beam-column elements are currently implemented in IDARC-BRIDGE: (i) a piece-wise linear hysteretic rule based on the "three-parameter" formulation of Park et al. (1987) and (ii) a smooth hysteretic rule derived from the model proposed by Bouc (1967, 1971).

#### 5.3.3.1 "Three-Parameter" Hysteretic Model

The "three-parameter" model was developed and implemented in the original release of IDARC in 1987. It ranks among the most advanced and versatile polygonal rules for characterizing response-dependent constitutive laws of beam-column members. Both the force-controlled and deformation-controlled versions use a non-symmetric trilinear monotonic moment-curvature envelope to define the strength and deformation limits in bending (figure 5-6). The model is capable of simulating a wide range of phenomena associated with plasticity: (i) loss of stiffness (termed stiffness degradation); (ii) loss of strength capacity (strength deterioration); (iii) slipping and locking of reinforcing steel inside concrete. The effect of the three parameters controlling the deterioration events in the model is illustrated in figure 5-7. The algorithm traces the hysteresis of the end sections of an element subjected to cyclic lateral load as it changes from one linear stage (branch) to another and establishes the instantaneous flexural rigidity EI at the ends. The spread plasticity concept is then employed along with a yield penetration model to generate the flexibility matrix relating the moments and rotations at the nodal points of the element as already discussed in previous sections of this report.

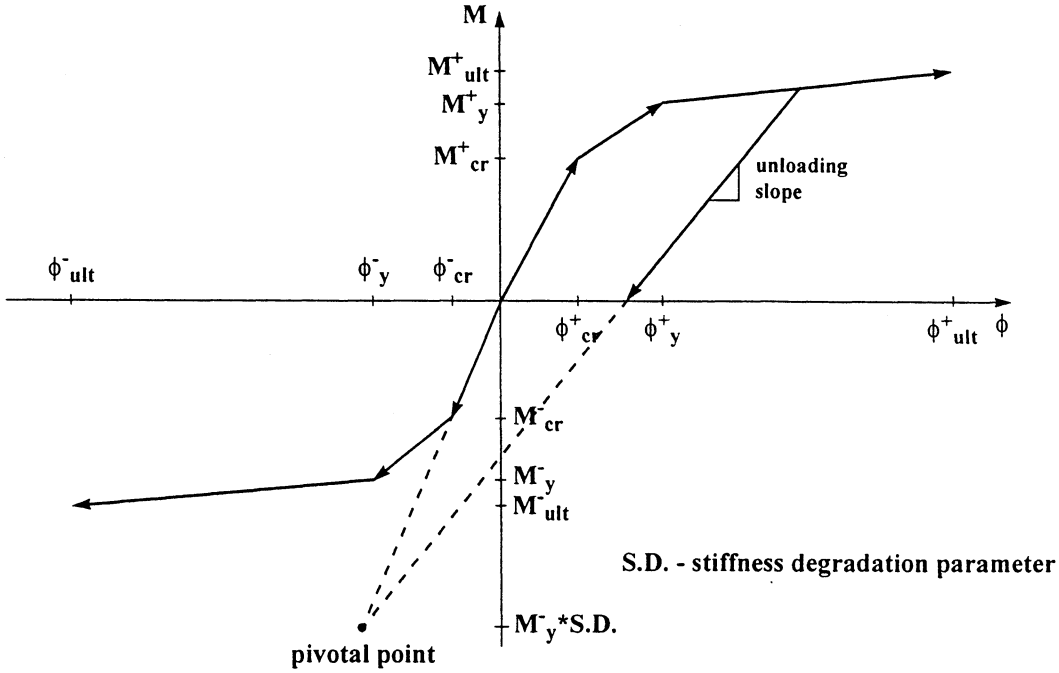


a)

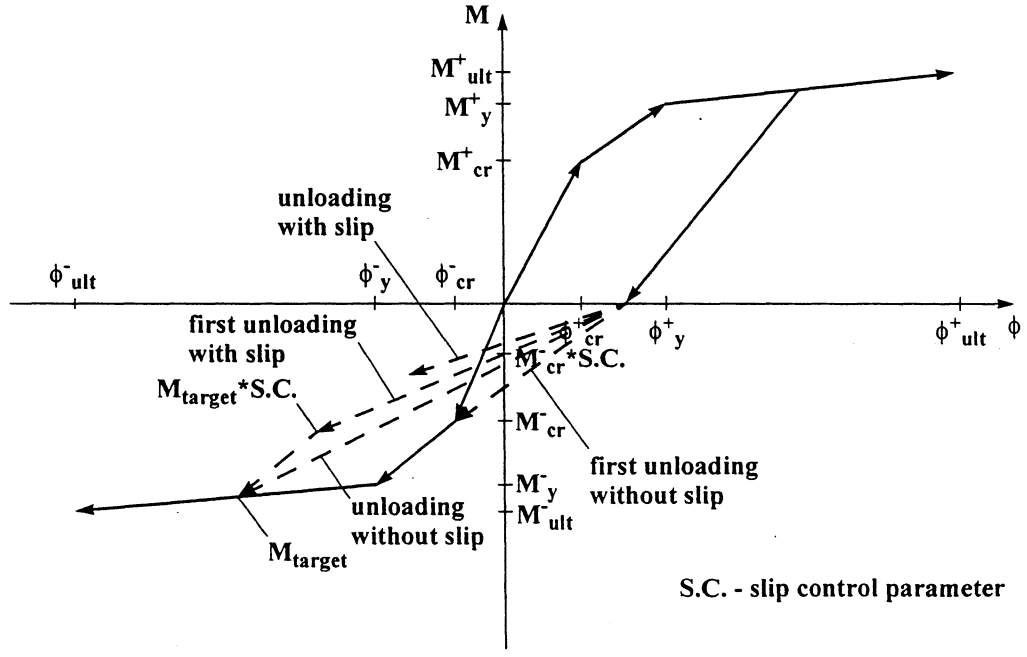


b)

**FIGURE 5-6 "Three-Parameter" Polygonal Hysteretic Model: a) Unloading Slope Definition, b) Slip Definition**

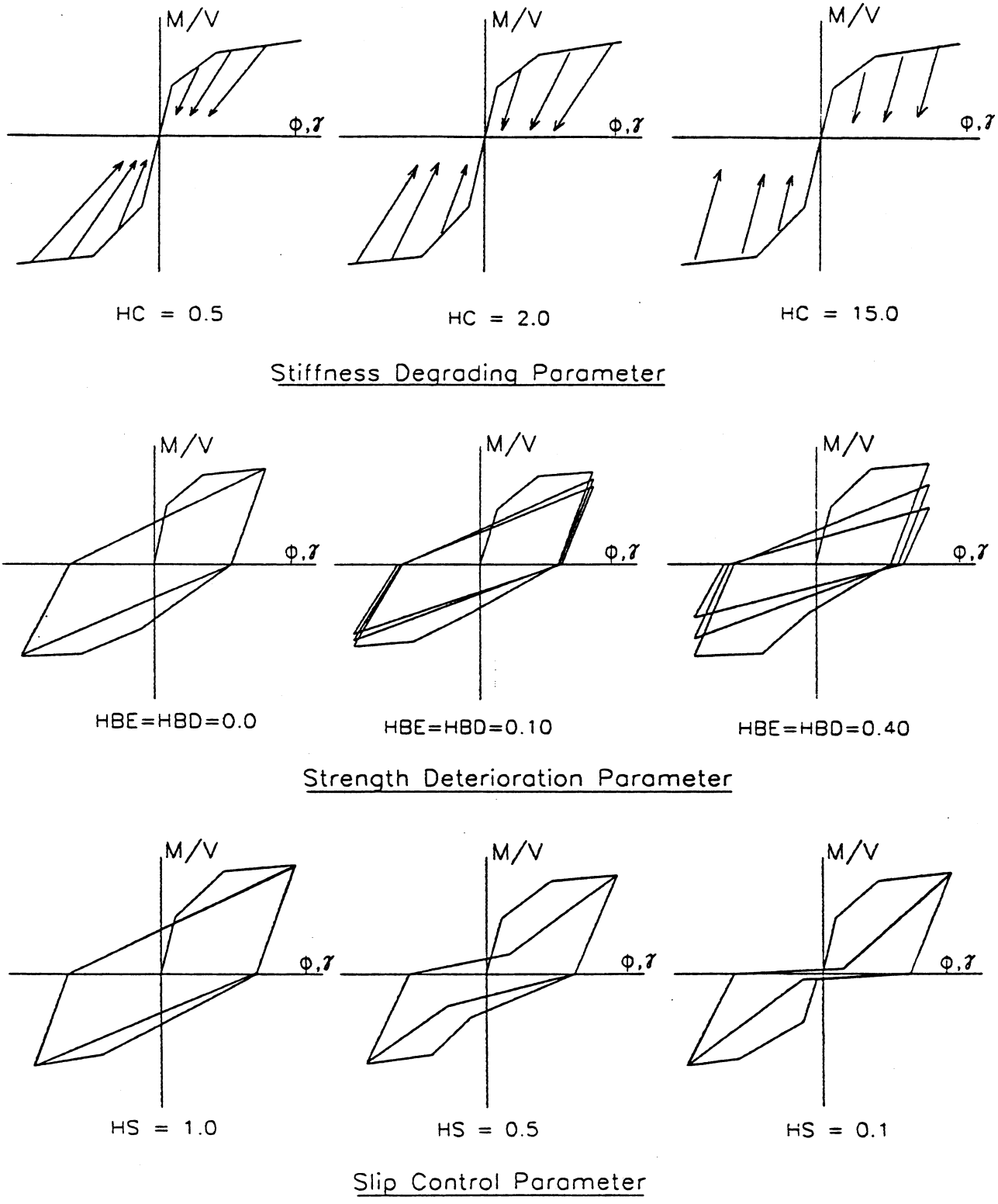


**FIGURE 5-7 Effect of Variation of Parameters Controlling the Deterioration Phenomena in the "Three-Parameter" Model**

### 5.3.3.2 Smooth Hysteretic Model

#### 5.3.3.2.1 Introduction

A smooth hysteretic model capable of simulating stiffness degradation, strength and progressive pinching effects is developed in this study to improve the accuracy of analysis of damaged elements. The model studied herein is an extension of the original formulation by Bouc (1967), modified by Wen (1976), and Baber and Wen (1981), and Baber and Noori (1985). Both the stiffness degradation and strength deterioration are controlled by an improved damage index, which is a function of hysteretic energy dissipation. Pinching of hysteretic loops due to shear cracking and bond slip commonly observed in reinforced concrete structures during cyclic loading is considered in the model by adding a slip lock function to the general hysteretic function.

The smooth hysteretic model is controlled by a small number of structural characteristics (the initial stiffness, the yield force and the post-yield stiffness ratio) along with the parameters of the loop. The polygonal model, on the other hand, is defined by numerous parameters (Valles et al., 1996) which require complex manipulations of the database during inelastic analyses.

In this study, the traditionally displacement-controlled Bouc-Wen model was modified to accommodate a force-controlled algorithm by inverting the rate-independent differential equation for the restoring force. The degradation models were then added making use of a new formulation for damage quantification.

#### 5.3.3.2.2 Original Bouc-Wen Hysteretic Model

The Bouc-Wen model is a hysteretic constitutive law, which has been widely used in recent years in studies of random vibrations of structures. The model can be visualized as a parallel combination of a linear and a nonlinear element (figure 5-8), which relate the generalized forces (or moments) and the generalized displacements (or curvatures):

$$M_i = M_y[\alpha\mu_i + (1-\alpha)Z_i] \tag{5-17}$$

where $\alpha$ is the ratio of the post-yield to the initial elastic stiffness; $Z(\phi)$ is the hysteretic component defined in (5-20) below; $\mu_i$ is the normalized curvature ductility:

$$\mu_i = \frac{\phi_i}{\phi_y} \tag{5-18}$$

where $\phi_i$, $\phi_y$ are the instantaneous and yield curvatures respectively.

Using the generalized force notation, commonly used in literature for the Bouc-Wen model, we can express (5-17) as follows:

$$F = \alpha ku + (1-\alpha)kZ \tag{5-19}$$

in which $F_1 = \alpha ku$ is the force resisted by a linear spring element simulating the post-yield hardening and $F_2 = (1-\alpha)kZ$ is the force resisted by the elastic-ideal-plastic nonlinear spring element (figure 5-8).

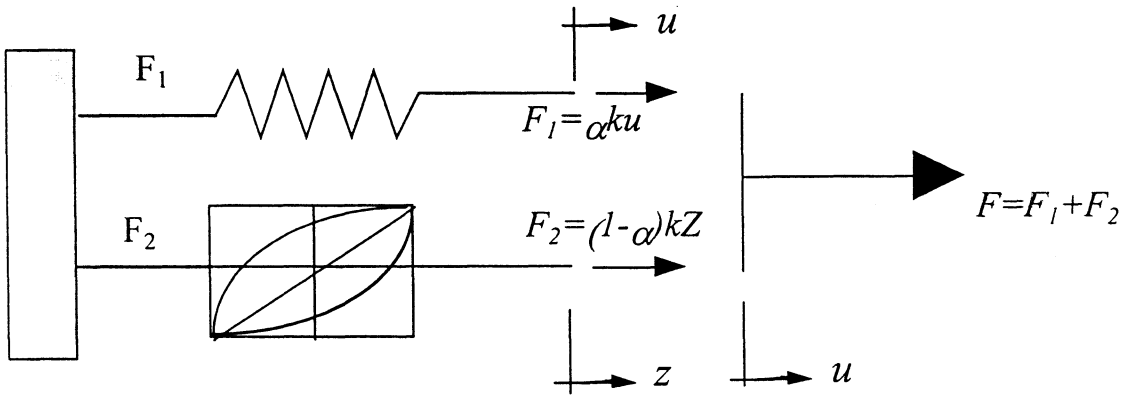


**FIGURE 5-8 Bouc-Wen Hysteretic Model**

The normalized hysteretic component $Z(\phi) \leq 1.0$ is obtained from the differential equation (Madan et al., 1997):

$$dZ_i = d\mu_i \left\{ A - |Z_i|^n \left[ \beta \, \mathrm{sgn}(d\mu_i Z_i) + \gamma \right] \right\} \tag{5-20}$$

where A, $\beta$ and $\gamma$ are constants, which control the shape of the hysteretic loops. Different values of the parameters $\gamma$ and $\beta$ produce different loading and unloading paths. The program defaults ($\gamma = \beta = 0.5$) cause unloading with the initial loading stiffness. The conditions ($\gamma + \beta$) = 1 and A = 1 are discussed later in this report. The exponent in (5-20) governs the transition from the elastic to the plastic state. Small values of *n* lead to a smooth transition, but as *n* increases the transition becomes sharper tending to a perfectly bilinear behavior in the limit ($n \rightarrow \infty$). More information on the subject can be found in Constantinou and Adnane (1987).

#### 5.3.3.2.3 Force-Controlled Hysteretic Model

The original displacement-controlled Bouc-Wen model can be modified to obtain a force-controlled hysteretic behavior. The basic moment-curvature relation in (5-17) can be rewritten as:

$$\phi_i = \frac{\phi_y}{\alpha}\left[\frac{M_i}{M_y} - (1-\alpha)Z_i\right] \tag{5-21}$$

where the curvature ductility $\mu$ was replaced by the actual curvatures.

The derivative of (5-17) produces information on the instantaneous flexural rigidity $(EI)_T$:

$$EI_T = \left(\frac{dM}{d\phi}\right) = \alpha \cdot \frac{M_y}{\phi_y} + (1-\alpha) \cdot \left(\frac{dZ}{d\phi}\right) \cdot M_y \tag{5-22}$$

in which the derivative $dZ/d\phi$ can be obtained by rewriting (5-20):

$$\left(\frac{dZ}{d\phi}\right) = \frac{1}{\phi_y} \cdot \left\{A - |Z|^n \cdot [\beta \cdot \mathrm{sgn}(d\phi \cdot Z) + \gamma]\right\} \tag{5-23}$$

The increment of the hysteretic parameter Z can be expressed from (5-23) as:

$$dZ = \frac{1}{1-\alpha} \cdot \left(\frac{dM}{M_y} - \alpha \cdot \frac{d\phi}{\phi_y}\right) \tag{5-24}$$

Using the formulations above, the increment of curvature $d\phi$, the curvature $\phi$, the increment of the hysteretic parameter $dZ(\phi)$ and the hysteretic parameter $Z(\phi)$ can be evaluated at the end of the current step of computation knowing only the curvature and the hysteretic parameter at the beginning of the step, and the increment of moment dM over the current time interval.

It is initially assumed that the hysteretic parameter $Z_{i+1}$ at the end of the $(i+1)^{st}$ step of computation is equal to $Z_i$, the value at the beginning of the step. The calculation of the unknown response quantities at the end of the step follows the sequence outlined next, which includes one-step iteration:

1) Derivative of the hysteretic function at the end of the current step:

$$\left(\frac{dZ}{d\phi}\right)_{i+1} = \frac{1}{\phi_y} \cdot \left\{A - |Z_i|^n \cdot (\beta \cdot \text{sgn}(d\phi_i \cdot Z_i) + \gamma)\right\} \tag{5-25}$$

2) Instantaneous flexural rigidity at the end of the current step:

$$\left(\frac{dM}{d\phi}\right)_{i+1} = \alpha \frac{M_y}{\phi_y} + (1-\alpha)\left(\frac{dZ}{d\phi}\right)_{i+1} M_y \tag{5-26}$$

3) Increment of curvature over the current step $\phi_{i+1}$:

$$d\phi_{i+1} = \frac{dM_{i+1}}{\left(\frac{dM}{d\phi}\right)_{i+1}} \tag{5-27}$$

4) Increment of the hysteretic function Z over the current step:

$$dZ_{i+1} = \frac{1}{1-\alpha} \cdot \left(\frac{dM_{i+1}}{M_y} - \alpha \cdot \frac{d\phi_{i+1}}{\phi_y}\right) \tag{5-28}$$

5) Hysteretic function at the end of the current step $Z_{i+1}$:

$$Z_{i+1} = Z_i + dZ_{i+1} \tag{5-29}$$

6) Curvature at the end of the current step $\phi_{i+1}$ (calculated from (5-21)):

$$\phi_{i+1} = \frac{\phi_y}{\alpha}\left[\frac{M_{i+1}}{M_y} - (1-\alpha)Z_{i+1}\right] \tag{5-30}$$

7) The increment of curvature over the current step can be re-calculated:

$$d\phi_{i+1} = \phi_{i+1} - \phi_i \tag{5-31}$$

8) Knowing $\phi_i$, $\phi_{i+1}$ and $Z_i$, the hysteretic parameter at the end of the current step $Z_{i+1}$ is obtained by solving (5-20) numerically using a semi-implicit Runge-Kutta method.

9) The final value of $Z_{i+1}$ can be compared with the value obtained in step 5. If the difference is large, the computation might be repeated from step 6 on.

#### 5.3.3.2.4 Slip-Lock Model

Pinching of hysteretic loops due to shear cracking and bond slip of the reinforcement is commonly observed in reinforced concrete structures during cyclic loading. Baber and Noori (1985) proposed a general degradation model combining the hysteretic element discussed above with a time-dependent non-linear hardening spring, which acts as a slip-lock element. To obtain a rate-independent model, Madan et al., (1997) modified the formulation by combining a slip-lock spring element in series with the basic hysteretic element (figure 5-9). The normalized deformation $\mu$ of the resulting element is the sum of the deformations of the basic smooth element $\mu_1$ and that of the slip lock element $\mu_2$:

$$d\mu = d\mu_1 + d\mu_2 \tag{5-32}$$

in which $d\mu_1$ and $d\mu_2$ are the incremental normalized curvatures of the hysteretic spring element and slip-lock element, respectively.

The hysteretic function $Z(\phi)$ is already related to the deformation contribution of the basic element in (5-20):

$$dZ = d\mu_1 \left\{ A - |Z|^n \left[ \beta \, \mathrm{sgn}(d\mu_1 Z) + \gamma \right] \right\} \tag{5-33}$$

Madan et al., (1997) proposed the following formulation for the deformation of the slip-lock element:

$$d\mu_2 = a \, f(Z) \, dZ \tag{5-34}$$

The function $f(Z)$ is defined by the expression (figure 5-9):

$$f(Z) = \exp\left[ -\frac{(Z - \bar{Z})^2}{Z_s^{\,2}} \right] \tag{5-35}$$

in which, $Z_s$ is the range, symmetric about Z = 0, where the slip occurs. The parameter is assumed independent of the response history. A non-zero value of the parameter $\bar{Z}$ will shift the effective slip region so that it is symmetric about $Z = \bar{Z}$. The "slip length" parameter a in (5-34) is function of the maximum attained deformation (Madan, 1996):

$$a = A_s(\mu^r - 1) \tag{5-36}$$

where $A_s$ is a control parameter which may be linked to the size of crack opening or reinforcement slip or both (Lobo, 1994) and $\mu^r$ is the normalized curvature attained at the load

load reversal prior the current loading cycle. The effects of varying the slip-lock parameters are illustrated in figure 5-10.

Rewriting (5-33) in terms of dZ and then substituting (5-33) and (5-34) into (5-32) yields:

$$\frac{dZ}{d\mu} = \frac{A - |Z|^n [\beta\, \mathrm{sgn}(d\mu \cdot Z) + \gamma]}{1 + a \cdot \exp\left[ -\frac{(Z - \bar{Z})^2}{Z_s^{\,2}} \right] \cdot \{A - |Z|^n [\beta\, \mathrm{sgn}(d\mu \cdot Z) - \gamma]\}} \tag{5-37}$$

with the assumption that $\mathrm{sgn}(d\mu) = \mathrm{sgn}(d\mu_1)$.

Equations (5-17) and (5-37) render a model for pinched hysteretic behavior.

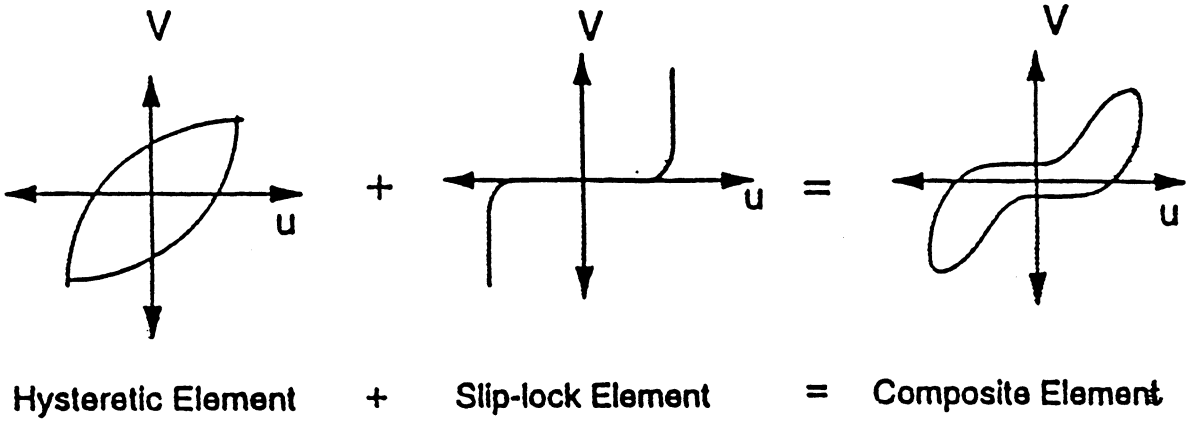


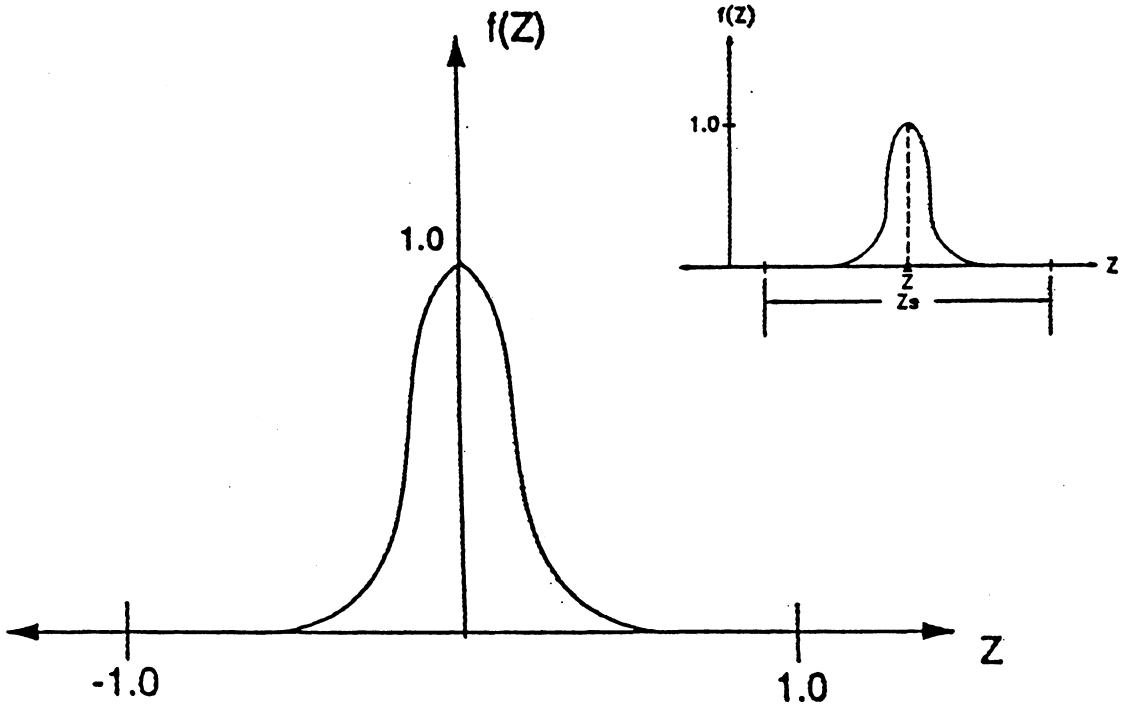


FIGURE 5-9 Slip-Lock Model

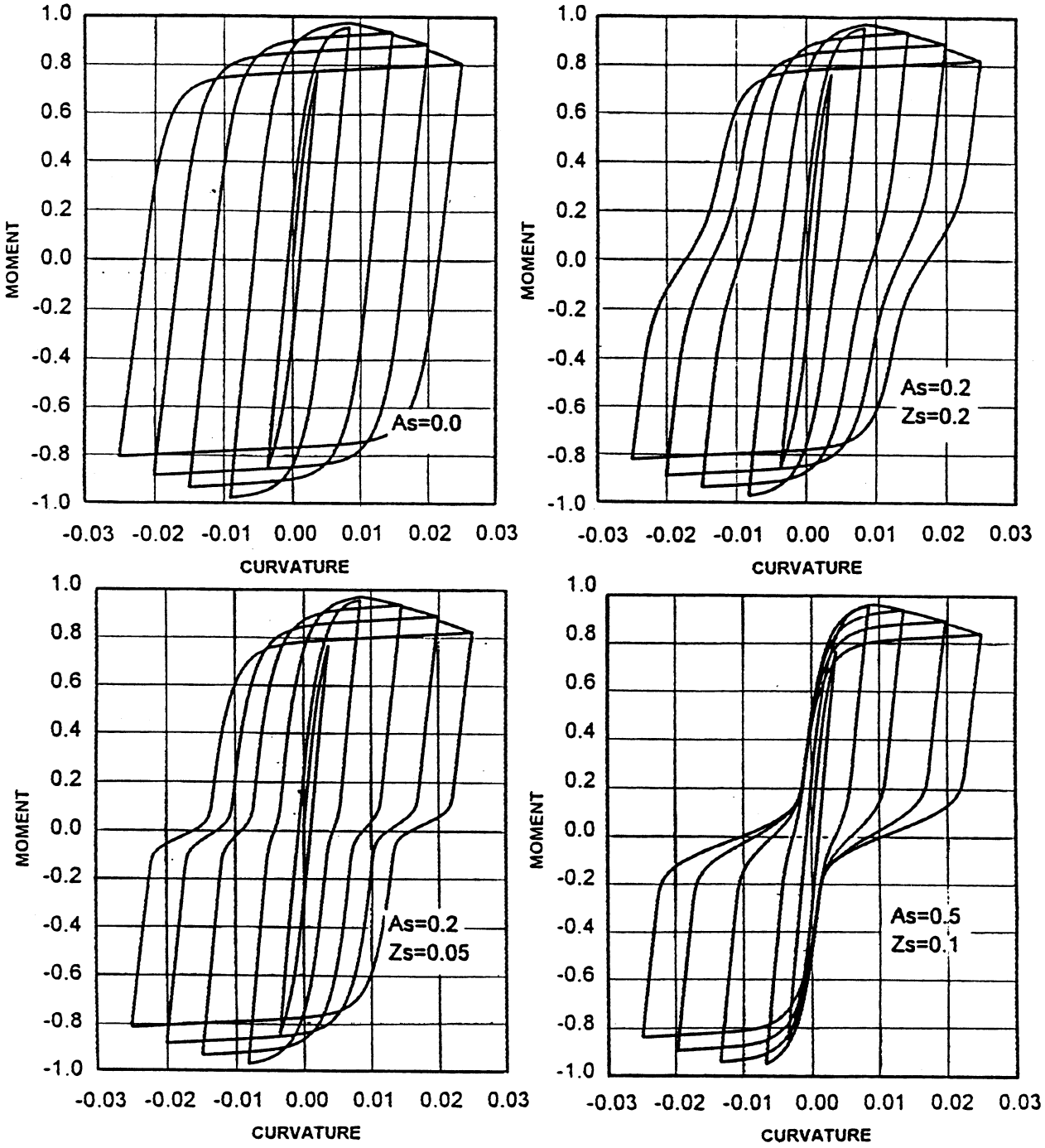


**FIGURE 5-10 Effects of Varying the Control Parameters of the Slip-Lock Model**

#### 5.3.3.2.5 Stiffness Degradation Model

Loss of stiffness is commonly observed in reinforced concrete and masonry infill members undergoing repeated inelastic deformations. The stiffness deterioration is incorporated directly in the hysteretic model, described so far, by using a control parameter. Equation (5-37) can be modified to as follows:

$$\frac{dZ}{d\mu} = \frac{A - |Z|^n [\beta \, sgn(d\mu \cdot Z) + \gamma]}{\eta \left( 1 + a \cdot \exp\left[ - \frac{(Z - \bar{Z})^2}{Z_s^{\,2}} \right] \cdot \{ A - |Z|^n [\beta \, sgn(d\mu \cdot Z) - \gamma] \} \right)} \tag{5-38}$$

The parameter $\eta$ is defined by the equation (Lobo, 1994):

$$\eta = \frac{S_k + 1 + \alpha(\mu - 1)}{S_k + \mu} \tag{5-39}$$

where, $S_k$ is a parameter, which represents the rate of stiffness decay as a function of the current normalized deformation $\mu$ using a pivotal method. This model is extensively used by the polygonal hysteretic model in IDARC-2D (Valles et al., 1996). A value of $S_k = 0$ is an origin pivot indicating high decay, while $S_k = \infty$ implies no degradation.

#### 5.3.3.2.6 Strength Deterioration Model

Structural members made of reinforced concrete, or even steel or elastomers, have often exhibited gradual reduction of force capacity when subjected to cyclic loading. The model of hysteresis, developed so far, can be modified to simulate strength deterioration by reducing the yield capacity of the element:

$$M_y^k = s_\beta \cdot M_y^0 \tag{5-40}$$

where, $M_y^k$ is the reduced yield moment for the $k^{th}$ cycle and $M_y^0$ is the yield force of an undamaged member. The factor $s_\beta$ determines the amount of deterioration from the original yield level and depends on the cumulative damage sustained by the element during the response history. The reduction factor $s_\beta$ can be related to a damage index (DI) used to quantify the detrimental effect of the cyclic load:

$$s_\beta = 1 - DI \tag{5-41}$$

The local damage index used in this development is a function of the attained curvature at an end section of a structural member and dissipated cyclic energy:

$$DI = \frac{\mu_{max} - 1}{\mu_c - 1} \cdot \frac{1}{\left(1 - \frac{s_{pl} \int dE_h}{E_{hy}}\right)^{s_{p2}}} \quad , \quad (0 \le DI \le 1.0) \tag{5-42}$$

where, $\mu_{max}$ is maximum deformation achieved throughout the response history and $\mu_c$ is the deformation capacity of the structural member. The parameters $s_{pl}$ and $s_{p2}$ control the rate of strength deterioration (both assumed equal to 1.0 in this development). The integral $\int dE_h$ represents the hysteretic energy dissipated before the start of the current reloading cycle and $E_{hy}$ is the maximum hysteretic energy that can be dissipated by the member in one cycle to failure:

$$E_{hy} = 4 \cdot M_y \cdot \phi_y \cdot (\mu_c - 1) \tag{5-43}$$

To encompass cases of monotonic loading without unloading (and not only cyclic loading), the damage index may also be expressed as:

$$DI = \frac{\mu_{max} - 1}{\mu_c - 1} \cdot \frac{1}{\left[1 - 0.25 s_{p1} \int \left(\frac{M}{M_y}\right) \frac{d\mu}{(\mu_c - 1)}\right]^{s_{p2}}} \qquad (5\text{-}44)$$

When an end section of a member reaches a curvature greater than the maximum curvature achieved in any of the previous cycles of response, the yield force at that end is reduced in accordance with (5-41). In a force-controlled analysis, a correction is needed to maintain equilibrium and avoid numerical instabilities. The lost capacity is applied as an external load at the nodal points of the element and held constant for the remainder of the analysis. Unless there are other members to sustain the released force, the system will fail.

Figures 5-11, 5-12 and 5-13 illustrate schematically and graphically the characteristics of hysteretic model presented so far.

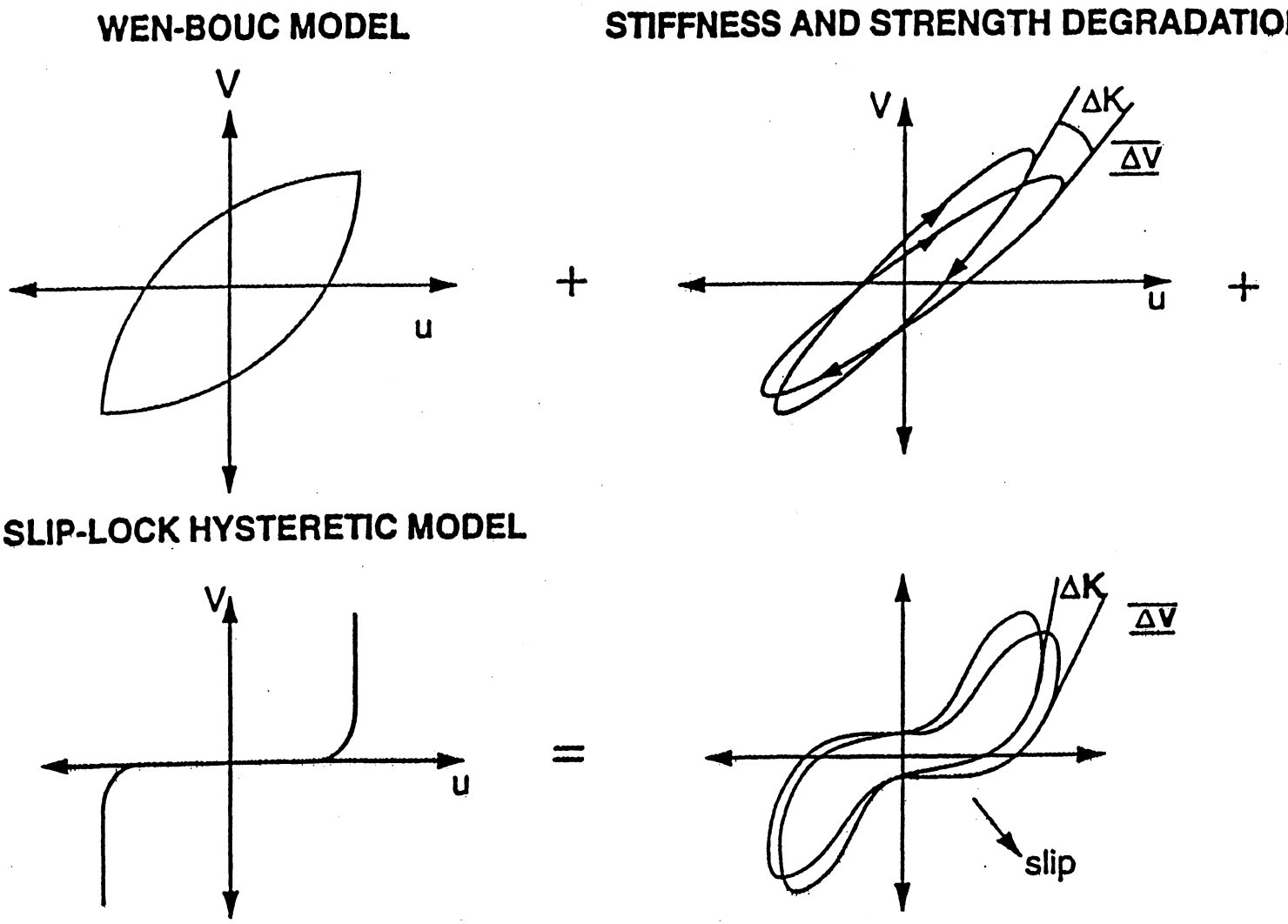


FIGURE 5-11 Integrated Hysteretic Model Capable of Simulating Slip-Lock, Stiffness Degradation and Strength Deterioration Phenomena

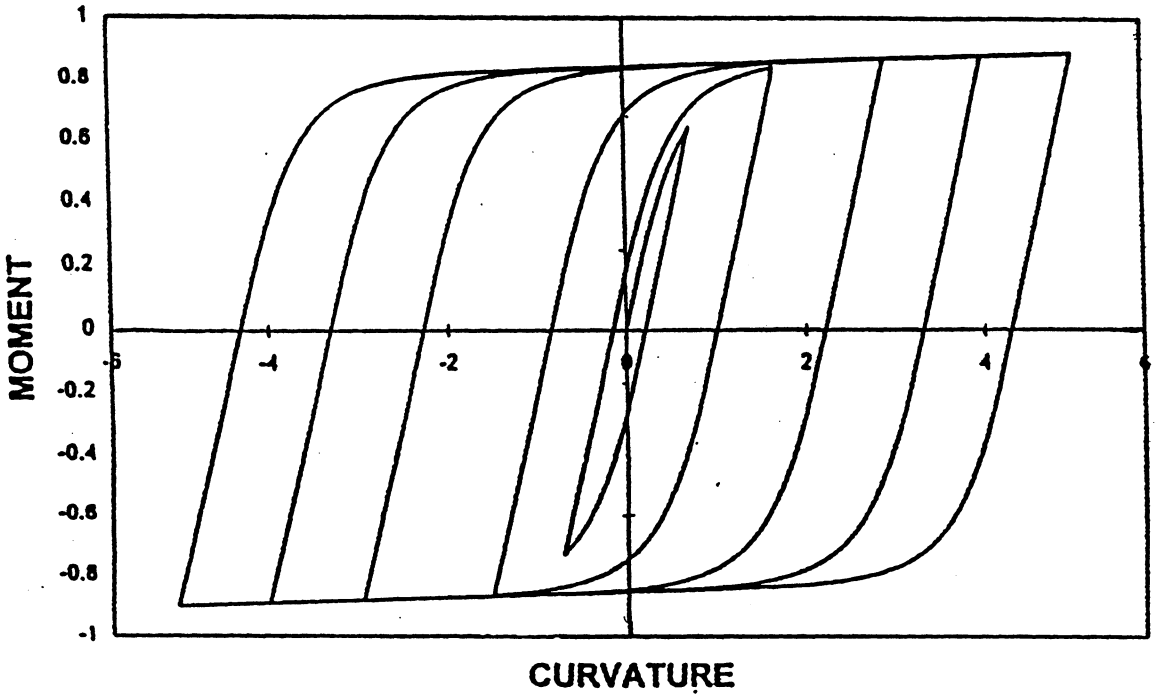


**Fig 3.4. Basic Continuous Hysteretic Model without Strength Degradation**

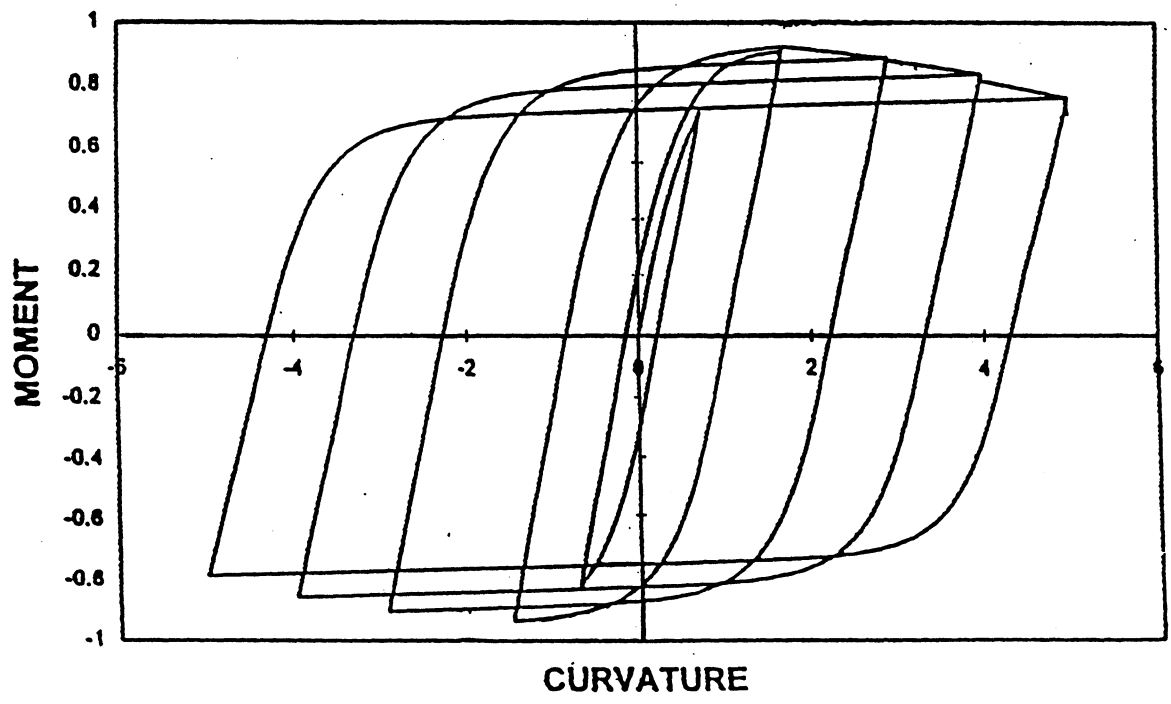


**FIGURE 5-12 Continuous Hysteretic Model: a) without Strength Deterioration, b) with Strength Deterioration**

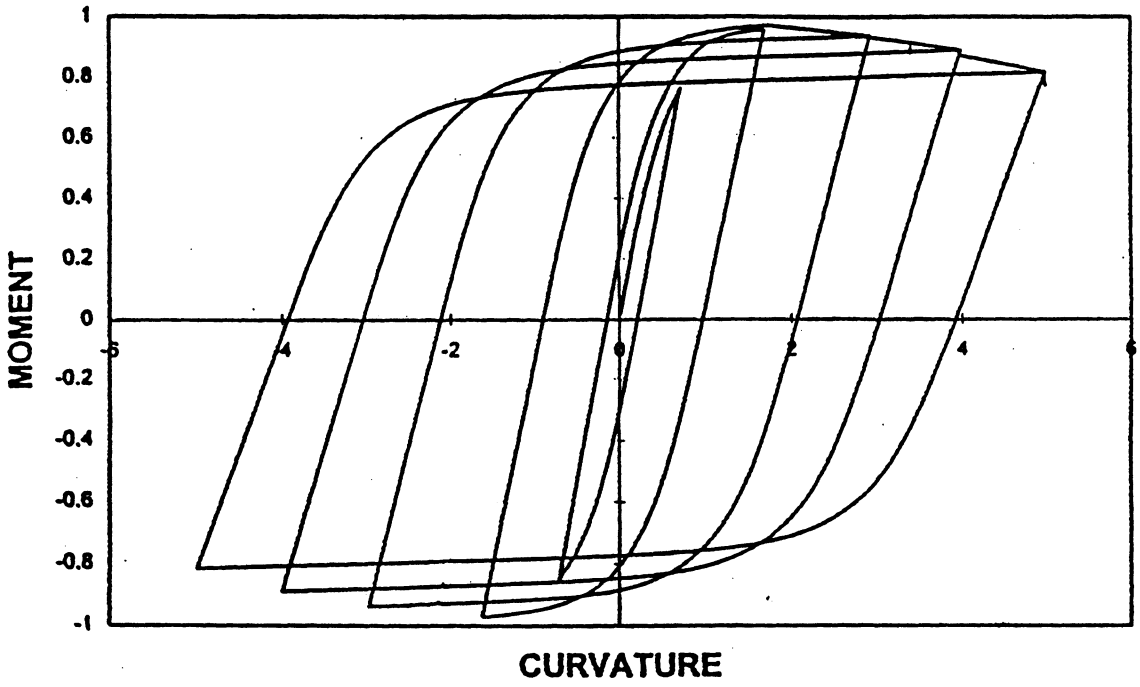


**Fig 3.6. Continuous Hysteretic Model with Strength and Stiffness Degradation**

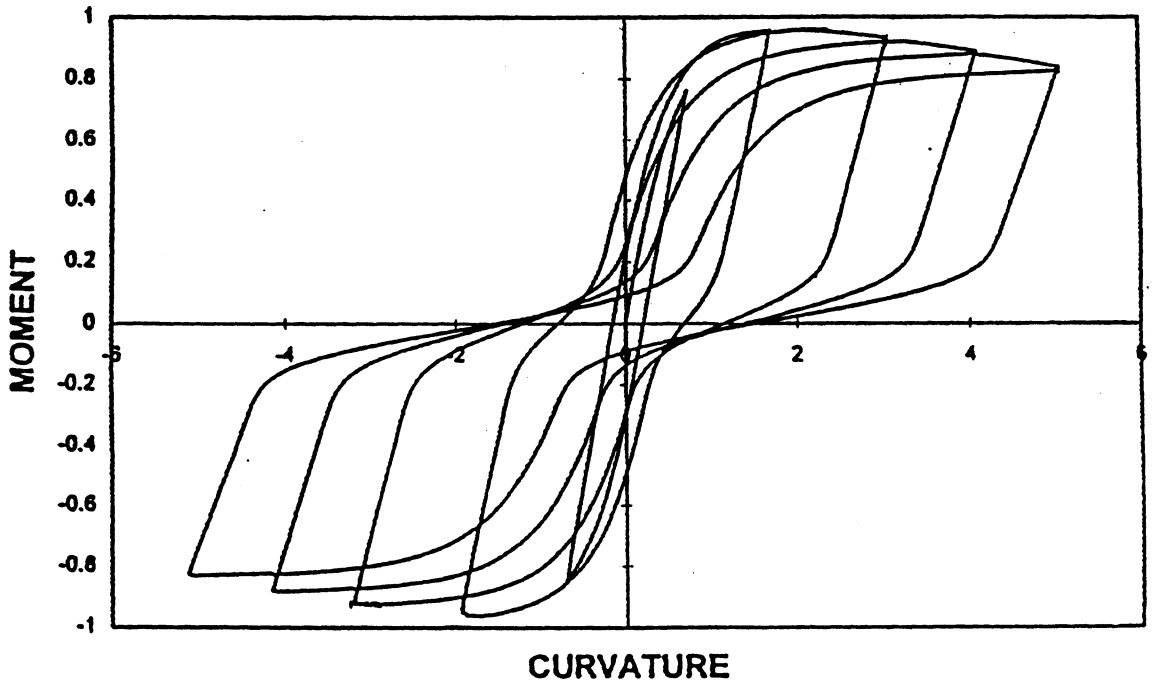


**FIGURE 5-13 Continuous Hysteretic Model: a) with Stiffness Degradation and Strength Deterioration, b) with Stiffness Degradation, Strength Deterioration and Slip-Lock Effects**

## 5.4 Elastomeric Isolator Element

A non-linear element is developed to model the smooth hysteresis of the restoring forces typical of some base isolation devices subjected to cyclic loading. The element type "isolator 1" is a three-dimensional element defined by two nodes with six degrees of freedom each, the yield force, yield displacement, ratio of the post-yielding to the initial elastic stiffness and two parameters controlling the shape of the force-displacement loop (figure 5-14). The local coordinate system is assumed parallel to the global coordinate system. A translation-of-axis option makes possible to transform the set of element degrees of freedom from one location to another and thus effectively redefine the locations of the end nodes (Section 5.9.1). The uniaxial shear force-relative displacement relationship is simulated by a model of hysteresis, originally proposed by Bouc (1967, 1971) and subsequently extended by Wen (1976), with the following governing equation (Constantinou and Adnane, 1987):

$$F = Z F_y \tag{5-45}$$

where $F_y$ is the ultimate restoring force and Z is a dimensionless hysteretic parameter defined by the differential equation:

$$\dot{Z} = A\frac{\dot{U}}{U_y} - |Z|^{\eta}\left[\gamma\,\mathrm{sgn}(\dot{U}Z) + \beta\right]\frac{\dot{U}}{U_y} \qquad \text{or} \qquad \frac{dZ}{dU} = \frac{A - |Z|^{\eta}\left[\gamma\,\mathrm{sgn}(dU\,Z) + \beta\right]}{U_y} \tag{5-46}$$

where:

A, $\eta$, $\gamma$, $\beta$ = Non-dimensional parameters controlling the shape of the hysteretic loop.

U = Relative displacement between top and bottom of the isolator.

$U_y$ = Displacement at yield.

$\mathrm{sgn}(\dot{U}Z) = 1$, if $(\dot{U}Z) > 0$

$\mathrm{sgn}(\dot{U}Z) = 1$, if $(\dot{U}Z) > 0$.

$\mathrm{sgn}(\dot{U}Z) = \mathrm{sgn}(dU\,Z)$.

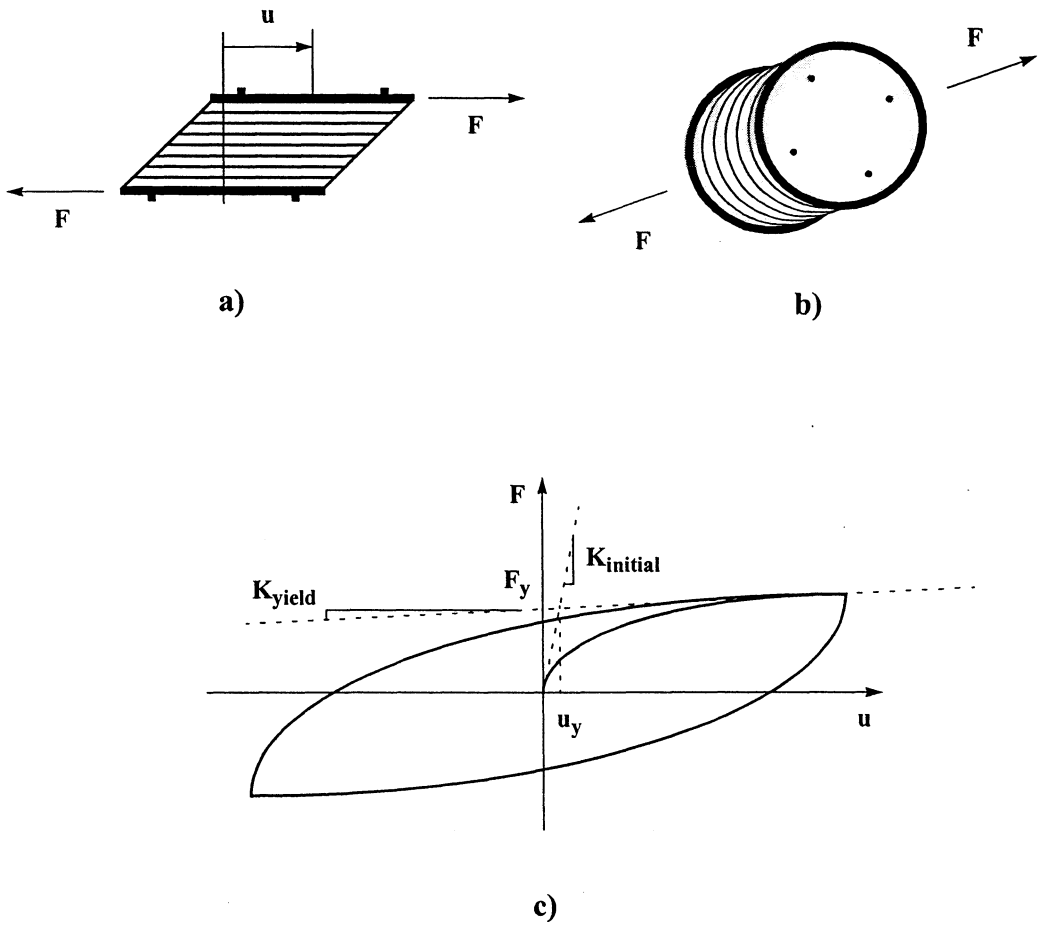


**FIGURE 5-14 Elastomeric Isolator:**
**a) Side View, b) Top View, c) Force-Displacement Relationship**

The maximum value of the hysteretic parameter Z, also termed "non-dimensional reactive force", is obtained by setting $\frac{dZ}{dU}$ equal to 0, after rearranging (5-46) with $\dot{U} > 0$ and $Z > 0$:

$$Z_{max} = \left(\frac{A}{\beta + \gamma}\right)^{\frac{1}{\eta}} \tag{5-47}$$

Strain hardening is introduced in the model by modifying (5-45):

$$F = \alpha \frac{F_y}{U_y} U + (1 - \alpha) F_y Z \tag{5-48}$$

or,

$$F = \alpha K_0 U + (1 - \alpha) F_y Z \tag{5-49}$$

where:

$K_0$ = Initial elastic stiffness.

$\alpha$ = Post-yield to initial stiffness ratio.

In the context of the mathematical model, the yield force $F_y$, yield displacement $U_y$ and stiffness ratio $\alpha$ correspond to the actual physical quantities if A = 1 and $(\gamma + \beta) = 1$. It is evident from (5-47) that for this set of values of A, $\gamma$ and $\beta$, the hysteretic parameter Z is limited to the range $-1 \leq Z \leq 1$. When $\beta = \gamma$ the slope of the unloading branch of the hysteresis loop is equal to the slope of the loading branch or the elastic stiffness. If $\beta > \gamma$, the unloading stiffness is initially higher than the elastic stiffness and the unloading curve is convex (figure 5-14). Alternatively, if $\beta < \gamma$, the unloading slope is initially smaller than the initial stiffness and the unloading curve is concave. Linear elastic behavior is obtained when $\alpha = 1$. The parameter $\eta$ controls the sharpness of transition to the inelastic range. Bilinear hardening or elastoplastic behavior is obtained for large values of $\eta$. In addition, the model exhibits strong rate dependency of the mode of transition into the inelastic range for small values of the parameter. The differential equation can be solved numerically by using an enhanced Runge-Kutta method (Nagarajaiah et al., 1989).

Analytical solution is possible for a limited range of values of $\eta$, the case $\eta = 1$ being the original formulation of the model by Bouc (1967). The solution for $\eta = 2$ is used for defining the hysteretic law of the isolator element in IDARC-BRIDGE and will be presented next. For this purpose equation (5-46) is rewritten as:

$$dU = \frac{dZ\, U_y}{A - Z^2(\gamma\, \mathrm{sgn}(dU\, Z) + \beta)} \tag{5-50}$$

Integrating both sides:

$$U = U_y \int \frac{dZ}{A - Z^2 \gamma\, \mathrm{sgn}(dU\, Z) + \beta} \tag{5-51}$$

It is useful to introduce the following parameters:

$$a = \sqrt{A} \qquad\qquad b = \sqrt{|\gamma\, \mathrm{sgn}(dU\, Z) + \beta|} \tag{5-52}$$

Several different cases should be considered in the solution of (5-51):

A) $\gamma > \beta$:

$$\gamma\, \mathrm{sgn}(dU\, Z) + \beta = b^2\, \mathrm{sgn}(dU\, Z) \tag{5-53}$$

Substitution of (5-52) into (5-51) yields:

$$U = U_y \int \frac{dZ}{a^2 - \mathrm{sgn}(dU\, Z) b^2 Z^2} \tag{5-54}$$

The solution of (5-54) can be derived for the following cases:

1) $\mathrm{sgn}(dU\, Z) > 0$

$$U = U_y \int \frac{dZ}{a^2 - b^2 Z^2} \tag{5-55}$$

Upon integration,

$$U = U_y \frac{1}{2ab} \log \left| \frac{a + bZ}{a - bZ} \right| + c \tag{5-56}$$

Equation (5-56) is simplified further assuming the following possible conditions:

(i) $b^2Z^2 < a^2$

$$U = \frac{U_y}{ab} \operatorname{atanh} \frac{bZ}{a} + c \tag{5-57}$$

$$Z = \frac{a}{b} \tanh\left( \frac{Uab}{U_y} + c \right) \tag{5-58}$$

(ii) $b^2Z^2 > a^2$

$$U = \frac{U_y}{ab} \operatorname{acoth} \frac{bZ}{a} + c \tag{5-59}$$

$$Z = \frac{a}{b} \coth\left( \frac{Uab}{U_y} + c \right) \tag{5-60}$$

2) $\operatorname{sgn}(dUZ) < 0$

A valid solution for case $\operatorname{sgn}(dUZ) < 0$ exists only when $b^2Z^2 < a^2$, since the conditions $\gamma > \beta$ and $b^2Z^2 > a^2$ produce $Z > 1$.

$$U = \frac{U_y}{ab} \operatorname{atan} \frac{bZ}{a} + c \tag{5-61}$$

$$Z = \frac{a}{b} \tan\left( \frac{Uab}{U_y} + c \right) \tag{5-62}$$

The instantaneous stiffness of the isolator can be expressed in terms of the displacement derivative of the hysteretic parameter Z by differentiating (5-49):

$$K = \frac{dF}{dU} = \alpha K_0 + (1-\alpha) F_y \frac{dZ}{dU} \tag{5-63}$$

The term $\frac{dZ}{dU}$ is obtained from (5-58), (5-60) and (5-62):

(i) $\text{sgn}(dU\,Z) = 1$ and $b^2Z^2 < a^2$:

$$\frac{dZ}{dU} = \frac{a^2}{U_y} \text{sech}^2 \frac{Uab}{U_y} \tag{5-64}$$

(ii) $\text{sgn}(dU\,Z) = 1$ and $b^2Z^2 > a^2$:

$$\frac{dZ}{dU} = -\frac{a^2}{U_y} \text{csec h}^2 \frac{Uab}{U_y} \tag{5-65}$$

(iii) $\text{sgn}(dUZ) = -1$ and $b^2Z^2 < a^2$:

$$\frac{dZ}{dU} = \frac{a^2}{U_y} \sec^2\left(\frac{Uab}{U_y}\right) \tag{5-66}$$

To limit the extreme value of Z to the range $-1 \le Z \le 1$, the ratio a/b in (5-58), (5-60) and (5-62) must be equal to 1. One way to achieve this is to fulfil the conditions $A = 1$ and $\gamma + \beta = 1$.

### 5.5 Sliding Isolator Element

The interaction model developed in this study and implemented in IDARC-BRIDGE has the capability to simulate the behavior of sliding isolators to triaxial loading. The horizontal response of these devices is influenced by the variation of the axial force transmitted through the contact interface.

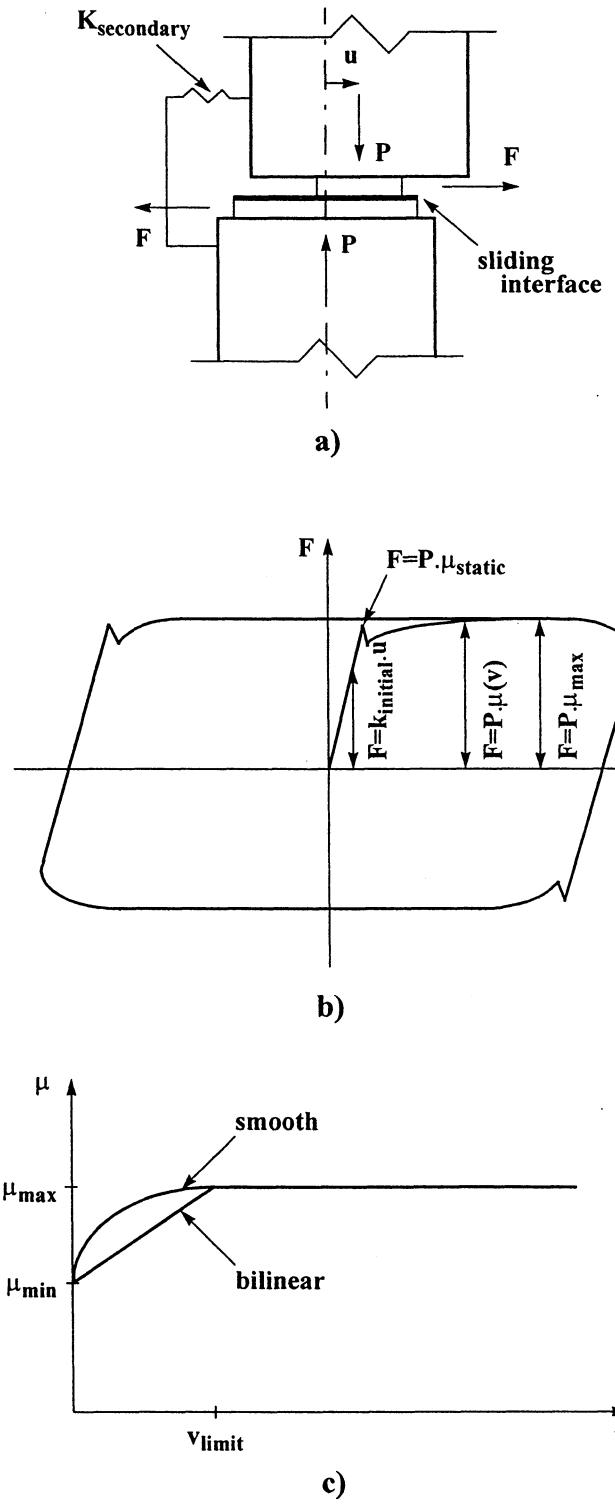


**FIGURE 5-15 Sliding Isolator: a) Side View, b) Sliding Force-Displacement Relationship, c) Dependency of the Coefficient of Friction on Velocity**

The element type "isolator slider" is a three-dimensional element defined by two nodes, the normal force on the isolator under static (dead load) conditions, the initial elastic stiffness, the stiffness of the re-centering spring, the velocity limit above which the coefficient of friction becomes constant and equal to the maximum coefficient of friction, the minimum coefficient of friction, the maximum coefficient of friction and the breakaway coefficient of friction (figure 5-15). The local coordinate system is parallel to the global coordinate system. The element degrees of freedom can be transformed to new nodal locations (without actually redefining the element) by "rigid-arm" transformations (Section 5.9.1).

Friction sliding isolators exhibit two distinct modes of behavior: "stick" and "slip". During the "stick" stage the isolator responds with the initial elastic stiffness $K_{initial}$. After breakaway the isolator slides, the coefficient of friction varying between the minimum $\mu_{min}$ and maximum $\mu_{max}$ coefficient of friction as a function of velocity (figure 5-15). When the velocity of sliding exceeds the threshold value, the coefficient of friction becomes constant and equal to the maximum coefficient of friction.

The force in the isolator F(t), can be expressed as a combination of three components: (i) a static friction component, (ii) a viscous component; and (iii) a "Coulomb" friction component, by the following incremental formulation:

$$\vec{F}(t) = \vec{F}(t - \Delta t) + \Delta\vec{F}(t) \tag{5-67}$$

$$\Delta\vec{F}(t) = k_j \Delta\vec{U}(t) + c_j \Delta\dot{\vec{U}}(t) + \mu_j \Delta N(t)\vec{i}(t) + s_j \left|\vec{F}(t - \Delta t)\right| \Delta\vec{i}(t) \tag{5-68}$$

where:

j = Indicator of the mode of response.

$\Delta\vec{U}(t)$ = Increment of displacement in the plane of sliding.

$\Delta\dot{\vec{U}}(t)$ = Increment of velocity.

$\Delta N(t)$ = Increment of the axial load.

$\vec{i}(t) = \frac{\dot{\vec{U}}(t)}{\left|\dot{\vec{U}}(t)\right|}$ = Sliding direction vector.

$s_j$ = Indicator for biaxial interaction effects in the sliding mode.

$\Delta\vec{i} = \vec{i}_{k+1} - \vec{i}_k$ = Increment of the sliding direction vector over the current step of computation.

The parameters of the model $k_j$, $c_j$, $\mu_j$ and $s_j$ take on the following values depending on the mode of response:

1) "Stick" phase: $\left|\vec{F}(t)\right| \le \mu_{static} N(t)$

$$\begin{aligned} j &= 1 \\ k_1 &= K_{initial} \\ c_1 &= 0 \\ \mu_1 &= 0 \\ s_1 &= 0 \end{aligned} \qquad (5\text{-}69)$$

where:

$\mu_{static}$ = Breakaway coefficient of friction.

N(t) = Total force normal to the sliding surface.

2) Transition "slip" phase $\mu_{min} N(t) \le \left|\vec{F}(t)\right| \le \mu_{max} N(t)$ and $\left|\dot{\vec{U}}(t)\right| \le \dot{U}_{limit}$

$$\begin{aligned} j &= 2 \\ k_2 &= 0 \\ c_2 &= c_{eq}(t) \\ \mu_2 &= \mu_{min} \\ s_2 &= 1 \end{aligned} \qquad (5\text{-}70)$$

where:

$\dot{U}_{limit}$ = Velocity threshold which, depending on the properties of the material of the friction interface, typically takes on values in the range 2-4 in/sec.

$c_{eq}(t) = \frac{N(t)(\mu_{max} - \mu_{min})}{\dot{U}_{limit}}$ = Equivalent damping coefficient.

3) "Slip" phase $\left|\vec{F}(t)\right| = \mu_{max} N(t)$ and $\left|\dot{\vec{U}}(t)\right| > \dot{U}_{limit}$

$$\begin{aligned} j &= 3 \\ k_3 &= 0 \\ c_3 &= 0 \\ \mu_3 &= \mu_{max} \\ s_3 &= 1 \end{aligned} \qquad (5\text{-}71)$$

When the restoring force $\left|\vec{F}(t)\right|$ drops below $\mu_{min} N(t)$ the system returns to the first stage.

## 5.6 Spring Element

The element type "elastic foundation" is a three-dimensional spring element defined by two nodes with six degrees of freedom each and twelve spring constants (figure 5-16). The element orientation is determined by the node locations. An additional rotation-of-axis option allows rotation of the local coordinate system about the longitudinal axis of the element. Furthermore, a translation-of-axis option makes possible to transform the set of element degrees of freedom from one location to another and thus effectively redefine the locations of the end nodes (Section 5.9.1). The spring constants enter directly the element stiffness matrix (figure 5-17). Interaction of degrees of freedom is considered if the corresponding cross stiffness coefficients are provided by the user. These features make the element applicable in a variety of situations, including simplified, yet rigorous enough for most applications, modeling of bridge bearings and shear keys, soil-structure interaction at deep and shallow foundations and abutments. An upgrade is currently under way which will allow response dependency of terms of the element stiffness matrix by use of the Bouc-Wen smooth hysteretic model.

The spring element and the beam element end springs discussed later in section 4 and are somewhat similar. The differences between the two cases are: (i) The end springs can be connected only to a single beam-column member, while the spring element can be connected to a joint of framing of several members. (ii) Definition of a spring element requires an additional

global node - a drawback for the addition of new degrees of freedom, on one hand, but a post-processing convenience, on the other. For example, if the displacements of the bridge substructure relative to the surrounding soil are of interest, spring elements can be defined between the foundation and the ground to obtain these response quantities. (iii) In the case of a mass or force acting on an internal node of a beam-column element (see section 4), the element-end-spring technique cannot be applied for deriving the stiffness matrix incorporating the end flexibility effect since the formulation assumes no masses or forces acting on the internal node.

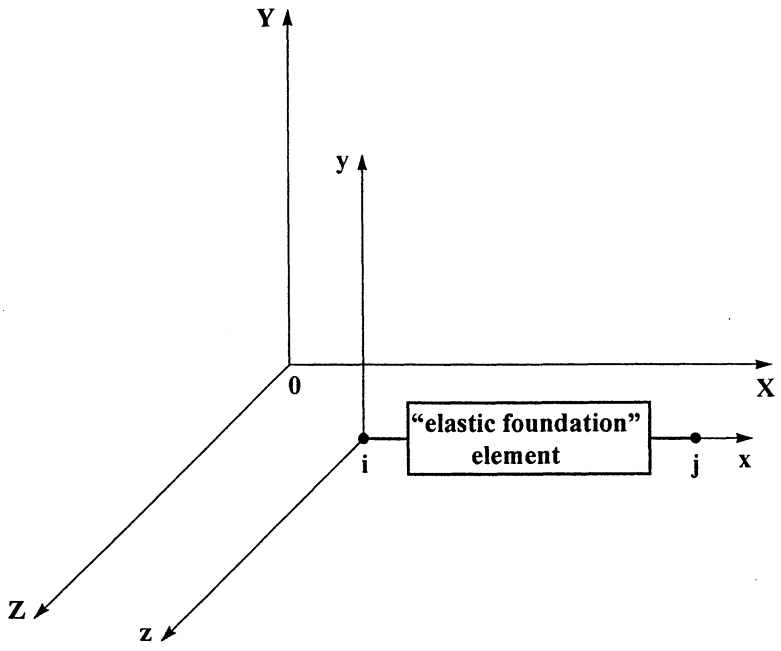


a)

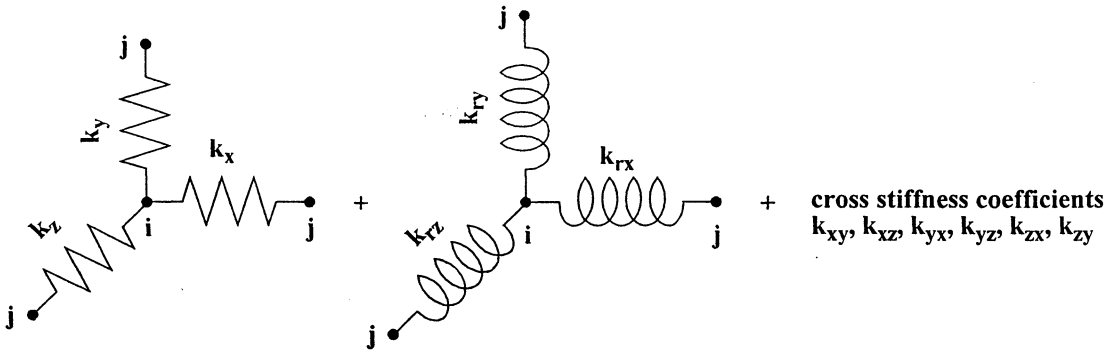


**Note: All stiffness coefficients are for member-oriented axes.**

b)

**FIGURE 5-16 Spring Element:**
**a) Local Coordinate System, b) Stiffness Coefficients**

$$[K_e]=\begin{bmatrix}
k_x & 0 & 0 & 0 & k_x kr_y & k_x kr_z & -k_x & 0 & 0 & 0 & -k_x kr_y & -k_x kr_z \\
 & k_y & 0 & k_y kr_x & 0 & k_y kr_z & 0 & -k_y & 0 & -k_y kr_x & 0 & k_y kr_z \\
 & & k_z & k_z kr_x & -k_z kr_y & 0 & 0 & 0 & -k_z & -k_z kr_x & -k_z kr_y & 0 \\
 & & & kr_x & 0 & 0 & 0 & 0 & 0 & -kr_x & 0 & 0 \\
 & & & & kr_y & 0 & 0 & 0 & 0 & 0 & -kr_y & 0 \\
 & & & & & kr_z & 0 & 0 & 0 & 0 & 0 & -kr_z \\
 & & & & & & k_x & 0 & 0 & 0 & k_x kr_y & k_x kr_z \\
 & & & & & & & k_y & 0 & k_y kr_x & 0 & k_y kr_z \\
 & & \text{symm.} & & & & & & k_z & k_z kr_x & -k_z kr_y & 0 \\
 & & & & & & & & & kr_x & 0 & 0 \\
 & & & & & & & & & & kr_y & 0 \\
 & & & & & & & & & & & kr_z
\end{bmatrix}$$

**FIGURE 5-17 Stiffness Matrix of Spring Element**

## 5.7 Expansion Joint Element

A non-linear element with tension and compression gaps, hysteretic behavior in tension and elastic stiffening behavior in compression is developed to model the complex interaction and force transfer in a bridge expansion joint. Figure 5-18a shows a typical hinge detail with gap of size $t_{gap}$ before the restrainer unit is activated and gap of size $c_{gap}$ before the sort material between the end diaphragm of the deck and the abutment is compressed. It is assumed that no reactions are generated at the ends of the hinge during travel from $-c_{gap}$ to $+t_{gap}$. Upon closing the compression gap the expansion joint stiffens until finally the deck and abutment collide. This behavior can be approximated by the bilinear elastic force-displacement relationship in figure 5-18b. In tension, the restrainer unit yields after the tension gap is closed and the tension gap increases with each inelastic excursion as the hysteresis progresses. The element type "bilinear gap", developed to model the behavior of a tributary section of an expansion joint, is a uniaxial one-dimensional element defined by two nodes with three translational degrees of freedom each, compression gap, tension gap, initial compression stiffness, initial tension stiffness, displacement at contact, displacement at yield, stiffness of contact and post-yielding stiffness. The rotation of the local coordinate system is determined by the location of the end nodes. This feature is particularly useful when dealing with skewed expansion joints or expansion joints in horizontally curved or inclined bridges. In addition, the line of action can be translated away from the deck centerline by rigid body transformations (Section 5.9.1). Several elements of this kind, often in parallel combination with isolators, are typically needed to properly model the force transfer along the entire width of a bridge expansion joint.

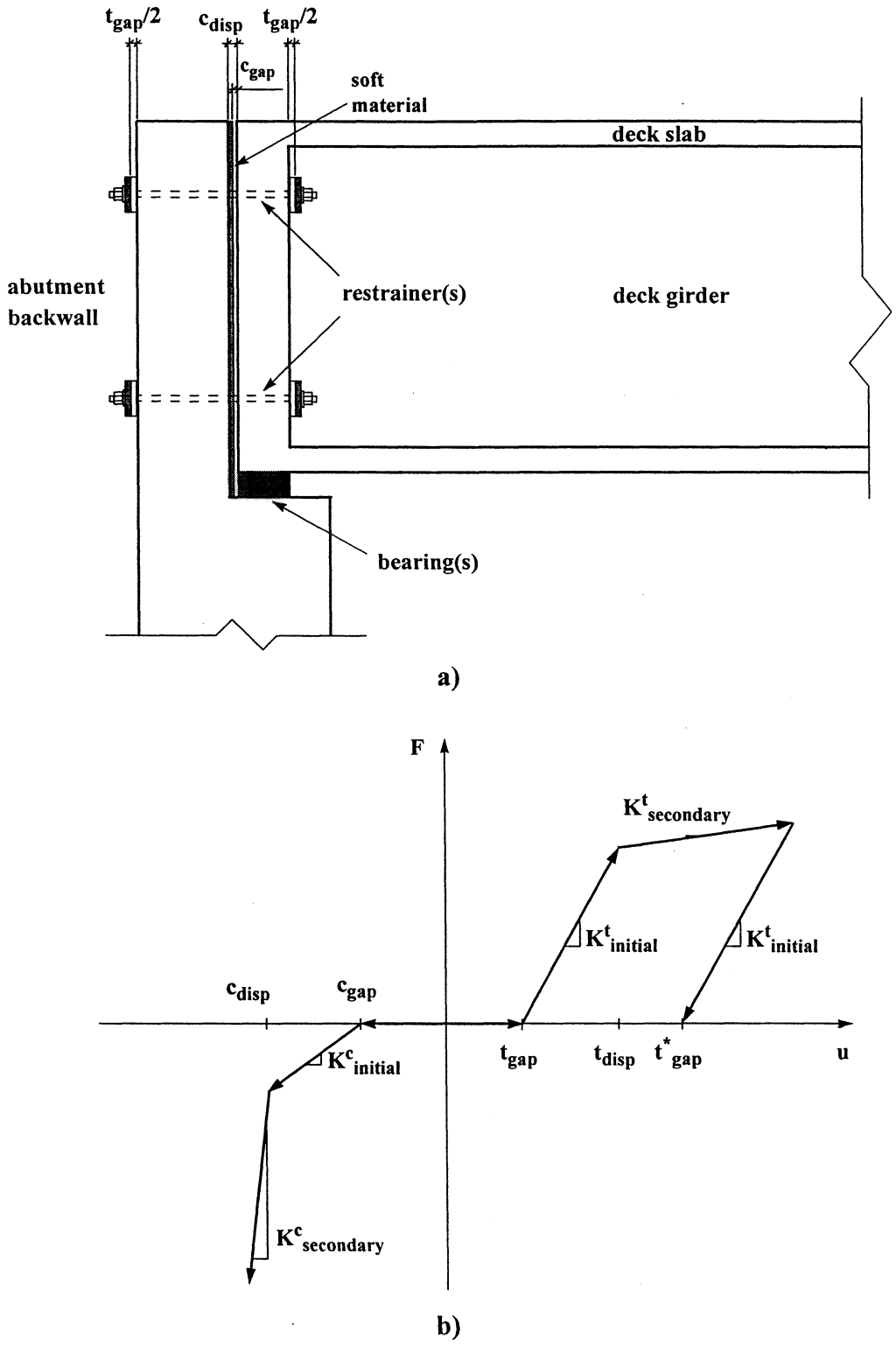


**FIGURE 5-18 Expansion Joint Element: a) Typical Abutment Expansion Joint b) Force-Displacement Relationship**

## 5.8 Damping Element

Elements with damping properties (such as metallic, fluid, viscoelastic, viscous fluid, tuned mass and tuned liquid dampers, as well as, some isolation devices) contribute to the global damping matrix in the same manner individual elements provide a portion of the system stiffness. The element type "linear damper" is a uniaxial three-dimensional element defined by two nodes with six degrees of freedom at each node and twelve damping constants (figure 5-19). The direction of the damper is determined by the node locations. The orientation in space can be elaborated further by specifying the rotation of the local coordinate system about the longitudinal axis of the element. Additionally, a translation-of-axis option allows transformations of the element nodal degrees of freedom from one location to another (Section 5.9.1). The damping constants, including those relating interacting degrees of freedom, are provided by the user and enter directly the element matrix (figure 5-20). The element has utility in modeling not only mechanical damping devices, but also in uncomplicated approximations of radiation damping effects in soil-structure interaction. A more versatile version, capable of representing nonlinear force-velocity relationships with a smooth hysteretic model, is planned for future development.

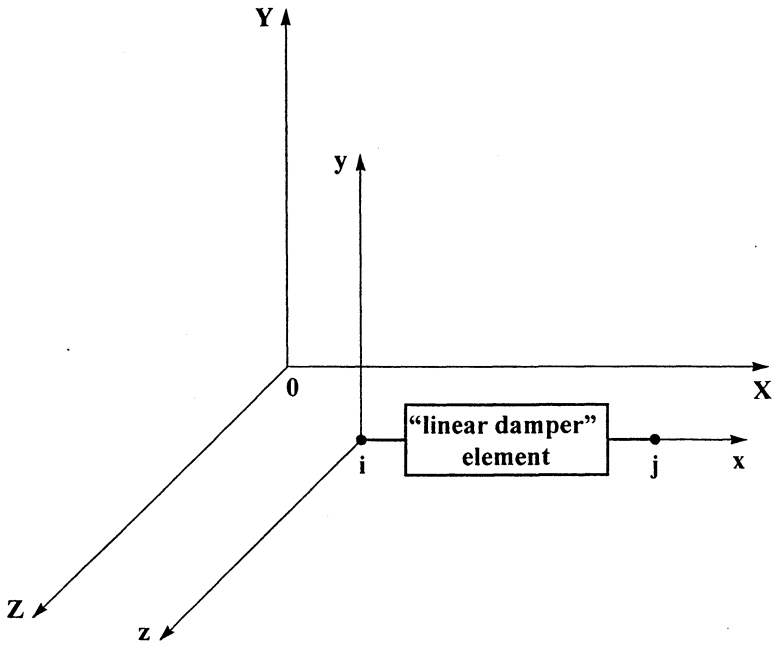


a)

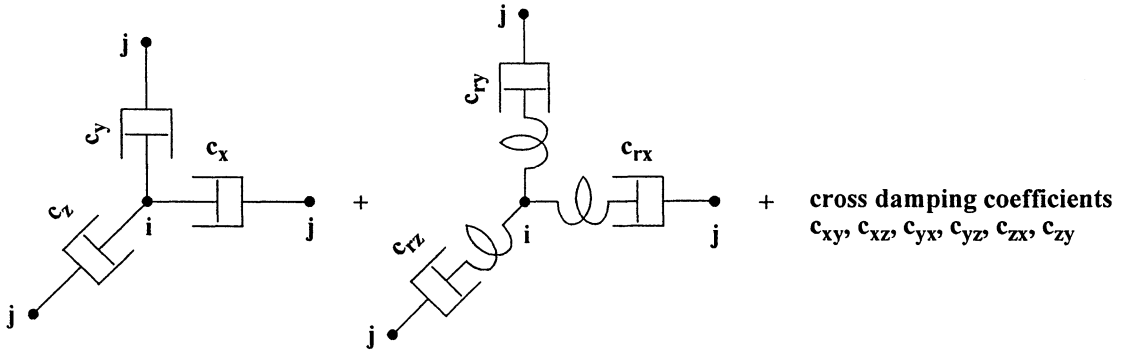


Note: All damping coefficients are for member-oriented axes.

b)

**FIGURE 5-19 Damper Element:**
**a) Local Coordinate System, b) Damping Coefficients**

$$[C_e]=\begin{bmatrix}
c_x & 0 & 0 & 0 & c_x cr_y & c_x cr_z & -c_x & 0 & 0 & 0 & -c_x cr_y & -c_x cr_z \\
 & c_y & 0 & c_y cr_x & 0 & c_y cr_z & 0 & -c_y & 0 & -c_y cr_x & 0 & c_y cr_z \\
 & & c_z & c_z cr_x & -c_z cr_y & 0 & 0 & 0 & -c_z & -c_z cr_x & -c_z cr_y & 0 \\
 & & & cr_x & 0 & 0 & 0 & 0 & 0 & -cr_x & 0 & 0 \\
 & & & & cr_y & 0 & 0 & 0 & 0 & 0 & -cr_y & 0 \\
 & & & & & cr_z & 0 & 0 & 0 & 0 & 0 & -cr_z \\
 & & & & & & c_x & 0 & 0 & 0 & c_x cr_y & c_x cr_z \\
 & & & & & & & c_y & 0 & c_y cr_x & 0 & c_y cr_z \\
 & & \text{symm.} & & & & & & c_z & c_z cr_x & -c_z cr_y & 0 \\
 & & & & & & & & & cr_x & 0 & 0 \\
 & & & & & & & & & & cr_y & 0 \\
 & & & & & & & & & & & cr_z
\end{bmatrix}$$

**FIGURE 5-20 Damping Matrix of Damper Element**

## 5.9 Modeling of Connections

Connections between bridge components may be complicated and difficult to model accurately. Representation of some essentially rigid zones and offsets, in particular, may require many nodes and beam-column elements. IDARC-BRIDGE offers several tools for modeling connection details: (i) rigid body transformations, (ii) element end springs and (iii) degree-of-freedom releases. The main benefit is reduction of the size of the problem by eliminating redundant nodes or degrees of freedom along with influence coefficients in the global structural matrices associated with them.

### 5.9.1 Rigid arms

Numerous nodes and elements would be required to model realistically a typical deck-cap beam connection detail such as that shown in figure 5-21a. The deck can be modeled using a single beam element ("elastic 3d beam" or "hysteretic 3d beam" in the program) with "equivalent" properties. In contrast, it may be inappropriate to lump the bearings supporting the bridge girders into a single isolator element ("isolator 1" or "isolator slider") at the deck centerline. The technique described below utilizes a rigid zone transformation, based on the premise of infinite in-plane rigidity of the deck. The displacements (rotations) of degrees of freedom used for describing of the load-deformation behavior of each of the isolator elements in their actual locations are obtained from the displacements (rotations) of degrees of freedom of the nodes used for defining these elements in the structural model and, thus, participate in the global solution. The displacement-dependent damping and stiffness matrices of the isolator elements are modified in accordance with the hysteretic rule and then transferred back to the degrees of freedom used in the analysis. The flexibility of the girder web to transverse translation of the bridge deck can be modeled by element end springs. In this manner, the entire deck-cap beam connection detail is modeled using only four nodes and three elements (figure 5-21c).

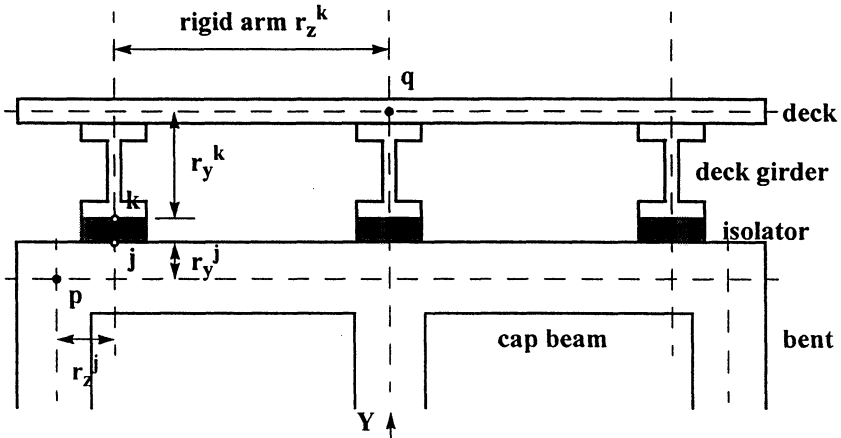


Nodes "p" and "q" are used for the FE discretization of the structure and, thus, for defining the isolator element. Nodes "j" and "k" describe the true position of the element and its force-displacement relation but they do not participate directly in the solution.

a)

**14-Node Representation in a Typical FEM Analysis**

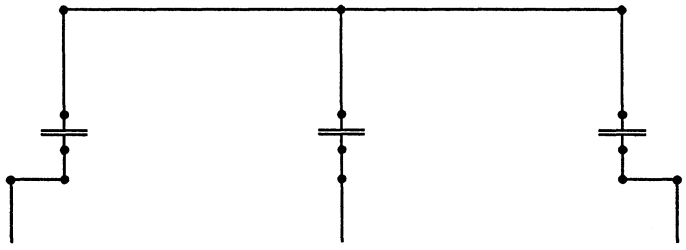

b)

**4-Node Representation Using Rigid BodyTransformations and Element End Springs**

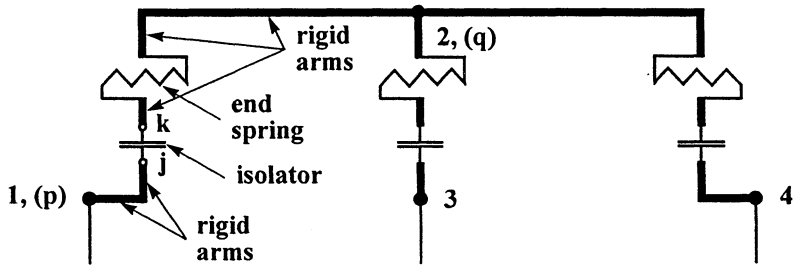


c)

**FIGURE 5-21 Typical Deck-Bent Connection:**
**a) Section, b) Typical Modeling, c) Modeling with Rigid Arms and End Springs**

In summary, the isolator element stiffness matrix is created with respect to the actual nodes and then transformed to the theoretical nodes. Following the solution of the global system, the displacements of the actual nodes (and subsequently, the element end forces) can be found using an inverse rigid body transformation.

The transformation of an action (force or moment) from node "j" to node "p" is schematically shown in figure 5-22.

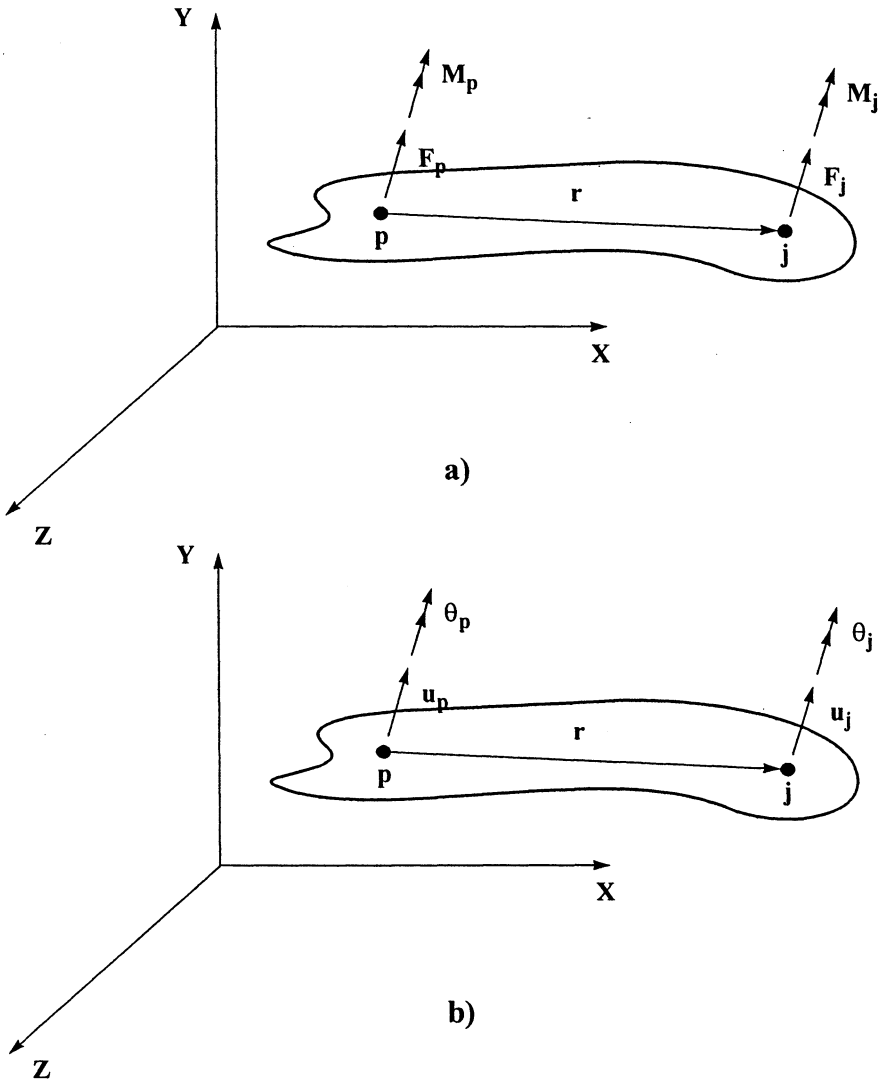


**FIGURE 5-22 Rigid Body Transformations of : a) Actions, b) Deformations**

The actions at node "p" can be expressed in terms of the actions at node "j":

$$\{A_p\} = \begin{Bmatrix} \{F_j\} \\ [c_{pj}]\{F_j\} + \{M_j\} \end{Bmatrix} \tag{5-72}$$

where:

$$\{A_p\} = \begin{Bmatrix} \{F_p\} \\ \{M_p\} \end{Bmatrix} \qquad [c_{pj}]\{F_j\} = \begin{bmatrix} 0 & -z_{pj} & y_{pj} \\ z_{pj} & 0 & -x_{pj} \\ -y_{pj} & x_{pj} & 0 \end{bmatrix} \begin{Bmatrix} F_j^x \\ F_j^y \\ F_j^z \end{Bmatrix} \qquad \{A_j\} = \begin{Bmatrix} \{F_j\} \\ \{M_j\} \end{Bmatrix}$$

$x_{pj}$, $y_{pj}$, $z_{pj}$ = Components of vector $r_{pj}$ from node "p" to node "j".

The relationship expressed by (5-72) can be written as:

$$\{A_p\} = [T_{pj}]\{A_j\} \tag{5-73}$$

where:

$$[T_{pj}] = \begin{bmatrix} [I_3] & [0] \\ [c_{pj}] & [I_3] \end{bmatrix} = \text{Transformation matrix}$$

$[I_3]$ = Identity matrix of size 3x3.

The displacements of nodes "p" and "j" can be related by the equation:

$$\{D_j\} = \begin{Bmatrix} \{u_p\} - [c_{pj}]\{\theta_j\} \\ \{\theta_p\} \end{Bmatrix} \tag{5-74}$$

where,

$$\{D_p\} = \begin{Bmatrix} \{u_p\} \\ \{\theta_p\} \end{Bmatrix} \qquad -[c_{pj}]\{\theta_j\} = \begin{bmatrix} 0 & z_{pj} & -y_{pj} \\ -z_{pj} & 0 & x_{pj} \\ y_{pj} & -x_{pj} & 0 \end{bmatrix} \begin{Bmatrix} \theta_j^x \\ \theta_j^y \\ \theta_j^z \end{Bmatrix} \qquad \{D_j\} = \begin{Bmatrix} \{u_j\} \\ \{\theta_j\} \end{Bmatrix}$$

Equation (5-74) can be rewritten as:

$$\{D_j\} = [T_{pj}]^T \{D_p\} \tag{5-75}$$

Consider the force-displacement relation of a structural element defined between node "j" and "k":

$$\{A_{j,k}\} = [K_{j,k}]\{D_{j,k}\} \tag{5-76}$$

The actions at the ends of the element may be transformed into statically equivalent actions at nodes "p" and "q":

$$\{A_{p,q}\} = [T]\{A_{j,k}\} \tag{5-77}$$

where:

$$\{A_{p,q}\} = \begin{Bmatrix}\{A_p\}\\ \{A_q\}\end{Bmatrix} \qquad [T] = \begin{bmatrix}[T_{pj}] & [0]\\ [0] & [T_{qk}]\end{bmatrix} \qquad \{A_{j,k}\} = \begin{Bmatrix}\{A_j\}\\ \{A_k\}\end{Bmatrix}$$

The displacements of the ends of the element may be expressed in terms of those of nodes "p" and "q":

$$\{D_{j,k}\} = [T]^T\{D_{p,q}\} \tag{5-78}$$

where:

$$\{D_{j,k}\} = \begin{Bmatrix}\{D_j\}\\ \{D_k\}\end{Bmatrix} \qquad [T]^T = \begin{bmatrix}[T_{pj}]^T & [0]\\ [0] & [T_{qk}]^T\end{bmatrix} \qquad \{D_{p,q}\} = \begin{Bmatrix}\{D_p\}\\ \{D_q\}\end{Bmatrix}$$

Substitution of (5-76) and (5-77) into (5-75) gives:

$$\{A_{j,k}\} = [K_{j,k}][T]^T\{D_{p,q}\} \tag{5-79}$$

$$[T]^{-1}\{A_{p,q}\} = [K_{j,k}][T]^T\{D_{p,q}\} \tag{5-80}$$

Pre-multiplying both sides by the transformation matrix [T] produces:

$$\{A_{p,q}\} = [T][K_{j,k}][T]^T\{D_{p,q}\} \quad (5\text{-}81)$$

The stiffness matrix relating the nodal forces and displacements at nodes "p" and "q" is:

$$[K_{p,q}] = [T][K_{j,k}][T^T] \quad (5\text{-}82)$$

The rigid body transformation procedure is internal and can be applied on any of the element types in the program with minimum interfacing effort. The current implementation assumes that nodes "p" and "q" are used for the finite-element discretization of the structure. The element is formally defined between nodes "p" and "q" and, therefore, the degrees of freedom of these nodes participate in the solution. Nodes, or rather points, "j" and "k", however, determine the true location of the ends of the element and its orientation in space. This feature allows the declaration of multiple but actually non-coincident elements between a pair of structural nodes. The "rigid arm" transformation tool is applicable in modeling of offset connections, complicated framing details, shear walls, expansion joints and abutments.

### 5.9.2 End Releases

Releases of selected degrees of freedom at the ends of an element are incorporated in the program to increase the ability of the user to model complicated connections with minimum effort (figure 5-23). The fixed-end element stiffness matrix is generated first and the effect of the end releases is applied subsequently by the procedure outlined next. The equilibrium of a single element can be expressed by the equation:

$$[k_e]\{d\} = \{A\} \quad (5\text{-}83)$$

where:

$[k_e]$ = Element stiffness matrix (12X12 in the general case).

$\{d\}$ = Element displacement vector (1X12).

$\{A\}$ = Element actions (1X12).

The matrix equation is then separated with regard to the released (subscript "r") and non-released (subscript "n") degrees of freedom. The element actions associated with the released degrees of freedom are set to zero.

$$\begin{bmatrix} [k_{n-n}] & [k_{n-r}] \\ [k_{r-n}] & [k_{r-r}] \end{bmatrix} \begin{Bmatrix} \{d_n\} \\ \{d_r\} \end{Bmatrix} = \begin{Bmatrix} \{A_n\} \\ \{0\} \end{Bmatrix} \tag{5-84}$$

Solving the second equation in (5-84) for $\{d_r\}$ and substituting the result in the first equation yields a new sub-matrix $[k^*_{n-n}]$ relating the element forces and displacements along the non-released degrees of freedom.

$$[k^*_{n-n}] = [k_{n-n}] - [k_{n-r}]^T [k_{r-r}]^{-1} [k_{r-n}] \tag{5-85}$$

The element matrix is obtained by eliminating the influence coefficients of the released degrees of freedom:

$$[k^*_e] = \begin{bmatrix} [k^*_{n-n}] & [0] \\ [0] & [0] \end{bmatrix} \tag{5-86}$$

The end-release procedure in IDARC-BRIDGE does not reduce the size of the element stiffness matrix. Furthermore, releases of the same local degree of freedom should not be applied to the ends of all members framing in a structural node; this will result in null diagonal terms in the global stiffness matrix. The number of releases in a particular element is subject to the limitation of avoiding a collapse mechanism. The above formulation significantly simplifies the manipulation of the element stiffness matrix since it allows combination of releases, rigid zones, and end springs in the same member. Another important benefit is that the release procedure can be applied on any type of element, including inelastic beams, springs, dampers, isolators, gaps, etc.

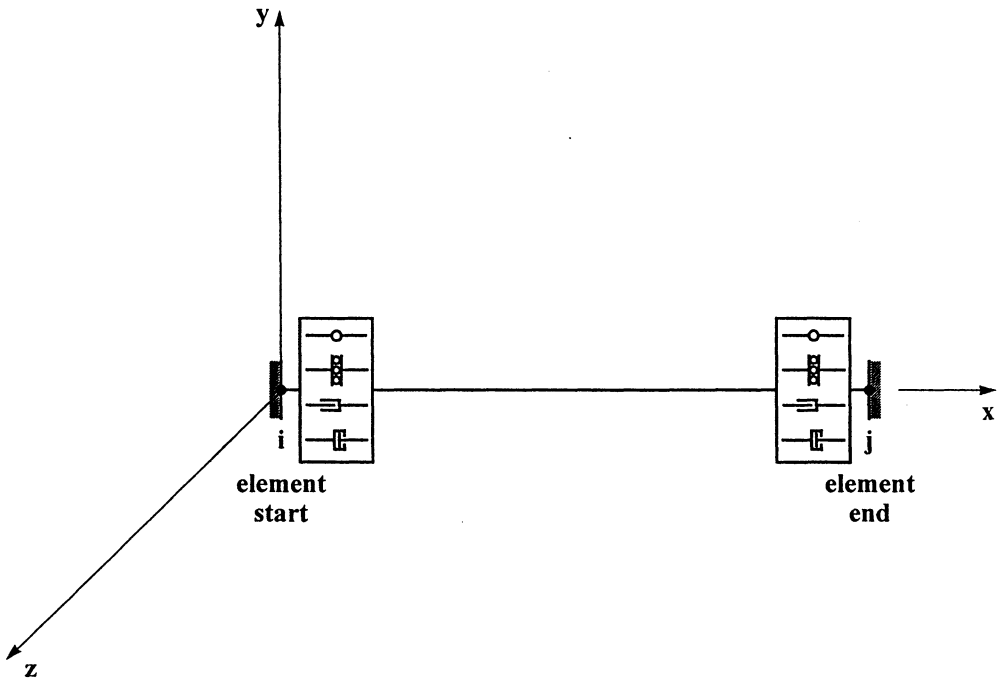


**Possibly released degrees of freedom at each end: $u_x$, $u_y$, $u_z$, $rot_x$, $rot_y$, $rot_z$.**
**All releases are in the element coordinate system.**

**FIGURE 5-23 Element End Releases**

### 5.9.3 End Springs

A set of springs attached to the ends of a beam-column element may be used to model a variety of structural connections, as well as soil-structure interaction (SSI). The flexibility method is commonly used to derive the element stiffness matrix. This approach, however, requires different formulations for members with and without springs and then for all possible combinations of end springs (Weaver and Gere, 1990). In IDARC-BRIDGE the element stiffness matrix is obtained by condensing the matrix of a system of three fixed-end elements (figure 5-22).

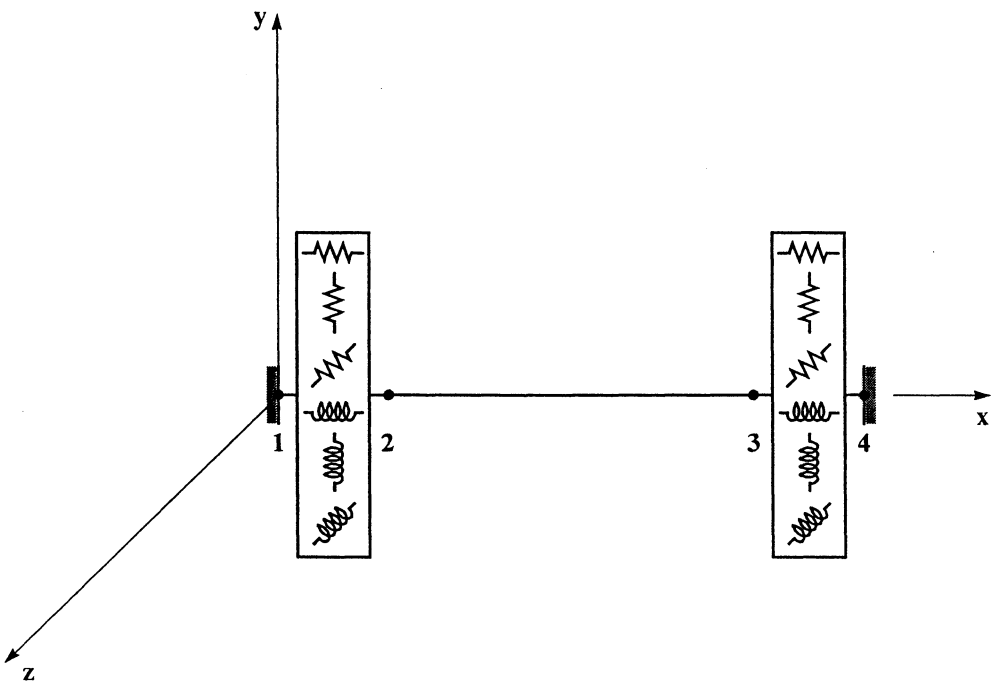


**Adding flexibility is possible along degrees of freedom: $u_x$, $u_y$, $u_z$, $rot_x$, $rot_y$, $rot_z$, at each end. All end springs are defined in the element coordinate system. Nodes 2 and 3 are virtual.**

**FIGURE 5-24 Element End Springs**

Two external and two internal nodes are needed to define the beam-column and end spring elements. The action equations of the system in matrix form are:

$$\begin{bmatrix} [k_{2,3-2,3}] & [k_{2,3-2,3}] \\ [k_{2,3-2,3}] & [k_{2,3-2,3}] \end{bmatrix} \begin{Bmatrix} \{u_{2,3}\} \\ \{u_{1,4}\} \end{Bmatrix} = \begin{Bmatrix} \{F_{2,3}\} \\ \{F_{1,4}\} \end{Bmatrix} \tag{5-87}$$

where:

$$\{F_{2,3}\} = \begin{Bmatrix} \{F_2\} \\ \{F_3\} \end{Bmatrix}, \qquad \{F_{1,4}\} = \begin{Bmatrix} \{F_1\} \\ \{F_4\} \end{Bmatrix}, \qquad \{u_{2,3}\} = \begin{Bmatrix} \{u_2\} \\ \{u_3\} \end{Bmatrix}, \qquad \{u_{1.4}\} = \begin{Bmatrix} \{u_1\} \\ \{u_4\} \end{Bmatrix}$$

in which $\{F_{i,j}\}$ are the forces and moments acting on nodes i and j, while $\{u_{i,j}\}$ are the corresponding displacements. The stiffness matrix of the system [K] is assembled in a standard manner by arranging the beam-column and end spring stiffness matrices $[K_b]$, $[K_{s1}]$ and $[K_{s2}]$ in relation to the nodal numbering and element connectivity.

Since no forces are applied on the internal nodes 2 and 3, $\{F_{2,3}\}$ in equation (5-87) is zero. Solving the set of equations yields:

$$\{u_{2,3}\} = -[k_{2,3-2,3}]^{-1}[k_{2,3-1,4}]\{u_{1,4}\} \tag{5-88}$$

The force-deflection relation for the external nodes 1 and 4 is then:

$$[K^*_{1,4}]\{u_{1,4}\} = \{F_{1,4}\} \tag{5-89}$$

where:

$$[K^*_{1,4}] = [k_{1,4}] - [k_{2,3\text{-}1,4}]^T [k_{2,3\text{-}2,3}]^{-1} [k_{2,3-1,4}] \tag{5-90}$$

In the end springs act along only a few of the degrees of freedom of the beam, the procedure can be simplified:

$$\begin{bmatrix} [k_{e-e}] & [k_{e-i}] \\ [k_{i-e}] & [k_{i-i}] \end{bmatrix} \begin{Bmatrix} \{u_e\} \\ \{u_i\} \end{Bmatrix} = \begin{Bmatrix} \{F_e\} \\ \{0\} \end{Bmatrix} \tag{5-91}$$

where $\{u_e\}$ are the displacements along the degrees of freedom of the "external" nodes (nodes 1 and 4 in the previous development) and $\{u_i\}$ are displacements of the "internal" nodes. Employing static condensation:

$$[k^*_{e-e}] = [k_{e-e}] - [k_{i-e}]^T [k_{i-i}]^{-1} [k_{i-e}] \tag{5-92}$$

The above expression is general and can be applied for rigid arms as well (Section 5.9.1).

# SECTION 6
# EXAMPLE PROBLEMS AND CASE STUDIES

All example problems are solved with the current edition of IDARC-BRIDGE (version 1.0) or the earlier β-version. To avoid confusion due to different input requirements of the two versions only input files of the most recent release of the program are listed here.

## 6.1 Example Problem 1: Quasi-Static Analysis for Force Input (IDARC-BRIDGE 1.0)

**Title**: Static analysis of a space frame.
**Type**: Analysis for force input.
**Reference**: Weaver, Jr. and Gere (1990), Page 354, Example 1.

**Problem**: A space frame having three members and four joints is subjected to static force loading (figure 6-1). Points A and D are fully restrained. All members have the same cross-sectional properties. The loads on the frame consist of a force 2P in the positive X direction at point B, a force P in the negative Y direction at point C, and a moment PL in the negative Z sense at C. Determine the final displaced shape of the structure. Include the effect of shearing deformations.

**Given**: $E = 200 \times 10^6$ kN/m$^2$, $G = 80 \times 10^6$ kN/m$^2$, $L = 3$ m, $A = 0.01$ m$^2$, $I_{xx} = 2 \times 10^{-3}$ m$^4$, $I_{zz} = I_{yy} = 1 \times 10^{-3}$ m$^4$, $P = 60$ kN.

**Input Data Listing**:

```
*analysis type
at 3d
*analysis options
ao quasistatic force
*units
un kilonewton meter degree
```

```
*joint coordinates
co 1 0.0 3.0 0.0
co 2 6.0 3.0 0.0
co 3 0.0 0.0 0.0
co 4 9.0 0.0 3.0
co 5 3.0 3.0 0.0
co 6 6.0 6.0 0.0
*boundary conditions
bc 111111 3 4
*element properties
elastic beam 3d
property 1
a 0.01 ixx 2.0e-3 iyy 1.0e-3 izz 1.0e-3 e 200.0e6 g 80.0e6 theta 0.0
fy 1.0 fz 1.0
property 2
a 0.01 ixx 2.0e-3 iyy 1.0e-3 izz 1.0e-3 e 200.0e9 g 80.0e9 theta 0.0
fy 1.0 fz 1.0
end elastic beam 3d properties
*element definition
element 1 1 5
element 2 3 1
element 3 2 4
element 4 5 2
element 5 2 6
*elements types
type 3d_e_b elements 1 2 3 4 5
*property number
property 1 element 1 2 3 4
property 2 element 5
*number of load steps
number of load steps 1
```

```
*joint load
pj dx 120 1
pj dz 240 5
pj dy -60 2
pj dx -60 2
pj dx 60 6
*output control
oc dis his dof 1 joi 1 2 3 4
oc dis his dof 2 joi 1 2 3 4
oc dis his dof 3 joi 1 2 3 4
oc dis his dof 4 joi 1 2 3 4
oc dis his dof 5 joi 1 2 3 4
oc dis his dof 6 joi 1 2 3 4
oc for his ele 3
*finish
```

**Solution Comparison:**

**TABLE 6-1 Displacements of Node 1**

| | $u_{x,1}$ [m] | $u_{y,1}$ [m] | $u_{z,1}$ [m] | $rot_{x,1}$ [rad] | $rot_{y,1}$ [rad] | $rot_{z,1}$ [rad] |
|---|---|---|---|---|---|---|
| **Reference** | -0.859E-03 | 0.578E-04 | 0.501E-02 | 0.239E-02 | -0.162E-02 | 0.681E-03 |
| **IDARC** | -0.859E-03 | 0.578E-04 | 0.501E-02 | 0.239E-02 | -0.162E-02 | 0.681E-03 |
| **Difference** | None | None | None | None | None | None |

**TABLE 6-2 End Actions at Node "i" of Element 3**

| | $F_{x,3}$ [kN] | $F_{y,3}$ [kN] | $F_{z,3}$ [kN] | $M_{x,3}$ [kNm] | $M_{y,3}$ [kNm] | $M_{z,1}$ [kNm] |
|---|---|---|---|---|---|---|
| **Reference** | 105.548 | -38.509 | -126.013 | 29.464 | 86.569 | -67.100 |
| **IDARC** | 105.548 | -38.509 | -126.013 | 29.464 | 86.569 | -67.100 |
| **Difference** | None | None | None | None | None | None |

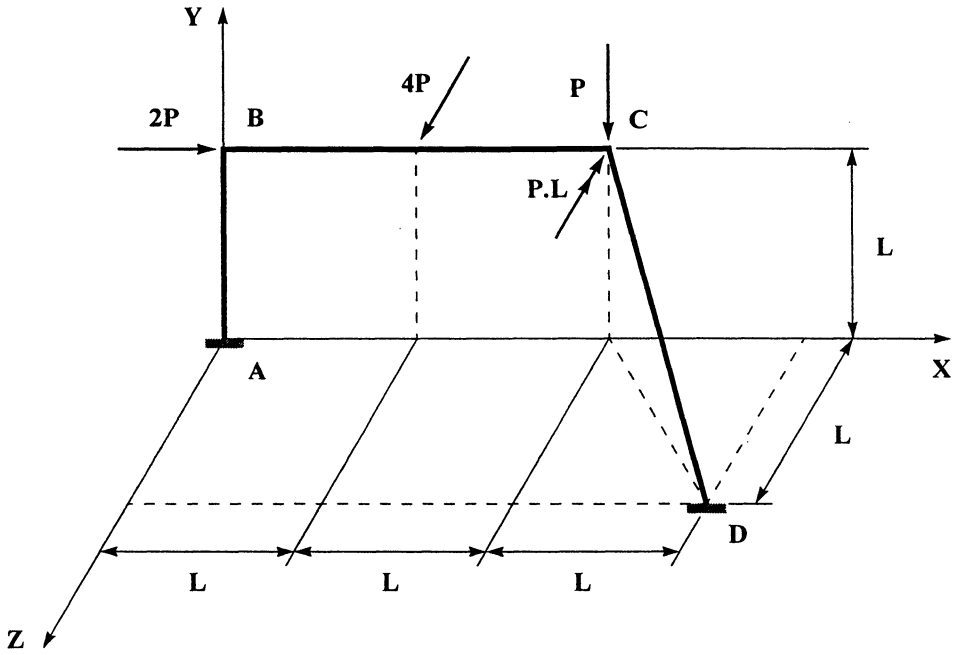


a)

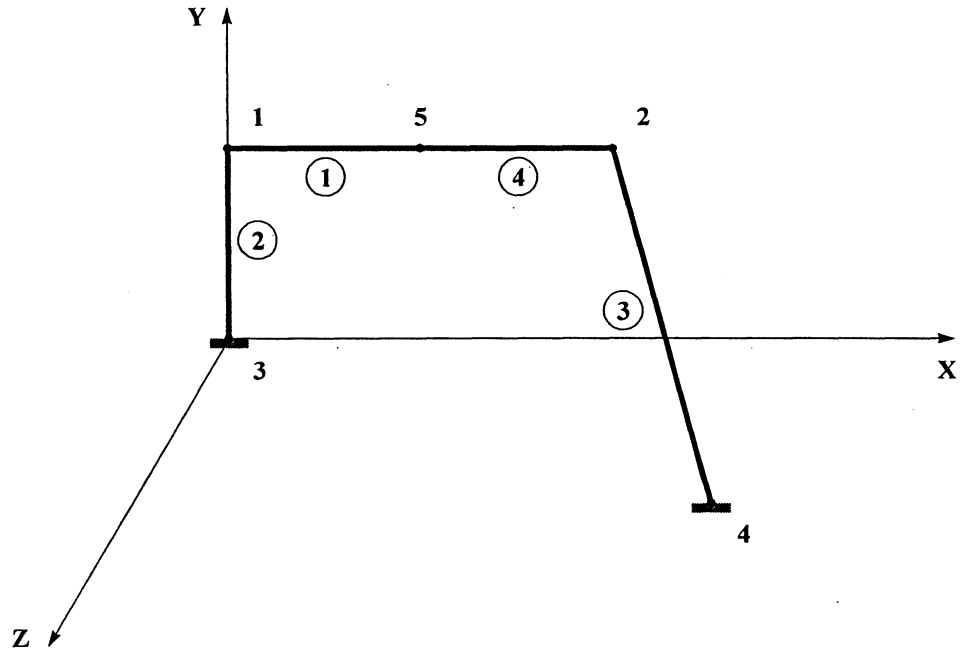


b)

**FIGURE 6-1 Example Structure 1: a) Geometric Properties and Loading, b) Computer Analysis Model**

## 6.2 Example Problem 2: Dynamic Analysis for Force Input (IDARC-BRIDGE 1.0)

**Title**: Dynamic analysis of a lumped-mass cantilever.

**Type**: Analysis for force input.

**Reference**: Chopra (1995), Page 570, Example 15.1.

**Problem**: A reinforced-concrete chimney idealized as a five degree-of-freedom lumped-mass system is subjected at the top to a step force p(t) of 1000 kips (figure 6-2). Determine the displacement response by direct integration of the equations of motion using the average acceleration method and a time step of $\Delta t = 0.1$ sec.

**Given**: $h = 120$ ft, $m = 208.6$ kip-sec$^2$/ft, $EI_{zz} = EI_{yy} = 5.469 \times 10^{-10}$ kip-ft$^2$.

**Input Data Listing**:

```
*analysis type
at 3d
*analysis options
ao dynamic force
*units
un feet kip degree
*joint coordinates
co 1 0.0 120.0 0.0
co 2 0.0 240.0 0.0
co 3 0.0 360.0 0.0
co 4 0.0 480.0 0.0
co 5 0.0 600.0 0.0
co 6 0.0   0.0 0.0
*boundary conditions
bc 111111 6
bc 011110 1 2 3 4 5
*element properties
```

```
elastic beam 3d
property  1
a  1.69  ixx  0.28  iyy  0.14  izz  1000.0  e  5.469e7  g  10.0  theta 0.0
end elastic beam 3d properties
*element definition
element  1  1  6
element  2  1  2
element  3  2  3
element  4  3  4
element  5  4  5
*elements types
type  3d_e_b  element  1  2  3  4  5
*property number
property  1  element  1  2  3  4  5
*excitation groups
ex  file  force.inp  dof  1  joi  5
*joint weight
weight  dx  6712.748  1 2  3  4
weight  dx  3356.374  5
*time history analysis
input time step  0.1
analysis time step  0.1
total analysis duration  2.0
damping  alpha  0.0  beta  0.0  gamma  0.0
type of input  force
direction of excitation  0.0
peak ground acceleration  1.0
*output control
oc  dis  his  dof  1  joint  1  2  3  4  5  6
oc  dis  max  dof  1  joint  1  2  3  4  5  6
oc  for  his  ele  1  2  3  4  5
```

*finish

**Solution Comparison:**

**TABLE 6-3 Natural Circular Frequencies of Vibration**

| | $\omega_1$ [rad/sec] | $\omega_2$ [rad/sec] |
|---|---|---|
| **Reference** | 1.701 | 10.220 |
| **IDARC** | 1.701 | 10.220 |
| **Difference** | None | None |

**TABLE 6-4 Modes of Vibration**

| | $\Phi_{1,1}$ | $\Phi_{1,2}$ | $\Phi_{1,3}$ | $\Phi_{1,4}$ | $\Phi_{1,5}$ |
|---|---|---|---|---|---|
| **Reference** | 0.386E-02 | 0.139E-01 | 0.280E-01 | 0.441E-01 | 0.610E-01 |
| **IDARC** | 0.386E-02 | 0.139E-01 | 0.280E-01 | 0.441E-01 | 0.610E-01 |
| **Difference** | None | None | None | None | None |

| | $\Phi_{2,1}$ | $\Phi_{2,2}$ | $\Phi_{2,3}$ | $\Phi_{2,4}$ | $\Phi_{2,5}$ |
|---|---|---|---|---|---|
| **Reference** | 0.173E-01 | 0.402E-01 | 0.370E-01 | 0.412E-03 | -0.550E-01 |
| **IDARC** | -0.173E-01 | -0.402E-01 | -0.370E-01 | -0.412E-03 | 0.550E-01 |
| **Difference** | None | None | None | None | None |

**TABLE 6-5 Maximum Displacements of Degrees of Freedom 1, 2, 3, 4 and 5**

| | $u_1$ [ft] | $u_2$ [ft] | $u_3$ [ft] | $u_4$ [ft] | $u_5$ [ft] |
|---|---|---|---|---|---|
| **Reference** | 0.160E+00<br>-0.0057 * | 0.578E+00<br>-0.0056 * | 0.116E+01<br>-0.0003 * | 0.184E+01<br>0.000E+00 | 0.255E+01<br>0.000E+00 |
| **IDARC** | 0.160E+00<br>-0.567E-02 | 0.578E+00<br>-0.563E-02 | 0.116E+01<br>-0.266E-03 | 0.184E+01<br>0.000E+00 | 0.255E+01<br>0.000E+00 |
| **Difference** | None | None | None | None | None |

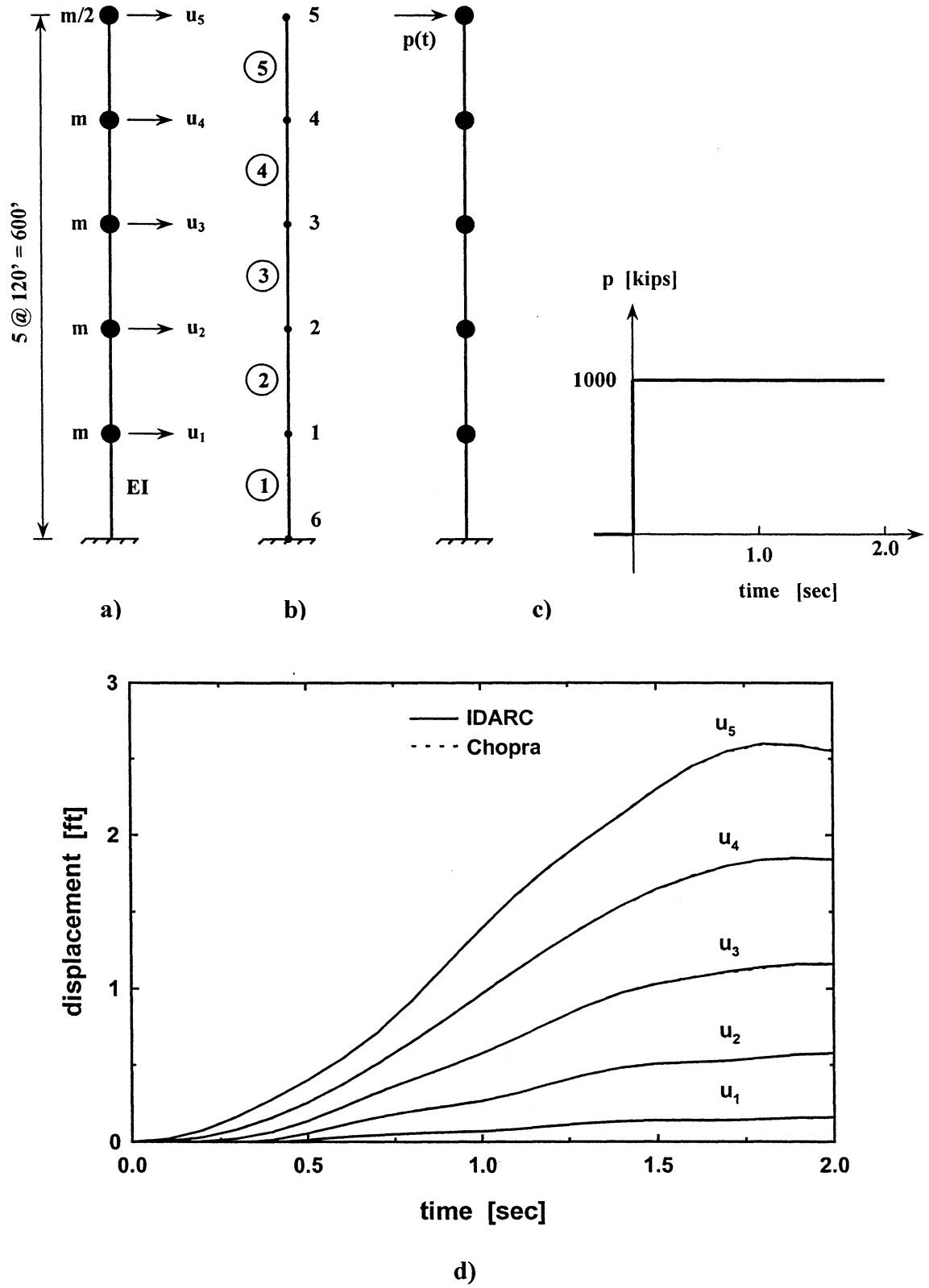


**FIGURE 6-3 Example Problem 2: a) Geometric and Material Properties, b) Computer Model, c) Dynamic Force Loading, d) Displacement Response**

## 6.3 Example Problem 3: Dynamic Analysis for Displacement Input (IDARC-BRIDGE 1.0)

**Title**: Dynamic analysis of a bridge.

**Type**: Analysis for ground displacement input.

**Reference**: ANSYS computer program.

**Problem**: A three-span reinforced-concrete bridge is subjected to the three-dimensional ground displacement records of the 1994 Northridge earthquake. The structure is identical to the collapsed first frame of the SR14/I5 southbound separation and overhead bridge located 25 miles north of downtown Los Angeles (figure 6-3). The ground motion is believed to have varied in space during the actual event due to wave passage and loss of coherence effects, as well as different local soil conditions at the supports. Determine the response of the structure to spatially varying support displacements by direct integration of the equations of motion with a time step of $\Delta t = 0.02$ sec. Assume the analysis height of the piers to be equal to the distance from the grade level to the center of gravity of the deck, and account for soil-structure interaction by using foundation springs. Use classical Rayleigh damping with 5% damping ratios for the first and fifth modes of vibration. Compare the solution of IDARC to the results of analysis of an identical model with the ANSYS finite-element package.

**Given**: Deck: $L_1 = 45.363$ m, $L_2 = 63.789$ m, $L_3 = 45.354$ m, $E = 23.2 \times 10^6$ kN/m$^2$, $G = 9.28 \times 10^6$ kN/m$^2$, $A = 8.800$ m$^2$, $I_{xx} = 16.299$ m$^4$, $I_{yy} = 188.566$ m$^4$, $I_{zz} = 5.854$ m$^4$.

Pier 2: $h_1 = 10.037$ m, $E = 24.3 \times 10^6$ kN/m$^2$, $G = 9.72 \times 10^6$ kN/m$^2$, $A = 4.207$ m$^2$, $I_{xx} = 1.746$ m$^4$, $I_{yy} = 4.770$ m$^4$, $I_{zz} = 0.682$ m$^4$.

Foundation springs at pier 2: $k_x = 2.7 \times 10^5$ kN/m, $k_y = 12.0 \times 10^5$ kN/m, $k_z = 5.1 \times 10^5$ kN/m, $k_{rx} = 290.0 \times 10^5$ kNm/rad, $k_{ry} = 1.0 \times 10^9$ kNm/rad, $k_{rz} = 49.9 \times 10^5$ kNm/rad.

Pier 3: $h_2 = 10.345$ m, $E = 24.3 \times 10^6$ kN/m$^2$, $G = 9.72 \times 10^6$ kN/m$^2$, $A = 4.207$ m$^2$, $I_{xx} = 1.746$ m$^4$, $I_{yy} = 4.752$ m$^4$, $I_{zz} = 0.680$ m$^4$.

Foundation springs at pier 3: $k_x = 3.1 \times 10^5$ kN/m, $k_y = 15.0 \times 10^5$ kN/m, $k_z = 6.2 \times 10^5$ kN/m, $k_{rx} = 306.0 \times 10^5$ kNm/rad, $k_{ry} = 1.0 \times 10^9$ kNm/rad, $k_{rz} = 54.0 \times 10^5$ kNm/rad.

Masses: $m_1 = 488$ kN.s$^2$/m, $m_2 = 1249$ kN.s$^2$/m, $m_3 = 59$ kN.s$^2$/m, $m_4 = 1249$ kN.s$^2$/m, $m_5 = 62$ kN.s$^2$/m, $m_6 = 555$ kN.s$^2$/m.

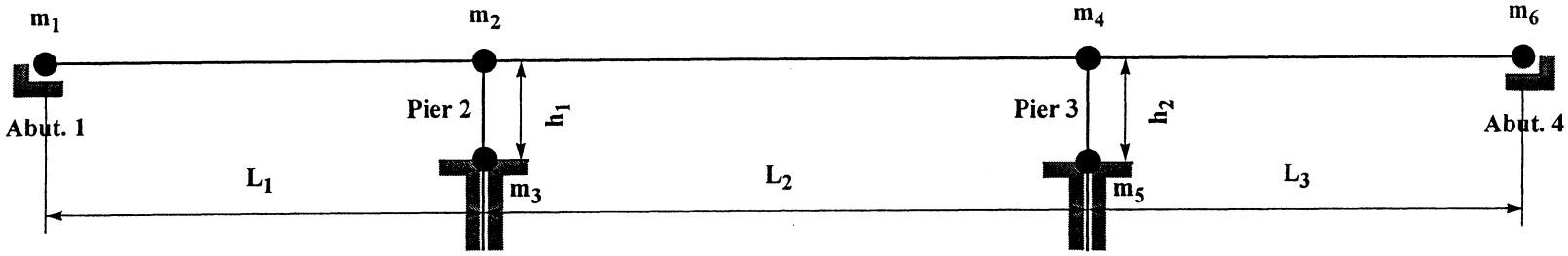


Abutments 1 and 4 are seat-type abutments. Piers 2 and 3 are founded on drilled shafts.

a)

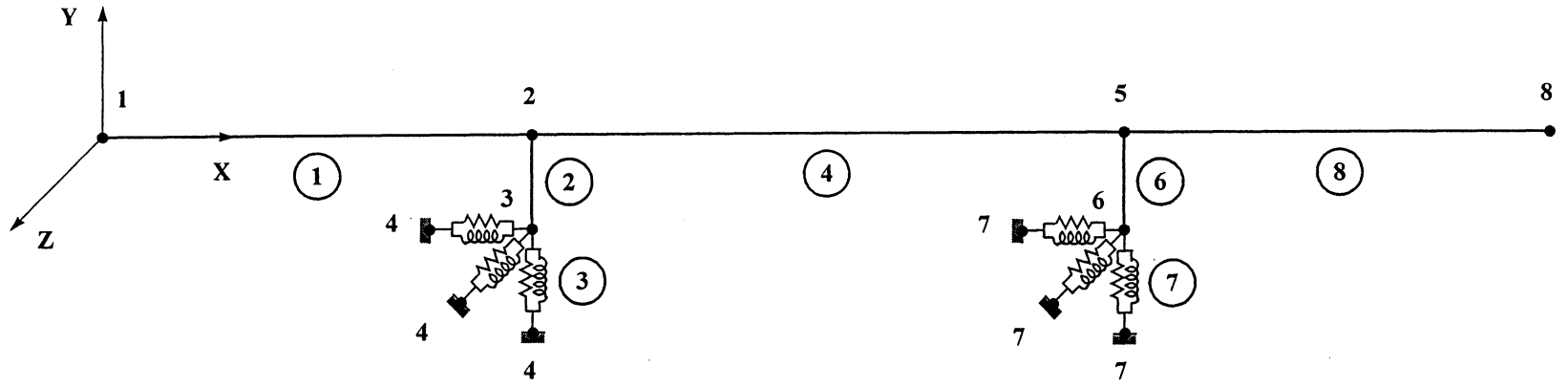


The transverse horizontal and vertical motions at the abutments are applied directly on nodes 1 and 8. All three components of the ground displacements at the piers are applied at the soil at the soil ends of the foundation springs, nodes 4 and 7.

b)

**FIGURE 6-3 Example Problem 3: a) Geometric and Material Properties of the Bridge Structure, b) Computer Analysis Model**

**Input Data Listing**:

```
*analysis type
at 3d
*analysis options
ao dynamic displacements
*units
un meter kilonewton degree
*joint coordinates
co 1    0.000    0.000 0.000
co 2   45.363    0.000 0.000
co 3   45.363  -10.037 0.000
co 4   44.363  -10.037 0.000
co 5  108.152    0.000 0.000
co 6  108.152  -10.345 0.000
co 7  107.152  -10.345 0.000
co 8  153.506    0.000 0.000
*boundary conditions
bc 011110 1 8
bc 111111 4 7
*element properties
elastic beam 3d
property 1
a 4.207 ixx 1.746 iyy 4.770 izz 0.682 e 24300000 g 9720000 theta 0.0
property 2
a 4.207 ixx 1.746 iyy 4.752 izz 0.680 e 24300000 g 9720000 theta 0.0
property 3
a 8.800 ixx 16.299 iyy 188.566 izz 5.854 e 23200000 g 9280000 theta 0.0
end elastic beam 3d properties
elastic foundation
property 1
kx 2.7e5 ky 12.0e5 kz 5.1e5 krx 290.0e5 kry 1.0e9 krz 49.9e5
```

property 2

kx 3.1e5 ky 15.0e5 kz 6.2e5 krx 306.0e5 kry 1.0e9 krz 54.0e5

end elastic foundation properties

linear damper

property 1

cx 0.0 cy 0.0 cz 0.0 crx 0.0 cry 0.0 crz 0.0

property 2

cx 0.0 cy 0.0 cz 0.0 crx 0.0 cry 0.0 crz 0.0

end linear damper properties

*element definition

element 1 1 2

element 2 2 3

element 3 3 4

element 4 3 4

element 5 2 5

element 6 5 6

element 7 6 7

element 8 6 7

element 9 5 8

*elements types

type 3d_e_b element 1 2 5 6 9

type e_foun element 3 7

type l_damp element 4 8

*property number

property 1 element 2 3 4

property 2 element 6 7 8

property 3 element 1 5 9

*excitation groups

ex file p2-sh.nd dof 1 joi 4

ex file p3-sh.nd dof 1 joi 7

ex file a1-sh.zd dof 2 joi 1

```
ex file p2-sh.zd dof 2 joi 4
ex file p3-sh.zd dof 2 joi 7
ex file p4-sh.zd dof 2 joi 8
ex file a1-sh.ed dof 3 joi 1
ex file p2-sh.ed dof 3 joi 4
ex file p3-sh.ed dof 3 joi 7
ex file p4-sh.ed dof 3 joi 8
*joint weight
weight all  4790 1
weight all 12253 2
weight all   581 3
weight all 12252 5
weight all   604 6
weight all  5443 8
*time history analysis
input time step 0.02
analysis time step 0.02
total analysis duration 15.00
damping alpha 0.523667 beta 0.002626 gamma 0.0
type of input displacements
direction of excitation 0.0
peak ground acceleration 0.01
*output control
oc dis his dof 1 joi 2 5
oc dis his dof 3 joi 2 5
oc dis add his dof 1 joi 2 3 coef 1 -1
oc dis add his dof 3 joi 2 3 coef 1 -1
oc dis add his dof 1 joi 5 6 coef 1 -1
oc dis add his dof 3 joi 5 6 coef 1 -1
oc dis max dof 1 joi 1 2 3 4 5 6 7 8
oc dis max dof 3 joi 1 2 3 4 5 6 7 8
```

```
oc dis add max dof 1 joi 2 3 coef 1 -1
oc dis add max dof 1 joi 5 6 coef 1 -1
oc dis add max dof 3 joi 2 3 coef 1 -1
oc dis add max dof 3 joi 5 6 coef 1 -1
oc for his ele 2 6
*finish
```

**Solution Comparison:**

**TABLE 6-6 Natural Periods of Vibration**

| | $T_1$ [sec] | $T_2$ [sec] | $T_3$ [sec] | $T_4$ [sec] | $T_5$ [sec] |
|---|---|---|---|---|---|
| **ANSYS** | 1.002 | 0.352 | 0.217 | 0.207 | 0.197 |
| **IDARC** | 1.002 | 0.352 | 0.217 | 0.207 | 0.197 |
| **Difference** | None | None | None | None | None |

**TABLE 6-7 Maximum Total Displacements of Nodes 2 and 5**

| | $u_{x,2}$ [m] | $u_{z,2}$ [m] | $u_{x,5}$ [m] | $u_{z,5}$ [m] |
|---|---|---|---|---|
| **ANSYS** | 0.503E+00<br>-0.425E+00 | 0.324E+00<br>-0.220E+00 | 0.503E+00<br>-0.425E+00 | 0.320E+00<br>-0.227E+00 |
| **IDARC** | 0.503E+00<br>-0.425E+00 | 0.324E+00<br>-0.220E+00 | 0.503E+00<br>-0.425E+00 | 0.320E+00<br>-0.227E+00 |
| **Difference** | None | None | None | None |

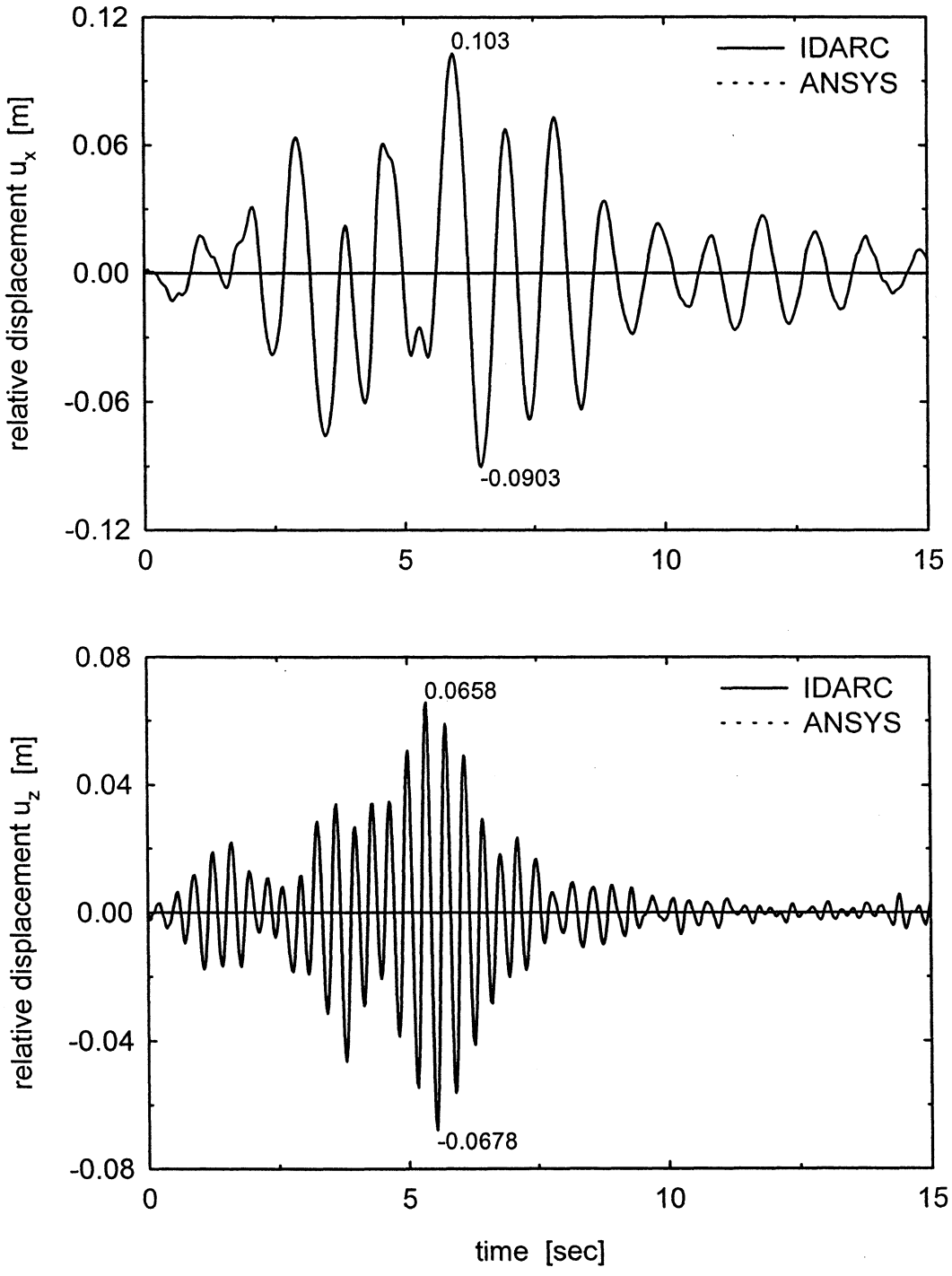


**FIGURE 6-4 Example Problem 3: Displacement Response of Pier 2**

## 6.4 Case Study 1: Analysis of a Small-Scale Isolated Bridge (Reichman, 1996)

Results of an experimental study performed by Tsopelas et al. (1994) are used to verify the capacity of the element models of IDARC-BRIDGE to represent the response of base-isolated structural systems. A shaking table test was performed on a scaled bridge model (1:4). A schematic of the bridge is shown in figure 6-5. The bridge consists of a deck (total weight 140 kN) supported by four flexible columns. Four Friction Pendulum System (FPS) bearings (Zayas et al., 1987) are placed on the top of the columns. Each of the bearings supports a load of 35 kN (figure 6-6). The bridge is subjected to a simulated ground motion categorized by the Japanese seismic design code as "level 2" for "ground condition 1" (figure 6-8). The frictional characteristics of the bearings are experimentally determined as shown in figure 6-7.

For analysis purposes, the bridge is modeled as a single frame (figure 6-9). A stiff elastic beam element is used for the deck. The weight of the structure is lumped in joints 5 and 6. The Bouc-Wen formulation ("isolator 1" element) is used to define the isolator load-displacement curve. It should be noted that the model for the bearings is velocity independent although their friction characteristics are velocity dependent. A dominant coefficient of friction of 9% is determined from shaking table tests of the bearing at low velocity (figure 6-7). The properties of the isolator: (i) initial stiffness $k_{initial}$, (ii) secondary stiffness $k_{yield}$, (iii) yielding force $F_y$, and (iv) post-yielding ratio $\alpha$ depend on the geometry, friction coefficient $\mu$ and supported weight W. The yielding force $F_y = W\mu$, yielding displacement $u_y$ and initial stiffness $k_{initial} = F_y/u_y$ are determined as 3.15 kN, 0.255 mm and 13059 kN/m respectively. The post-yield stiffness is calculated from the relation $k_{yield} = W/R = 35/0.5588 = 62.4\,kN/m$, where R is radius of the concave spherical surface of the isolator, and the post-yield ratio is $\alpha = k_{yield}/k_{initial} = 62.4/13059 = 0.006$. The stiffness of the columns is determined from the tabulated geometric properties. The degree of fixity at the base is concluded from the observed free vibration characteristics of the bridge at very low amplitudes, which do not cause sliding of the bearings.

The simulated ground motion is applied to the frame in the longitudinal direction. The response results are shown in figures 6-10 and 6-11. One of the parameters required for the analysis is the global structural equivalent damping. As mentioned in a previous section, it can be either mass

or stiffness proportional, or combination of the two (Rayleigh damping). To investigate the influence of the type and magnitude of global structural damping on the solution, analyses with different levels of damping are performed. A good agreement between analytically predicted and experimental results for the displacement of the deck for most types of damping can be noticed in figure 6-11. The comparison demonstrates that with careful representation of global damping, the behavior of isolated bridges with flexible columns can be adequately analyzed using the modeling tools of IDARC-BRIDGE.

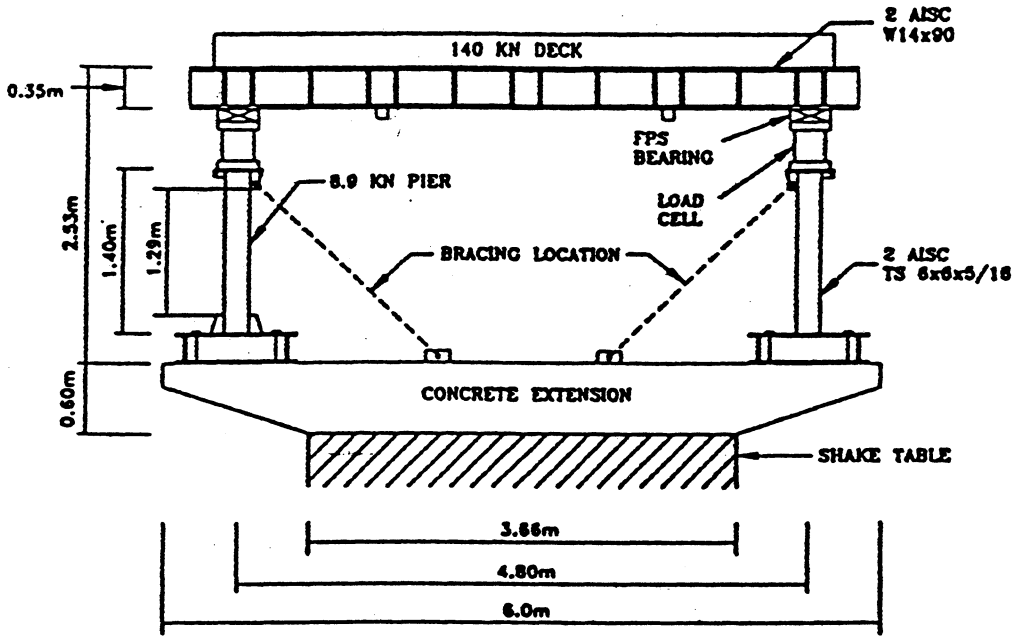


**FIGURE 6-5 Experimental Model**

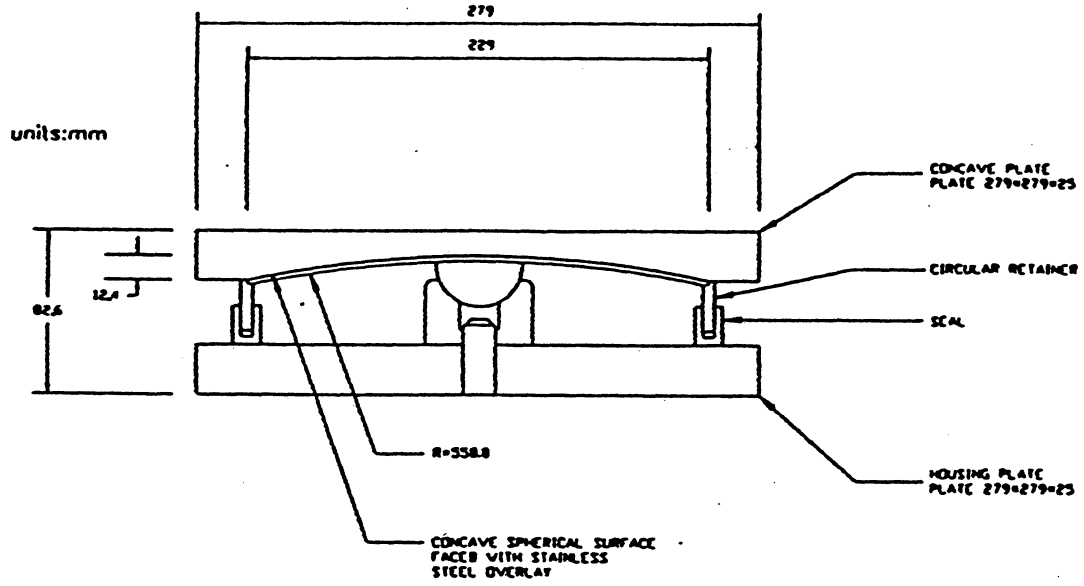


FIGURE 6-6 FPS Bearing Used in Experiment

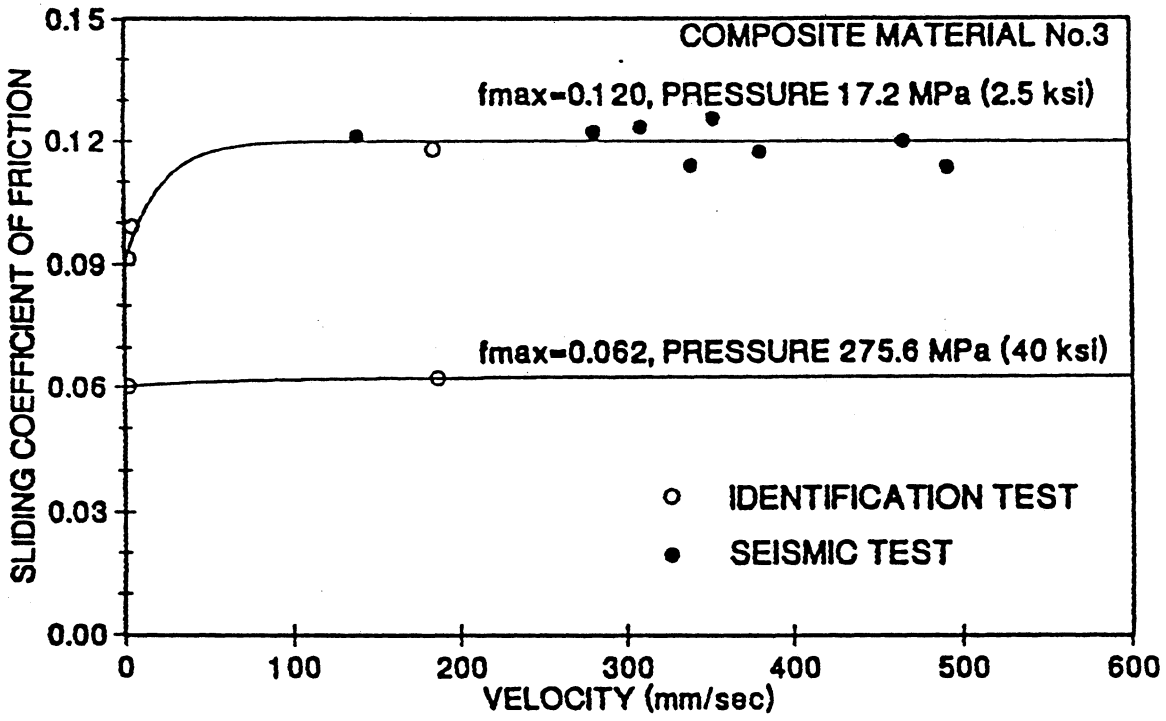


FIGURE 6-7 Experimentally Determined Coefficient of Friction

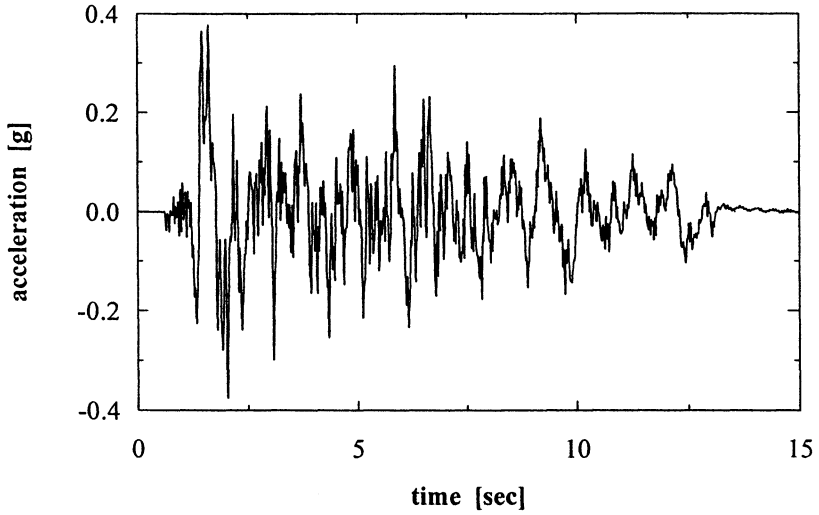


**FIGURE 6-8 Input Motion (Japanese Code, Level 2, Ground Condition 1)**

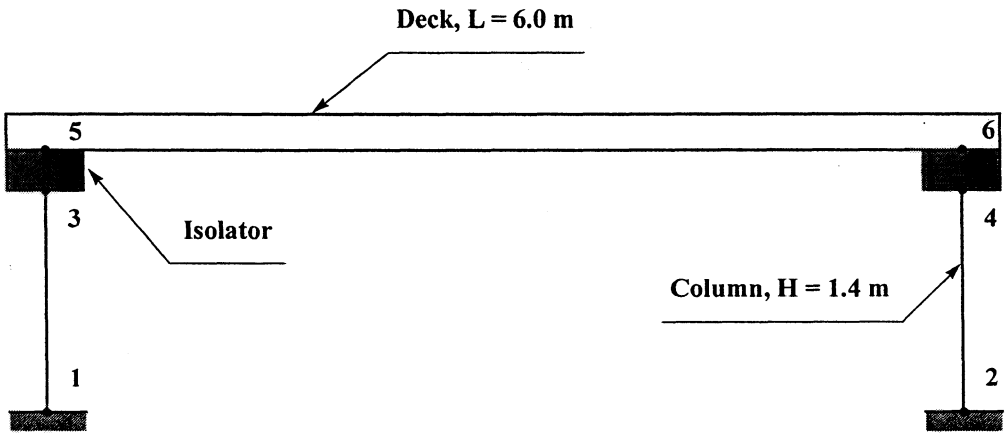


**FIGURE 6-9 Computer Analysis Model of Base-Isolated Bridge**

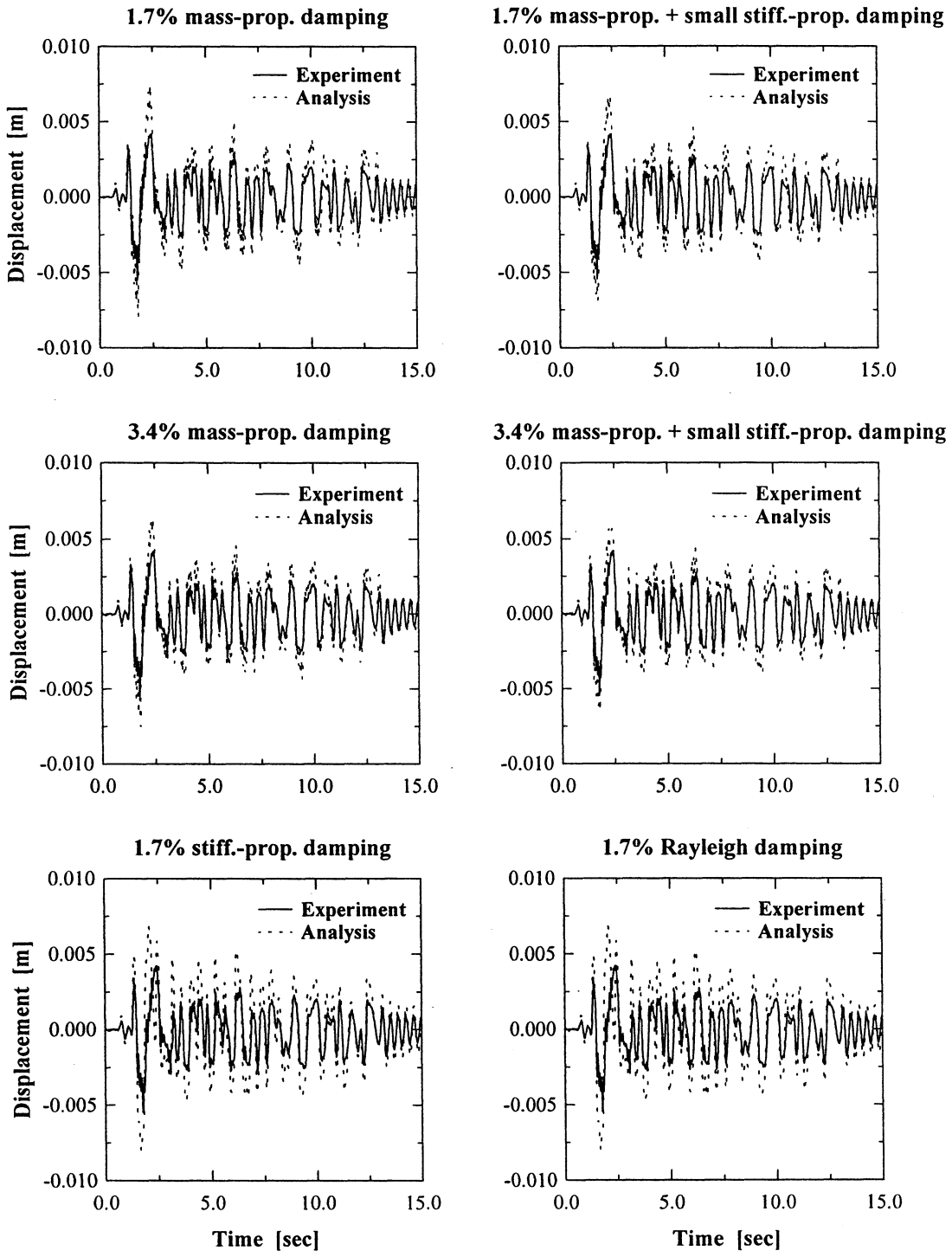


**FIGURE 6-10 Displacements of the Top of the Piers (Nodes 3 and 4)**

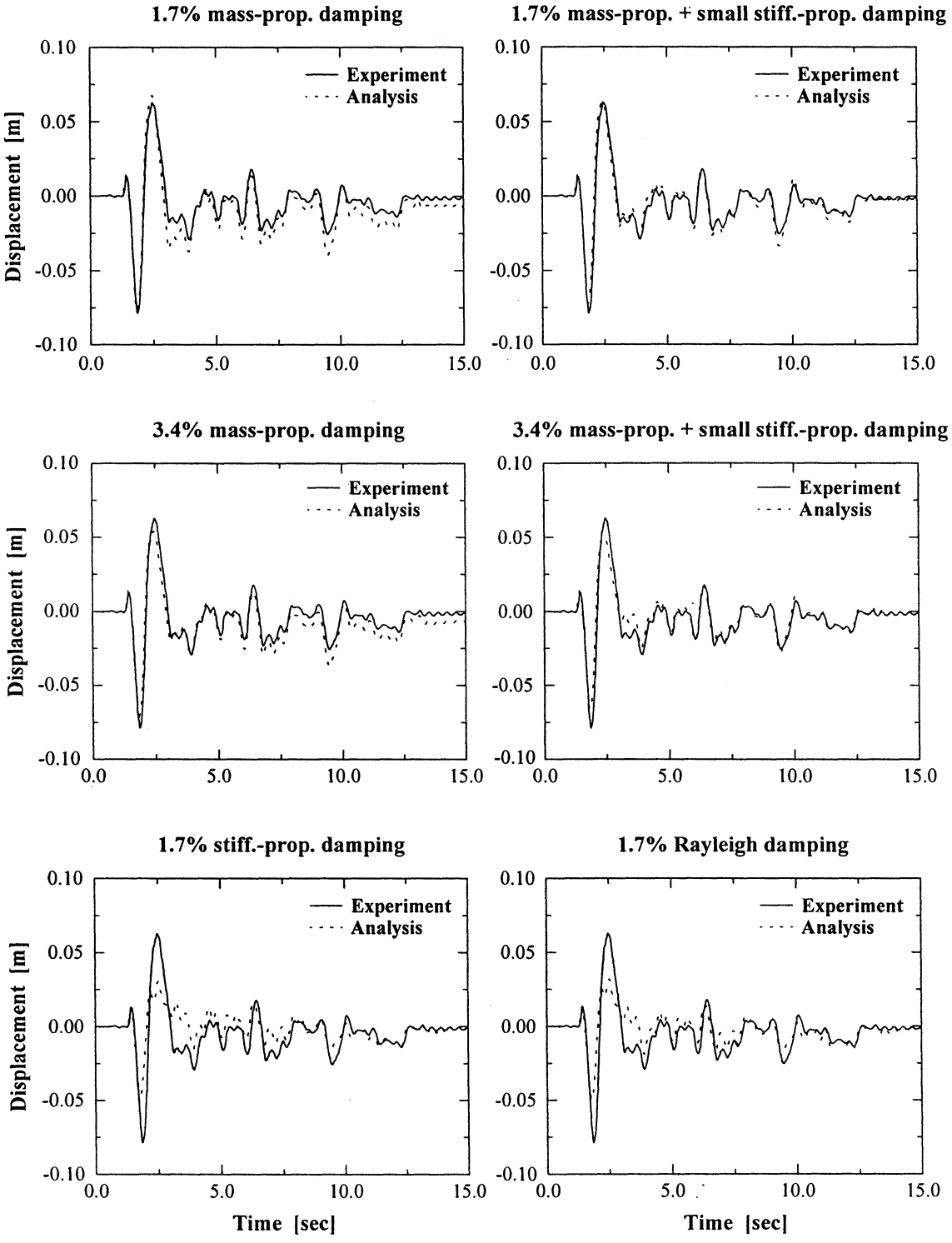


**FIGURE 6-11 Displacements of the Deck (Nodes 5 and 6)**

## 6.5 Case Study 2: East Aurora Bridge - Field Test (Reichman, 1996)

Results of a full-scale field test performed by Wendichansky (1996) on the southbound highway bridge spanning Cazenovia Creek on Route 400 in East Aurora, New York and laboratory component experiments (Mander et al., 1996) are used to assess the capability of IDARC-BRIDGE to predict the dynamic response of bridges with various types of bearings. The structure is a three-span continuous bridge supported on frame bents and abutments (figures 6-12, 6-13, 6-14, 6-15). The deck is carried by seven girders laterally connected with stringers (figures 6-13, 6-14, 6-15). Originally, the girders were supported on steel bearings. Three of the supports were equipped with expansion bearings while one of the bents provided a restraint in the longitudinal direction. The bridge was retrofitted and the steel bearings were replaced by lead-rubber bearings at the abutments and laminated rubber isolation bearings at the bents. Several snap-back tests are performed with both types of bearings. The bridge is pulled by two jacks connected to the deck above the bents and then quick-released to observe its free vibration response. The history of the force applied to bridge is presented in figure 6-16 as measured by the load cells.

A model of the bridge (figure 6-17) is analyzed using IDARC-BRIDGE for both types of bearing settings. The deck and bents are modeled as elastic beam elements. Foundation springs account for the flexibility of the soil medium at the supports. The participating mass of the soil is introduced into the corresponding joints. The rigid zones in the deck-bent connection are modeled by rigid arms (figure 6-18). As a result, the motion in the connection can be described by the degrees of freedom of a single node and only one beam element can be used for the deck in each span. The flexibility of the stringers in the lateral direction is represented by element end springs. The "isolator 1" element in IDARC-BRIDGE is used for the bearings whose properties before and after the retrofit were established experimentally (Mander et al., 1996).

The response measured in the snap-back tests of the bridge equipped first with steel and later with lead-rubber and elastomeric bearings is compared to results of the computer simulation. In both cases the agreement between analysis and experiment is very good (figure 6-19).

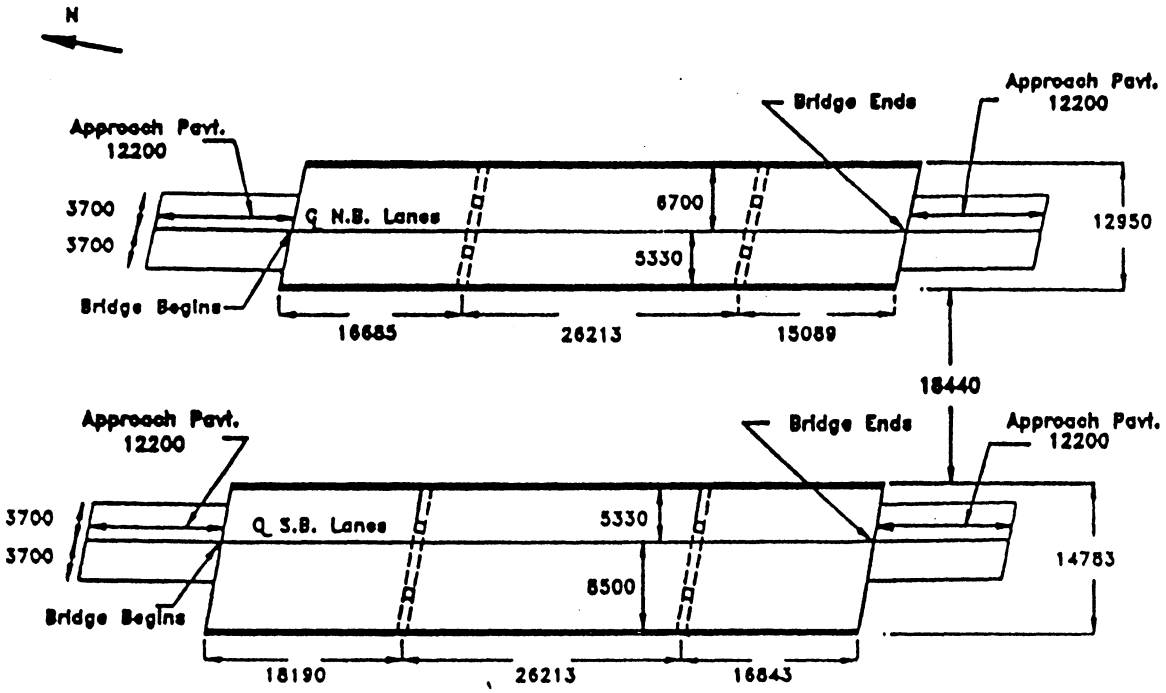


**FIGURE 6-12 Plan of East Aurora Bridge**

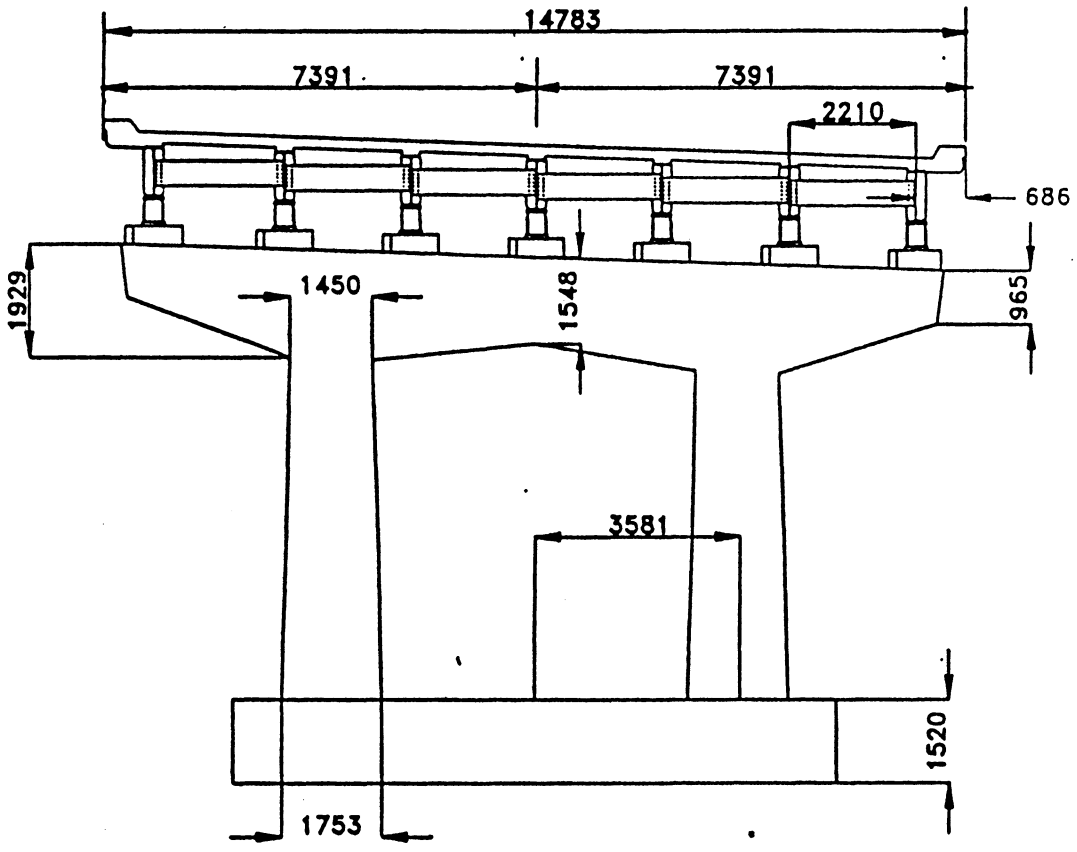


**FIGURE 6-13 Typical Bent**

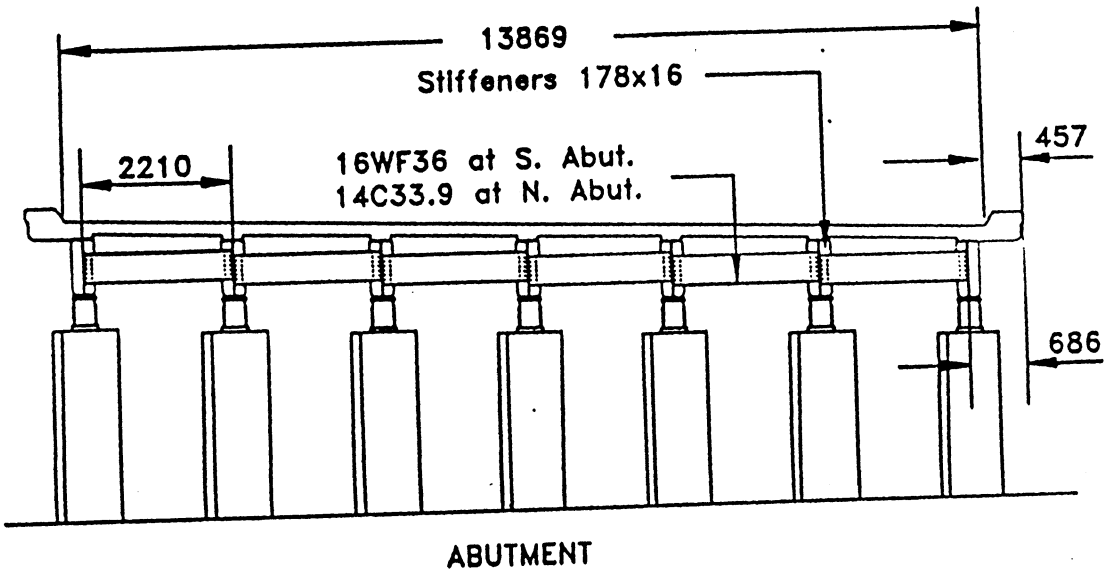


FIGURE 6-14 Typical Abutment

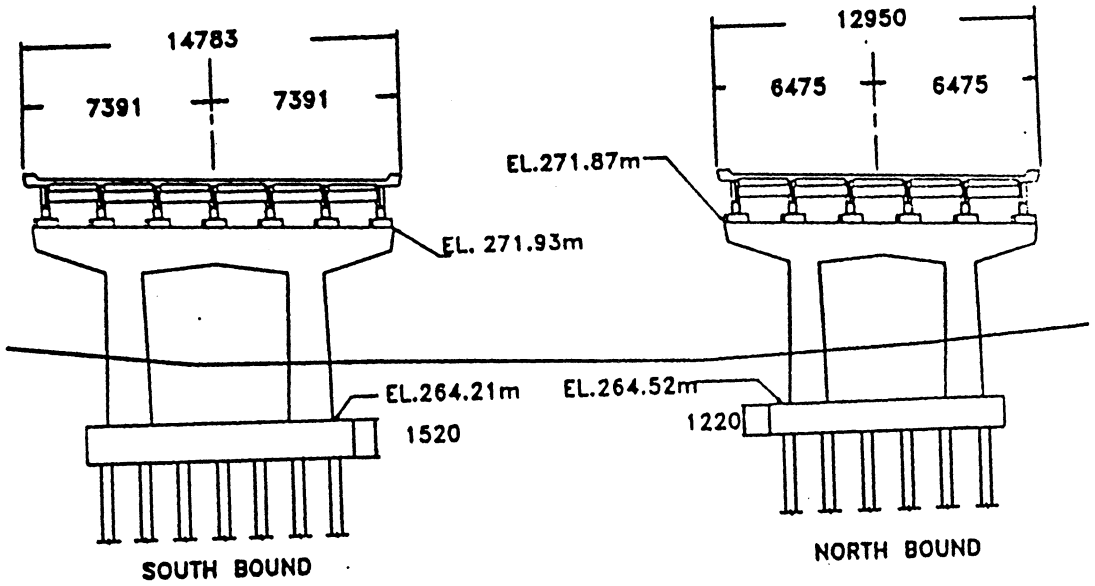


FIGURE 6-15 Typical Bridge Cross Section

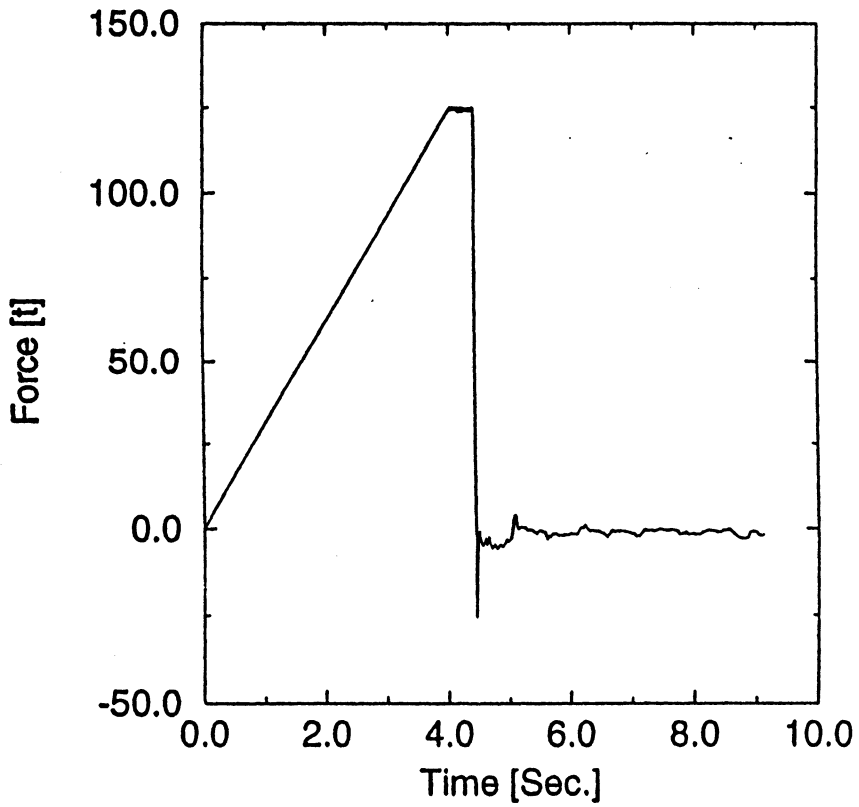


**FIGURE 6-16 Input Force History Measured During the Test**

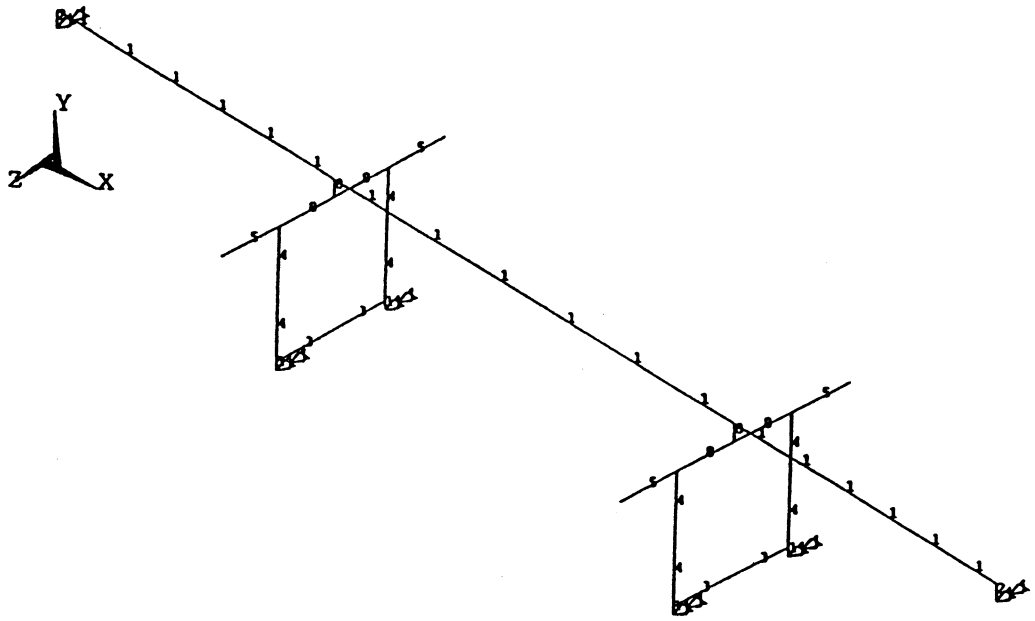


**FIGURE 6-17 East Aurora Bridge: Computer Analysis Model**

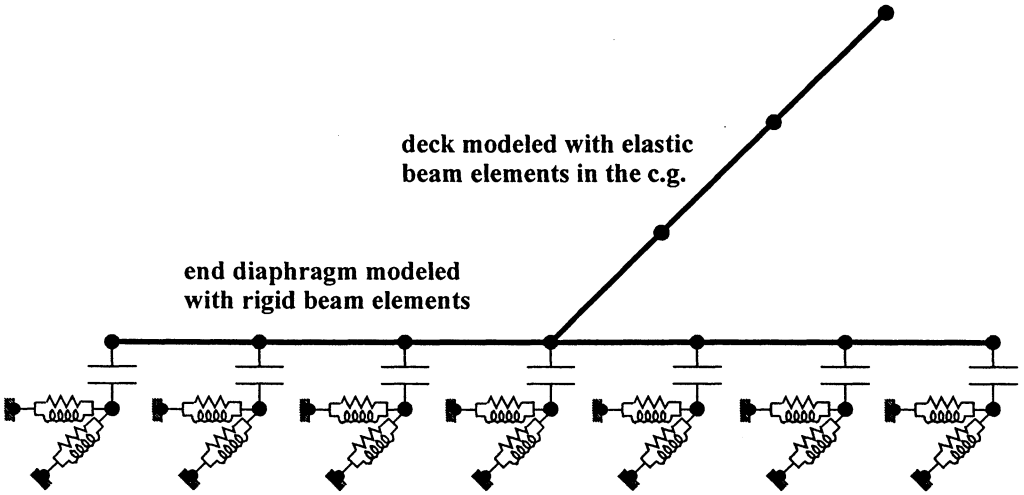


a)

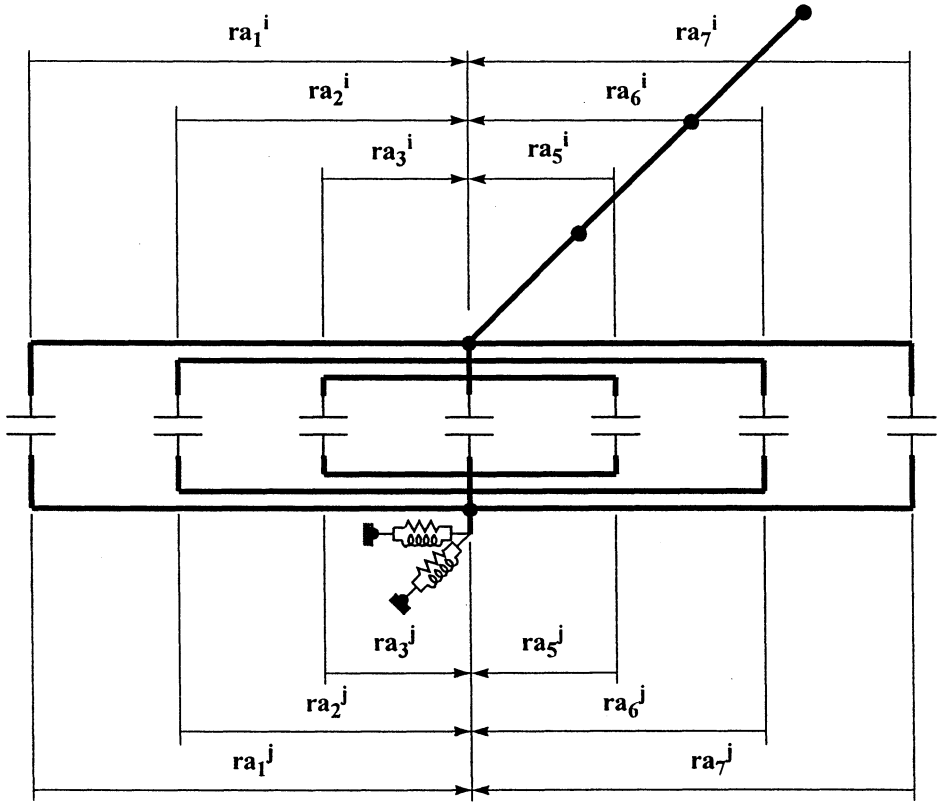


b)

**FIGURE 6-18 Modeling of the Deck-Abutment Connection: a) Modeling Using Rigid Beam Elements, b) Modeling Using Rigid Body Transformations**

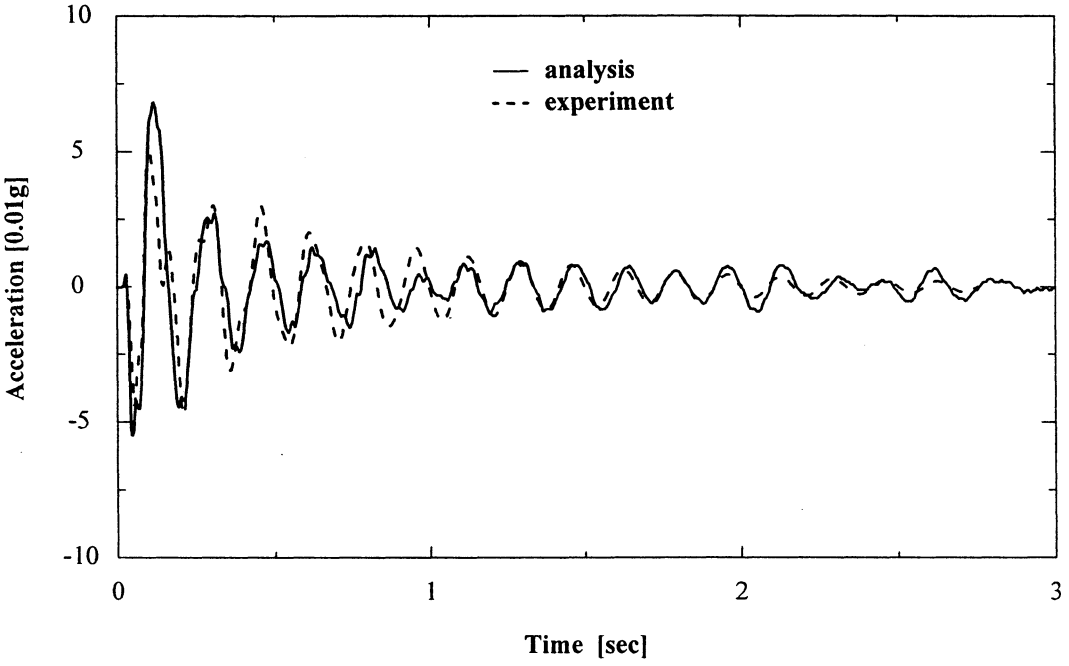


a)

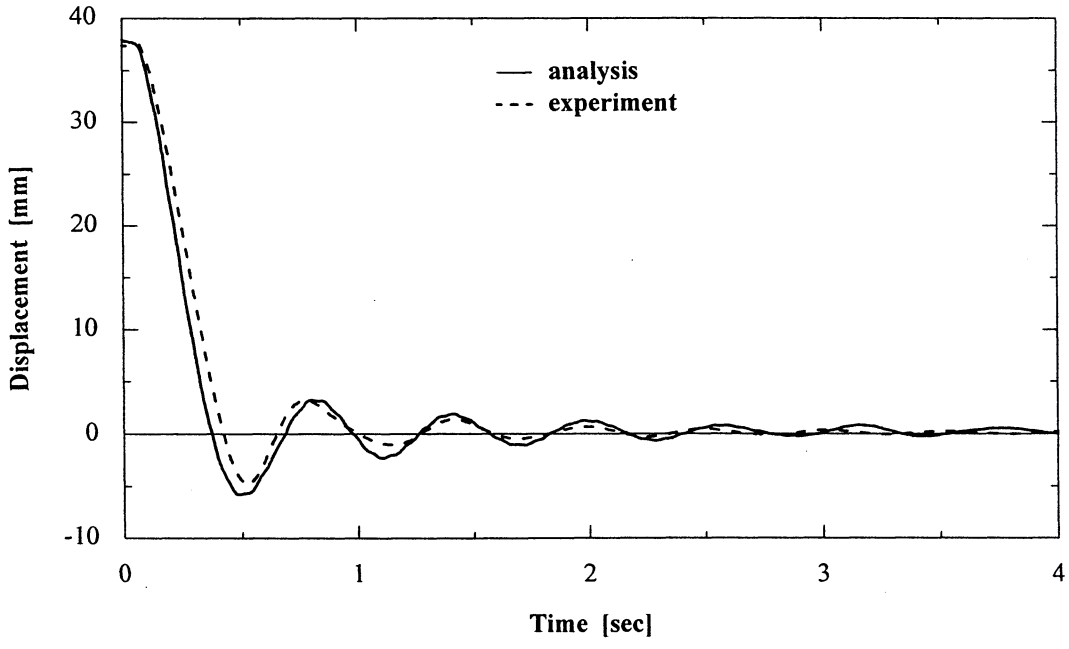


b)

**FIGURE 6-19 Comparison of Analytical and Experimental Results: a) Steel Bearings at Abutment, b) Rubber Bearings at Abutment**

## 6.6 Case Study 3: Broadway Bridge in Los Angeles - Retrofit Solution (Reichman, 1996)

The model of a bridge in Los Angeles is analyzed to validate the capacity of the computational platform to predict the response of bridge structures subjected to differential ground motion and assess the efficiency of retrofit using base isolation. The case study illustrates the utility of the program to cases, in which ground displacement (instead of the more usual acceleration) histories are available. Different support displacements were used to capture the effect of spatial variability of seismic motion on the response of the bridge. The case study demonstrates the ability of the program to model the behavior of nonlinear isolators with the "triaxial isolator" element. The analytical results also show the influence, which details like skewed supports and differential ground motion may have on the response of bridge structures.

### 6.6.1 Description of the Bridge Structure before Retrofitting

The bridge has seven spans ranging from 30 m to 39 m in length (figure 6-20a). The deck ribs are carried by concrete arches (figures 6-20b and 6-21a). The later are supported by abutments and bents on continuous foundations. Supports B1 to B5 are bents of the type shown in figures 6-20b and 6-21b. Abutment A1, bent B1, bent B2 and abutment A2 are skewed at angles of $48^{o}$, $54^{o}$, $61^{o}$ and $67^{o}$ respectively.

The bridge is modeled as a space frame system (figure 6-22). The deck (along with the ribs and arches) in each span is divided into four equal longitudinal segments having different section properties depending on the arch depth. The bents are modeled as beam elements with rigid arms to account for rigid zones in the deck-bent connection. The load-displacement behavior of soil surrounding the foundations was modeled using elastic springs with properties based on information provided by a geotechnical consulting company. The soil conditions vary along the length of the bridge from very stiff soils around bent B1 and supports A1 and A3 to very soft soils at some of the remaining support locations.

### 6.6.2 Retrofit Solution

Because of the low seismic capacity of the bents, a retrofit solution utilizing a PTFE isolation system is suggested. In this proposition, bents B1 to B5 are cut 2 m below the arch framing line (figure 6-20b). Eight isolators with elastomeric restoring springs are inserted in the cut elevating the deck on the isolation system. Consequently, the forces in the bents are expected to reduce due to transferring some of the horizontal load to supports A1-A3.

The isolators in bents B3, B4 and B5 are lumped and modeled by a single element. More than one isolator, however, is needed to capture the effect of the skewed configuration of bents B1 and B2 on the response of the isolation system and the bridge as a whole. Computer analysis models of the bridge before and after retrofitting are presented in figures 6-22 and 6-23.

### 6.6.3 Spatial Variability of Ground Excitation

The soil conditions at the supports vary significantly and so does the ground motion. The motions were calculated analytically considering soil amplification and wave-propagation effects. Non-linear soil response and associated residual displacements were not considered. Figure 6-25 shows that the displacements of the base of bents B2 through B5 and abutment 2 (all founded on soft soils) are amplified considerably more than the motion (figure 6-24) at supports on stiff soils - abutments A1, A3 and bent B1.

### 6.6.4 Analysis Results

To evaluate the seismic demand on the bridge and the influence of the variable ground motion, models of the original and retrofitted structure were analyzed for both uniform and variable ground motions.

#### 6.6.4.1 Uniform Motion

The bridge is extremely stiff in both the in-plane (X) and transverse (Z) directions. The period of vibration is about 0.2 sec before and 0.4 sec after the retrofit (figures 6-26 and 6-31). This relatively small increase is attributed to the fact that the superstructure is isolated only in-plane - at bents B1 through B5 and abutment A2. In the longitudinal direction, the retrofitted bridge vibrates mostly between supports A1 and A2 while floating (sliding) over the bents. The responses in the two horizontal directions interact through the skew of bents B1 and B2. In the case of uniform motion, there is no significant reduction in the shear forces in bents B1 to B5 due to isolation (figure 6-30). The displacements, on the other hand, increase significantly in the retrofitted structure (figure 6-26). The influence of isolation is more noticeable in the transverse direction especially in the bents, which are not skewed. This translates into a reduction of 50% in shear forces in bent B5 to a low of 20% in bent B1 (figure 6-35).

#### 6.6.4.2 Differential motion

In the case of differential support excitation of the bridge prior to retrofitting, the bents undergo larger in-plane relative displacements (figure 6-27) compared to the rigid base condition, resulting in significantly bigger shear forces (figure 6-29). The isolated structure, however, experiences much smaller shear forces (figure 6-30) due to the "floating behavior" mentioned earlier. The deformation of the bents is reduced at the expense of larger relative displacements of the isolators. The isolation has even stronger effect on the transverse response of the bridge in the case of differential ground motion. While the shear forces in the original bridge increase tenfold (figure 6-34) in comparison with the uniform base excitation case, the increase in the isolated bridge is only of the order of 2.5 (figures 6-33 and 6-35).

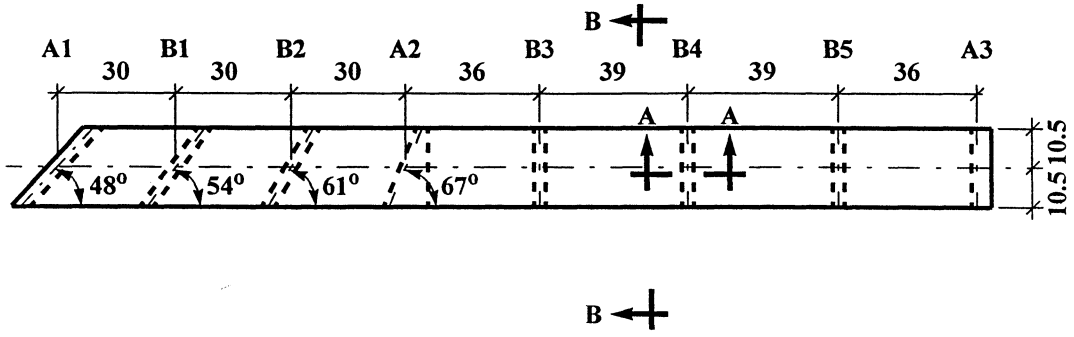


a)

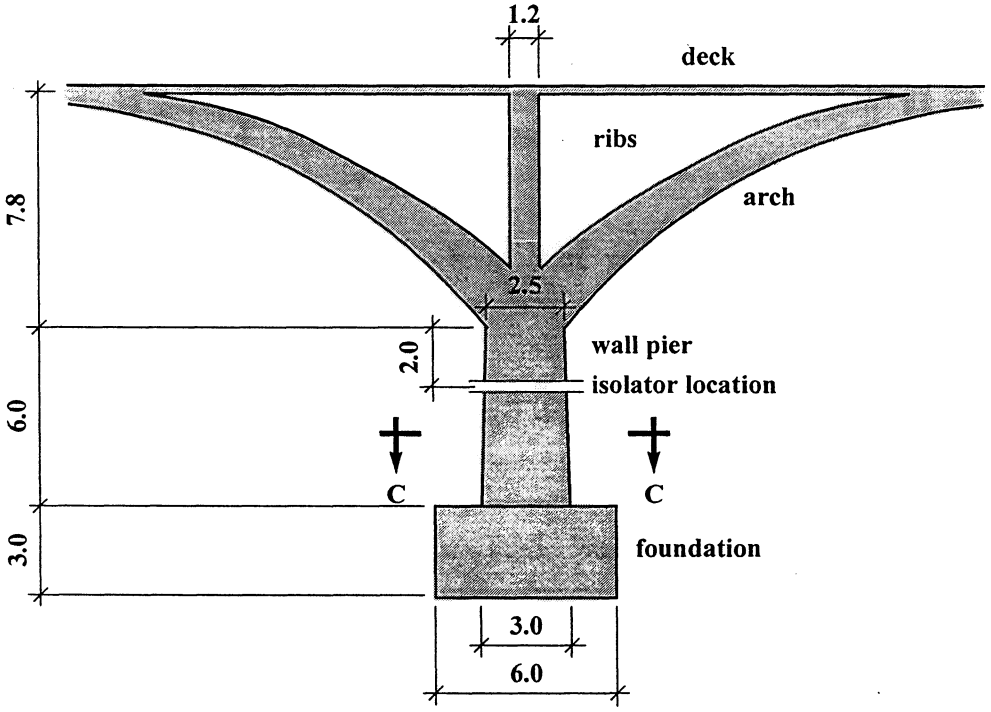


b) Section A-A (bent side view)

**FIGURE 6-20 Broadway Bridge: a) Plan, b) Cross Section of Typical Bent**

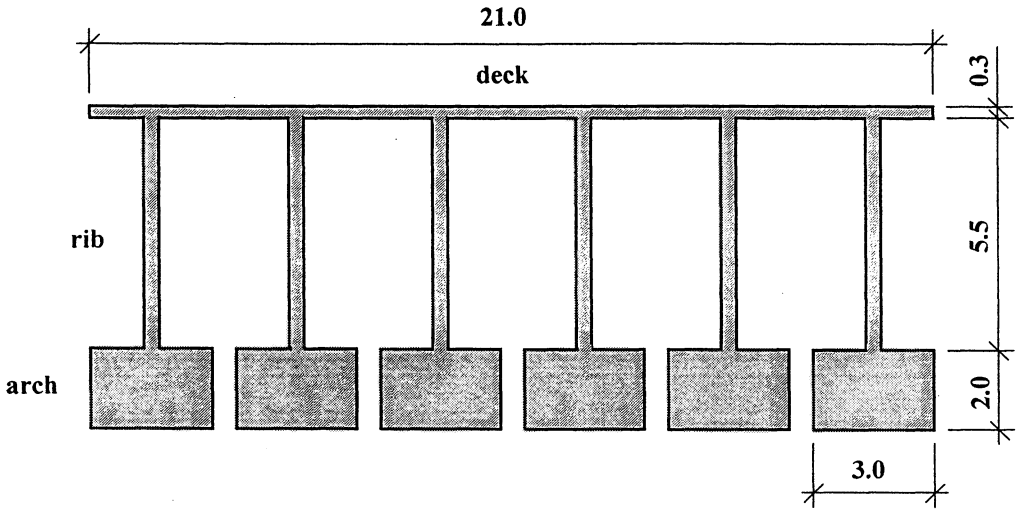


a) Section B-B

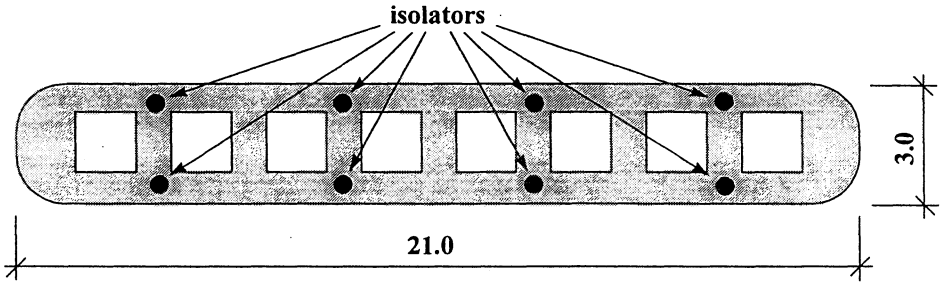


b) Section C-C

**FIGURE 6-21 Broadway Bridge: a) Cross Section of Deck, b) Cross Section of Typical Wall Pier**

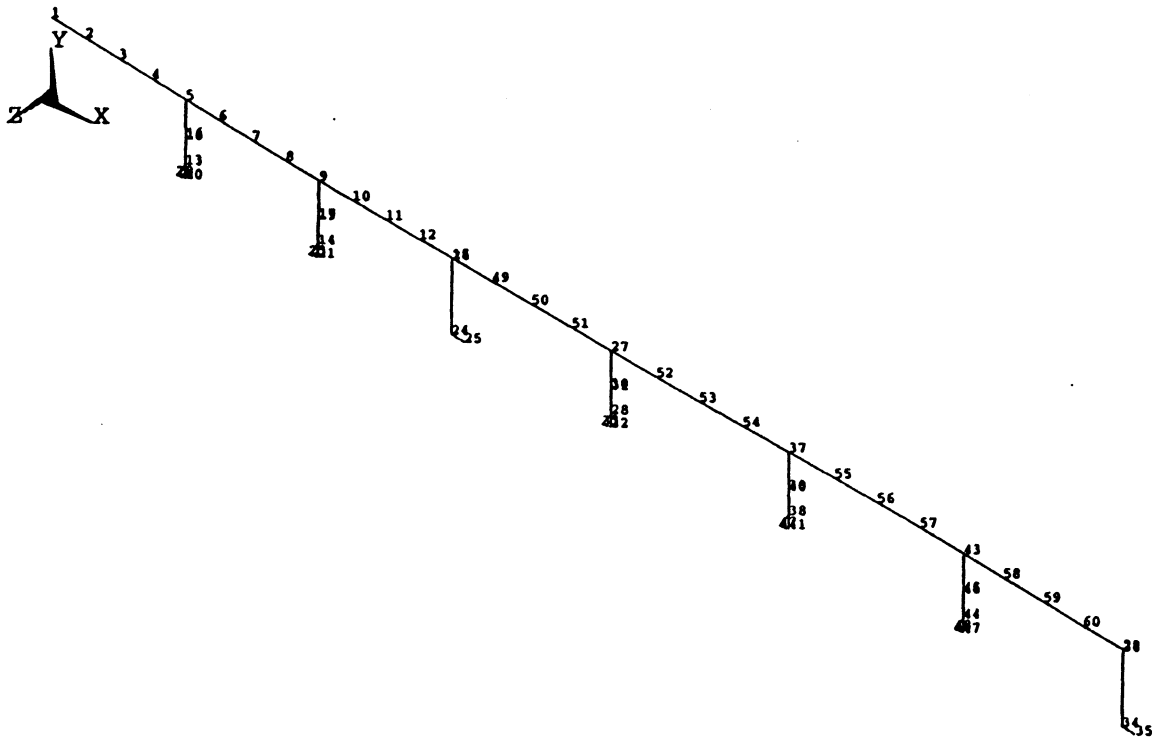


**FIGURE 6-22 Broadway Bridge: Computer Analysis Model of the Structure before Retrofitting**

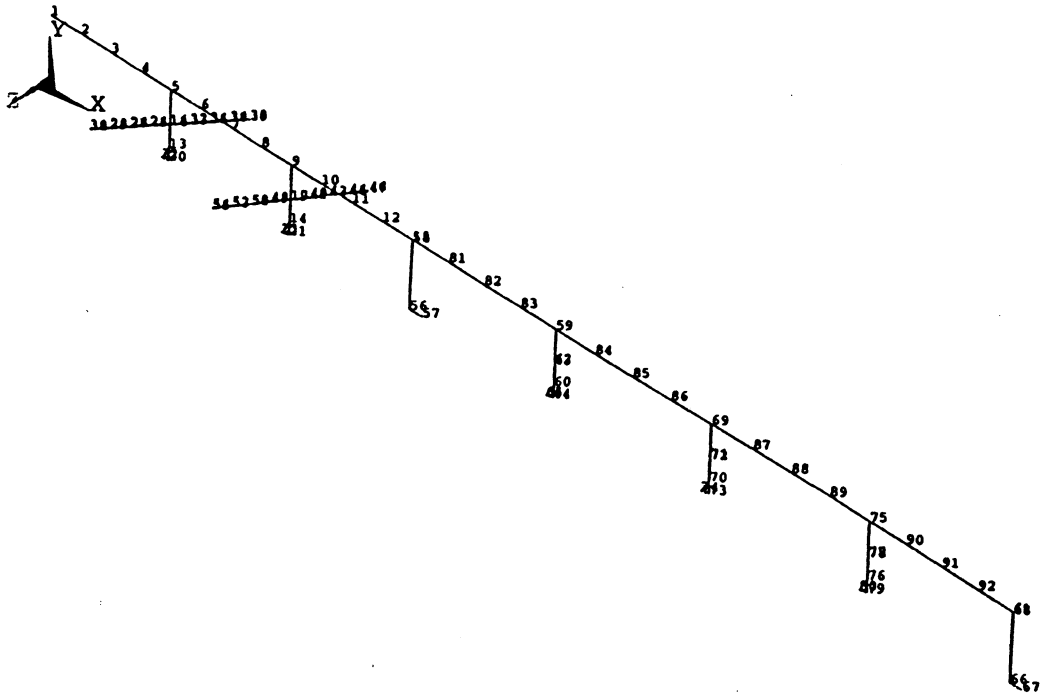

**FIGURE 6-23 Broadway Bridge: Computer Analysis Model of the Structure after Retrofitting**

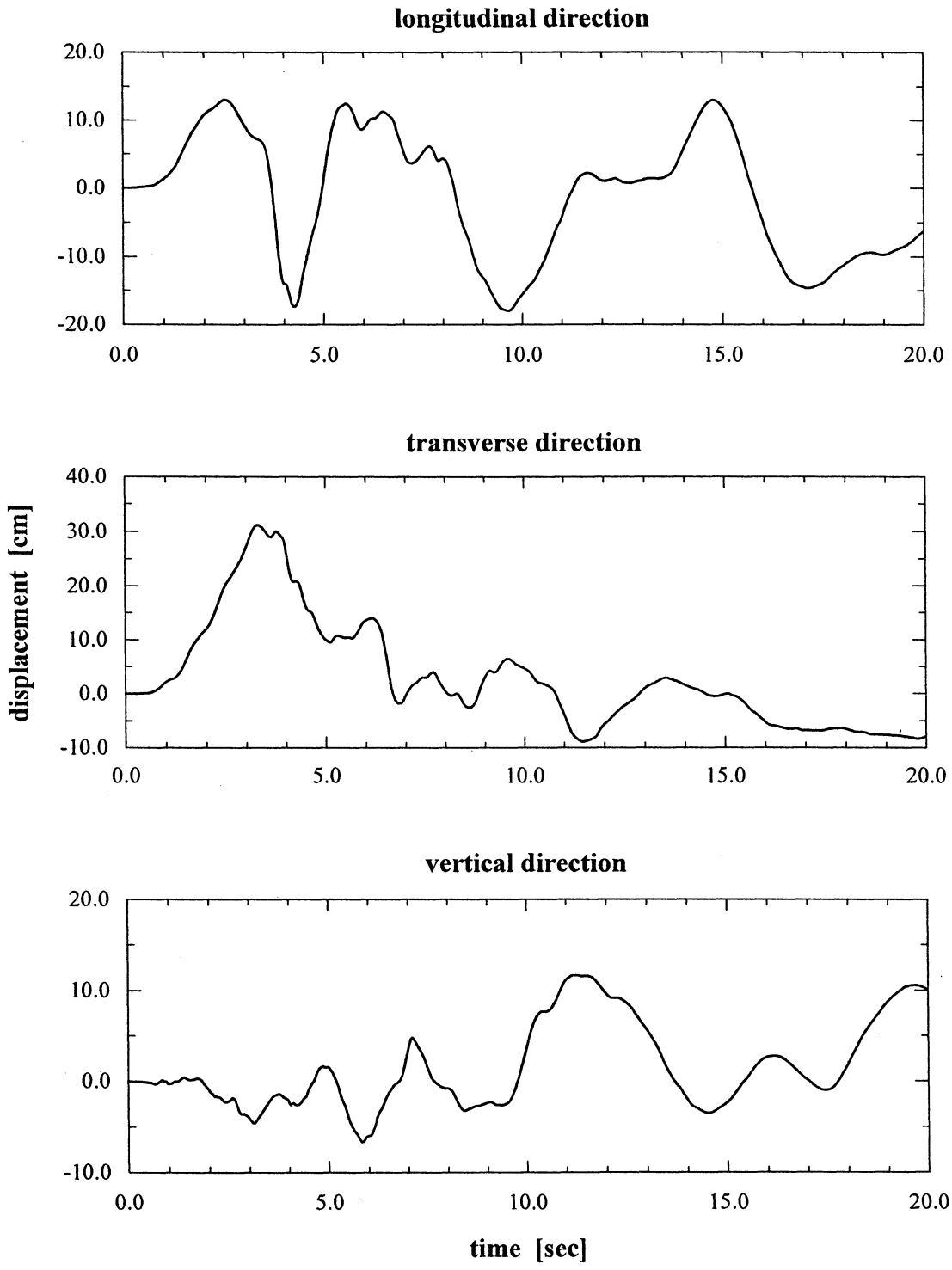


**FIGURE 6-24 Ground Displacements (Stiff Soil)**

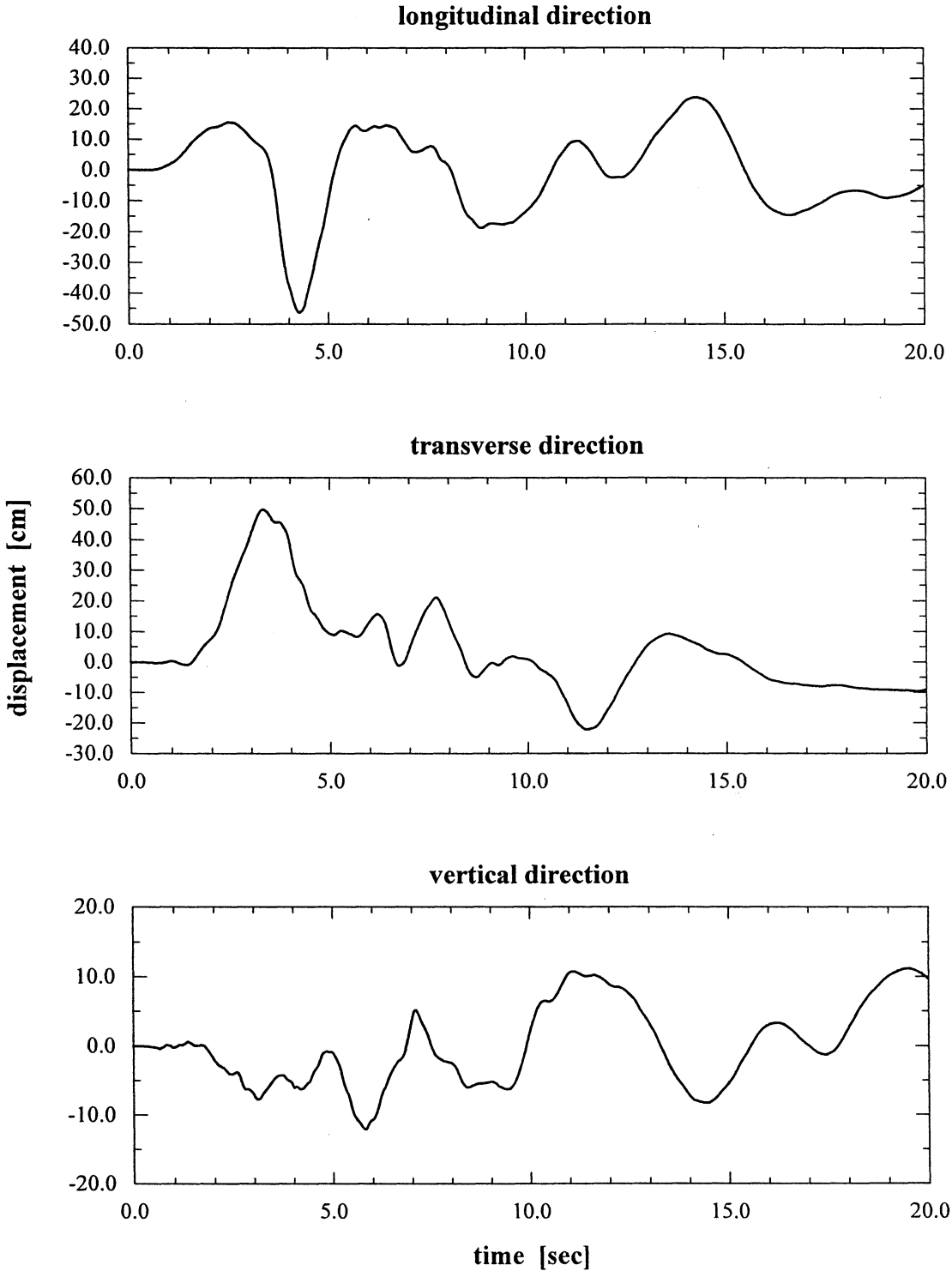


**FIGURE 6-25 Ground Displacements (Soft Soil)**

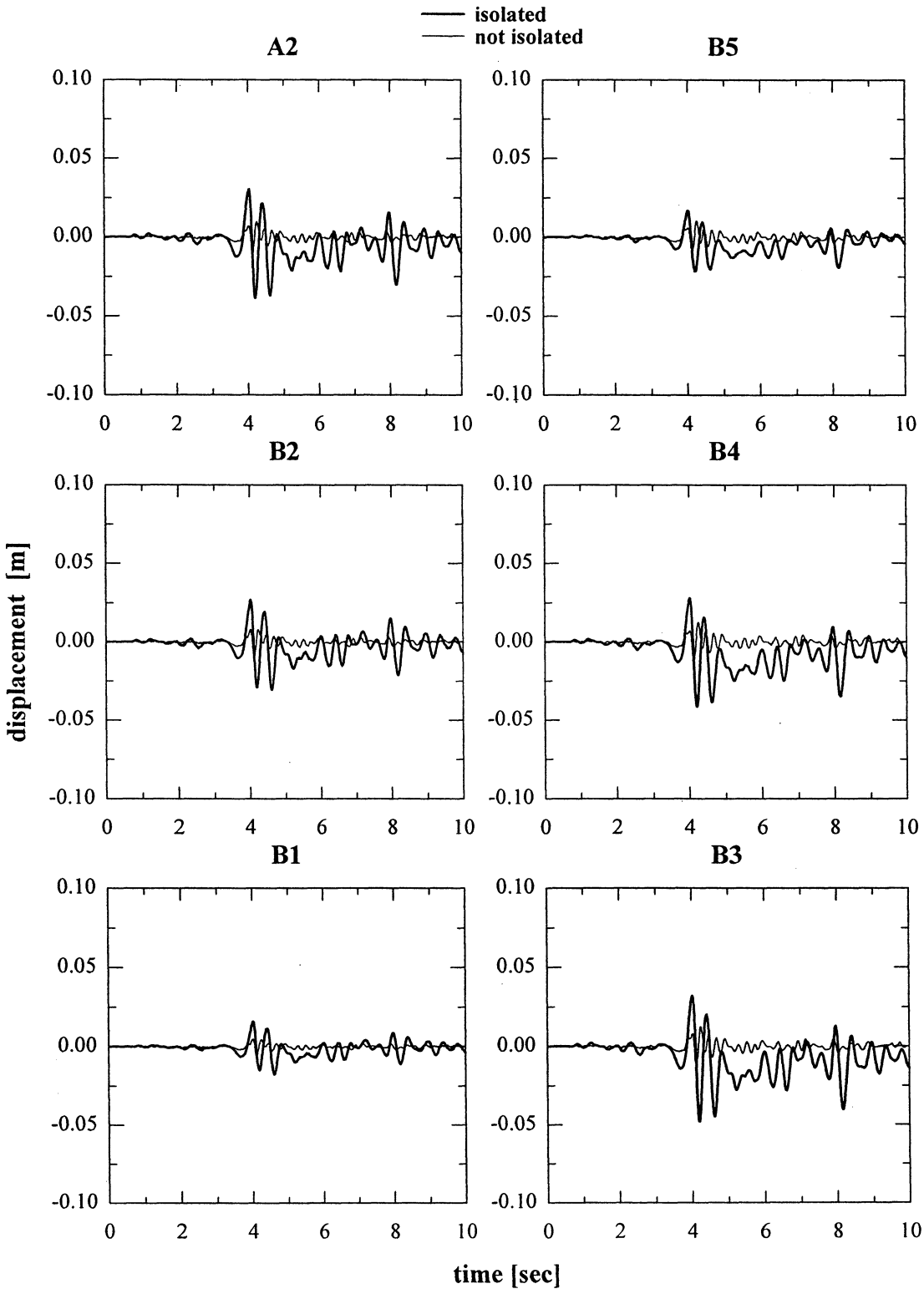


**FIGURE 6-26 Longitudinal Displacement of the Deck (at Pier Centerline) Relative to the Ground (Uniform Ground Motion)**

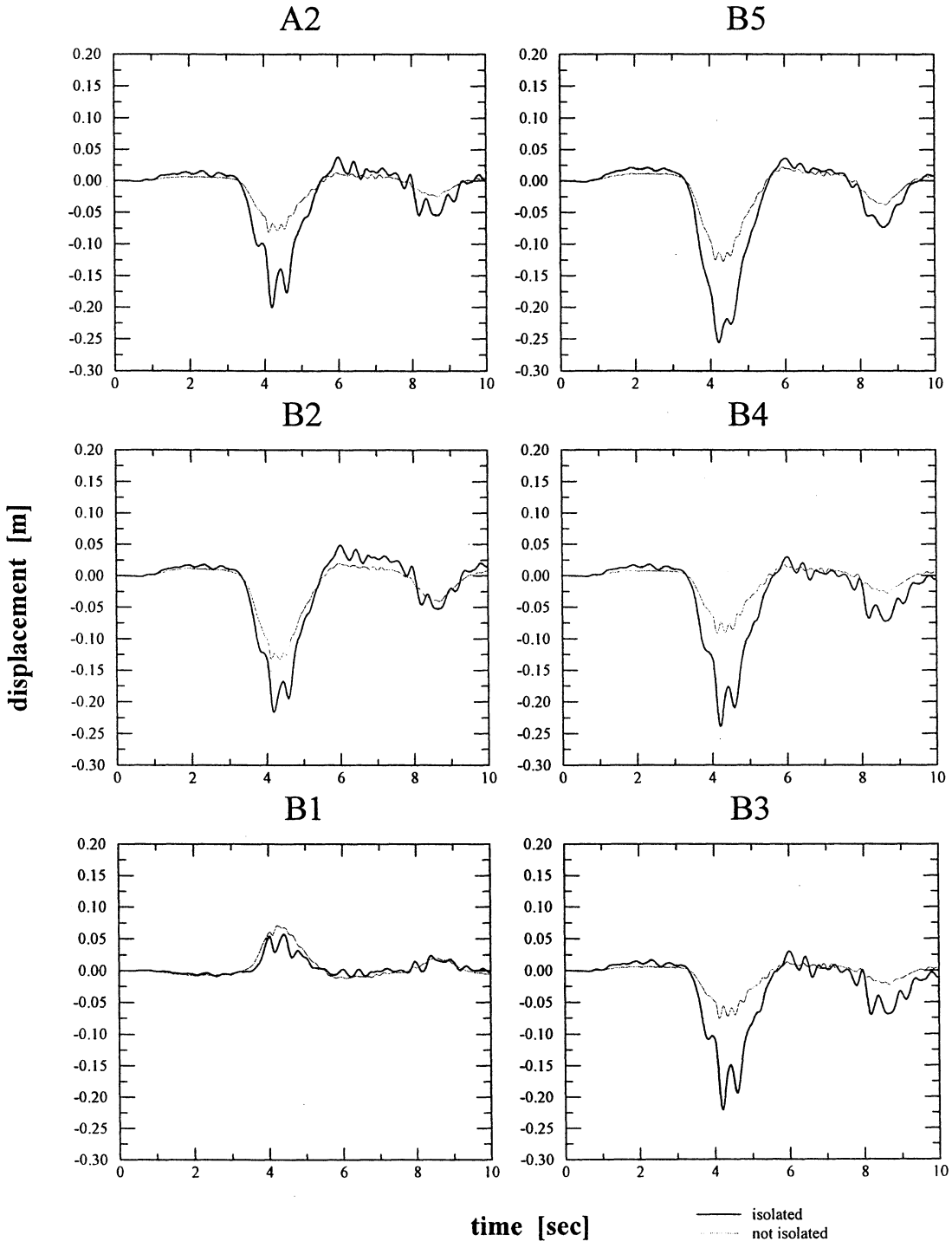


**FIGURE 6-27 Longitudinal Displacement of the Deck (at Pier Centerline) Relative to the Base (Variable Ground Motion)**

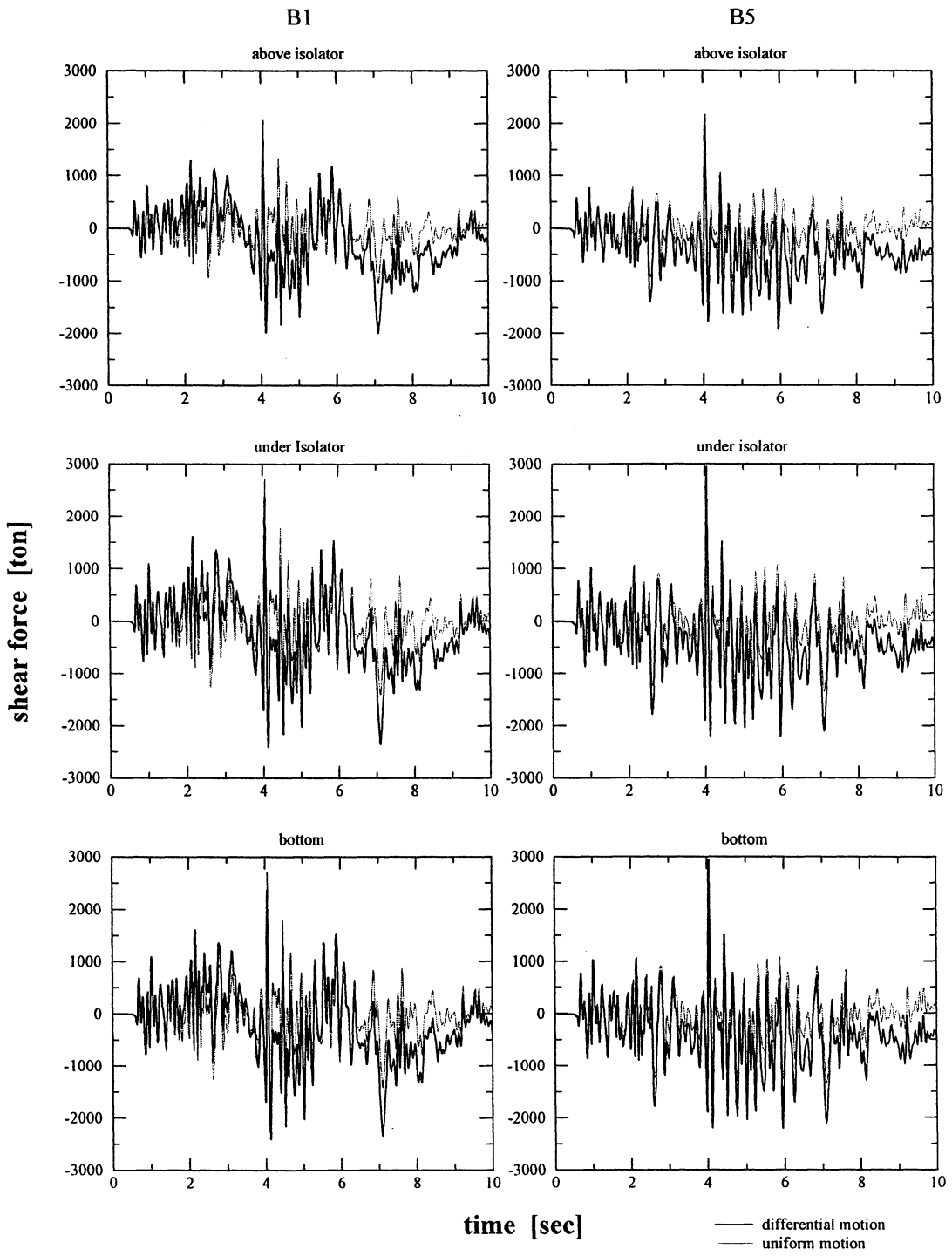


**FIGURE 6-28 Longitudinal Shear Forces in Piers B1 and B5 (Isolated Bridge)**

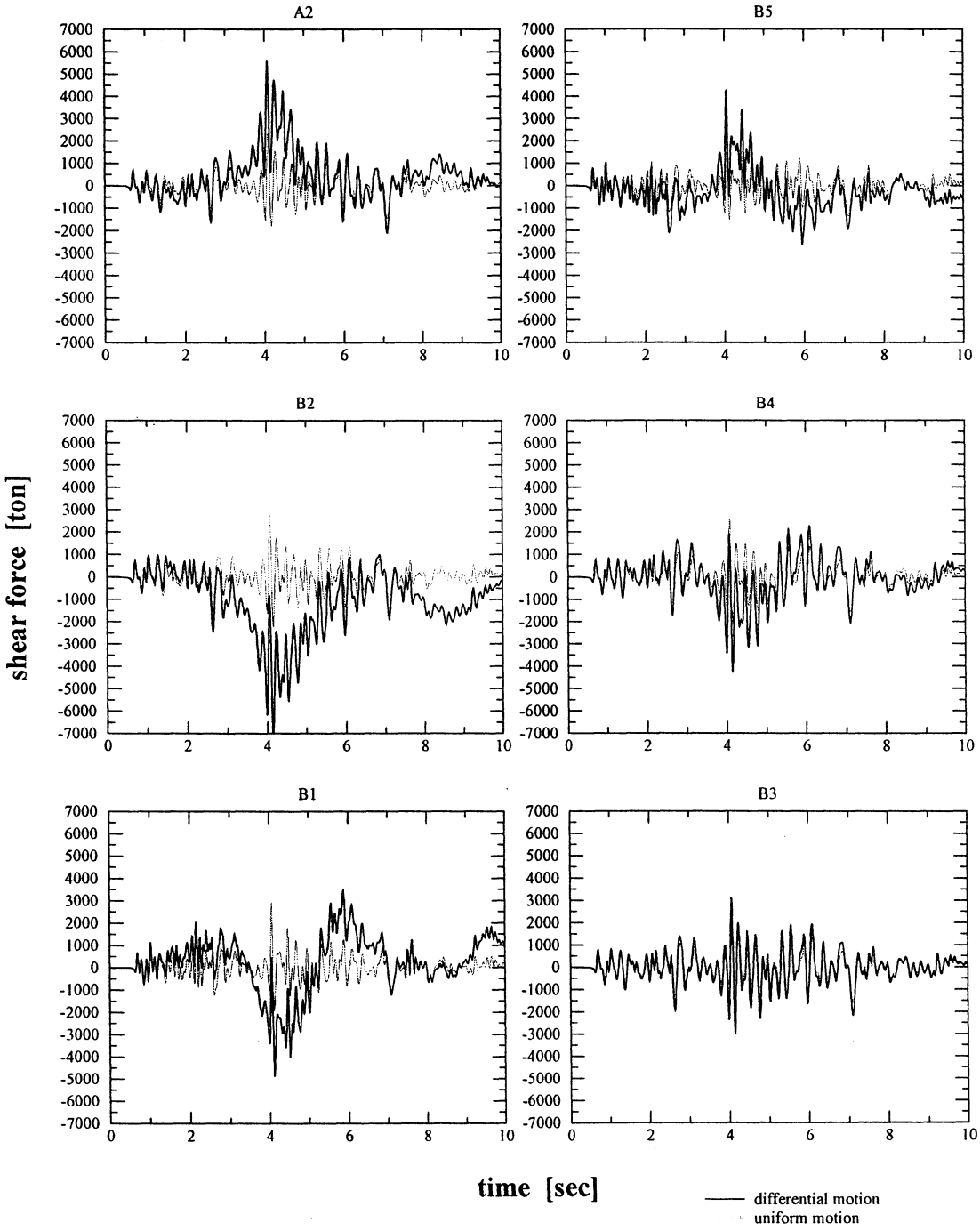


**FIGURE 6-29 Longitudinal Shear Forces at the Pier Bases (Non-Isolated Bridge)**

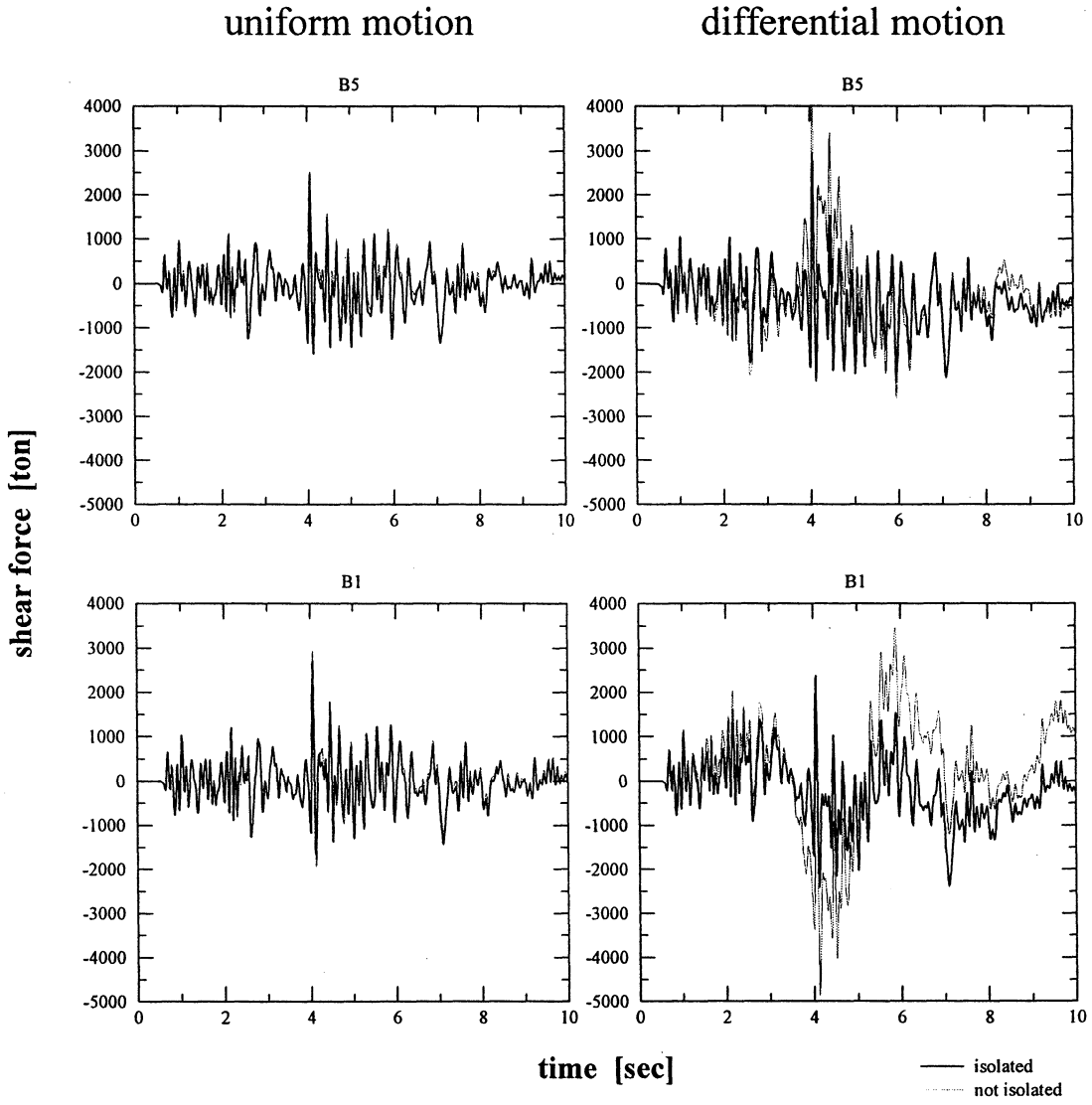


**FIGURE 6-30 Comparison of Longitudinal Shear Forces in Piers B1 and B5**

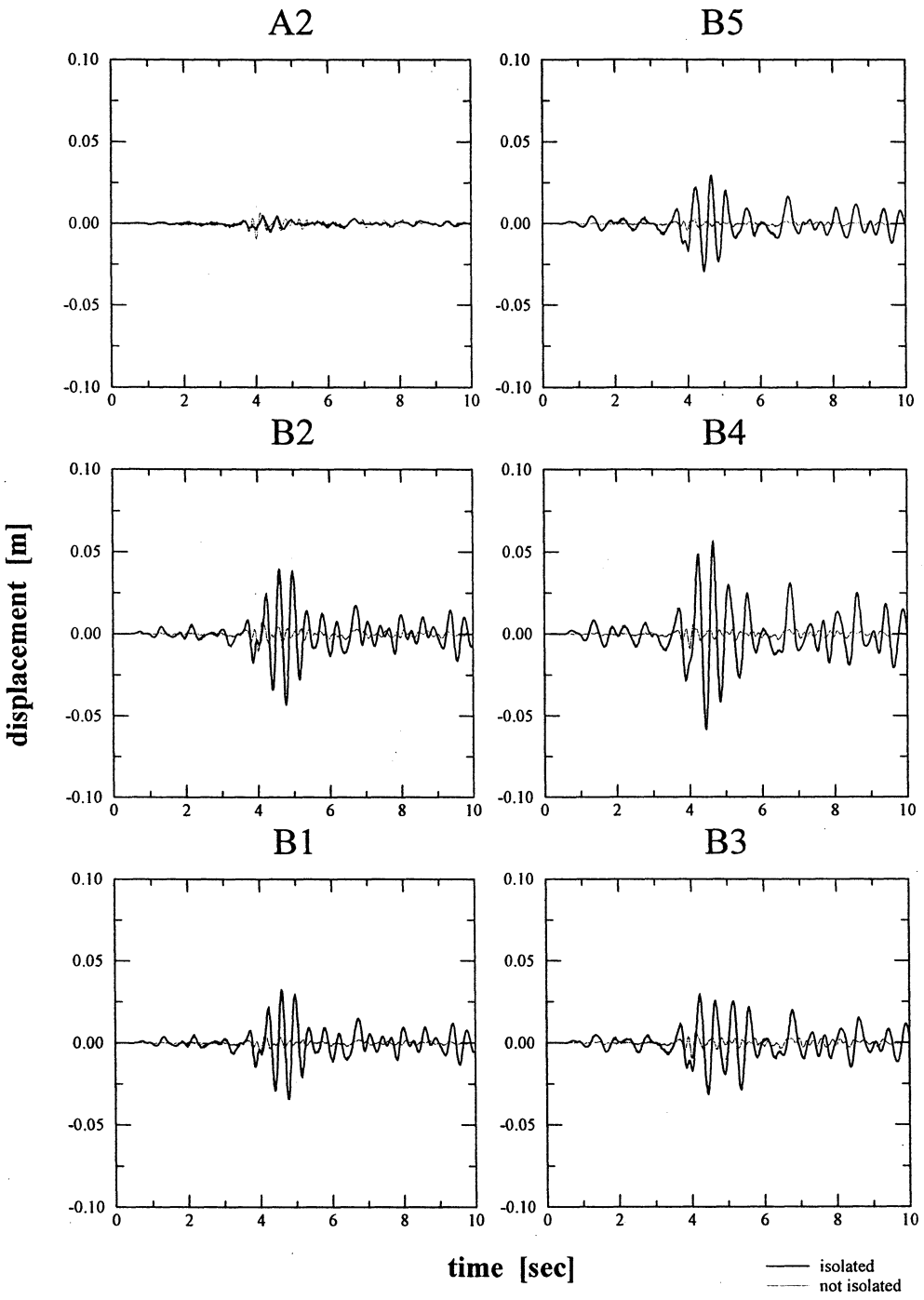


**FIGURE 6-31 Transverse Displacement of the Deck (at Pier Centerline) Relative to the Ground (Uniform Ground Motion)**

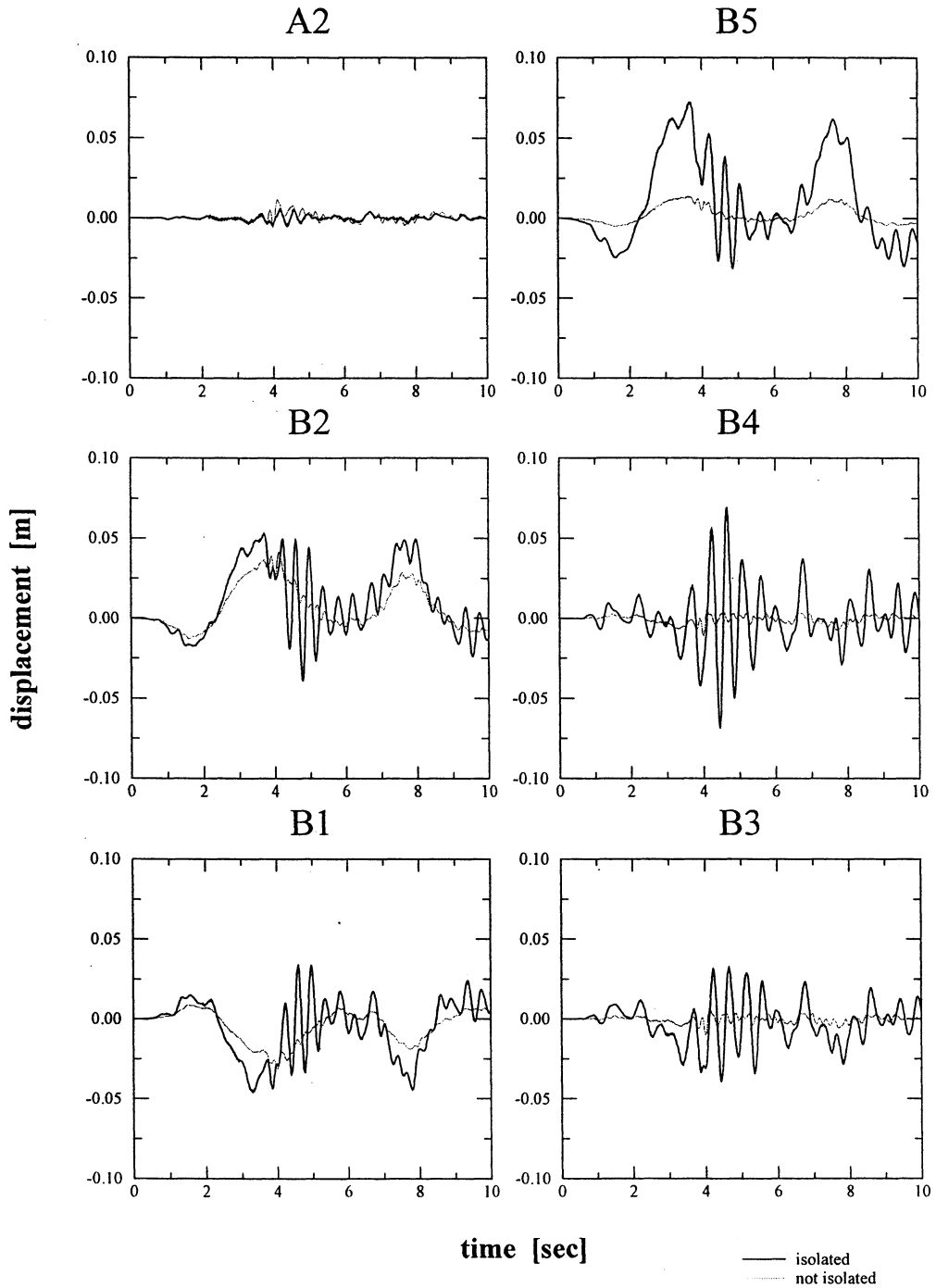


**FIGURE 6-32 Transverse Displacement of the Deck (at Pier Centerline) Relative to the Base (Variable Ground Motion)**

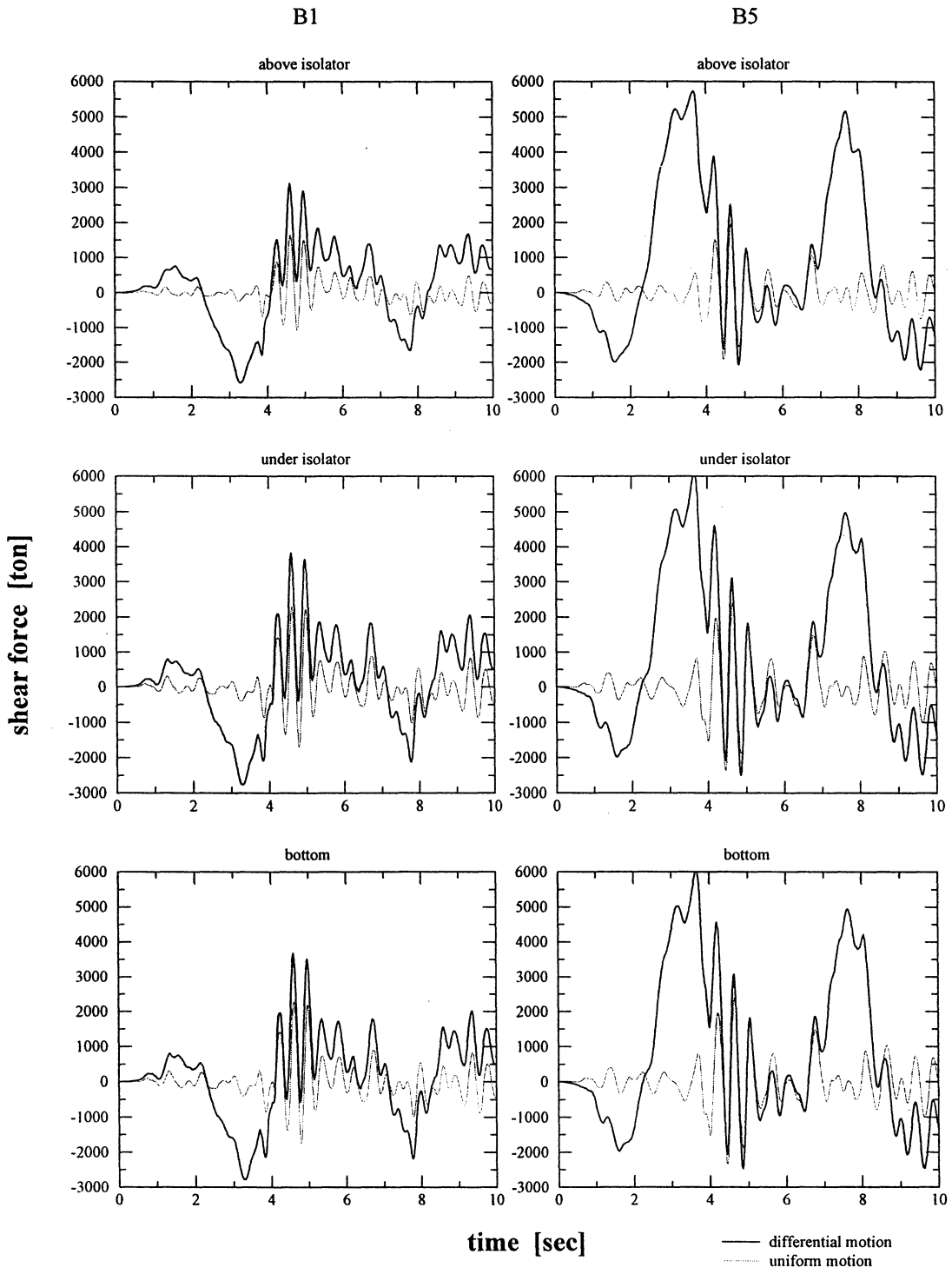


**FIGURE 6-33 Transverse Shear Forces in Piers B1 and B5 (Isolated Bridge)**

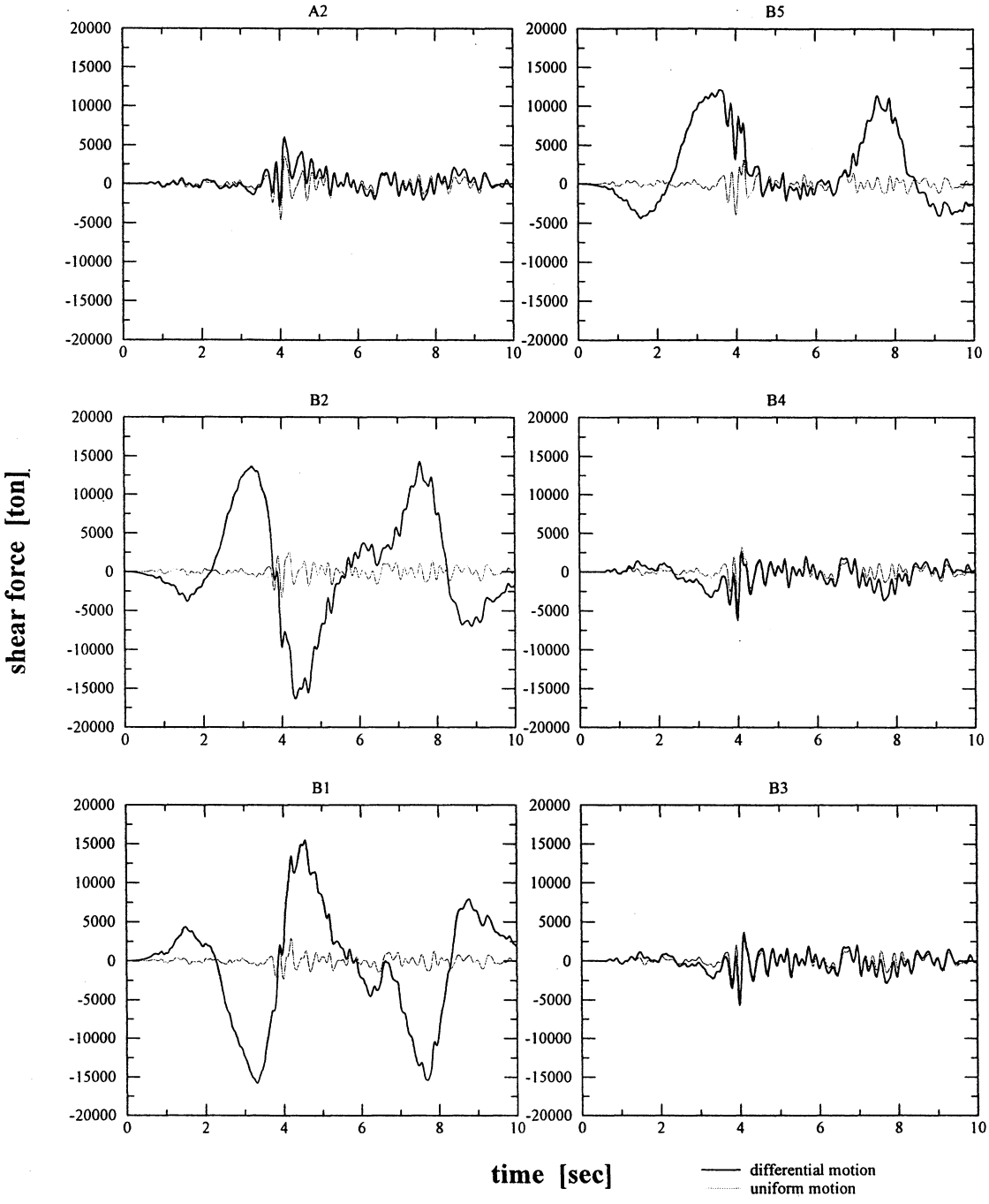


**FIGURE 6-34 Transverse Shear Forces at the Pier Bases (Non-Isolated Bridge)**

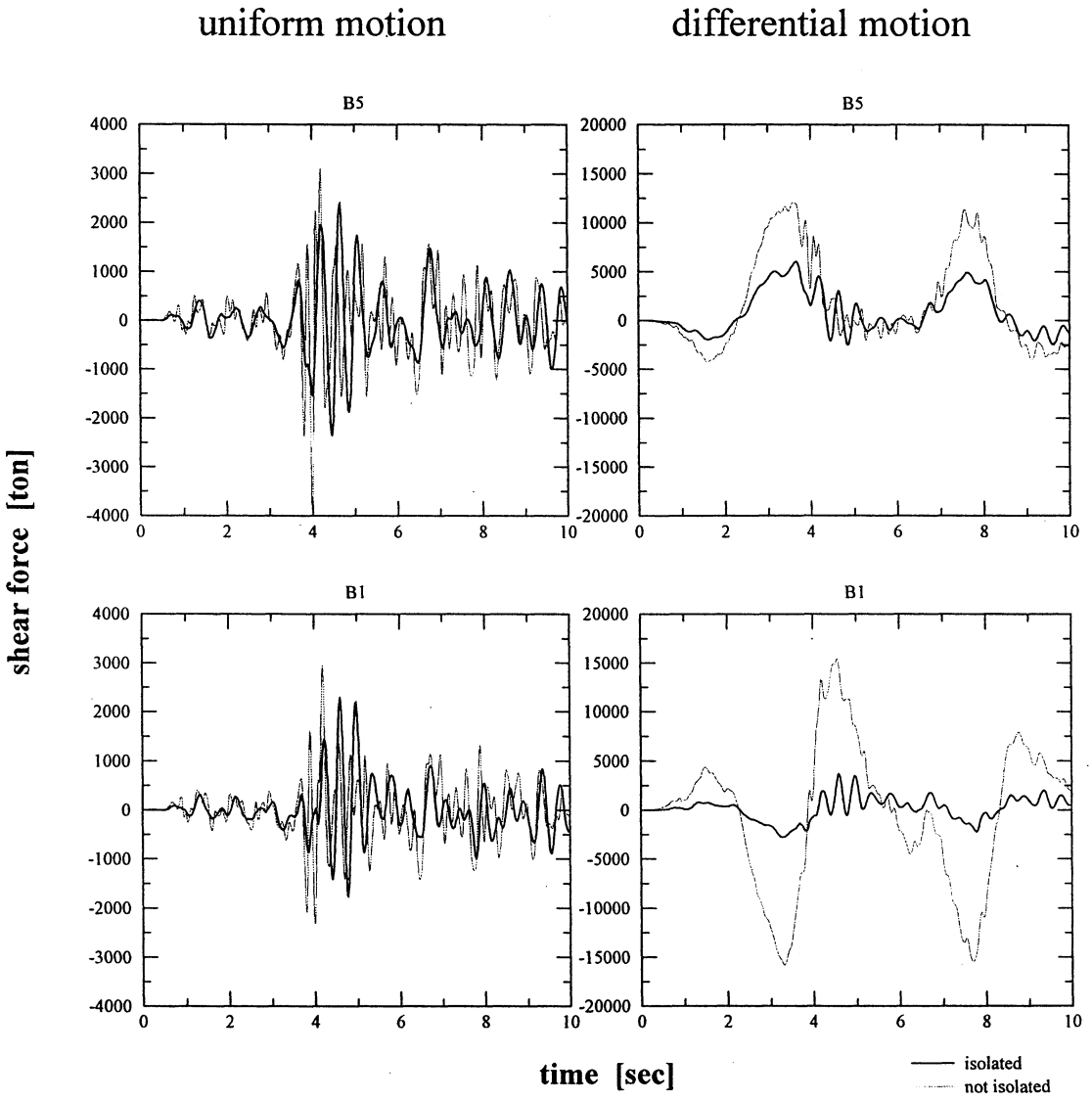


**FIGURE 6-35 Comparison of Longitudinal Shear Forces in Piers B1 and B5**

## 6.7 Case Study 4: Sixth Street Bridge in Los Angeles – Comparison of Retrofit Solutions (Reichman, 1996)

The model of large-size bridge over Los Angeles River is used to demonstrate the capability of the computer program to analyze the response of an isolated bridge with multiple restrained expansion joints. Investigation with simplified methods indicates that the seismic capacity of the bridge is smaller than the predicted demand in future events. The structure is a multiple arch reinforced concrete bridge with 12 spans ranging between 17.5 m and 35 m in length, supported on bents of heights between 8 m and 19 m (figure 6-36a). The deck, which is about 20-m wide and 5-m high, is carried by 5 parallel-arch girders in each span. The bridge was constructed with monolithic deck-abutment and deck-bent connections, but later had thermal expansion joints with 20-mm gaps built at bents b3, b6 and b9 (figure 6-36b).

The bridge is modeled as a space frame of elastic beam elements (figure 6-37). The nonlinear behavior is assumed localized in the isolation system and expansion joints. Each span is divided into two segments of equal length. Each deck segment is modeled by use of a single beam element. Coupling of motions of degrees of freedom is employed to create rigid blocks at the bent-deck connections. The expansion joints are modeled using multiple "bilinear gap" elements. The latter are transferred from the deck centerline to the actual locations of the restrainers by rigid body transformations (rigid arms).

### 6.7.1 Retrofit Solutions

Alternative 1: The bridge is fully isolated with teflon and stainless steel friction devices installed just under the cap beam of bents b3, b6 and b9 and above ground level in the remaining bents (figure 6-38a). A horizontal and vertical gap is created at the abutments and the isolation system is inserted between the bridge deck and the abutment. Elastomeric re-centering springs are installed near the sliding bearings (figure 6-38c). Since these springs are more flexible than the isolators, they do not transfer any vertical load. The isolated bridge is designed to have a natural period of vibration T = 2.5 sec. The relation between the initial vertical force $P_{initial}$ on the isolator and the restoring spring stiffness $K_{isolated}$ is:

$$K_{isolated} = \frac{4\pi^2}{T^2} \cdot \frac{P_{initial}}{g} \qquad (6\text{-}1)$$

The coefficient of friction is assumed to vary from 5% at zero velocity to 10% at velocity of 0.1 m/sec and higher. The isolation system is modeled using the triaxial isolation element ("isolator slider") in IDARC-BRIDGE.

Alternative 2: This retrofit scheme is similar to the one above with the only difference that the deck remains monolithically connected to the abutments. The second option is considered because of the significant cost involved in isolating the abutments.

### 6.7.2 Behavior of Bridge under Seismic Loading

Under seismic excitation, there is a transfer of force through the deck from the long to the short bents in the original bridge. The deformed shape of the bridge at $t = 2\,sec$ shows that bents b7 to b10 experience the largest displacements in contrast to bents b1, b2 and b3 (figure 6-39a). At the same time, the displacements of the isolated bridge (retrofit solution 1) are almost uniform indicating that the deck is floating over the isolators (figure 6-39b). Consequently, the forces in bents b9 and b10 are almost three times smaller than those in the original bridge (figure 6-41). The deformed shape of a typical bent frame before and after the retrofit is plotted in figure 6-40. In the original bridge, the movement of the cap beam causes bending and shearing of columns. In the isolated case, the transverse displacement is shared between the isolation system and the bent structure.

In conclusion, the response of the bridge in the alternative retrofit cases is comparable except for the transverse displacements of the two end spans (figure 6-46). Similarly, the shear forces in the bent columns are alike except for the bents adjacent to the abutments (figure 6-43). Both arrangements of the isolation system result in significant reduction of the force demand on the bents at the expense of increased displacement demand of the superstructure (alternatives 1 and 2) and force demand on the abutments (alternative 2) in comparison with the original structure (figures 6-41, 6-42, 6-44 and 6-45).

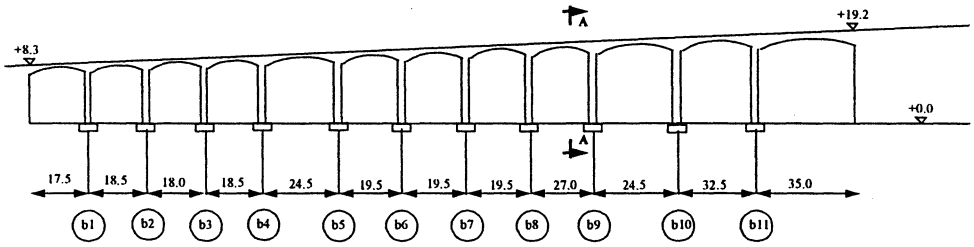


a) Bridge Side View (As Built)

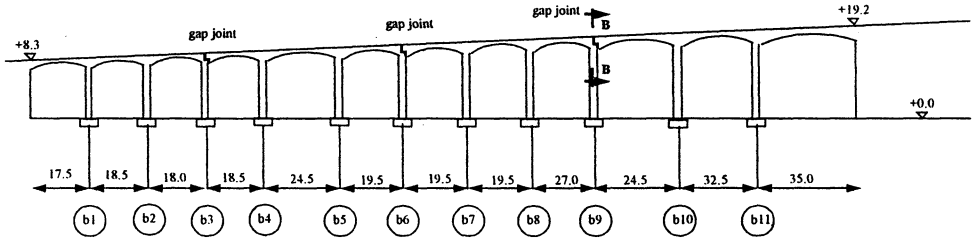


b) Bridge Side View With Expansion Joint (After first retrofit)

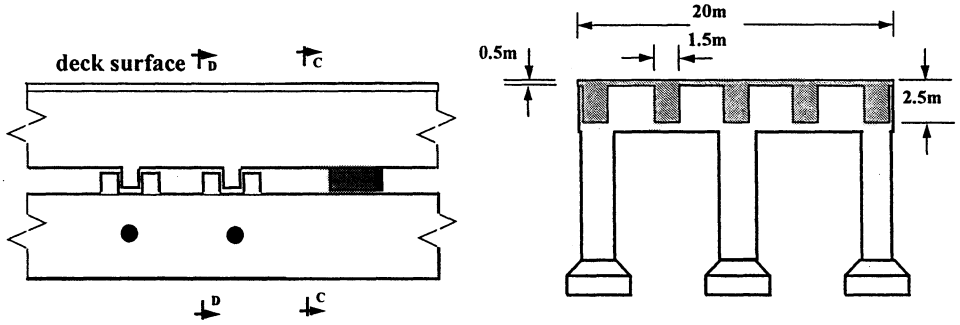


Sec B-B
Section through joint

Sec A-A
Cross Section

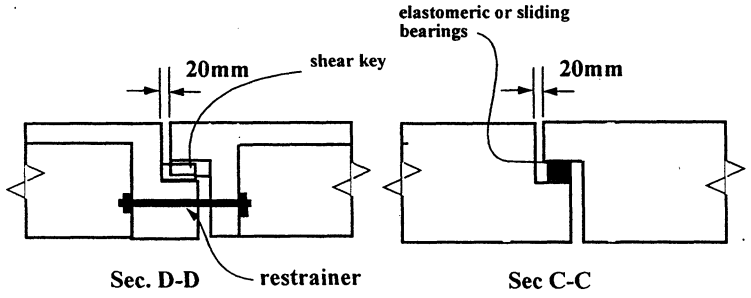


Sec. D-D

Sec C-C

**FIGURE 6-36 Sixth Street Bridge: a) As Built, b) after First Retrofit with Expansion Joints**

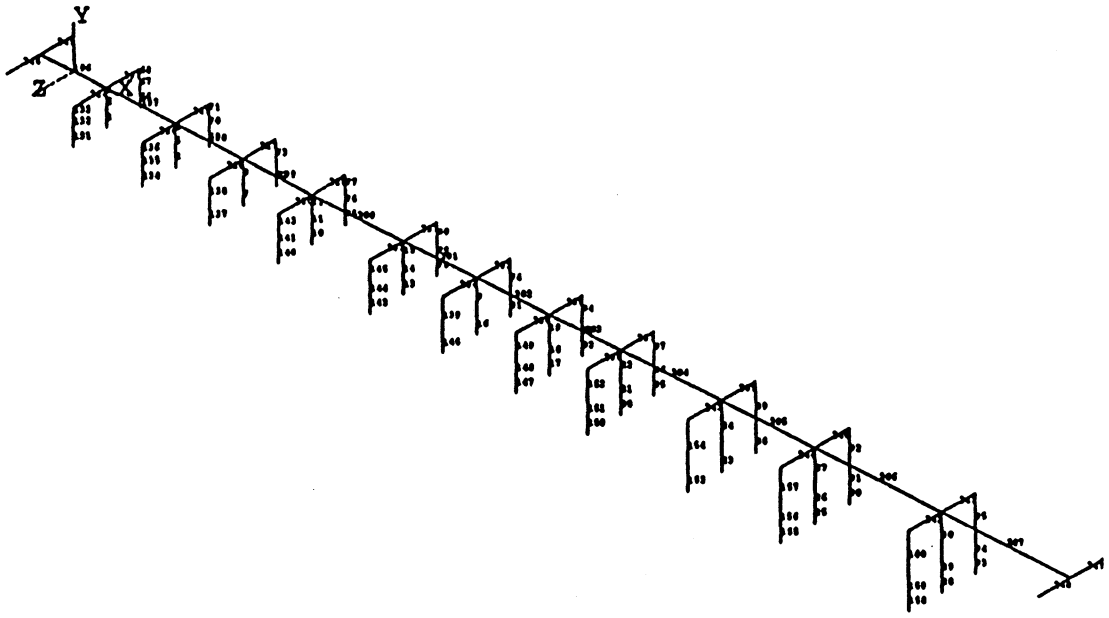


**FIGURE 6-37 Sixth Street Bridge: Computer Analysis Model**

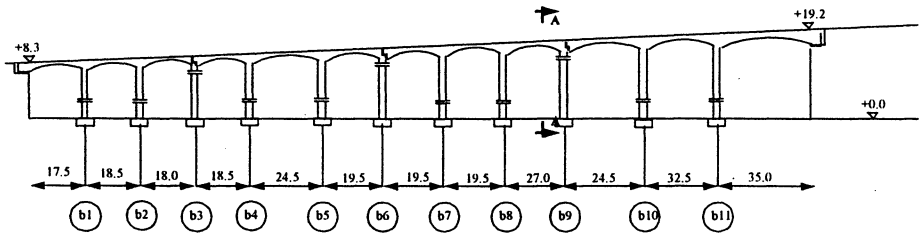


**a) Base Isolated Bridge With Expansion Joints**

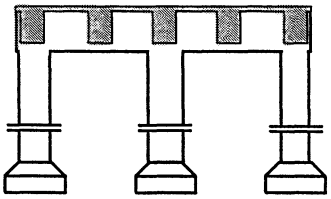

Sec A-A

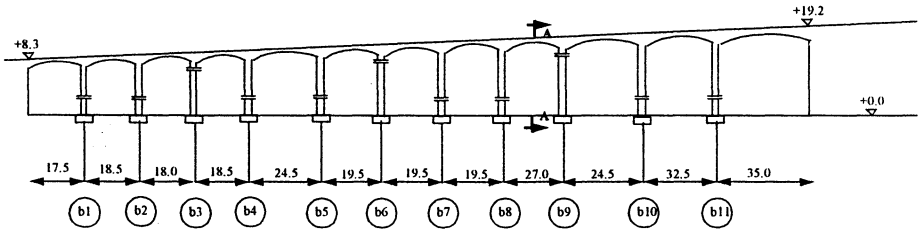


**b) Base Isolated Bridge Without Expansion Joints**

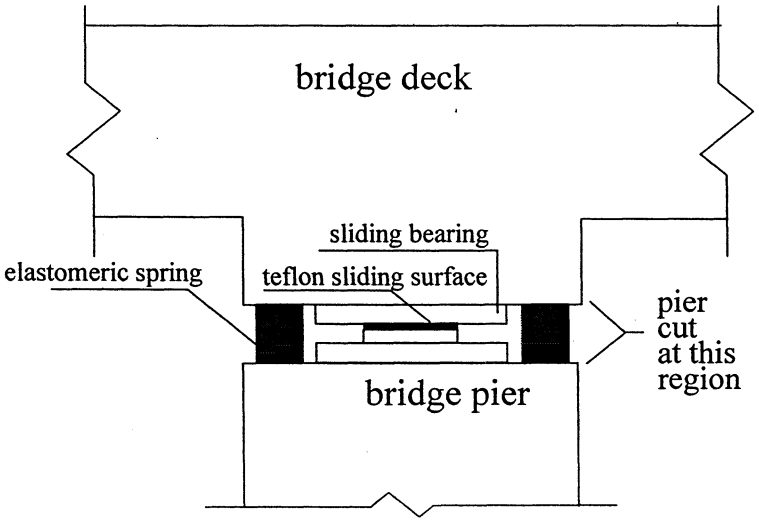


**c) Retrofit Isolation System Detail**

**FIGURE 6-38 Sixth Street Bridge: Base-Isolated Structure with and without Expansion Joints**

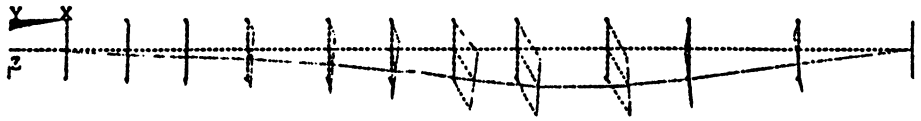

(a)

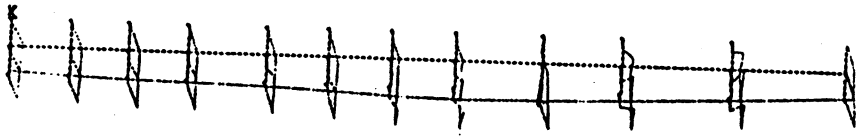

(b)

**FIGURE 6-39 Sixth Street Bridge: Displaced Shape for Transverse Loading: a) without Base Isolation, b) with Base Isolation**

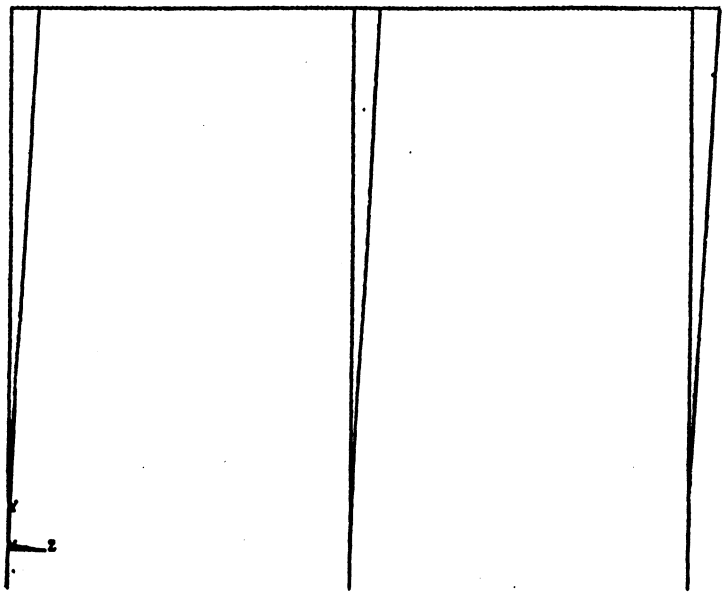

(a)

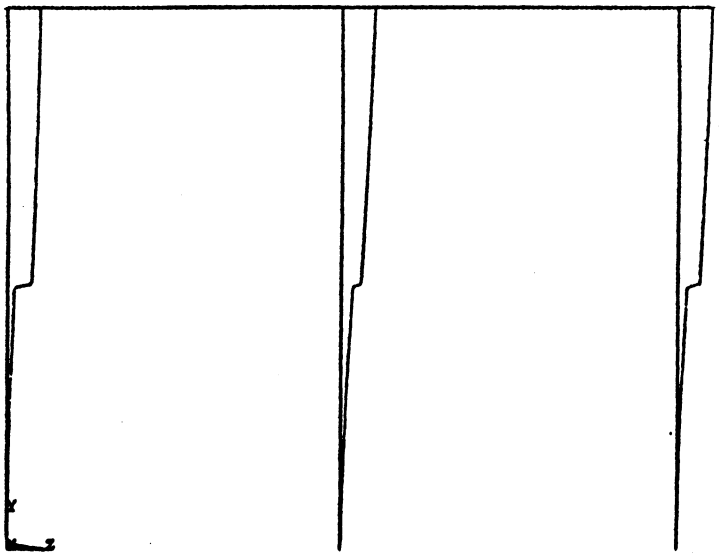

(b)

**FIGURE 6-40 Sixth Street Bridge: Displaced Shape of a Typical Frame for Transverse Loading: a) without Base Isolation, b) with Base Isolation**

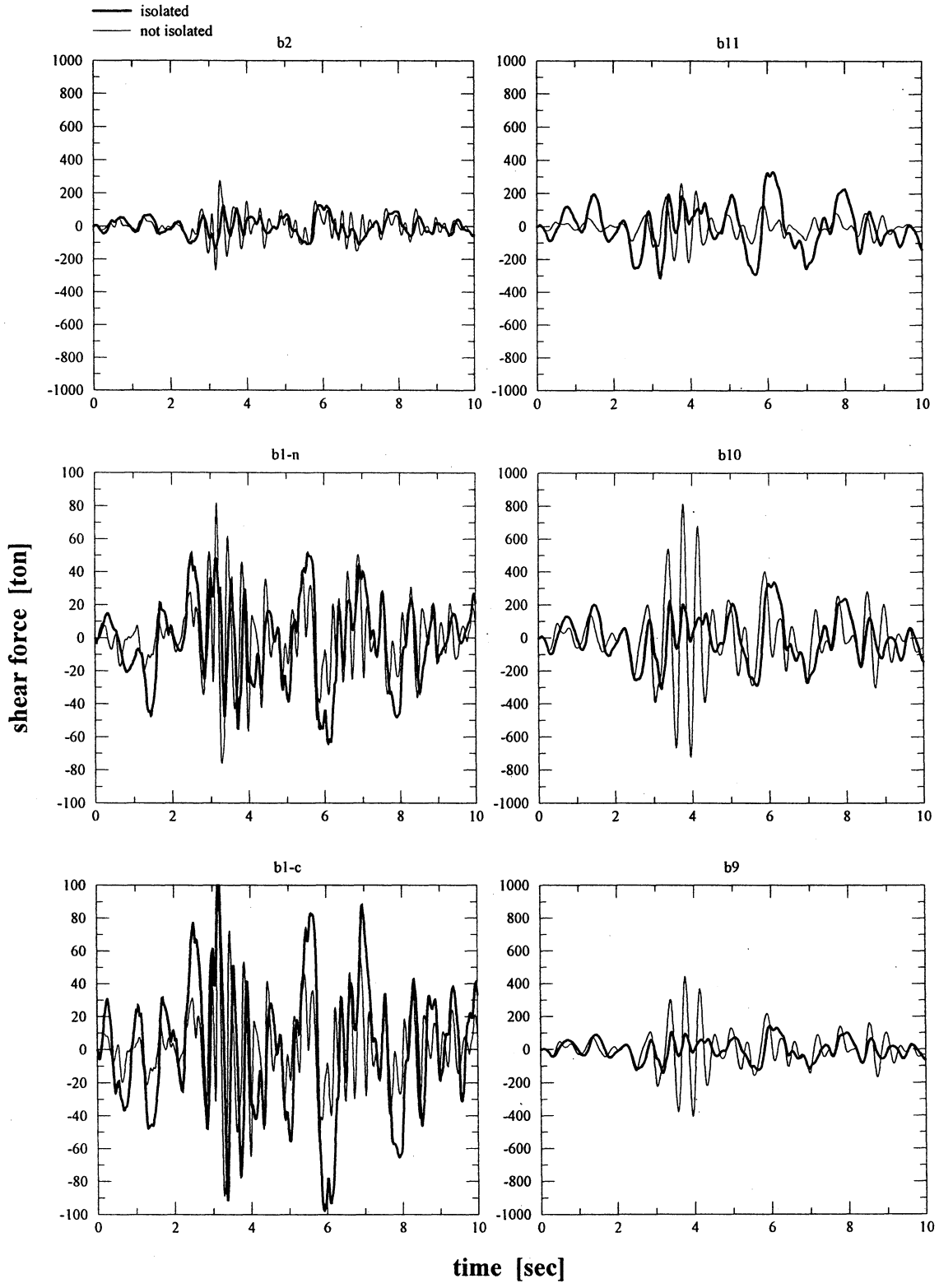


**FIGURE 6-41 Sixth Street Bridge: Comparison of Bent Shear Forces before and after Retrofit (Alternative 1)**

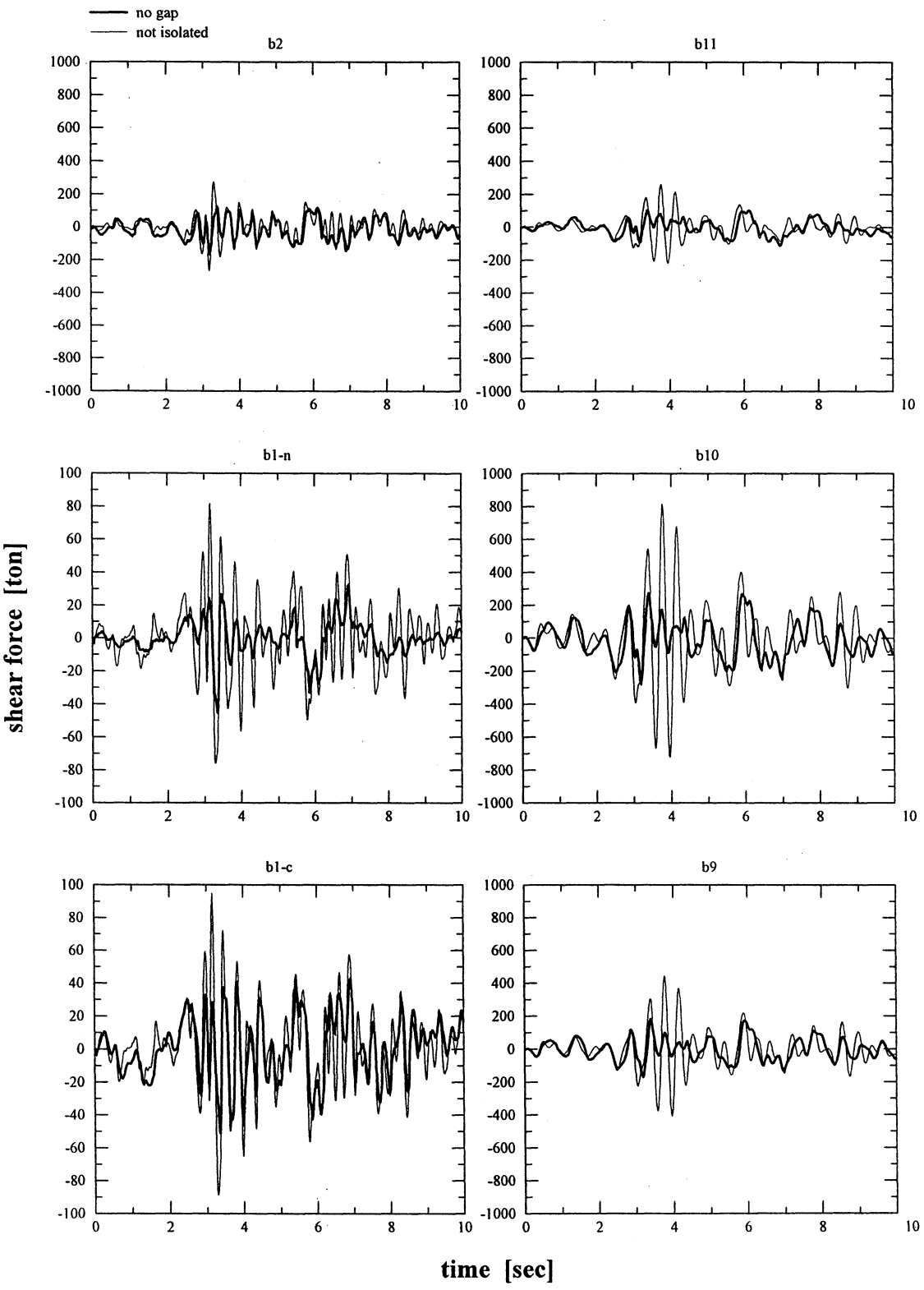


**FIGURE 6-42 Sixth Street Bridge: Comparison of Bent Shear Forces before and after Retrofit (Alternative 2)**

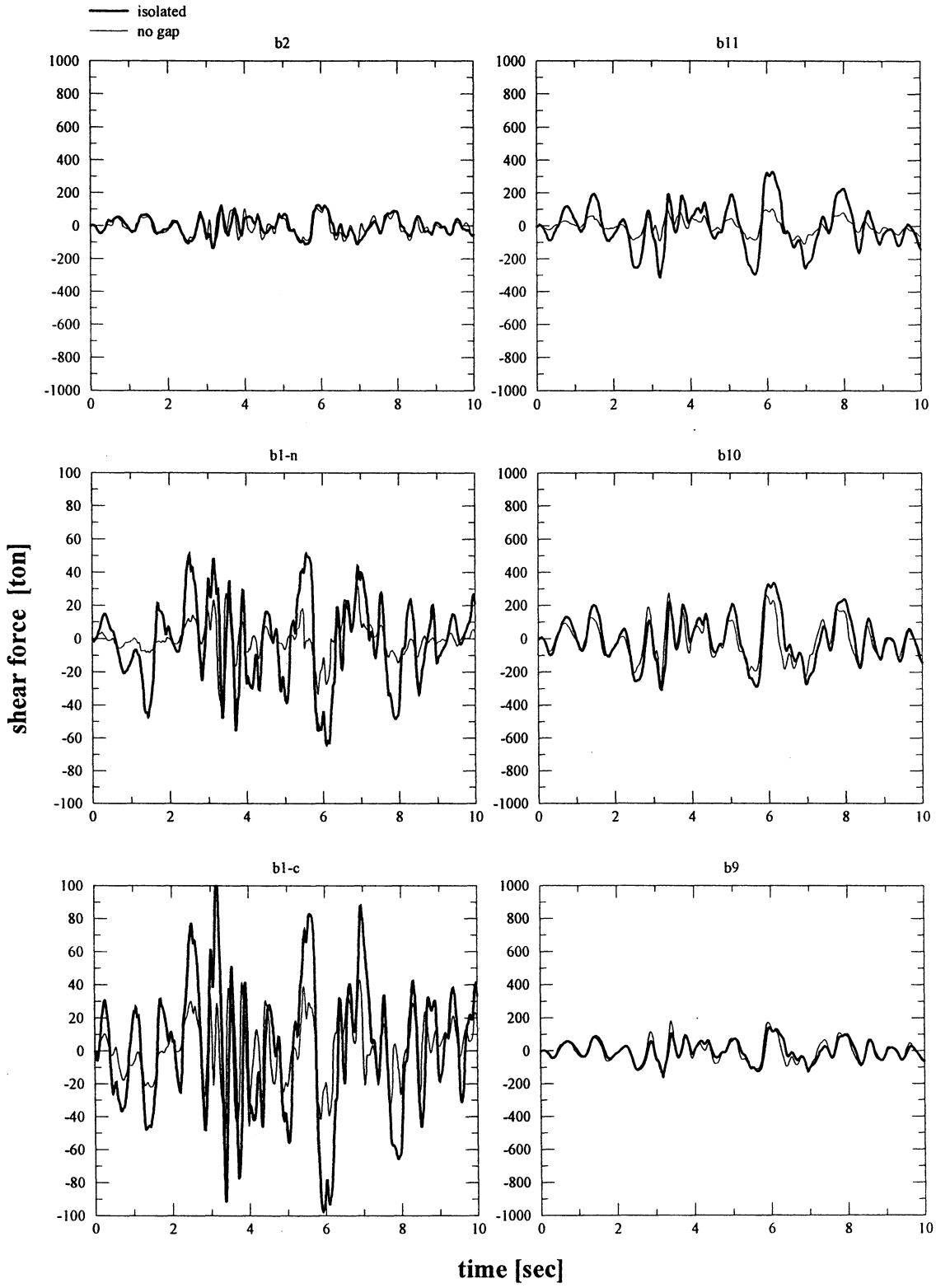


**FIGURE 6-43 Sixth Street Bridge: Comparison of Bent Shear Forces in Retrofit Alternatives 1 and 2**

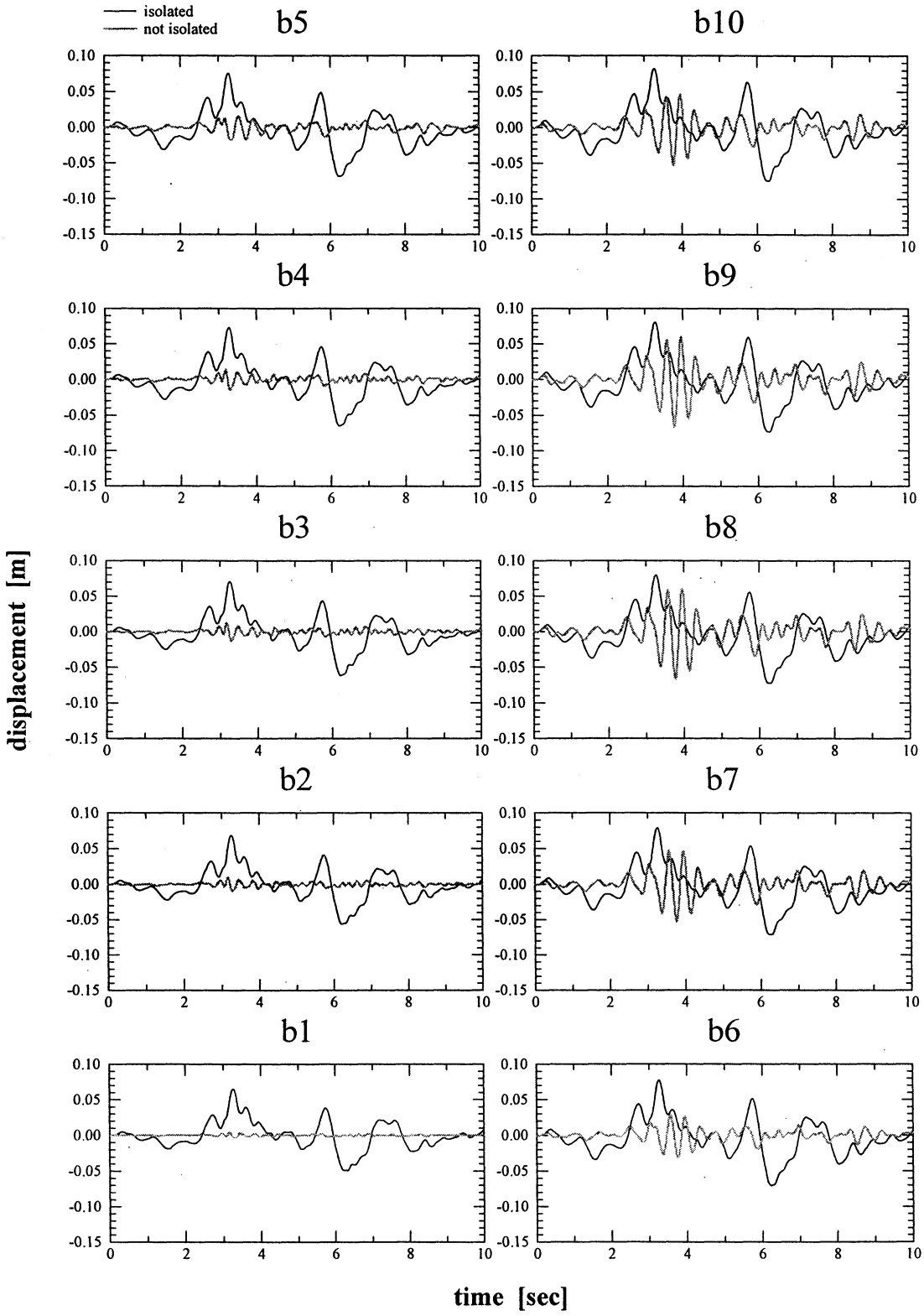


**FIGURE 6-44 Sixth Street Bridge: Comparison of Deck Displacements before and after Retrofit (Alternative 1)**

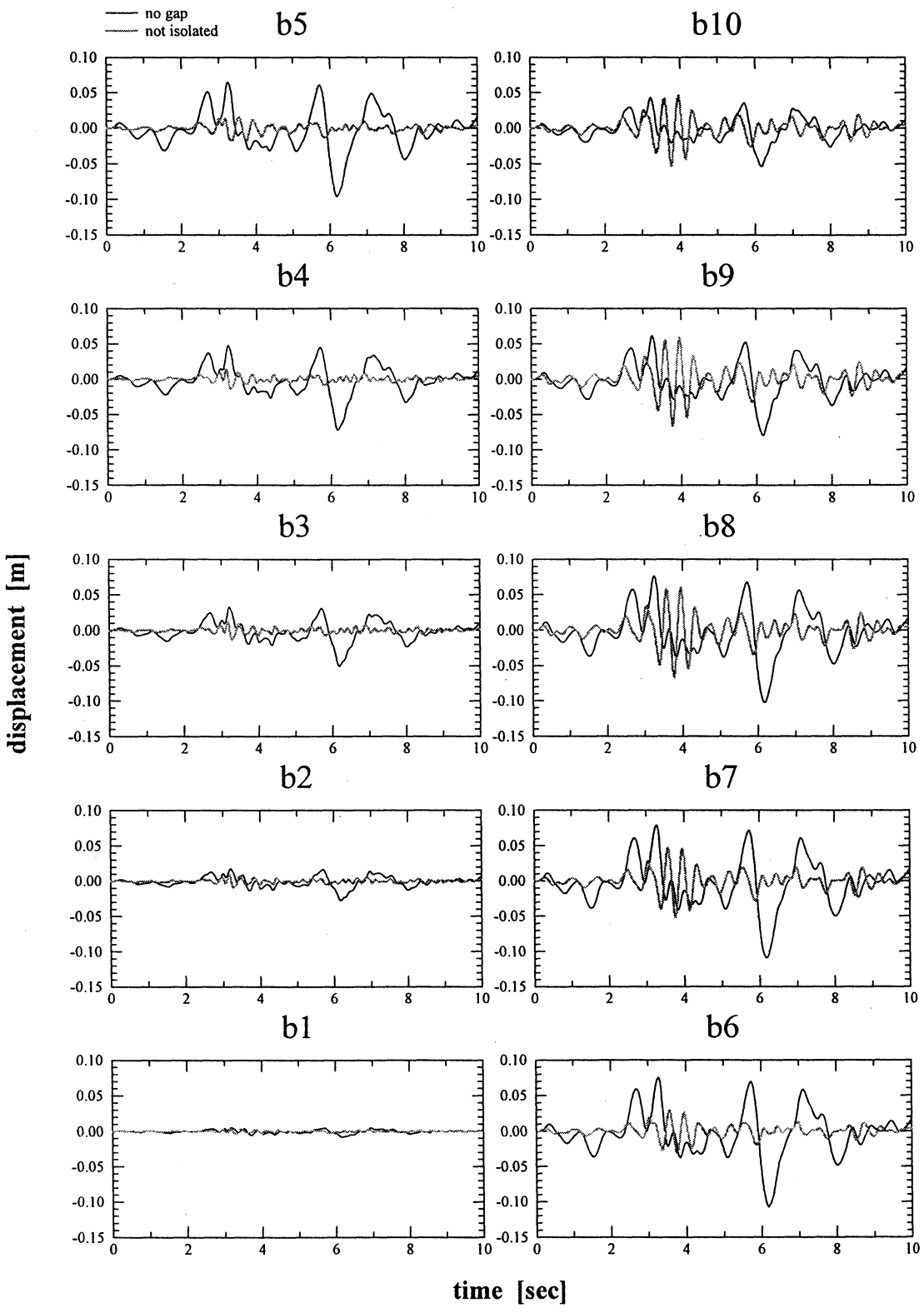


**FIGURE 6-45 Sixth Street Bridge: Comparison of Deck Displacements before and after Retrofit (Alternative 2)**

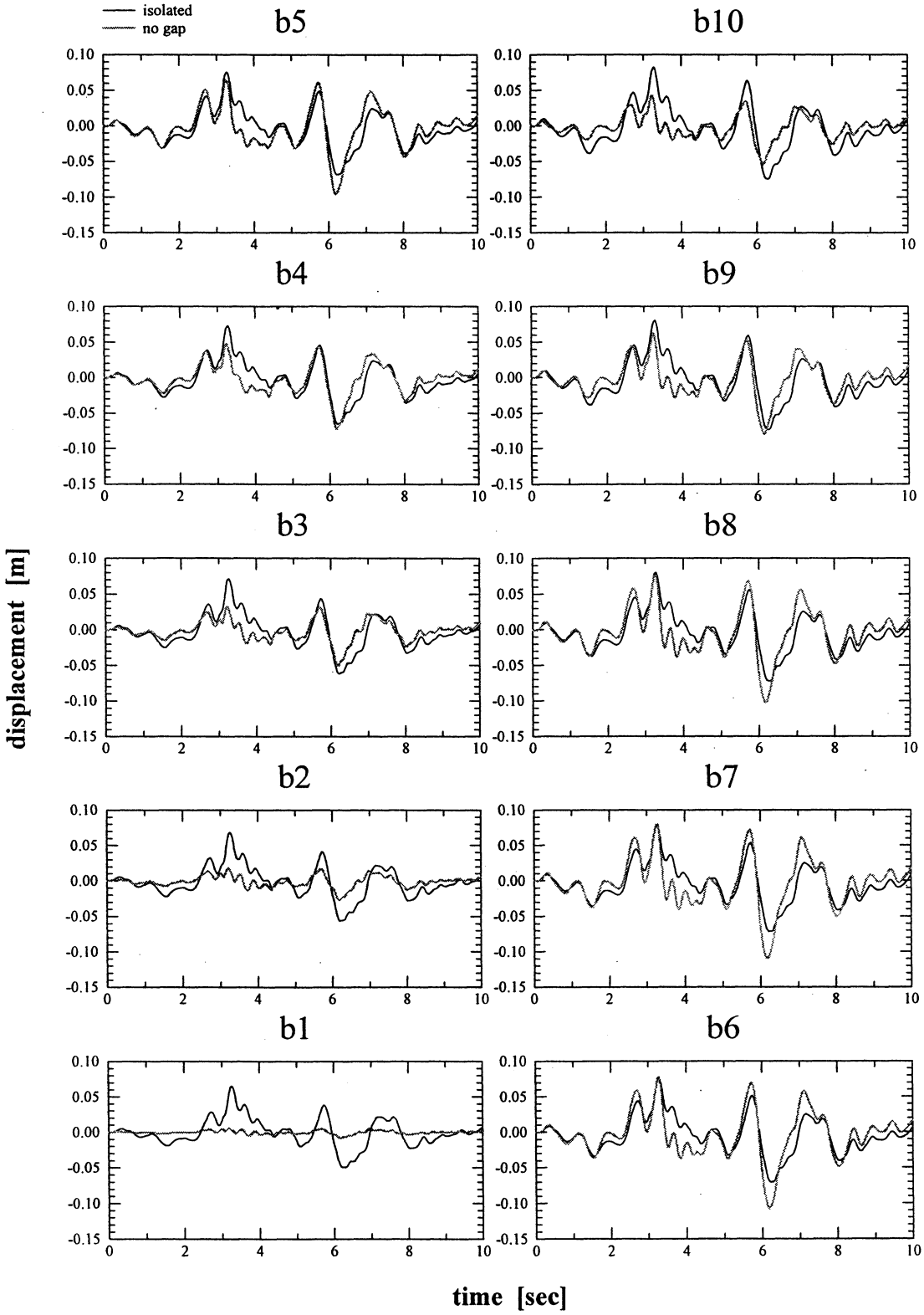


**FIGURE 6-46 Sixth Street Bridge: Comparison of Deck Displacements in Retrofit Alternatives 1 and 2**

## 6.8 Case Study 5: Miyagawa Bridge, Japan (Reichman, 1996)

An existing bridge structure (examined recently by TAISEI Corp, Tokyo, Japan) is investigated to demonstrate the ability of IDARC-BRIDGE to model and analyze the nonlinear inelastic behavior of base isolated bridges. The prototype, a pilot project for base isolated bridges in Japan, belongs to a class referred to as Menshin. The Menshin design aims at increasing the energy dissipation capacity of the bridge system rather than shifting its period.

The Miyagawa Bridge is a three-span continuous bridge with a total length of 105.5 m and a width of 10.5 m (figure 6-47). It was erected across the Keta River on National Highway No. 326 (Buckle, 1992). Lead-rubber bearings isolate the deck from the base in the in-plane direction only. The bearings are locked in the transverse direction. Figures 6-48 and 6-49 contain description of the lead-rubber bearings at the abutments and piers respectively. Their force-displacement curves are established in field tests (figure 6-51). The total weight of the deck is 1320 metric tons. The dimensions of the cross section and reinforcement of the piers vary with height (figure 6-50).

The analysis model of the bridge is shown in figure 6-52. The piers are divided into several elements to account for the variation of stiffness and mass. The pier foundations are represented by four infinitely rigid elastic beam elements (elements 1 to 4 in figure 6-52). The weight of the foundations (300 tf) is lumped in nodes 5 and 6. Elements 5 to 12 are nonlinear inelastic beams with hysteretic properties depending on the section geometry, reinforcement and axial load (table 6-8). The isolators are inserted immediately below the deck soffit at all piers and abutments. The weight of the superstructure is concentrated in nodes 19 to 22. The deck is modeled as a series of elastic beam elements. The flexibility of the soil medium around the pier bases is modeled by translational and rotational foundation springs.

**TABLE 6-8 Miyagawa Bridge: Moment-Curvature Relations of Bridge Piers**

| Element Number | Cracking Moment [t.m] | Cracking Curvature [rad/m] | Yielding Moment [t.m] | Yielding Curvature [rad/m] | Ultimate Moment [t.m] | Ultimate Curvature [rad/m] |
|---|---|---|---|---|---|---|
| **5, 6** | 819.75 | 0.9389e-4 | 1509.50 | 0.1129e-2 | 1632.42 | 0.3005e-1 |
| **7, 8** | 859.89 | 0.8832e-4 | 1568.16 | 0.1109e-2 | 1687.06 | 0.3207e-1 |
| **9, 10** | 886.02 | 0.8279e-4 | 1126.48 | 0.1057e-2 | 1217.59 | 0.3939e-1 |
| **11, 12** | 1001.87 | 0.7714e-4 | 1135.92 | 0.1029e-2 | 1225.71 | 0.4402e-1 |

The Japanese code requires that: (i) at least two ground motions are used for design, (ii) the bridge has to remain elastic during a moderate earthquake, termed "level 1" design earthquake and (iii) the structure must survive without collapse a strong earthquake designated as "level 2" design earthquake. The site can be classified under the "ground condition 1" category of the code (stiff soil).

Two types of analysis are performed: (i) elastic analysis with the initial stiffness of the piers and (ii) inelastic analysis where the flexural rigidity of the piers is derived from the moment-curvature relationships in table 6-8. Since the focus of this study is on behavior of bridges beyond the elastic limit, only results for the severe earthquake case are presented in figures 6-53 and 6-54. The relative displacements of the piers obtained from nonlinear analysis are as large as 230 mm compared to displacements of only about 130 mm computed by linear analysis. Consequently, the elastic moments at the base are approximately 50% bigger. The results also indicate that the displacements of the isolated deck are hardly affected by the nature of the analysis.

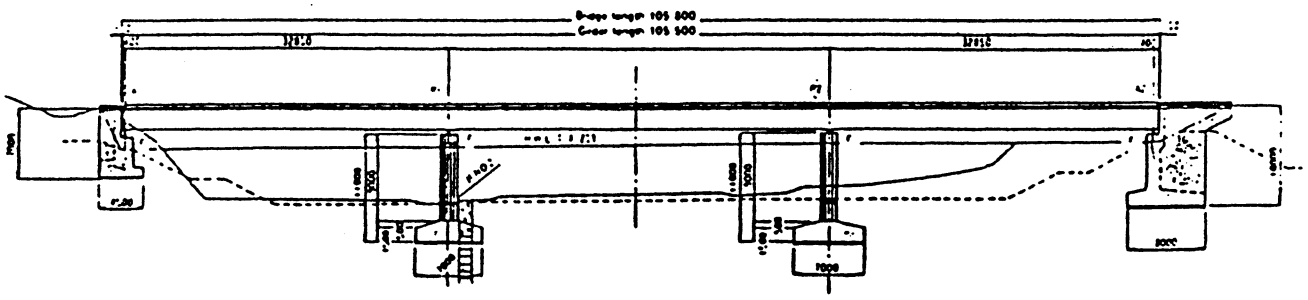

Side View

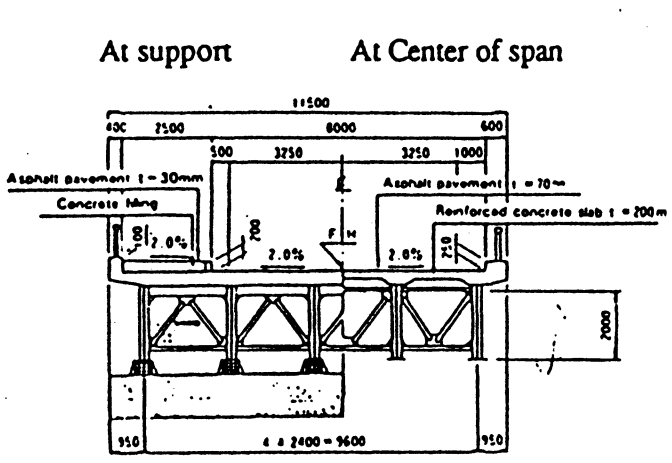


Superstructure

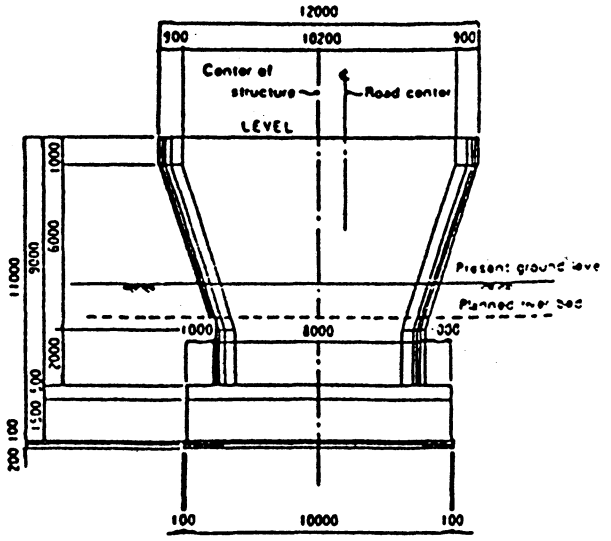


Bridge Pier

**FIGURE 6-47 Miyagawa Bridge: Geometric Properties**

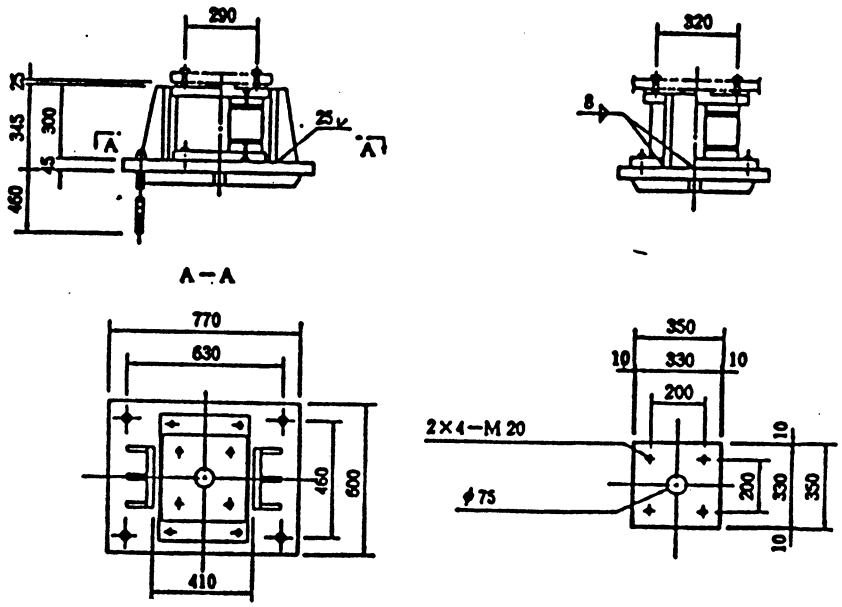


FIGURE 6-48 Miyagawa Bridge: Lead-Rubber Bearings at the Abutments

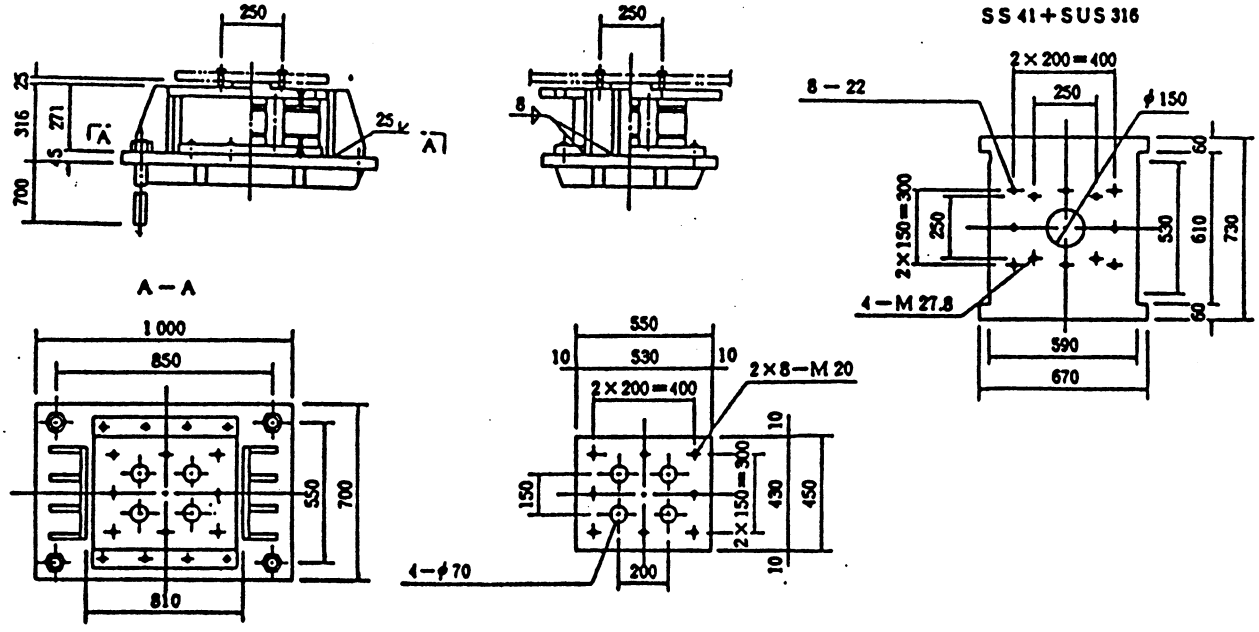


FIGURE 6-49 Miyagawa Bridge: Lead-Rubber Bearings at the Piers

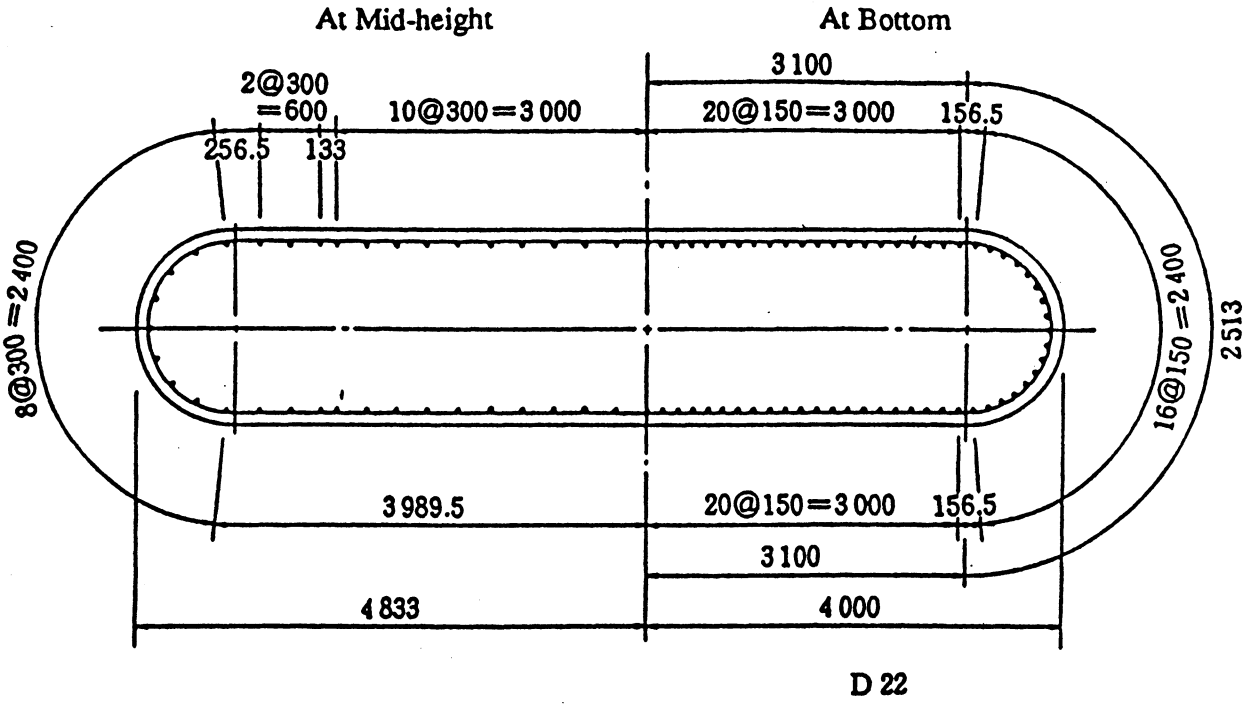


FIGURE 6-50 Miyagawa Bridge: Cross Section of Pier

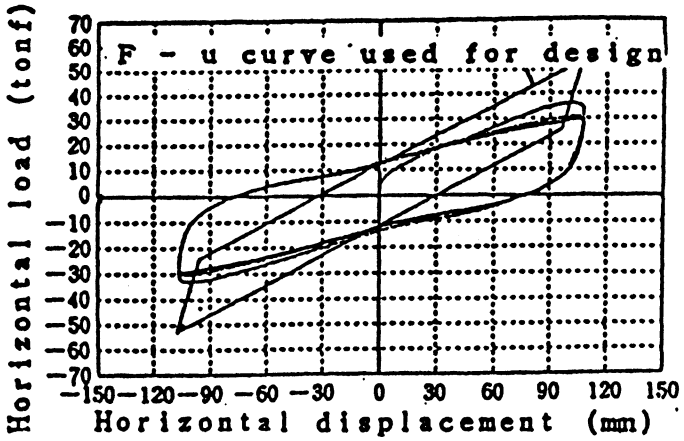


FIGURE 6-51 Miyagawa Bridge: Force-Displacement Curves of Lead-Rubber Bearings

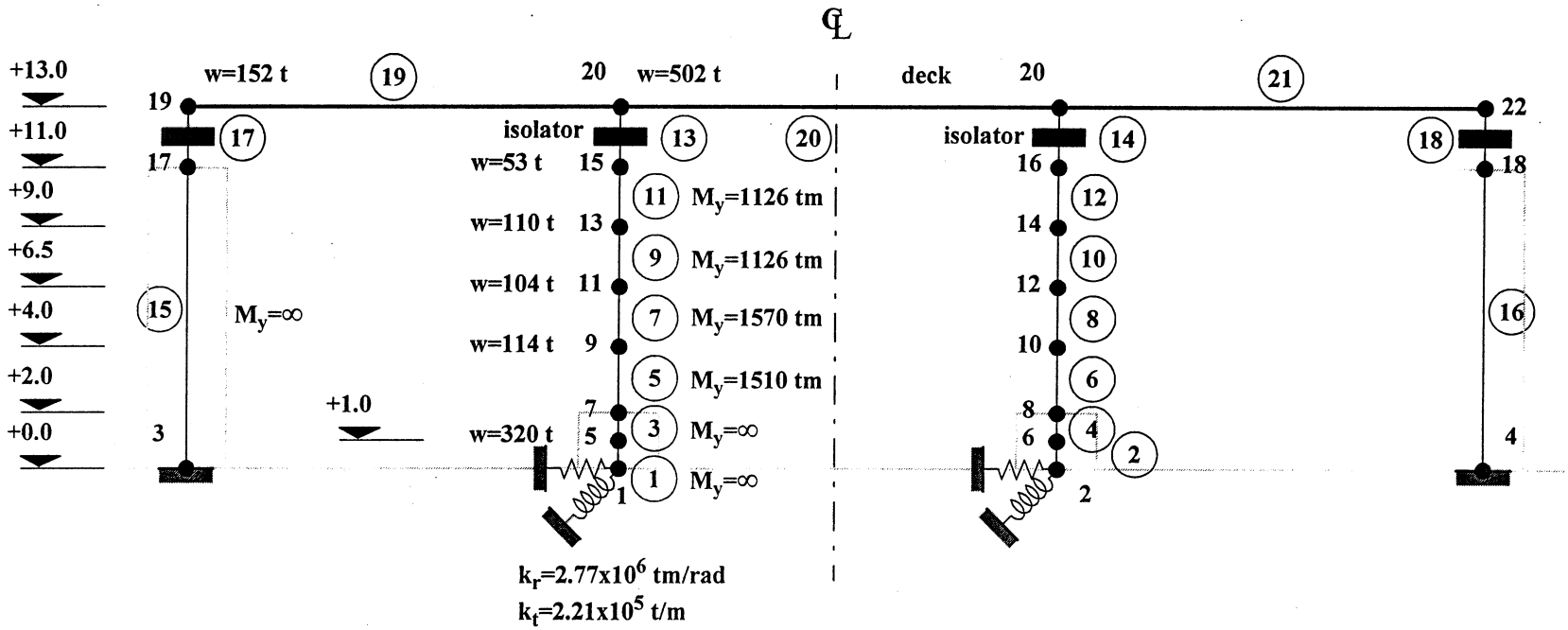


**FIGURE 6-52 Miyagawa Bridge: Computer Analysis Model**

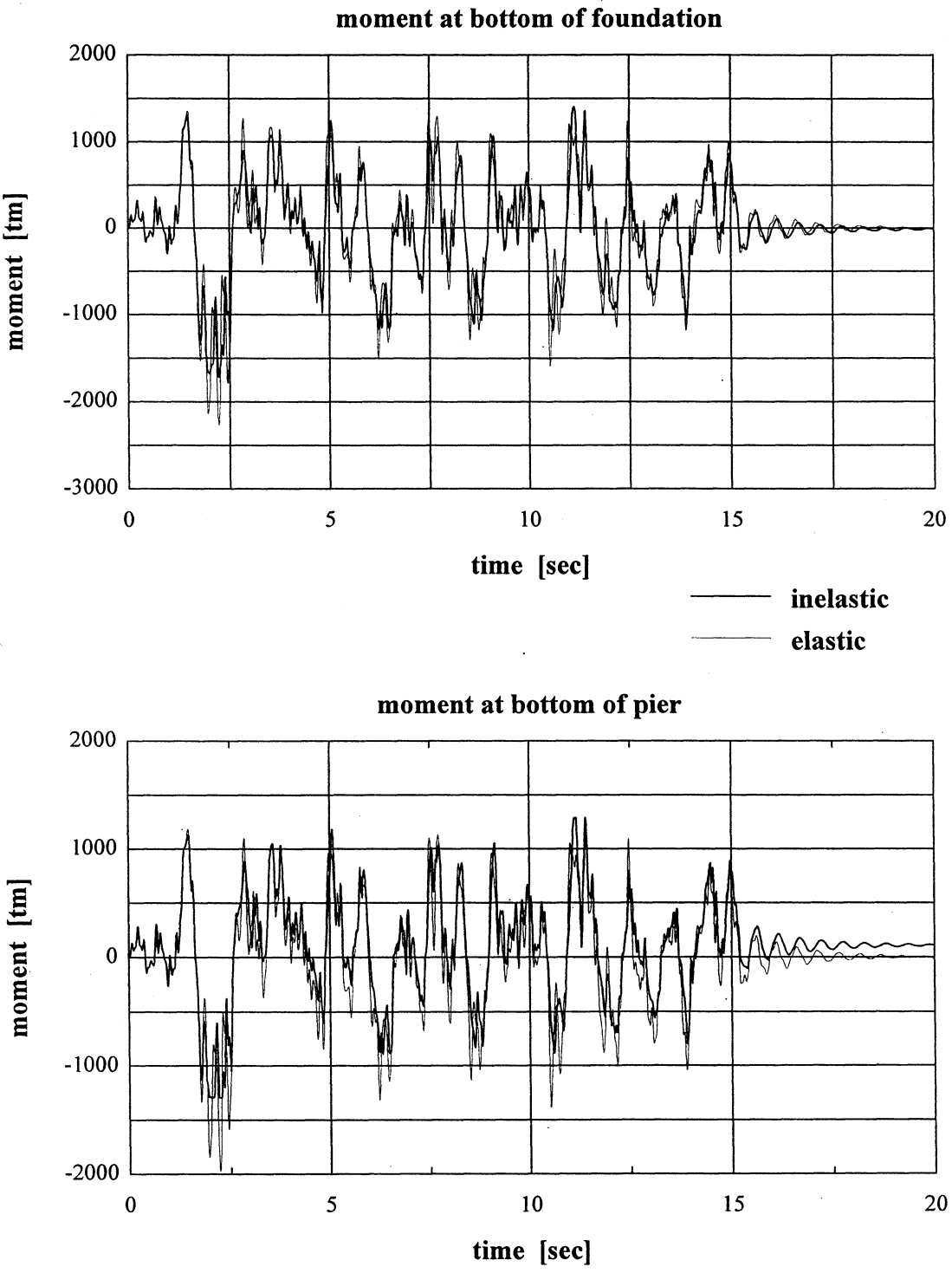


**FIGURE 6-53 Miyagawa Bridge: Bending Moments in Pier and Soil-Foundation Interface**

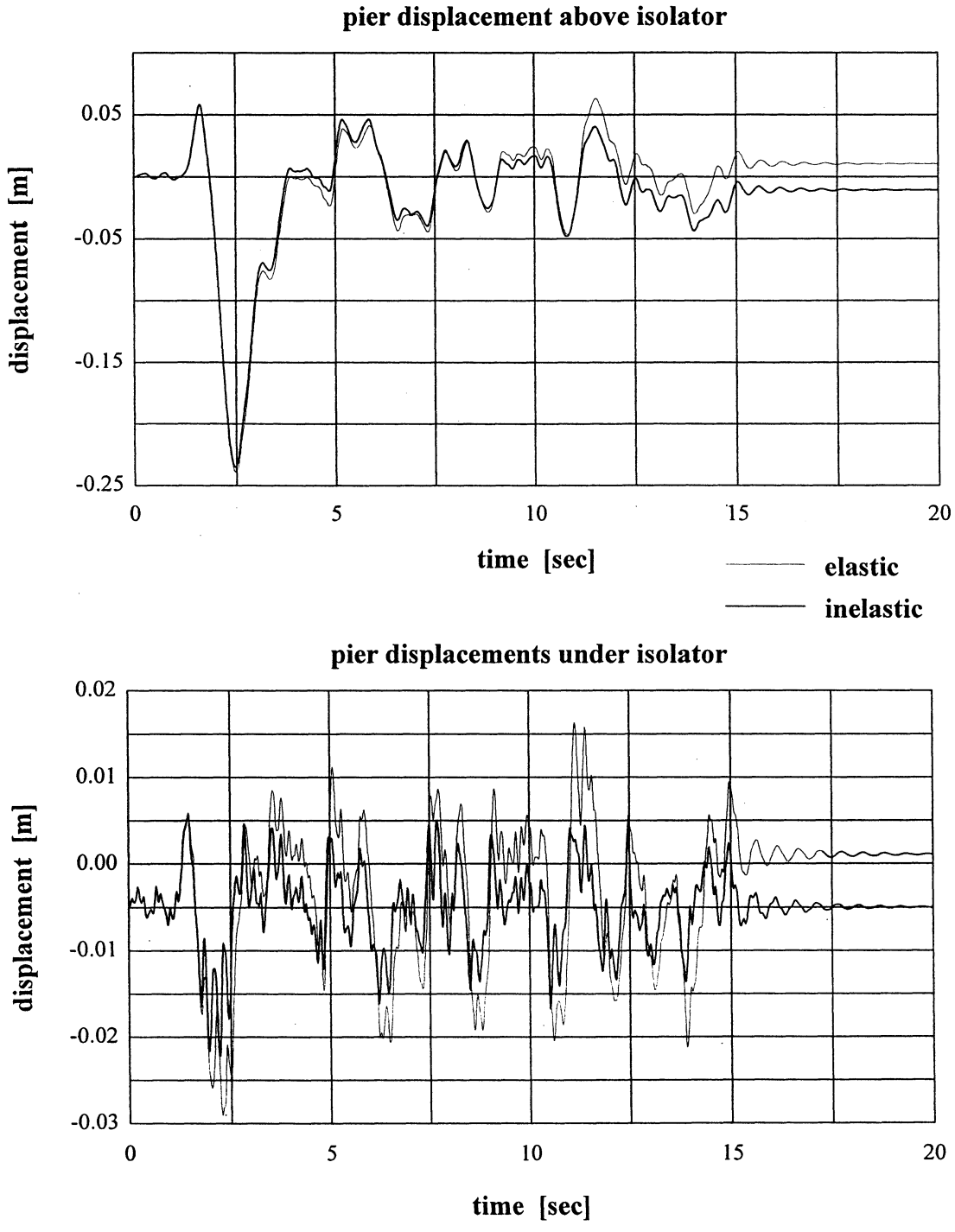


**FIGURE 6-54 Miyagawa Bridge: Displacements of Pier at Isolator Level**

## 6.9 Case Study 6: Evaluation of Capacity of SR14/I5 Separation Bridge by Pushover Analysis (Reichman, 1996)

The capacity of a bridge in Los Angeles County, which collapsed in the 1994 Northridge earthquake, is established by various methods: (i) static pushover analysis with constant lateral load distribution (ii) static pushover analysis with modal adaptive distribution (iii) dynamic analysis with linearly increasing base acceleration input (iv) dynamic analysis with base acceleration pulse input (half-cycle short-duration excitation). The capacity is compared to the response of the bridge to a recorded actual earthquake.

### 6.9.1 Description of Bridge Structure and Analytical Model

The SR14/I5 southbound separation and overhead bridge is located approximately 24 miles from downtown Los Angeles. The southbound structure is a ten-span continuous concrete box girder bridge constructed in five frame segments adjoining at four restrained expansion joints (Buckle, 1994). The deck is supported on single column bents with vastly different stiffness properties. The bents are founded on drilled shafts of large depth. Figures 6-55 and 6-56 show the general plan and elevation, and a typical cross section of the deck.

The superstructure is modeled by a combination of elastic and inelastic beam-column elements (figure 6-57). The nonlinear elements are used for the piers where hysteretic behavior is anticipated (table 6-10). Both the pre-stressed and reinforced concrete parts of the deck are expected to remain elastic throughout the analysis. The depths to fixity of the piers are added to their actual heights to reflect the influence of the soil properties on the location of the plastic hinges below ground (table 6-9).

**TABLE 6-9 SR14/I5 Bridge: Geometry and Cross Section Properties of Components**

| Location | Height [m] | $A_x$ [$m^2$] | $I_y$ [$m^4$] | $I_z$ [$m^4$] | J [$m^4$] |
|---|---|---|---|---|---|
| **Pier 2** | 13.4 | 4.2 | 0.49 | 4.23 | 1.74 |
| **Pier 3** | 13.7 | 4.2 | 0.49 | 4.23 | 1.74 |
| **Pier 4** | 17.5 | 4.2 | 0.49 | 4.23 | 1.74 |
| **Pier 5** | 18.0 | 4.2 | 0.49 | 4.23 | 1.74 |
| **Pier 6** | 29.2 | 3.7 | 0.85 | 4.60 | 2.37 |
| **Pier 7** | 41.2 | 4.0 | 1.35 | 5.20 | 3.70 |
| **Pier 8** | 30.9 | 4.0 | 1.35 | 5.20 | 3.70 |
| **Pier 9** | 32.6 | 4.0 | 1.35 | 5.20 | 3.70 |
| **Pier 10** | 17.6 | 4.2 | 0.49 | 4.23 | 1.74 |
| **Deck** | N/A | 8.8 | 5.85 | 188.56 | 16.30 |

**TABLE 6-10 SR14/I5 Bridge: Moment-Curvature Relations for Strong-Axis Bending and Shear Capacities of Piers**

| Location | $M_{cr}$ [kNm] | $\phi_{cr}$ [rad/m] | $M_y$ [kNm] | $\phi_y$ [rad/m] | $M_{ult}$ [kNm] | $\phi_{ult}$ [rad/m] | $V_{ult}$ [kN] |
|---|---|---|---|---|---|---|---|
| **Pier 2** | 22600 | 0.21 | 68740 | 1.29 | 75000 | 3.99 | 6925 |
| **Pier 3** | 23100 | 0.21 | 69740 | 1.31 | 75000 | 3.95 | 7065 |
| **Pier 4** | 20435 | 0.21 | 54570 | 1.18 | 70000 | 4.65 | 6345 |
| **Pier 5** | 20435 | 0.21 | 54570 | 1.18 | 70000 | 4.65 | 6365 |
| **Pier 6** | 26160 | 0.20 | 78250 | 1.39 | 85000 | 3.89 | 7347 |
| **Pier 7** | 24900 | 0.18 | 64260 | 1.25 | 70000 | 5.34 | 7041 |
| **Pier 8** | 19130 | 0.15 | 56360 | 1.23 | 70000 | 5.27 | 5770 |
| **Pier 9** | 22960 | 0.18 | 61670 | 1.27 | 70000 | 4.76 | 6608 |
| **Pier 10** | 22660 | 0.21 | 57320 | 1.16 | 70000 | 4.46 | 7885 |

### 6.9.2 Distribution of Lateral Load in Pushover Analyses. Type and Magnitude of Excitation in Dynamic Analyses.

The distribution of lateral force in a monotonic pushover analysis is typically governed by the distribution of seismic weight (figure 6-60a). The modal adaptive procedure, however, applies a non-stationary loading pattern, which is proportional to the instantaneous mode shapes (figure 6-59a). The eigenvectors reflect all changes in the capability of structural elements to resist load due to cracking and yielding, and the redistribution of forces in the structure associated with softening of some of its components.

Linear acceleration histories with rates of increase of 0.25 m/sec$^3$, 0.5 m/sec$^3$ and 5.0 m/sec$^3$ respectively are applied to the analytical model until failure (figures 6-61a, 6-62a and 6-63a). In the next round of analyses, the structure is subjected to acceleration pulse loading with duration of the records of 0.1 sec and 0.05 sec (figures 6-64a and 6-65a). Finally, the ground motion recorded at the Santa Monica City Hall during the Northridge earthquake is used as input for dynamic analysis (figure 6-66a).

### 6.9.3 Interpretation of Results

The onset of collapse is detected by monitoring the structure for: (i) flexural failure, where one of the piers reaches its ultimate bending capacity or (ii) shear failure of a pier due to exceeding its respective capacity in table 6-10. The histories of applied loading and shear forces in piers 2 to 7 are presented in figures 6-60 to 6-66 for various analysis cases. The distribution of the shear forces at the beginning of collapse is summarized in table 6-11 and charted in figure 6-58. The magnitude of the bending moment in each pier in that instant is given in table 6-12 as well. Comparison of the performance of the bridge under different loading conditions is presented in table 6-13. In all cases, the first failure occurred in one of the shorter piers belonging to either the frame, which collapsed in the Northridge earthquake, or to the adjacent segment (figure 6-55).

It is worthwhile mentioning that the analysis for ramp acceleration with the highest rate of increase (5.0 m/sec$^3$) identifies pier 5 as the critical component but predicts 30% higher shear

force in pier 2 compared to similar analyses with the lower rates of increase. The response in the two cases of acceleration pulse excitation is characterized by concentration of shear forces in the supporting members of the first frame and failure of pier 2. Shearing of this pier is speculated to have triggered the collapse in the actual event. The Santa Monica City Hall ground motion, recorded during the Northridge earthquake and selected to represent near-fault phenomena, has similar effect on the structure. It is scaled to 150% to bring the bridge to failure during the first large pulse (half-cycle) of the earthquake (figure 6-66). Again very large shear forces are resisted by the columns of the collapsed segment. Pier 3 is identified as the critical component.

Two distinct patterns of out-of-plane response of the bridge are observed in the series of static pushover and dynamic analyses. The magnitude of deformations and distribution of base shear in the substructure resulting from pulse loading follow closely those from time-history analysis. It can be hypothesized that the dynamic procedures for predicting the collapse mode of a bridge during a future event, which rely on analysis with simplified loading patterns are applicable to cases of ground motion of highly impulsive nature, whereas, the static pushover methods have utility in cases of structural response dominated by the first (or first few) transverse modes typical of vibratory earthquakes. In this case, however, a single-mode approach (model) may not be sufficient to identify the vulnerable components.

**TABLE 6-11 Shear Force Distribution at Time of Failure of Critical Pier**

| Analysis Method | Pier 2 [kN] | Pier 3 [kN] | Pier 4 [kN] | Pier 5 [kN] | Pier 6 [kN] | Pier 7 [kN] | Total [kN] |
|---|---|---|---|---|---|---|---|
| **Modal Adaptive** | -21.9 | 2530 | 3480 | 6365 | 3680 | 1410 | 17470 |
| **[%] of total** | 0 % | 14 % | 20 % | 37 % | 21 % | 8 % | N/A |
| **Constant Distribution** | 3800 | 7065 | 3720 | 6030 | 3210 | 868 | 23908 |
| **[%] of total** | 15 % | 29 % | 15 % | 25 % | 13 % | 4 % | N/A |
| **Ramp Acc. 0.25 m/sec$^3$** | 3880 | 6780 | 3760 | 6365 | 3400 | 1550 | 25750 |
| **[%] of total** | 15 % | 27 % | 14 % | 25 % | 13 % | 6 % | N/A |
| **Ramp Acc. 0.5 m/sec$^3$** | 3980 | 6710 | 3730 | 6365 | 3390 | 1580 | 25760 |
| **[%] of total** | 15 % | 27 % | 14 % | 25 % | 13 % | 6 % | N/A |
| **Ramp Acc. 5.0 m/sec$^3$** | 5150 | 6600 | 3590 | 6365 | 3520 | 1870 | 27100 |
| **[%] of total** | 19 % | 25 % | 13 % | 23 % | 13 % | 7 % | N/A |
| **Pulse Acc. 0.1 sec** | 6925 | 5080 | 2150 | 2330 | 1500 | 2170 | 19980 |
| **[%] of total** | 34 % | 25 % | 10 % | 12 % | 8 % | 11 % | N/A |
| **Pulse Acc. 0.05 sec** | 6925 | 4840 | 2160 | 2310 | 222 | 3860 | 20317 |
| **[%] of total** | 34 % | 24 % | 11 % | 11 % | 1 % | 19 % | N/A |
| **Ground Motion** | 4830 | 7065 | 2250 | -218 | -1510 | 1740 | 14242 |
| **[%] of total** | 34 % | 50 % | 16 % | 0 % | 11 % | 12 % | N/A |
| **Shear Capacity** | 6925 | 7065 | 6345 | 6365 | 7347 | 7041 | N/A |
| **Pier Height** | 10.5 m | 10.8 m | 14.7 m | 15.2 m | 26.3 m | 38.4 m | N/A |

**TABLE 6-12 Bending Moment in Piers at Shear Failure in Different Pushover Procedures**

| Type of Loading | Pier 2 [kN.m] | Pier 3 [kN.m] | Pier 4 [kN.m] | Pier 5 [kN.m] | Pier 6 [kN.m] | Pier 7 [kN.m] |
|---|---|---|---|---|---|---|
| **Modal Adaptable Dist.** | -1980 | 40100 | 60000* | 67600** | 84900** | 60700 |
| **Constant Distribution** | 38400 | 73100** | 59300* | 65800* | 80900** | 46500 |
| **Ramp Acc. 0.25 m/sec$^3$** | 32800 | 68300* | 56700* | 62400* | 78600* | 50200 |
| **Ramp Acc. 0.5 m/sec$^3$** | 49700 | 74400** | 61400* | 69900** | 81200** | 62200 |
| **Ramp Acc. 5.0 m/sec$^3$** | 53800 | 74000** | 61700* | 69500** | 82200** | 65300* |
| **Pulse Acc. 0.1 sec** | 64600 | 71100* | 43700 | 45200 | 27500 | 51000 |
| **Pulse Acc. 0.05** | 53500 | 48300 | 32300 | 32300 | 15600 | 39100 |
| **THA** | 43300 | 63500 | 38800 | 3820 | -20000 | 18000 |
| **Yielding moment** | **68740** | **69740** | **54570** | **54570** | **78250** | **64260** |
| **Ultimate moment** | **75000** | **75000** | **70000** | **70000** | **85000** | **70000** |

* Yielding moment exceeded.

** Within 5% of ultimate moment.

**TABLE 6-13 Comparison of Performance of SR14/I5 Bridge in Pushover Analyses**

| Type of Loading | Type of Failure | Failed Pier | Critical Acc. [g] |
|---|---|---|---|
| **Modal Adaptable Dist.** | Flexure | P5 | 0.21 |
| **Constant Distribution** | Flexure | P3 | 0.29 |
| **Ramp Acc. 0.25 m/sec$^3$** | Shear | P5 | 0.34 |
| **Ramp Acc. 0.5 m/sec$^3$** | Flexure | P5 | 0.38 |
| **Ramp Acc. 5.0 m/sec$^3$** | Flexure | P5 | 0.54 |
| **Pulse Acc. 0.1 sec** | Shear | P2 | 1.50 |
| **Pulse Acc. 0.05 sec** | Shear | P2 | 3.00 |
| **THA** | Shear | P3 | 0.35 |

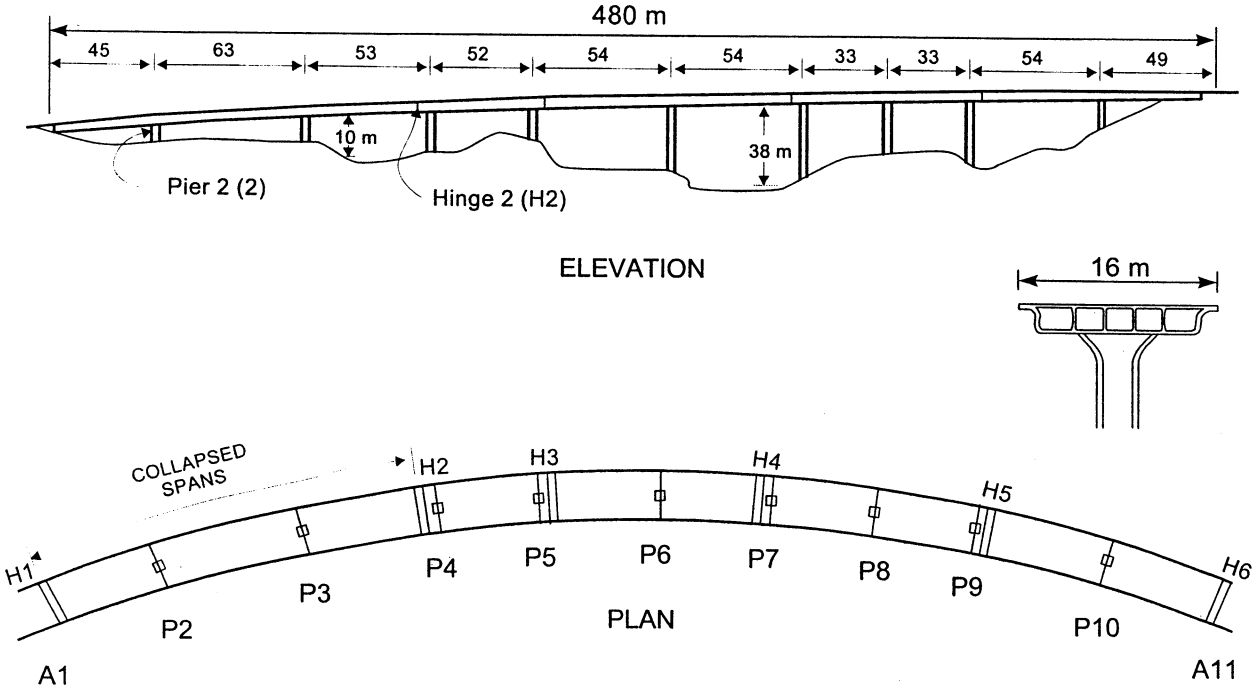


**FIGURE 6-55 SR14/I5 Bridge: Elevation and Plan**

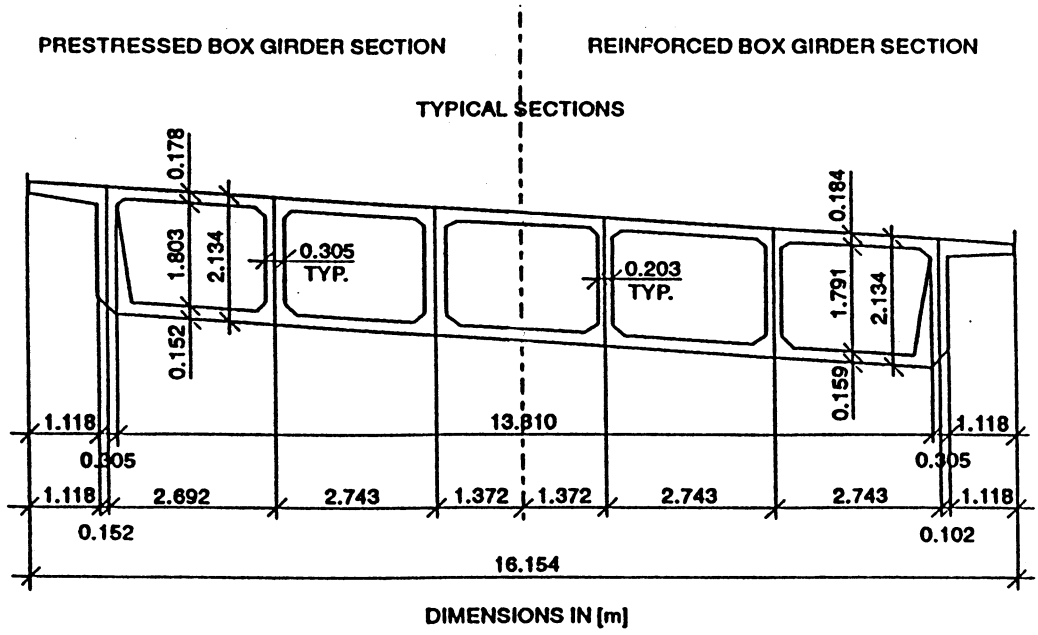


**FIGURE 6-56 SR14/I5 Bridge: Typical Deck Cross Section**

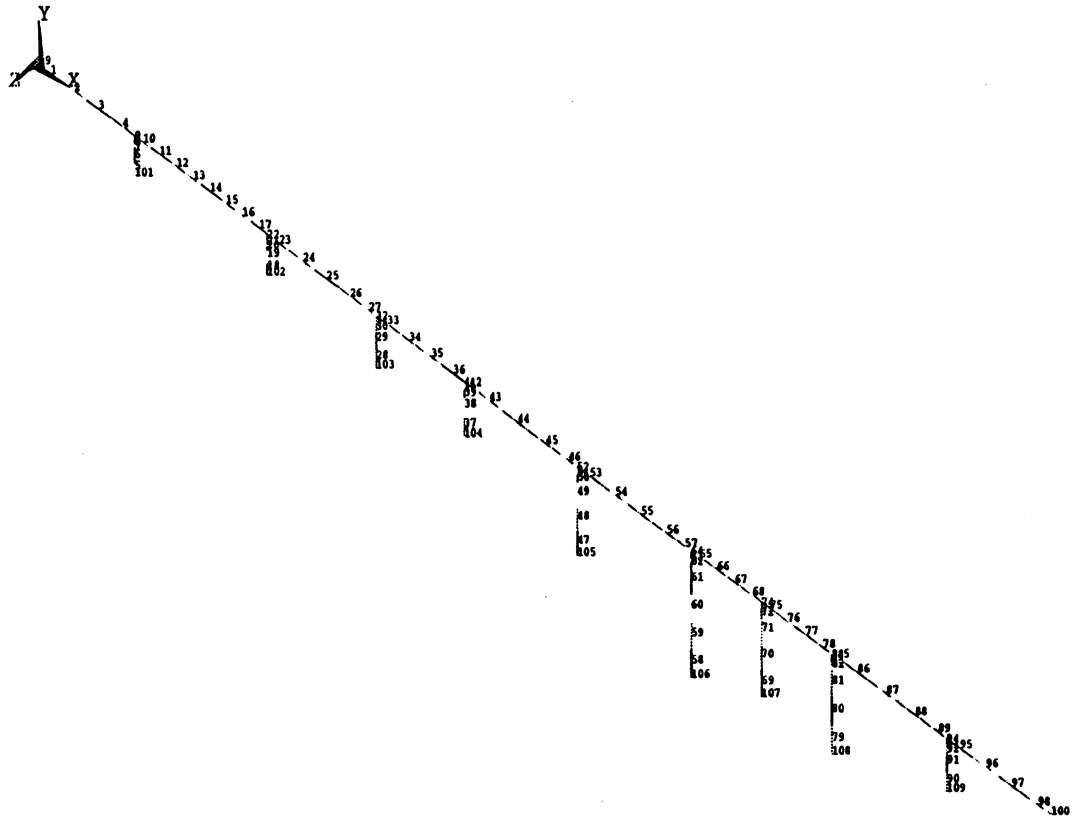

**FIGURE 6-57 SR14/I5 Bridge: Computer Analysis Model**

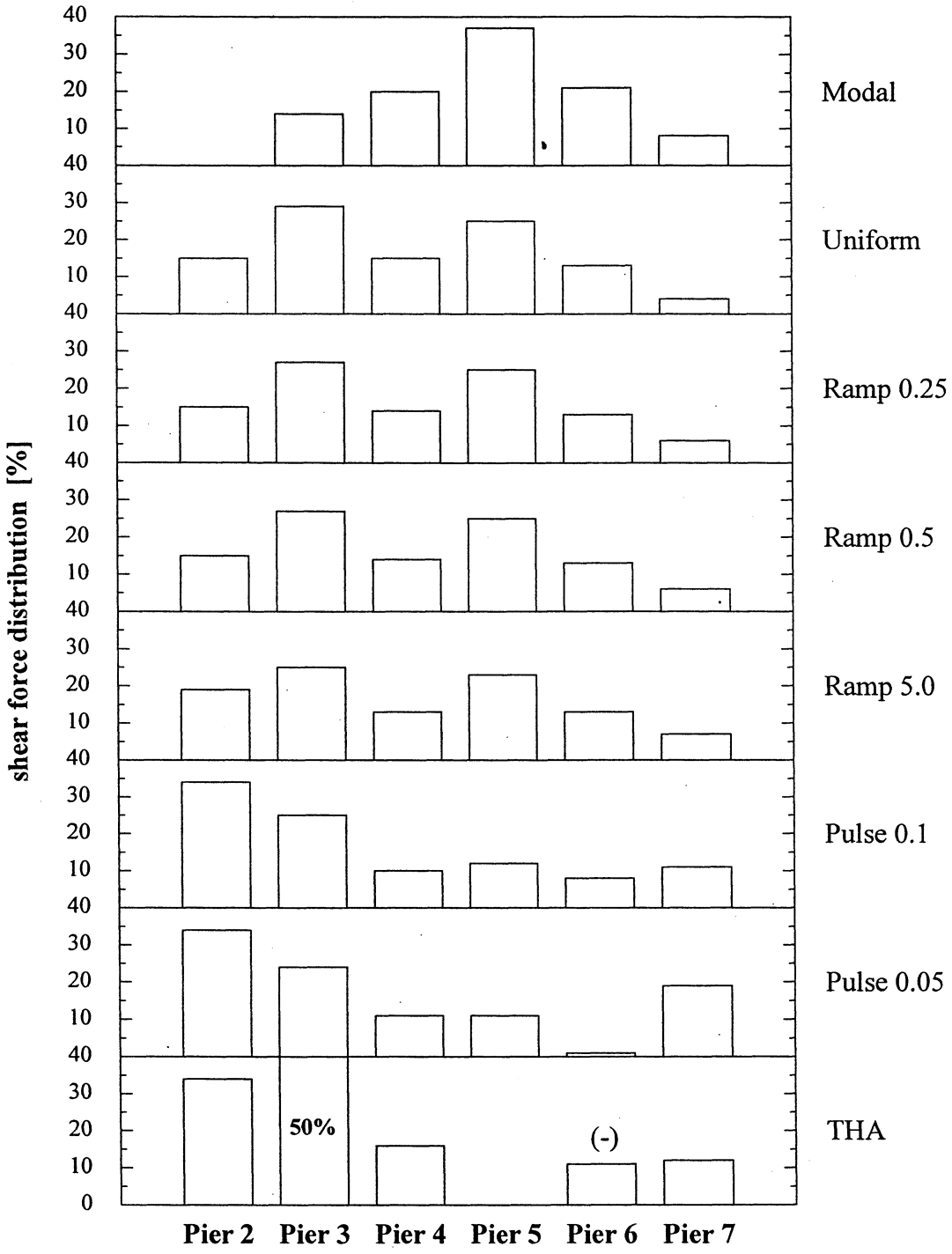


**FIGURE 6-58 SR14/I5 Bridge: Distribution of Shear Forces in Piers 2 to 7 for Different Analysis Procedures**

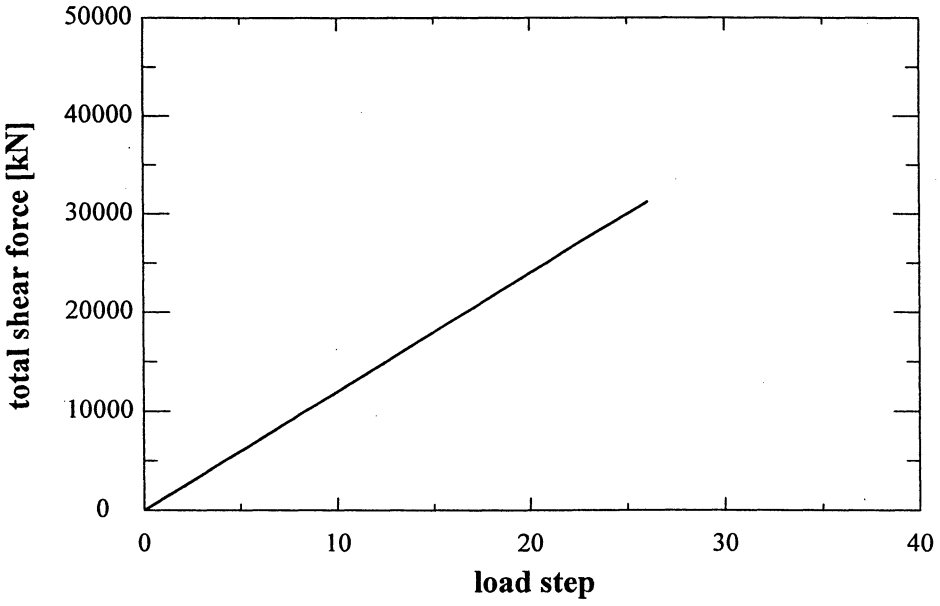


a)

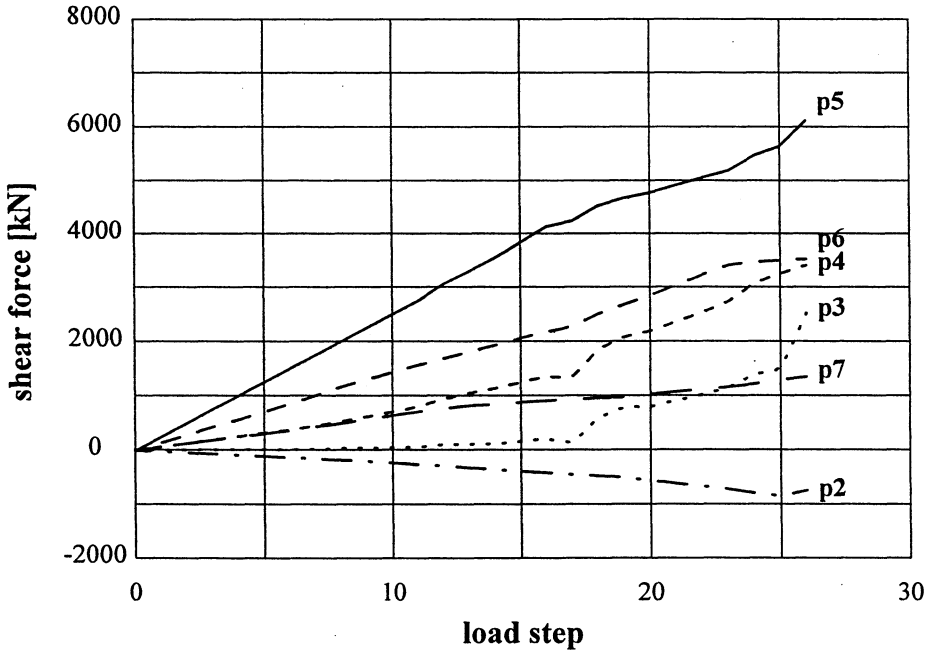


b)

**FIGURE 6-59 SR14/I5 Bridge: Response to Transverse Loading Proportional to Instantaneous Mode Shapes: a) Loading History, b) Shear Forces in Piers 2 to 7**

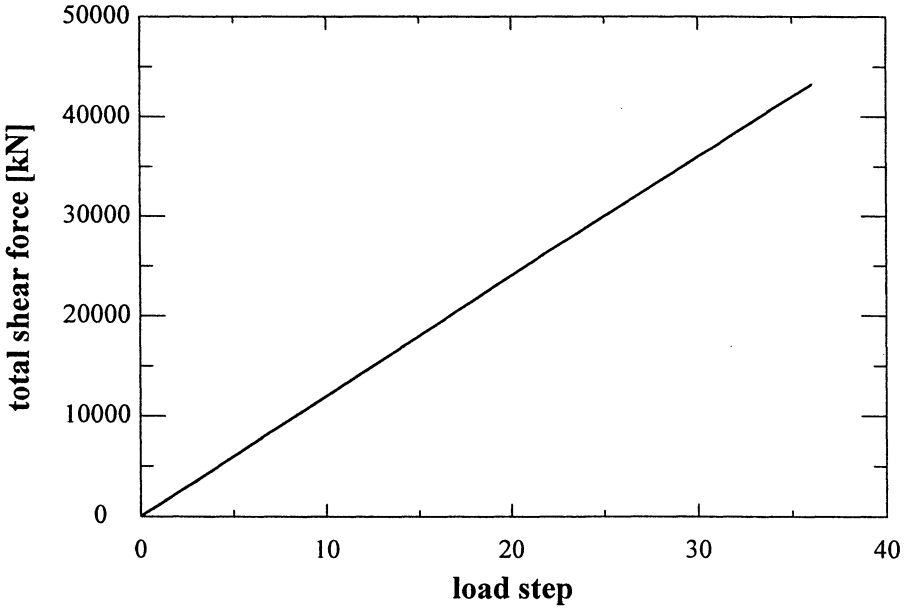


a)

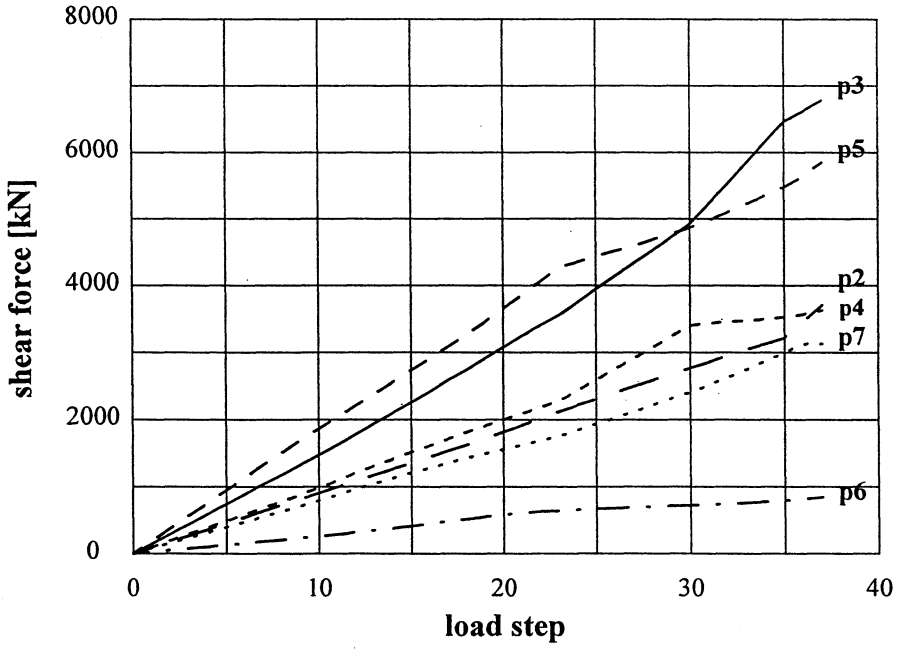


b)

**FIGURE 6-60 SR14/I5 Bridge: Response to Transverse Loading Distributed Relative to Mass: a) Loading History, b) Shear Forces in Piers 2 to 7**

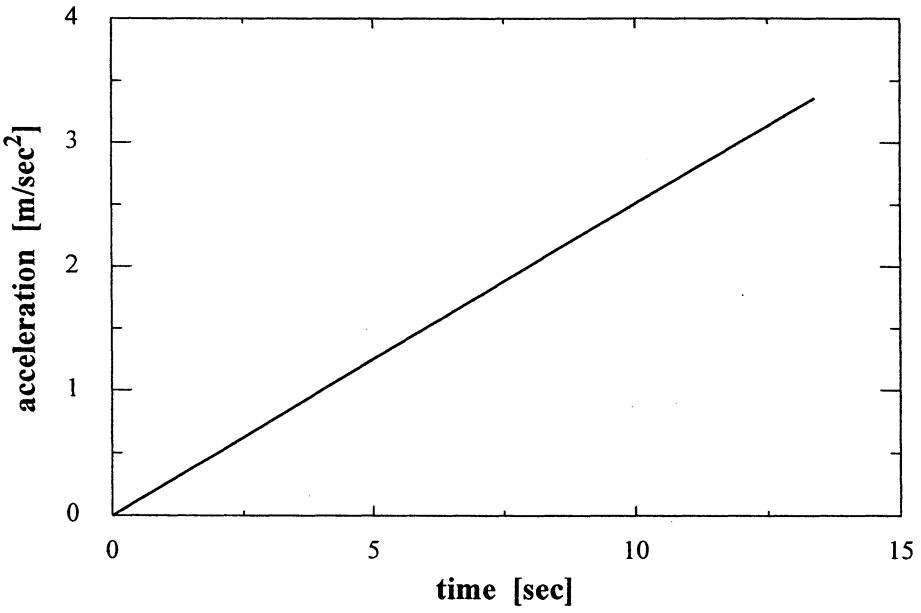


a)

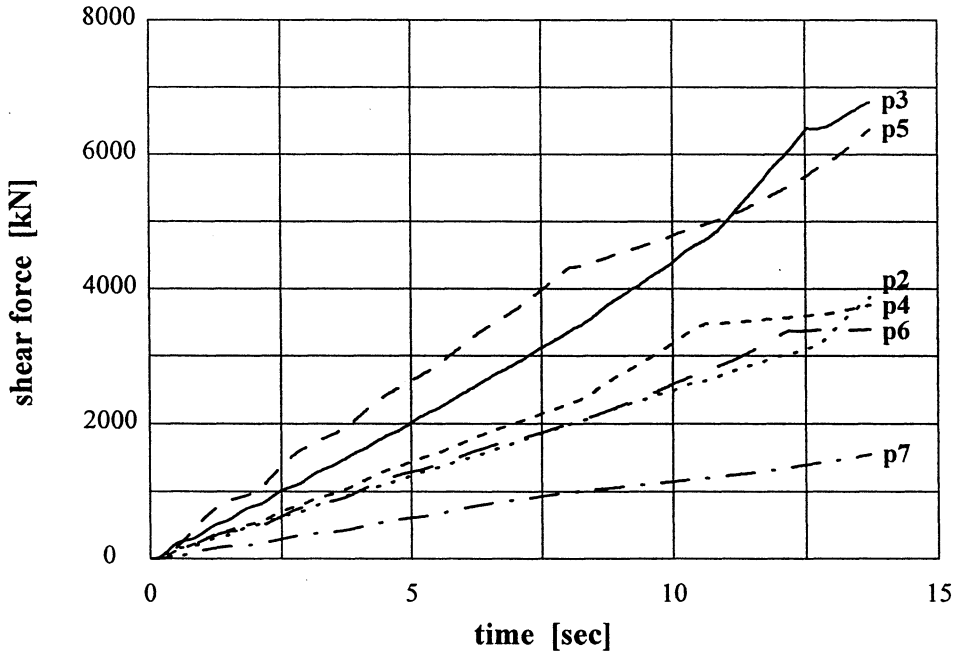


b)

**FIGURE 6-61 SR14/I5 Bridge: Response to Ramp Loading of Rate 0.25 m/sec$^3$: a) Loading History, b) Shear Forces in Piers 2 to 7**

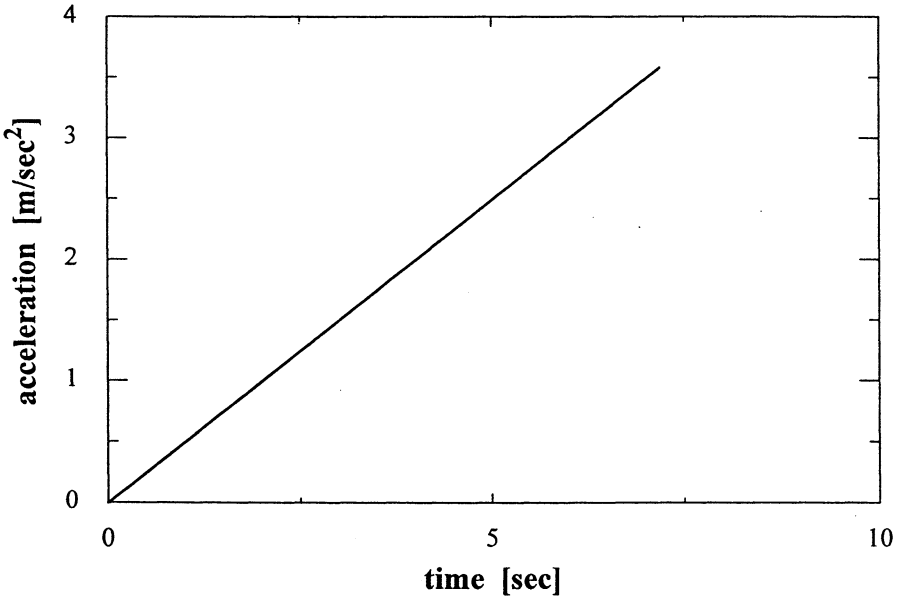


a)

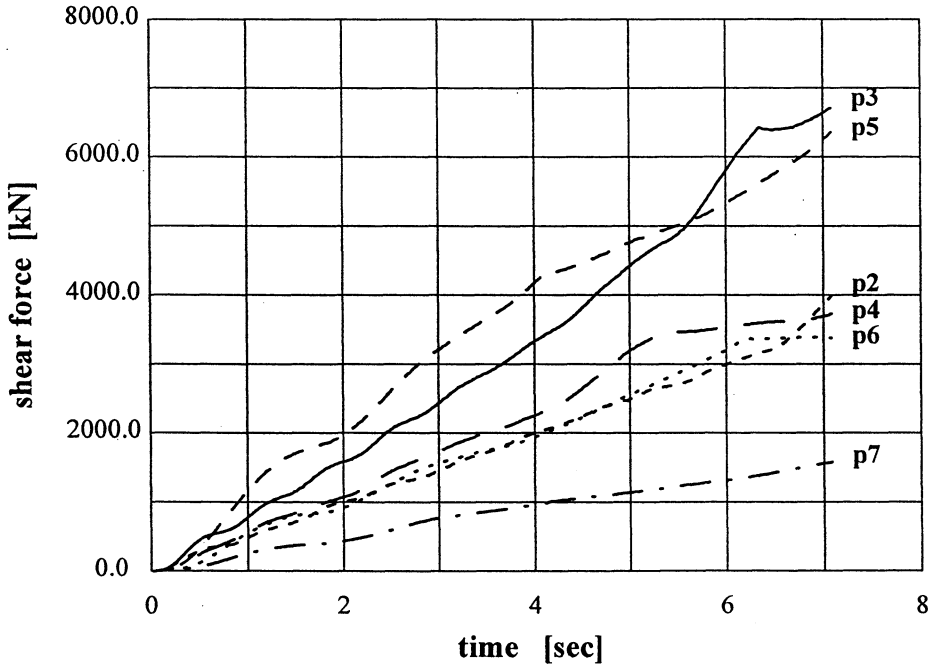


b)

**FIGURE 6-62 SR14/I5 Bridge: Response to Ramp Loading of Rate 0.5 m/sec$^3$ : a) Loading History, b) Shear Forces in Piers 2 to 7**

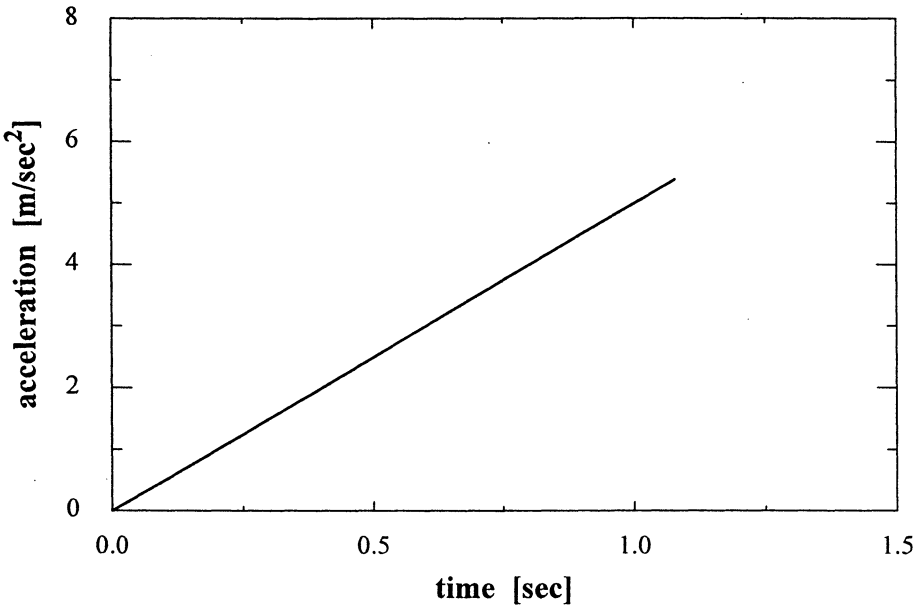


a)

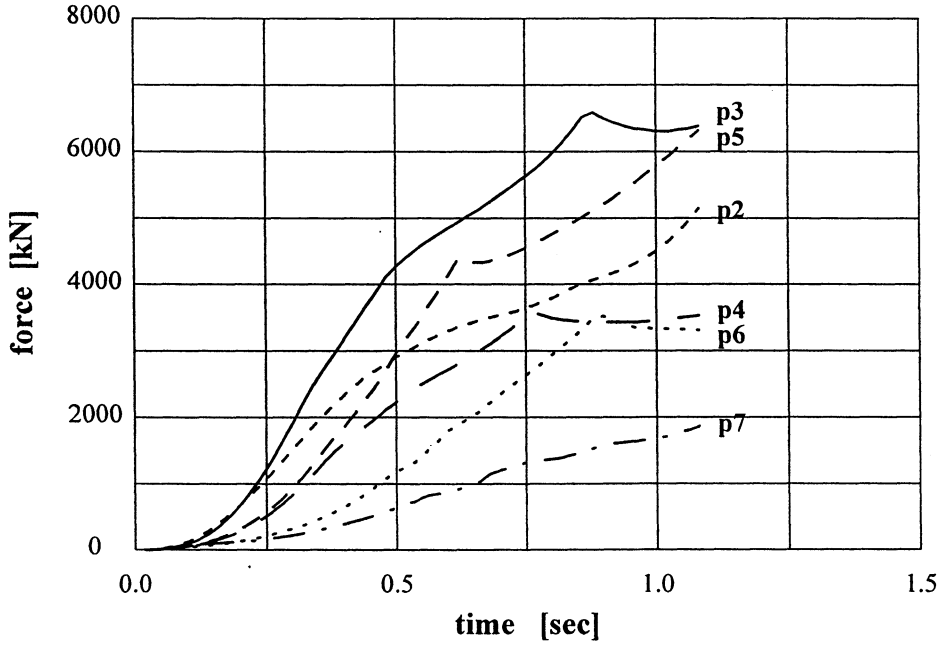


b)

**FIGURE 6-63 SR14/I5 Bridge: Response to Ramp Loading of Rate 5.0 m/sec$^3$: a) Loading History, b) Shear Forces in Piers 2 to 7**

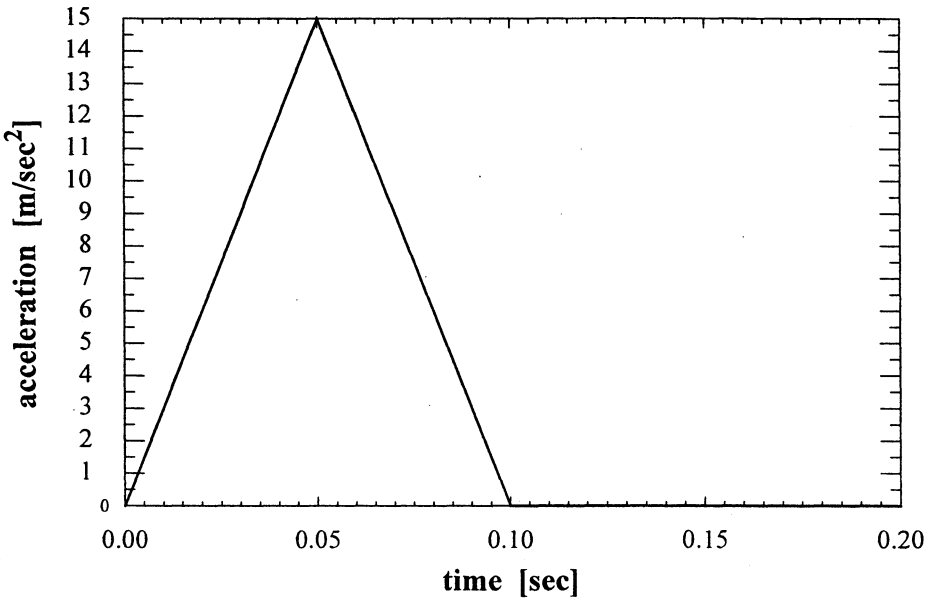


a)

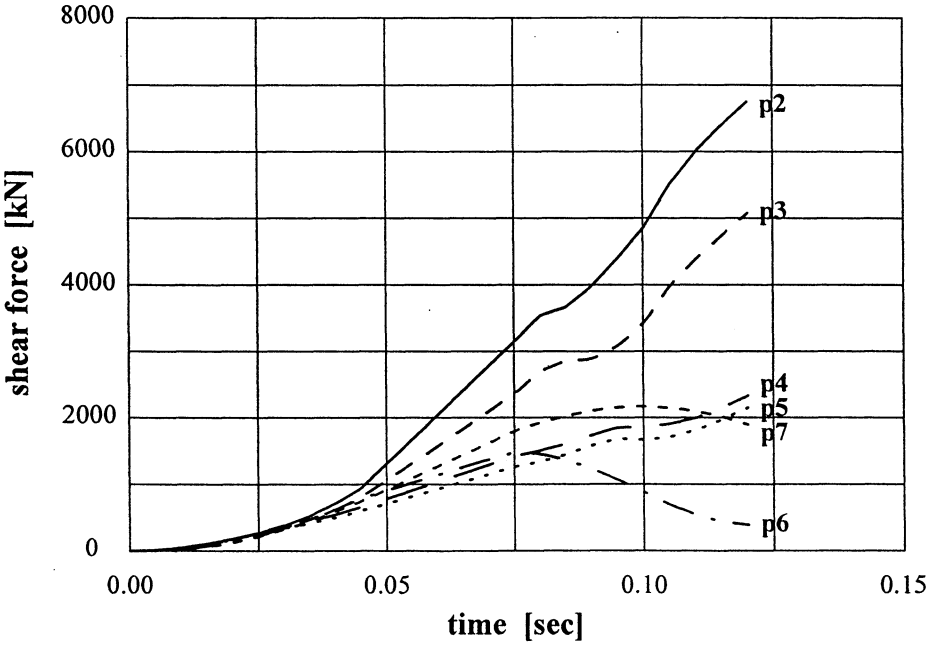


b)

**FIGURE 6-64 SR14/I5 Bridge: Response to Pulse Loading of Duration 0.1 sec: a) Loading History, b) Shear Forces in Piers 2 to 7**

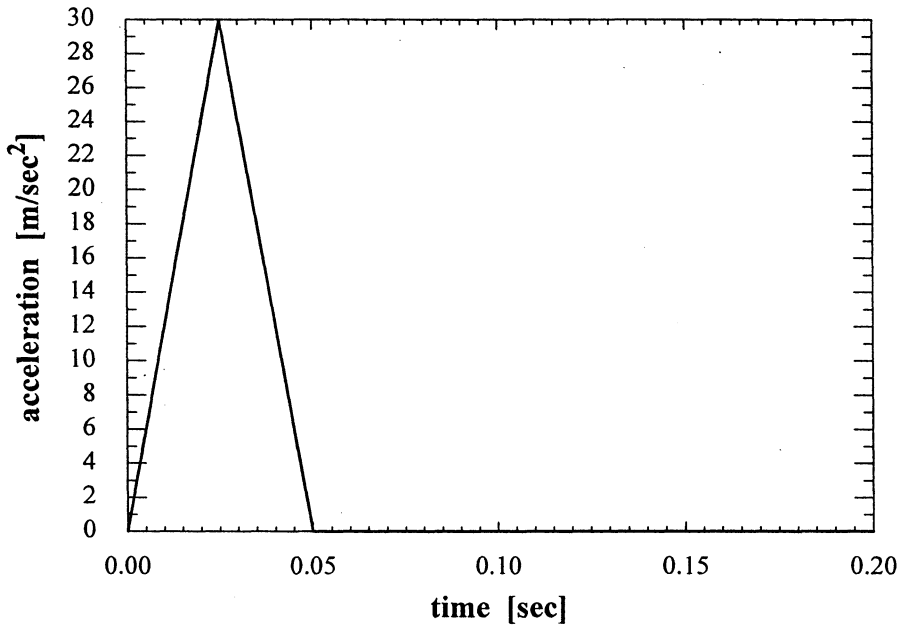


a)

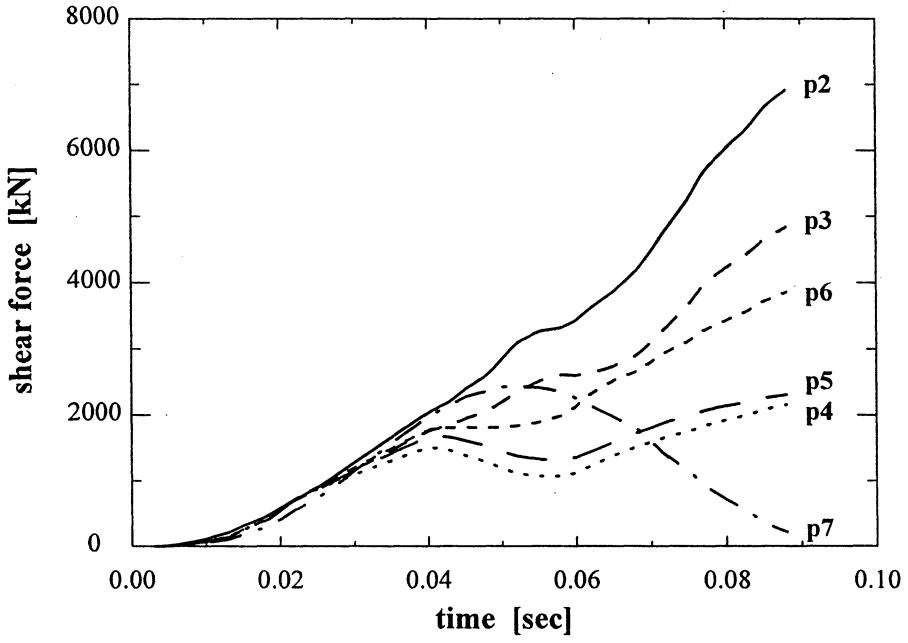


b)

**FIGURE 6-65 SR14/I5 Bridge: Response to Pulse Loading of Duration 0.05 sec: a) Loading History, b) Shear Forces in Piers 2 to 7**

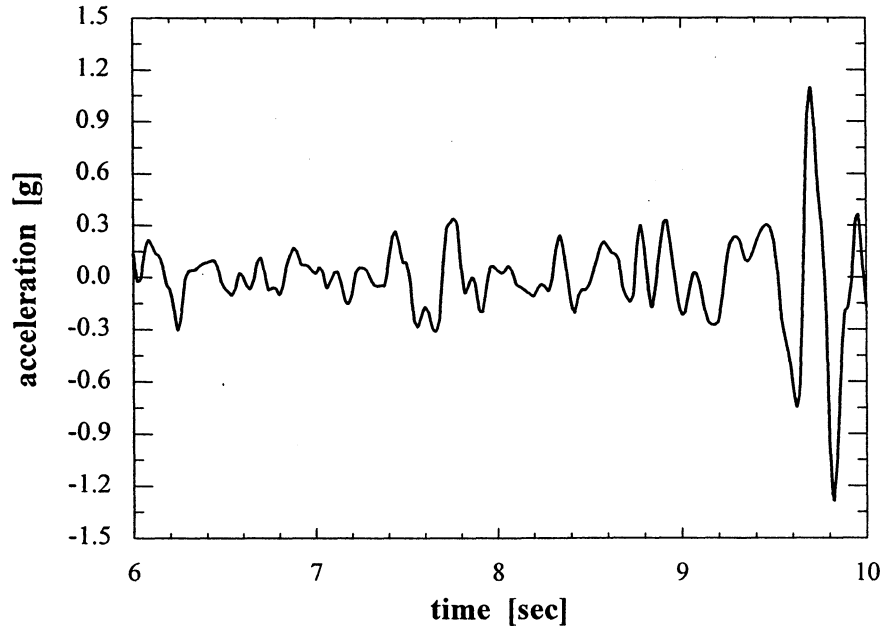


a)

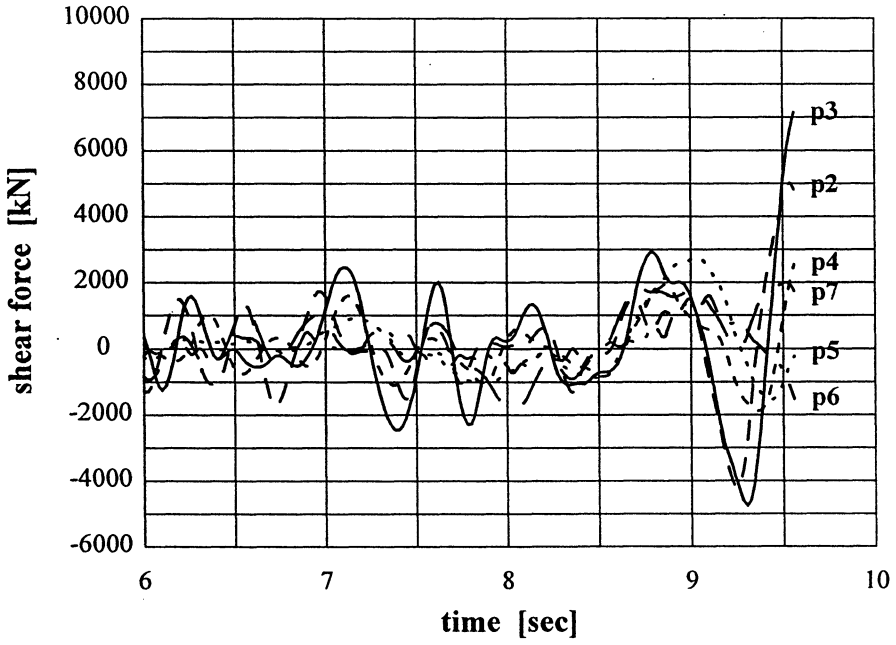


b)

**FIGURE 6-66 SR14/I5 Bridge: Response to Impulsive Earthquake Loading: a) Northridge 1994 Record (Santa Monica City Hall), b) Shear Forces in Piers 2 to 7**

# SECTION 7
# REFERENCES


1. Aydinoglu, M.N, and Erdik, M., (1995), "17 January 1995 Hyogo-ken Nanbu (Kobe) Earthquake Reconnaissance and Assessment Report", Kandilli Observatory and Earthquake Research Institute, Bebek-Istanbul, Turkey, 1995.

2. Baber, T.T., and Noori, M.N., (1985), "Random Vibration of Degrading Pinching Systems", Journal of Engineering Mechanics, ASCE, Vol. 111, No. 8, pp. 1010-1026.

3. Baber, T.T., and Wen, Y.K., (1981), "Random Vibration of Hysteretic Degrading Systems", Journal of Engineering Mechanics, ASCE, Vol. 107.

4. Bathe, K.-J., (1982), "Finite Element Procedures in Engineering Analysis", Prentice-Hall, Inc.

5. Bathe, K.-J., and Wilson, E.L., (1976), "Numerical Methods in Finite Element Analysis", Prentice-Hall, Inc.

6. Bouc, R. (1967), "Forced Vibrations of Mechanical Systems with Hysteresis", Proceedings of the 4th Conference on Nonlinear Oscillations, Prague.

7. Bouc, R. (1971), "Model Mathematique D'hysteresis", Acustica, Vol. 24, pp. 16-25, (in French).

8. Bracci, J.M., Reinhorn, A.M., and Mander, J.B., (1992), "Evaluation of Seismic Retrofit of Reinforced Concrete Frame Structures: Part III – Experimental Performance and Analytical Study of Retrofitted Structural Model Structure", Report No. NCEER-92-0031, National Center for Earthquake Engineering Research, State University of New York at Buffalo.

9. "Bridge Retrofit Procedures", Caltrans Interim Memo to Designers, 20-4, April 1992.

10. Buckle, I.G. (ed.), (1992), "Proceedings from the First US-Japan Workshop on Earthquake Protective Systems for Bridges", Report No. NCEER-92-0004, National Center for Earthquake Engineering Research, State University of New York at Buffalo.

11. Buckle, I.G., (1994), "The Northridge California Earthquake of January 17, 1994: Performance of Highway Bridges", Report No. NCEER-94-0008, National Center for Earthquake Engineering Research, State University of New York at Buffalo.

12. Carr, A.J., (1992), "Ruaumoko Inelastic Analysis Program", University of Canterbury, Christchurch, New Zealand.

13. Chopra, A.K., (1995), "Dynamics of Structures – Theory and Applications to Earthquake Engineering", Prentice-Hall, Inc.

14. Chung, Y.S., Meyer, C., and Shinozuka, M., (1987), "Seismic Damage Assessment of Reinforced Concrete Members", Report No. NCEER-87-0022, National Center for Earthquake Engineering Research, State University of New York at Buffalo.

15. Clough, R.W., and Penzien, J., (1993), "Dynamics of Structures", McGraw-Hill, Inc.

16. Collins, M.P., and Mitchell, D., (1991), "Prestressed Concrete Structures", Prentice-Hall Inc.

17. Constantinou, M.C. and Adnane, M.A., (1987), "Dynamics of Soil-Base-Isolated-Structure Systems – Evaluation of Two Models for Yielding Systems", Report to the National Science Foundation, September 1987, Drexel University.

18. Cosenza, E. and Manfredi, G., (1992), "Seismic Analysis of Degrading Models by Means of Damage Functional Concept", Monograph on Nonlinear Seismic Analysis of RC buildings, Editors: Fajfar, P., and Krawinkler, H., Elsevier Applied Science.

19. EERI, (1995), "Northridge Earthquake Reconnaissance Report", Vol. 1, Earthquake Spectra, Supplement to Vol. 11.

20. Fajfar, P., and Vidic T., (1994), "Consistent Inelastic Design Spectra: Hysteretic and Input Energy", Earthquake Engineering and Structural Dynamics, Vol. 23, 523-537.

21. Fischinger, M., Isakovic, T., and Fajfar, P., (1997), "Seismic Analysis of Viaduct Structures – Which Method to Use", Workshop on Seismic Design Methodology for the Next Generation of Codes, Bled, Slovenia, June 24-27, 1997, Balkema.

22. Hilber, H.M., Hughes, T.J.R., and Taylor, R.L., (1977), "Improved Numerical Dissipation for Time Integration Algorithms in Structural Dynamics", Earthquake Engineering and Structural Dynamics", Vol.5, pp. 283-292.

23. Housner, G. (ed.), (1990), "Competing Against Time", Report to the Governor of California.

24. Imbsen, R.A., and Penzien, J., (1986), "Evaluation of Energy Absorption Characteristics of Highway Bridges Under Seismic Conditions", Report No. UCB/EERC-84/17, Earthquake Engineering Research Center, University of California at Berkeley.

25. Iwasaki, T., Penzien, J., and Clough, R.W., (1972), "Literature Survey – Seismic Effects on Highway Bridges", Report No. UCB/EERC-72/11, Earthquake Engineering Research Center, University of California at Berkeley.

26. Kanaan, A.M., and Powell, G.H., (1973), "DRAIN-2D - A General purpose Computer Program for Dynamic Analysis of Inelastic Plane Structures with Users Guide", Report No. UCB/EERC-73/22, Earthquake Engineering Research Center, University of California at Berkeley.

27. Kincaid, D.R., Respess, J.R., Young, D.M., and Grimes, R.G., (1990), "ITPACK 2C: A Fortran Package for Solving Large Sparse Linear Systems by Adaptive Accelerated Iterative Methods", Download from NetLib.

28. Kunnath, S.K., Reinhorn, A.M., and Lobo, R.F., (1992), "IDARC Version 3.0: A Program for the Inelastic Damage Analysis of Reinforced Concrete Structures. " Report No. NCEER-92-0022, National Center for Earthquake Engineering Research, State University of New York, Buffalo, New York.

29. Lobo, F.L., (1994), "Inelastic Dynamic Analysis of Reinforced Concrete Structures in Three Dimensions", Ph.D. Dissertation, State University of New York at Buffalo.

30. Madan, A., (1996), "Non-Linear Modeling of Masonry Walls for Planar Analysis of Building Structures", Ph.D. Dissertation, Department of Civil Engineering, State University of New York at Buffalo.

31. Madan, A., Reinhorn, A.M. and Mander, J.B., (1997), "Flexural Behavior of Reinforced Masonry Shear Walls with Unbonded Reinforcement", The Masonry Journal, Professional Journal of Masonry Society.

32. Mander, J.B., Kim, J.H., Chen, S.S., and Premus, G.J., (1996), "Response of Steel Bridge Bearings to Reversed Cyclic Loading", Report No. NCEER-96-xxxx, National Center for Earthquake Engineering Research, State University of New York at Buffalo.

33. Manfredi, G., (1993), "Modeling of Damage in Seismic Analysis of Structures", Ph.D. Dissertation, Department of Civil Engineering, University of Naples "Federico II", Italy (in Italian).

34. Menun, C., (1996), "Multicomponent Excitation: A Replacement for the SRSS and 30 Percent Rules", News EERI, Vol. 17, No. 4, pp. 4-5.

35. Mokha, A.S., Constantinou, M.C., and Reinhorn, A.M., (1993), "Verification of Friction Model of Teflon Bearings under Triaxial Load", Journal of Structural Engineering, Vol. 119, No. 1, pp. 240-260.

36. Mylonakis, G., Simeonov, V.K., Reinhorn, A.M., and Buckle, I.G., (1997), "Implications of Spatial Variations of Ground Motion on the Seismic Response of Bridges: Case Study", ACI Journal, (in press).

37. Nagarajaiah, S., Reinhorn, A.M., and Constantinou, M.C., (1989), "Nonlinear Dynamic Analysis of Three-Dimensional Base Isolated Structures (3D-BASIS)", Report No. NCEER-89-0019, National Center for Earthquake Engineering Research, State University of New York at Buffalo.

38. Newmark, N.M., (1959), "A Method of Computing for Structural Dynamics" Journal of the Engineering Mechanics Division, Vol. 85, No. EM 3, pp. 67-94, July 1959.

39. Newmark, N.M., and Hall, W.J., (1981), "Earthquake Spectra and Design", Engineering Monographs on Earthquake Criteria, Structural Design, and Strong Motion Records, Editor: Agbabian, M.S., EERI, 1981.

40. Okamoto, S., (1983), "Introduction to Earthquake Engineering", 2nd edition, University of Tokyo Press.

41. Park, Y.J., and Ang, A.H-S., (1985), "Mechanistic Seismic Damage Model for Reinforced Concrete", Journal of Structural Engineering, ASCE, 111(4), 740-757.

42. Park, Y.J., Reinhorn, A.M. and Kunnath, S.K. (1987), "IDARC: Inelastic Damage Analysis of Reinforced Concrete Frame - Shear-Wall Structures", Report No. NCEER-87-0008, National Center for Earthquake Engineering, State University of New York, Buffalo, New York.

43. Paulay, T., and Priestley, M.J.N., (1992), "Seismic Design of Reinforced Concrete and Masonry Buildings", Wiley, 1992.

44. Powel, G.H., and Allahabadi, R., (1988), "Seismic Damage Prediction by Deterministic Methods: Concepts and Procedures", Earthquake Engineering and Structural Dynamic, Vol. 16, 719-734.

45. Priestley, M.J.N., and Calvi, G.M., (1997), "Concepts and Procedures for Direct Displacement-Based Design and Assessment", Workshop on Seismic Design Methodology for the Next Generation of Codes, Bled, Slovenia, June 24-27, 1997, Balkema.

46. Priestley, M.J.N., Seible, F., and Uang, C.M., (1991), "The Northridge Earthquake of January 17, 1994", Research Report SSRP-94/06, Department of Applied Mechanics and Engineering Sciences, University of California, San Diego.

47. Reichman, Y., (1996), "Evaluation of Bridge Structures Subjected to Severe Earthquakes", Ph.D. Dissertation, State University of New York at Buffalo.

48. Reinhorn, A.M., (1997), "Inelastic Analysis Techniques in Seismic Evaluations", Workshop on Seismic Design Methodology for the Next Generation of Codes, Bled, Slovenia, June 24-27, 1997, Balkema.

49. Reinhorn, A.M., and Barron, R., (1998), "Spectral Approach for Fragility Analysis of Structures", 11th European Conference in Earthquake Engineering, Paris, September 1998, (in print).

50. Reinhorn, A.M., Valles-Mattox, R., Lysiak, M., (1996), "Simplified Inelastic Response Evaluation Using Composite Spectra", ", Report No. NCEER-96-xxxx, National Center for Earthquake Engineering Research, State University of New York at Buffalo.

51. Smeby, W., and Der Kiureghian, A., (1985), "Modal Combination Rules for Multicomponent

Earthquake Excitation", Earthquake Engineering and Structural Dynamics, Vol. 13, pp. 1-12.

52. "Standard Specifications", (1992), State of California, Department of Transportation, July 1992.

53. "Standard Specifications for Highway Bridges", (1992), 15th Ed., American Association of State Highway and Transportation Officials, Including Interim Specifications for 1993, 1994 and 1995.

54. Tseng, W.S., and Penzien, J., (1975), "Seismic Analysis of Long Multiple-Span Highway Bridges", Earthquake Engineering and Structural Dynamics, Vol. 4, 3-24.

55. Tsopelas, P., Okamoto, S., Constantinou, M.C., Ozaki, D., Fujii, S., (1994), "NCEER-TAISEI Corporation Research Program on Sliding Seismic Isolation Systems for Bridges: Experimental and Analytical Study of Systems Consisting of Sliding Bearings, Rubber Restoring Force Devices and Fluid Dampers, Volume II", Report No. NCEER-94-0002, National Center for Earthquake Engineering Research, State University of New York at Buffalo.

56. Valles, R.E., Reinhorn, A.M., Kunnath, S.K., Li, C., and Madan, A., (1996), "IDARC2D Version 4.0: A Computer Program for the Inelastic Damage Analysis of Buildings", Report No. NCEER-96-0010, National Center for Earthquake Engineering Research, State University of New York at Buffalo.

57. Weaver, W., and Gere, J.M., (1990), "Matrix Analysis of Framed Structures", Van Nostrand Reinhold.

58. Wen, Y.K., (1976), "Method of Random Vibration of Hysteretic Systems", J. of Eng. Mech. Div. ASCE, 102(EM2), 249-263.

59. Wendichansky, D.A., (1996), "Experimental Investigation of the Dynamic Response of Two Bridges before and after Retrofitting with Elastomeric Bearings", Ph.D. Dissertation, State University of New York at Buffalo.

60. Williams, M.S., and Sexsmith, R.G., (1994), "Review of Methods of Assessing Seismic Damage in Concrete Structures", Report No. UBC 94-02, Earthquake Engineering Research Facility, University of British Columbia.

61. Wolf, J.P., (1985), "Dynamic Soil-Structure Interaction", Prentice-Hall, Inc.

62. Zayas, V.A., Low, S.S., and Mahin, S.A., (1987), "FPS Earthquake Resisting System Experimental Report", Report No. UCB/EERC-87/01, Earthquake Engineering Research Center, University of California at Berkeley.

63. Zenkiewicz, O.C., (1977), "The Finite Element Method", McGraw-Hill, London, England.

# APPENDIX A
# USER MANUAL

## INTRODUCTION

The following general instructions will aid the user in creating the input files for the computer program IDARC-BRIDGE. It will be beneficial to refer to the example problems in section 6 of this report.

The general input file must be named "in_file". It is divided into sections whose titles start with the "*" symbol. The user must input the title of each section exactly as suggested in the presentation of the sets in this manual. Only titles of sections and commands may appear in the input file, blank lines are not permitted.

The order in which different sections appear in "in_file" is not significant unless information from one section is used in the subsequent sections. For example, definition of elements must be preceded by definition of joints. It is, therefore, preferable to follow the sequence used in this guide.

The order in which input data appears in each command must be adhered to strictly. One or more blanks but no tabs can be used as separators. As many commands as needed may be issued within each section of the format typical of that section.

Titles of sections and keywords in commands are printed in **bold normal typeface**. Titles of sections and the first keyword of each command can not be altered. All other keywords can be shortened to only three letters.

Parts of commands printed in ***bold italic typeface*** can take any of the values (typically alpha-numerical strings) following the equal sign in the "Description" paragraph to each command or will require assigning of numerical values.

One or more loading files will be needed to perform dynamic analysis. Details about their format are provided in the "***excitation groups**" and "***time history analysis**" sections.

The global coordinate system is an arbitrary rectangular coordinate system in space, which follows the right hand rule. The global Y axis is always vertical. This coordinate system is used to define the joint (node) locations and loading direction. The translational degrees of freedom are denoted by: $u_1$ (or $u_x$), $u_2$ ($u_y$), $u_3$ ($u_z$) and the rotational degrees of freedom - by $u_4$ ($rot_x$), $u_5$ ($rot_y$), $u_6$ ($rot_z$). The degrees of freedom are also referred to as numbers: 1, 2, 3, 4, 5 and 6 respectively.

## INSTALLATION INSTRUCTIONS

The IDARC-BRIDGE program will compile, link and execute on Sun™ workstations running SunOS™ or SOLARIS operating system. The compiler must support the Sun FORTRAN language extensions (dynamic arrays, integer pointers etc.). A separate compilation will be needed for computers running SunOS and SOLARIS. Executable files for PC using -386, -486 or Pentium processors can be created using the appropriate options for the Sun FORTRAN compiler.

The following commands must be issued at the command line prompt to compile and link the program:

| **UNIX Command:** | **Description:** |
|---|---|
| **mkdir bridge** | Creates a new directory **bridge** |
| **cd bridge** | Changes directory to **bridge** |
| **set path = ($path $cwd)** | Sets path to the current working directory, i.e. **bridge** |

Copy archive tar file **bridge.tar** from the distribution diskette (or its current location) to directory **bridge**. The appropriate UNIX command is:

**cp** ***copy_from_file_name copy_to_file_name***

| | |
|---|---|
| **tar xvf bridge.tar** | Extracts multiple files containing source code from the single archive tar file **bridge.tar** |
| **makemake1 r** or | Runs program **makemake1** - a Makefile generation script provided with the distribution diskette (the **r** option will force the compiler to recursively traverse the directories) |
| **makemake1 r -g** or, | Runs program **makemake1** - a Makefile generation script (the **r** option will force the compiler to recursively traverse the directories, the **-g** option will cause compilation with debugging) |
| **makemake1 r -o** or, | Runs program **makemake1** - a Makefile generation script (the **r** option will force the compiler to recursively traverse the directories, the **-o** option will cause compilation with optimization) |
| **makemake1 r -l** | Runs program **makemake1** - a Makefile generation script (the **r** option will force the compiler to recursively traverse the directories, the **-l** option will cause generation of archived library at top level) |
| **make** | Compiles and links the source code |
| **bridge** | Executes the program |

## USER MANUAL

## GENERAL INFORMATION

SET A1:

Title of section:

***analysis type**

Command:

**at *dimension***

Description:

| | |
|---|---|
| **at** | keyword |
| ***dimension*** | = **3d** |
| | = **2d** |

Notes:

1) The user must input only one of the options for the variable ***dimension***. Choice of the option **3d** will result in the program performing three-dimensional analysis. Similarly, the option **2d** means two-dimensional analysis.

2) The option **2d** is not available in the current version of the program.

**SET A2:**

Title of section:

***analysis options**

Command:

**ao** ***input***

Description:

| | |
|---|---|
| **ao** | keyword |
| ***input*** | **= quasistatic force** |
| | **= quasistatic displacements** |
| | **= dynamic acceleration** |
| | **= dynamic displacements** |
| | **= dynamic force** |
| | **= modal analysis** |
| | **= push modal** |
| | **= push user** |
| | **= push ramp** |

Notes:

1) The user must use only one of the options for the variable ***input***. Choice of **quasistatic force** results in analysis of the structure for incremental force loading, **quasistatic displacements** - analysis for incremental displacement loading, **dynamic acceleration** - dynamic analysis for ground acceleration input, **dynamic displacements** - dynamic analysis for ground displacement

input, **dynamic force** - analysis for dynamic force loading, **modal analysis** - analysis for determining the natural frequencies and mode shapes of the structure.

2) The first two pushover analysis options differ by the distribution of the forces acting on (pushing) the structure: (i) in **push modal** it is controlled by the instantaneous mode shapes and the weights lumped at the joints (nodes) of the structural model, (ii) in **push user** - by concentrated loads acting on the joints (nodes) of the structural model. Both the weights and the loads are provided by the user. Two criteria are used to stop either analysis: 1) maximum displacement at a joint along a degree of freedom and/or 2) fraction of the total base shear.

3) The **push ramp** pushover analysis requires the input of the application rates of linearly increasing acceleration acting in the two horizontal (x and z) global directions in units of [m/sec$^3$]. The analysis ends when the displacement at a joint along a degree of freedom specified by the user is reached.

**SET A3:**

Title of section:

***units**

Command:

**un** ***length weight angle***

Description:

| | |
|---|---|
| **un** | keyword |
| ***length*** | **= meter** |
| | **= centimeter** |
| | **= millimeter** |
| | **= feet** |
| | **= inch** |
| ***weight*** | **= kilogram** |
| | **= newton** |
| | **= pound** |
| | **= ton** |
| | **= kilonewton** |
| | **= kips** |
| ***angle*** | **= degrees** |
| | **= radians** |

Notes:

1) The user must choose only one of the options for the fields ***length***, ***weight*** and ***angle***. For example, the command **un meter kilonewton degrees** means that all dimensions in the input file are in units of [m], weights - in units of [kN] and angles - in units of [deg]. Any combination of consistent units is valid.

## STRUCTURAL COMPONENTS AND PROPERTIES

As many commands as needed can be input following the title of a section but only with the command syntax typical of that section.

**SET B1:**

Title of section:

***joint coordinates**

Command:

**co** ***joint_number x y z***

Description:

| | |
|---|---|
| **co** | keyword |
| ***joint_number*** | number of joint (node) assigned by the user |
| ***x*** | number (global x coordinate of joint) |
| ***y*** | number (global y coordinate of joint) |
| ***z*** | number (global z coordinate of joint) |

Notes:

1) This command is used for defining joint coordinates in the global coordinate system.
2) Joint numbers must be consecutive.

**SET B2:**

Title of section:

***boundary conditions**

Command:

**bc** ***bound_cond joint_list***

Description:

| | |
|---|---|
| **bc** | keyword |
| ***bound_cond*** | number (a string of six digits each either 0 or 1) identifying the boundary condition<br>**= pinned**<br>**= fixed** |
| ***joint_list*** | list of joint numbers separated by spaces and/or<br>joint number to joint number |

Notes:

1) This command defines translational and rotational constraints on joints. Each joint has six degrees of freedom ($u_x$, $u_y$, $u_z$, $rot_x$, $rot_y$, $rot_z$) in the global coordinate system. A value of **1** in any of the six positions in the ***bound_cond*** string indicates that the corresponding degree of freedom is restrained. Conversely, a value of **0** shows that the degree of freedom is unrestrained (free). Therefore, the string **111110** will denote that the only possible motion that a joint (at a support location, etc.) can experience is rotation about the global z axis. If the second option for the ***bound_cond*** field is adopted for use, **pinned** would indicate that all translational degrees of

freedom are restrained while the rotational degrees of freedom are unrestrained. Use of **fixed** would mean that all six degrees of freedom of a joint are restrained.

2) The second option for the ***joint_list*** field can be used to apply a boundary condition to a group of joints having consecutive numbers. It can also be combined with the first option. For example, the command **bc 111000 4 6 8 to 11** will result in applying translational constraints on joints 4, 6, 8, 9, 10, 11.

3) Boundary conditions at no more than ***30*** joints can be defined with a single command.

**SET B3:**

Title of section:

***coupled equations**

Command:

**ce** ***slaved_joint slaved_dof*** **slave joint** ***joint_list*** **dof** ***dof_list*** **coefficient** ***coef_list***

Description:

| | |
|---|---|
| **ce** | keyword |
| ***slaved_joint*** | number of slaved joint |
| ***slaved_dof*** | number of slaved degree of freedom |
| **slave joint** | keyword |
| ***joint_list*** | list of joint numbers |
| **dof** | keyword |
| ***dof_list*** | list of degrees of freedom |
| **coefficient** | keyword |
| ***coef_list*** | list of coefficients |

Notes:

1) This command is used for relating the displacements or rotations of one joint to displacements and/or rotations of other joints in the structure. For example, the command **ce 6 2 slave joint 7 7 dof 2 6 coefficient -1.0 -2.5** will express the fact that the displacement of joint 6 along the global y axis (dof 2) is equal to the displacement of joint 7 along the global y axis (dof 2) multiplied by 1.0 plus the rotation of joint 7 about the global z axis (dof 6) multiplied by 2.5. In equation format this can be written as:

$$u_{y_6} + (-1.0)u_{y_7} + (-2.5)rot_{z_7} = 0 \Rightarrow u_{y_6} = 1.0u_{y_7} + 2.5rot_{z_7}$$

The origin and meaning of the coefficients in the coupled equations command becomes apparent from this representation.

**SET B4:**

Title of section:

***element properties**

Command:

This multiple-line command has different syntax depending on the type of the element whose properties are defined. Properties of elements of a similar kind are defined in a list after the element type. Each property is assigned a number in the list and consists of various cross-sectional and/or material attributes. A property number can be associated with an element after the structural geometry is defined.

If the entry in the ***element_type*** field below is any of the following: **elastic beam 3d**, **elastic beam 2d**, **isolator 1**, **isolator slider**, **bilinear gap**, **elastic foundation** or **linear damper**, the command has the syntax:

***element_type***
**property 1**
***label_1 value_1 label_2 value_2 label_3 value_3 ...***
***label_1 value_1 label_2 value_2 label_3 value_3 ...***
***label_1 value_1 label_2 value_2 label_3 value_3 ...***
**property 2**
***label_1 value_1 label_2 value_2 label_3 value_3 ...***
***label_1 value_1 label_2 value_2 label_3 value_3 ...***
***label_1 value_1 label_2 value_2 label_3 value_3 ...***
**... ...**
**end *element_type* properties**

Description:

| | |
|---|---|
| ***element_type*** | = **elastic beam 3d** |
| | = **elastic beam 2d** (not available in the current version) |
| | = **isolator 1** |
| | = **isolator slider** |
| | = **bilinear gap** |
| | = **elastic foundation** |
| | = **linear damper** |
| **property** | keyword |
| **1** | number of property |
| ***label_1*** | first label in the first input line (specific for each element type - see notes) |
| ***value_1*** | value of the attribute identified by the first label |
| ***label_2*** | second label in the first input line (specific for each element type – see notes) |
| ***value_2*** | value of the attribute identified by the second label |
| ***label_3*** | third label in the first input line (specific for each element type - see notes) |
| ***value_3*** | value of the attribute identified by the third label |

Continue until all attribute labels in the first input line of the first property are assigned values.

| | |
|---|---|
| ***label_1*** | first label in the second line |
| ***value_1*** | value of the attribute identified by the first label |
| ***label_2*** | second label in the second line |
| ***value_2*** | value of the attribute identified by the second label |
| ***label_3*** | third label in the second line |
| ***value_3*** | value of the attribute identified by the third label |

Continue until all attribute labels in the second input line of the first property are assigned values.

| | |
|---|---|
| ***label_1*** | first label in the third line |
| ***value_1*** | value of the attribute identified by the first label |
| ***label_2*** | second label in the third line |
| ***value_2*** | value of the attribute identified by the second label |
| ***label_3*** | third label in the third line |
| ***value_3*** | value of the attribute identified by the third label |

Continue until all attribute labels in the third input line of the first property are assigned values.

Repeat until all properties necessary for the definition of different elements of the same element type are input.

| | |
|---|---|
| **end** | keyword |
| ***element_type*** | = **elastic beam 3d** |
| | = **elastic beam 2d** (not available in the current version) |
| | = **isolator 1** |
| | = **isolator slider** |
| | = **bilinear gap** |
| | = **elastic foundation** |
| | = **linear damper** |
| **properties** | keyword |

Repeat until all properties of all element types used in the analysis are assigned numbers and all attribute labels within each property are assigned values.

Notes:

Labels of geometric and material attributes of the **elastic beam 3d** element:

First Input Line:

| | |
|---|---|
| **a** | area of cross section |
| **ixx** | torsional moment of inertia |
| **iyy** | moment of inertia about the y-y axis of the section (typically the vertical axis orthogonal to the beam centerline or the weak axis) |
| **izz** | moment of inertia about the z-z axis of the section (typically the horizontal axis orthogonal to the beam centerline or the strong axis) |
| **e** | modulus of elasticity of material |
| **g** | modulus of shear deformations |
| **theta** | angle of rotation of the local coordinate system about the element axis |

Second Input Line (optional):

| | |
|---|---|
| **fy** | form factor for shear along the y-y axis of the section |
| **fz** | form factor for shear along the z-z axis of the section |

Notes on the **elastic beam 3d** element:

1) The relationship between the local coordinate system of a beam element and the global coordinate system is determined by the ***theta*** angle. The origin of the local coordinate system is typically located at the first joint (node) of the element; the positive X axis is along the beam centerline toward the second joint (node); the Y axis is the weak axis and the Z axis is the strong axis of the beam cross section. When the local X axis is parallel to the global Y axis, i.e. vertical, the ***theta*** angle is the angle between the local Z axis and the global Z axis. If the local X axis is not vertical, ***theta*** is the angle through which the local coordinate system has been rotated about the local X axis from a position where the local Z axis is parallel to the global XZ plane and the local Y axis is pointing in the same positive direction as the global Y axis.

2) The form factors for shear relate the total area to the reduced (shear) area of the cross section:

$$A_y = \frac{A}{f_y} \qquad A_z = \frac{A}{f_z}$$

where:

A = Total area of the cross section.

$A_y$ and $A_z$ = Shear areas of the section.

Typical values of the form factor are: (I) rectangle f = 6/5, (ii) circle f = 10/9, (iii) thin-walled tube f = 2. A zero input for either $f_y$ or $f_z$, or both will eliminate the shearing deformations in the respective local direction of the beam.

3) All attributes in the first line of input must be given numerical values.

4) Omitting the optional input line has the effect of assigning zero values to all attributes in it.

Labels of geometric and material attributes of the **isolator 1** element:

First Input Line:

| | |
|---|---|
| **alpha** | ratio of post-yield to elastic stiffness |
| **beta** | loop controlling parameter |
| **gamma** | loop controlling parameter |
| **uy** | yield displacement |
| **fy** | yield force |

Second Input Line (optional):

| | |
|---|---|
| **theta angle** | angle of rotation of the local coordinate system about the element axis |

Notes on the **isolator 1** element:

1) The position of the local coordinate system with respect to the end joints follows rules identical to those for the **elastic beam 3d** element, presented earlier.
2) The element axis has to be vertical. To achieve that, the end joints have to be one above the other either by definition or by rigid body transformations (see the "*rigid arms" command).
3) Omitting the optional input line has the effect of assigning zero values to all attributes in it.

Labels of geometric and material attributes of the **isolator slider** element:

First Input Line:

| | |
|---|---|
| **iforce** | initial compression force from static load (i.e. without dynamic contribution) – typically the compression force resulting from dead load |
| **istiffness** | stiffness of the device before sliding occurs |
| **sstiffness** | stiffness of the device after sliding (due to the re-centering spring) |
| **vlimit** | velocity limit above which the friction coefficient is constant and equal to $\mu_{max}$ |
| **mmin** | minimum value of the coefficient of friction (at low velocity) |
| **mmax** | maximum value of the coefficient of friction (at high velocity) |
| **mstatic** | breakaway coefficient of friction |

Notes on the **isolator slider** element:

1) The orientation of the local coordinate system is independent of the location of the end joints. It is assumed parallel to the global coordinate system.
2) The program, however, uses the spatial coordinates of the end nodes to calculate the "rigid arms" of the element, if such are defined (see the "*rigid arms" command).

Labels of geometric and material attributes of the **bilinear gap** element:

First Input Line:

| | |
|---|---|
| **cgap** | compression gap (displacement at the beginning of the initial compression branch) |
| **tgap** | tension gap (displacement at the beginning of the initial tension branch) |
| **cistiffness** | initial compression stiffness |
| **tistiffness** | initial tension stiffness |
| **cdisp** | displacement at the beginning of second compression branch |
| **tdisp** | displacement at the beginning of the second tension branch |
| **cstiffness** | secondary compression stiffness |
| **tstiffness** | secondary tension stiffness |

Notes on the **bilinear gap** element:

1) The position of the local coordinate system with respect to the end joints follows rules identical to those for the **elastic beam 3d** element, presented earlier.
2) Steep changes of stiffness (say, more than three orders of magnitude between adjacent branches of the force-displacement relation) may cause convergence problems.

Labels of geometric and material attributes of the **elastic foundation** element:

First Input Line

| | |
|---|---|
| **kx** | translational stiffness in the local X direction |
| **ky** | translational stiffness in the local Y direction |
| **kz** | translational stiffness in the local Z direction |
| **krx** | rotational stiffness about the local X axis |
| **kry** | rotational stiffness about the local Y axis |
| **krz** | rotational stiffness about the local Z axis |

Second Input Line (optional)

| | |
|---|---|
| **kxkry** | cross stiffness coefficient relating the translational DOF in the local X direction and the rotational DOF about the local Y axis |
| **kxkrz** | cross stiffness coefficient relating the translational DOF in the local X direction and the rotational DOF about the local Z axis |
| **kykrx** | cross stiffness coefficient relating the translational DOF in the local Y direction and the rotational DOF about the local X axis |
| **kykrz** | cross stiffness coefficient relating the translational DOF in the local Y direction and the rotational DOF about the local Z axis |
| **kzkrx** | cross stiffness coefficient relating the translational DOF in the local Z direction and the rotational DOF about the local X axis |
| **kzkry** | cross stiffness coefficient relating the translational DOF in the local Z direction and the rotational DOF about the local Y axis |

Third Input Line (optional)

| | |
|---|---|
| **theta angle** | angle of rotation of the local coordinate system about the element axis |

Notes on the **elastic foundation** element:

1) The position of the local coordinate system with respect to the end joints follows rules identical to those for the **elastic beam 3d** element, presented earlier.

2) Omitting the optional input lines has the effect of assigning zero values to all attributes in them.

Labels of geometric and material attributes of the **linear damper** element:

First Input Line

| | |
|---|---|
| **cx** | translational damping in the local X direction |
| **cy** | translational damping in the local Y direction |
| **cz** | translational damping in the local Z direction |
| **crx** | rotational damping about the local X axis |
| **cry** | rotational damping about the local Y axis |
| **crz** | rotational damping about the local Z axis |

Second Input Line (optional)

| | |
|---|---|
| **cxcry** | cross damping coefficient relating the translational DOF in the local X direction and the rotational DOF about the local Y axis |
| **cxcry** | cross damping coefficient relating the translational DOF in the local X direction and the rotational DOF about the local Z axis |
| **cycrx** | cross damping coefficient relating the translational DOF in the local Y direction and the rotational DOF about the local X axis |
| **cycrz** | cross damping coefficient relating the translational DOF in the local Y direction and the rotational DOF about the local Z axis |
| **czcrx** | cross damping coefficient relating the translational DOF in the local Z direction and the rotational DOF about the local X axis |
| **czcry** | cross damping coefficient relating the translational DOF in the local Z direction and the rotational DOF about the local Y axis |

Third Input Line (optional)

| | |
|---|---|
| **theta angle** | angle of rotation of the local coordinate system about the element axis |

Notes on the **linear damper** element:

1) The position of the local coordinate system with respect to the end joints follows rules identical to those for the **elastic beam 3d**, presented earlier.

2) Omitting the optional input lines has the effect of assigning zero values to all attributes in them.

**SET B4 (CONTINUED):**

Command:

If the entry in the ***element_type*** field below is **hysteretic beam 3d** or **hysteretic beam 2d**, the command has the syntax:

***element_type***
**property 1**
**axial stiffness** ***axial_stiff_value***
**torsional stiffness** ***tors_stiff_value***
**theta angle** ***theta***
**sign** ***sign***
**member** ***location***
**direction** ***direction***
**moment** ***cracking_moment yielding_moment ultimate_moment***
**curvature** ***cracking_curvature yielding_curvature ultimate_curvature***
**loop parameters**
**stren deter** ***value*** **stiff degra** ***value*** **slip control** ***value*** **slip factor** ***value***
**property 2**
...
**end** ***element_type*** **properties**

Description:

| | |
|---|---|
| ***element_type*** | = **hysteretic beam 3d** |
| | = **hysteretic beam 2d** (not available in the current version) |
| **property** | keyword |
| **1** | number of property |
| **axial stiffness** | keyword |

| | |
|---|---|
| ***axial_stiff_value*** | elastic axial stiffness of the element |
| **torsional stiffness** | keyword |
| ***tors_stiff_value*** | elastic torsional stiffness of the element |
| **theta angle** | keyword |
| ***theta*** | angle of rotation of the local coordinate system about the element axis |
| **sign** | keyword |
| ***sign*** | **= positive** |
| | **= negative** |
| | **= all** |
| **member** | keyword |
| ***location*** | **= start** |
| | **= end** |
| | **= all** |
| **direction** | keyword |
| ***direction*** | **= y** |
| | **= z** |
| | **= all** |
| **moment** | keyword |
| ***cracking_moment*** | bending moment that initiates cracking of the element at a section the location of which is specified in ***location***, from bending in a plane identified in ***direction*** (**y** means local XY plane, etc.) and pointing in the direction (indicated in ***sign***) of the axis orthogonal to that plane following the right-hand rule |
| ***yielding_moment*** | bending moment that initiates yielding of the element |
| ***ultimate_moment*** | bending moment that causes failure of the element |
| **curvature** | keyword |
| ***cracking_curvature*** | curvature of the section (at which the element cracks) at the location specified in ***location***, from bending in a plane identified in ***direction*** (**y** means local XY plane, etc.) and pointing in the direction (indicated in ***sign***) of the axis orthogonal to that plane following the right-hand rule |

| | |
|---|---|
| ***yielding_curvature*** | curvature of the section at which the element yields |
| ***ultimate_curvature*** | curvature of the section at which the element fails |
| **loop parameters** | keyword |
| **stren deter** | keyword |
| ***value*** | strength deterioration parameter (see Note 2) |
| **stiff degra** | keyword |
| ***value*** | stiffness degradation parameter (see Note 3) |
| **slip control** | keyword |
| ***value*** | slip control parameter - used for modeling pinching behavior (see Note 4) |
| **slip factor** | keyword |
| ***value*** | slip closing parameter - used for modeling pinching behavior (see Note 5) |

Notes on the **hysteretic beam 3d** element:

1) In this version of IDARC-BRIDGE, the parameters controlling the hysteretic behavior at the ends of the element are assumed identical for negative and positive moment-curvature relations. The subroutine, however, has the capability to handle different values in the positive and negative loading branches.

2) The **strength deterioration parameter** (β parameter in other programs of the IDARC family) represents the ratio of plastic deformation increase per unit increase of absorbed energy. The change of the target deformation is proportional to the parameter divided by the corresponding yield moment. Typical values:

* No strength deterioration (steel): 0.0
* Severe strength deterioration: 0.4
* Recommended value for reinforced concrete: **0.1**

3) Stiffness degradation in the hysteretic model is accounted for by forcing the unloading branches to aim at the same point. The target unloading point is found by multiplying the

yielding moment by the **stiffness degradation parameter** (formerly $\alpha$ parameter). Typical values:

* Severe stiffness degradation: 0.1
* Negligible stiffness degradation (steel): 10.0
* Recommended value for reinforced concrete: **2.0**

4) After the beam element has passed a full cycle of cracking and yielding at a given section slipping of steel inside concrete may occur. The yielding moment after slipping is obtained by multiplying the **slip control parameter** (formerly $\gamma$ parameter) by the yielding moments thus defining a lower target point for the reloading branch. Typical values:

* Extremely pinched loops: 0.1
* No pinching (steel): 1.0
* Recommended value for reinforced concrete: **0.5**

5) Range of values for the **slip closing parameter** (formerly SLPF parameter): $0 \div 1$.

* Recommended value for steel: 1.0.
* Recommended value for reinforced concrete: **0.8**.

6) The moment-curvature (M-$\phi$) relationships at the ends of the element are trilinear or, rather, the monotonic envelopes are trilinearized so that the initial, post-cracking and post-yielding stiffnesses of reinforced and prestressed concrete members or the initial and post-yielding stiffnesses of steel members are realistic. A section analysis program may be needed to establish these envelopes in cases of complicated section geometry or reinforcing pattern. A typical example of such software, capable of handling section of any size, geometry, multiple reinforcing steel layers, prestressing, strain hardening of steel, etc., is "RESPONSE" (Collins and Mitchell, 1991).

7) The slope of the post-yielding branch of the M-$\phi$ relationship can not be negative or zero, i.e. the input value in the ***ultimate_moment*** field above must always be greater than that in the ***yielding_moment*** field.

8) A practical approach to obtain the ultimate moment that can be sustained at a section is to perform analysis of the section for a curvature that causes the extreme concrete fiber to attain compressive strain of 0.005 (0.003 recommended by ACI).

9) Convergence can become a problem if the post-yielding slope of the M-$\phi$ relationship is close to zero. The recommended ratio of the post-yielding to post-cracking slope (or initial in the case of structural steel) is in the range 0.001÷0.01. This is easy to achieve if the strain hardening of reinforcing (or structural) steel is accounted for in the section analysis.

10) Boundary conditions at the ends of a **hysteretic beam 3d** element can be implemented by applying stiff springs. An **elastic foundation** element can be created between the joint at the end of the member and a joint defined in the near vicinity representing the surrounding soil. The latter joint is then fixed and appropriate stiffnesses are assigned to the **elastic foundation** element. To simulate full fixity, for example, the rotational stiffness to bending in a given global plane must be greater by an order of magnitude than the flexural rigidity EI of the end section of the **hysteretic beam 3d** element to bending in that direction (EI = ***cracking_moment*** / ***cracking_curvature***).

11) The relationship between the local coordinate system of a beam element and the global coordinate system is determined by the ***theta*** angle. The origin of the local coordinate system is typically at the first joint (node) of the element, the positive X axis is along the beam centerline toward the second joint (node), the Y axis is the weak axis and the Z axis is the strong axis of the beam cross section. When the local X axis is parallel to the global Y axis, i.e. vertical, the ***theta*** angle is the angle between the local Z axis and the global Z axis. If the local X axis is not vertical, ***theta*** is the angle through which the local coordinate system has been rotated about the local X axis from a position where the local Z axis is parallel to the global XZ plane and the local Y axis is pointing in the same positive direction as the global Y axis.

**SET B4 (CONTINUED):**

Command:

If the entry in the ***element_type*** field below is **hysteretic beam 3d shear**, the command has the syntax:

***element_type***
**property 1**
**axial stiffness** ***axial_stiff_value***
**torsional stiffness** ***tors_stiff_value***
**sign** ***sign***
**member** ***location***
**direction** ***direction***
**moment** ***cracking_moment yielding_moment ultimate_moment***
**curvature** ***cracking_curvature yielding_curvature ultimate_curvature***
**shear** ***yielding_shear ultimate_shear***
**displacement** ***yielding_disp ultimate_disp***
**loop parameters**
**stren deter** ***value*** **stiff degra** ***value*** **slip control** ***value*** **slip factor** ***value***
**property 2**
**...**
**end** ***element_type*** **properties**

Description:

| | |
|---|---|
| ***element_type*** | = **hysteretic beam 3d shear** |
| | = **hysteretic beam 2d shear** (not available in the current version) |
| **property** | keyword |
| **1** | number of property |

| | |
|---|---|
| **axial stiffness** | keyword |
| ***axial_stiff_value*** | elastic axial stiffness of the element |
| **torsional stiffness** | keyword |
| ***tors_stiff_value*** | elastic torsional stiffness of the element |
| **theta angle** | keyword |
| ***theta*** | angle of rotation of the local coordinate system about the element axis |
| **sign** | keyword |
| ***sign*** | **= positive** |
| | **= negative** |
| | **= all** |
| **member** | keyword |
| ***location*** | **= start** |
| | **= end** |
| | **= all** |
| **direction** | keyword |
| ***direction*** | **= y** |
| | **= z** |
| | **= all** |
| **moment** | keyword |
| ***cracking_moment*** | bending moment that initiates cracking of the element at a section the location of which is specified in ***location***, from bending in a plane identified in ***direction*** (**y** means local XY plane, etc.) and pointing in the direction (indicated in ***sign***) of the axis orthogonal to that plane following the right-hand rule |
| ***yielding_moment*** | bending moment that initiates yielding of the element |
| ***ultimate_moment*** | bending moment that causes failure of the element |
| **curvature** | keyword |
| ***cracking_curvature*** | curvature of the section (at which the element cracks) at the location specified in ***location***, from bending in a plane identified in ***direction*** (**y** means local XY plane, etc.) and pointing in the direction (indicated in |

| | |
|---|---|
| | ***sign***) of the axis orthogonal to that plane following the right-hand rule |
| ***yielding_curvature*** | curvature of the section at which the element yields |
| ***ultimate_curvature*** | curvature of the section at which the element fails |
| **shear** | keyword |
| ***yielding_shear*** | force coordinate of the first point on the force-displacement curve (yielding shear force) |
| ***ultimate_shear*** | force coordinate of the second point on the force-displacement curve (ultimate shear force) |
| **displacement** | keyword |
| ***yielding_disp*** | displacement coordinate of the first point on the force-displacement curve (displacement at yield) |
| ***ultimate_disp*** | displacement coordinate of the second point on the force-displacement curve (ultimate displacement) |
| **loop parameters** | keyword |
| **stren deter** | keyword |
| ***value*** | strength deterioration parameter (see Note 2) |
| **stiff degra** | keyword |
| ***value*** | stiffness degradation parameter (see Note 3) |
| **slip control** | keyword |
| ***value*** | slip control parameter - used for modeling pinching behavior (see Note 4) |
| **slip factor** | keyword |
| ***value*** | slip closing parameter - used for modeling pinching behavior (see Note 5) |

Notes on the **hysteretic beam 3d shear** element:

1) In this version of IDARC-BRIDGE, the parameters controlling the hysteretic behavior at the ends of the element are assumed identical for negative and positive moment-curvature relations.

The subroutine, however, has the capability to handle different values in the positive and negative loading branches.

2) The **strength deterioration parameter** (β parameter in other programs of the IDARC family) represents the ratio of plastic deformation increase per unit increase of absorbed energy. The change of the target deformation is proportional to the parameter divided by the corresponding yield moment. Typical values:

* No strength deterioration (steel): 0.0
* Severe strength deterioration: 0.4
* Recommended value for reinforced concrete: **0.1**

3) Stiffness degradation in the hysteretic model is accounted for by forcing the unloading branches to aim at the same point. The target unloading point is found by multiplying the yielding moment by the **stiffness degradation parameter** (formerly α parameter). Typical values:

* Severe stiffness degradation: 0.1
* Negligible stiffness degradation (steel): 10.0
* Recommended value for reinforced concrete: **2.0**

4) After the beam element has passed a full cycle of cracking and yielding at a given section slipping of steel inside concrete may occur. The yielding moment after slipping is obtained by multiplying the **slip control parameter** (formerly γ parameter) by the yielding moments thus defining a lower target point for the reloading branch. Typical values:

* Extremely pinched loops: 0.1
* No pinching (steel): 1.0
* Recommended value for reinforced concrete: **0.5**

5) Range of values for the **slip closing parameter** (formerly SLPF parameter): $0 \div 1$.

* Recommended value for steel: 1.0.
* Recommended value for reinforced concrete: **0.8**.

6) The moment-curvature (M-ϕ) relationships at the ends of the element are trilinear or, rather, the monotonic envelopes are tri-linearized so that the initial, post-cracking and post-yielding stiffnesses of reinforced and prestressed concrete members or the initial and post-yielding stiffnesses of steel members are realistic. A section analysis program may be needed to establish

these envelopes in cases of complicated section geometry or reinforcing pattern. A typical example of such software, capable of handling section of any size, geometry, multiple reinforcing steel layers, prestressing, strain hardening of steel, etc., is "RESPONSE" (Collins and Mitchell, 1991).

7) The slope of the post-yielding branch of the M-$\phi$ relationship can not be negative or zero, i.e. the input value in the ***ultimate_moment*** field above must always be greater than that in the ***yielding_moment*** field.

8) A practical approach to obtain the ultimate moment that can be sustained at a section is to perform analysis of the section for a curvature that causes the extreme concrete fiber to attain compressive strain of 0.005 (0.003 recommended by ACI).

9) Convergence can become a problem if the post-yielding slope of the M-$\phi$ relationship is close to zero. The recommended ratio of the post-yielding to post-cracking slope (or initial in the case of structural steel) is in the range 0.001÷0.01. This is easy to achieve if the strain hardening of reinforcing (or structural) steel is accounted for in the section analysis.

10) Boundary conditions at the ends of a **hysteretic beam 3d** element can be implemented by applying stiff springs. An **elastic foundation** element can be created between the joint at the end of the member and a joint defined in the near vicinity representing the surrounding soil. The latter joint is then fixed and appropriate stiffnesses are assigned to the **elastic foundation** element. To simulate full fixity, for example, the rotational stiffness to bending in a given global plane must be greater by an order of magnitude than the flexural rigidity EI of the end section of the **hysteretic beam 3d** element to bending in that direction (EI = ***cracking_moment*** / ***cracking_curvature***).

11) The relationship between the local coordinate system of a beam element and the global coordinate system is determined by the ***theta*** angle. The origin of the local coordinate system is typically at the first joint (node) of the element, the positive X axis is along the beam centerline toward the second joint (node), the Y axis is the weak axis and the Z axis is the strong axis of the beam cross section. When the local X axis is parallel to the global Y axis, i.e. vertical, the ***theta*** angle is the angle between the local Z axis and the global Z axis. If the local X axis is not vertical, ***theta*** is the angle through which the local coordinate system has been rotated about the

local X axis from a position where the local Z axis is parallel to the global XZ plane and the local Y axis is pointing in the same positive direction as the global Y axis.

12) This element is still under construction in the current version. Use of the ***hysteretic beam 3d*** element instead is recommended.

**SET B5:**

Title of section:

***element definition**

Command:

**element** ***elem_number joint_1 joint_2***

Description:

| | |
|---|---|
| **element** | keyword |
| ***elem_number*** | number of the element |
| ***joint_1*** | number of joint (node) located at the first end of the element |
| ***joint_2*** | number of joint (node) located at the second end of the element |

Notes:

1) This command is used for definition of elements by specifying the end joints (nodes).

SET B6:

Title of section:

***element types**

Command:

**type** ***type_name*** **elements** ***element_list***

Description:

| | |
|---|---|
| **type** | keyword |
| ***type_name*** | = **3d_e_b** |
| | = **2d_e_b** (not available in this version) |
| | = **3d_h_b** |
| | = **2d_h_b** (not available in this version) |
| | = **3d_s_h_b** (not available in this version) |
| | = **iso_1** |
| | = **iso_sli** |
| | = **bi_gap** |
| | = **e_foun** |
| | = **l_damp** |
| **elements** | keyword |
| ***element_list*** | list of element numbers separated by spaces and/or element number **to** element number |

Notes:

1) This command assigns type name to elements. For example, elements that are assigned the type name **3d_e_b** will be three-dimensional elastic beam elements, **2d_e_b** - two-dimensional elastic beam elements, **3d_h_b** - three-dimensional hysteretic beam elements, **2d_h_b** - two-dimensional hysteretic beam elements, **3d_s_h_b** - three-dimensional hysteretic beam elements with varying shear stiffness, **iso_1** - elastomeric isolator elements, **iso_sli** - isolator slider elements, **bi_gap** - bilinear gap elements, **e_foun** - elastic foundation elements and **l_damp** - linear damper elements.

2) The second option for the ***element_list*** field can be used to apply a type name to a group of elements having consecutive numbers. For example, the command **type 3d_e_b elements 8 to 11** will define elements 8, 9, 10 and 11 as three-dimensional elastic beam elements.

3) No more than **30** elements can be assigned a type name with a single command.

**SET B7:**

Title of section:

***property number**

Command:

**property** ***prop_number*** **elements** ***element_list***

Description:

| | |
|---|---|
| **property** | keyword |
| ***prop_number*** | number of property (defined in the ***element properties** section for all element types used in the analysis) |
| **elements** | keyword |
| ***element_list*** | list of element numbers separated by spaces and/or element number **to** element number |

Notes:

1) The property number is the same number that follows the keyword **property** (for a given element type) in the ***element properties** section. For example, the commands:

***units**
**un meter kilonewton degrees**
***element properties**
**elastic beam 3d**
**property** 1
**a** 0.64 **ixx** 0.068 **iyy** 0.034 **izz** 0.034 **e** 30000000 **g** 12000000 **theta** 0
**property** 2

**a** 0.81 **ixx** 0.109 **iyy** 0.055 **izz** 0.055 **e** 30000000 **g** 12000000 **theta** 0

**end elastic beam 3d properties**

***element types**

**type 3d_e_b elements** 8 **to** 11

***property number**

**property** 2 **elements** 8 **to** 11

will assign the three-dimensional elastic beam elements with numbers 8, 9, 10, 11 the following list of cross-sectional and material attributes: $A = 0.81\,m^2$, $I_{xx} = 0.109\,m^4$, $I_{yy} = 0.055 m^4$, $I_{zz} = 0.055\,m^4$, $E = 30000000\,kPa$, $G = 12000000\,kPa$, $\theta = 0'$. Note that, [kPa] = [kN/m$^2$].

2) No more than **30** elements can be assigned a property number with a single command.

**SET B8:**

Title of section:

***rigid arm**

Command:

**ra xs** ***value*** **ys** ***value*** **zs** ***value*** **xe** ***value*** **ye** ***value*** **ze** ***value*** **element** ***element_number***

Description:

| | |
|---|---|
| **ra** | keyword |
| **xs** | keyword |
| ***value*** | global X coordinate of the actual position of the joint at the beginning of the element |
| **ys** | keyword |
| ***value*** | global Y coordinate of the actual position of the joint at the beginning of the element |
| **zs** | keyword |
| ***value*** | global Z coordinate of the actual position of the joint at the beginning of the element |
| **xe** | keyword |
| ***value*** | global X coordinate of the actual position of the joint at the end of the element |
| **ye** | keyword |
| ***value*** | global Y coordinate of the actual position of the joint at the end of the element |
| **ze** | keyword |
| ***value*** | global Z coordinate of the actual position of the joint at the end of the |

| | |
|---|---|
| | element |
| **element** | keyword |
| ***element_number*** | element number |

Notes:

1) This command can be used to transfer to new locations the end nodes of elements of type **isolator 1**, **bilinear gap**, **elastic foundation** or **linear damper**.

2) This command can be used to create in-line rigid zones at the ends of elements of type **elastic beam 3d**, **hysteretic beam 3d** or **hysteretic beam 3d shear**.

3) The beginning and end of an element is determined by the order in which the joints defining the element appear in the respective command in the ***element definition** section.

4) The position of the end nodes determine the orientation of the local coordinate system with respect to the global directions (the **isolator slider** being the only exception), as well as the length (for stiffness calculations) of elements of type **elastic beam 3d**, **hysteretic beam 3d** or **hysteretic beam 3d shear**. This command redefines the locations of the end joints and, therefore, affects both the local coordinate system and the length of the element.

**SET B9:**

Title of section:

***member releases**

Command:

**release** ***location released_dof element_list***

Description:

| | |
|---|---|
| **release** | keyword |
| ***location*** | = **start** |
| | = **end** |
| ***released_dof*** | number (a string of six digits each either 0 or 1) identifying the released degrees of freedom. |
| | **= pinned** |
| ***element_list*** | list of element numbers separated by spaces and/or |
| | element number **to** element number |

Notes:

1) Six degrees of freedom describe the displacements and rotations at each end of a three-dimensional beam element. A value of **1** in any of the six positions in the ***released_dof*** string indicates that the corresponding degree of freedom is fixed (restrained). Conversely, a value of **0** shows that the degree of freedom is released (unrestrained). Therefore, the string **111101** will denote that the rotation about the local Y axis is released (i.e. unopposed by internal forces). A consequence of such condition is that the internal force associated with the displacement along the released degree of freedom will become zero. If the second option for the ***released_dof*** field

is adopted for use, **pinned** would indicate that all translational degrees of freedom are fixed while the rotational degrees of freedom are released.

2) It is not necessary to release both identical degrees of freedom at the common joint of adjacent elements - releasing the desired degree of freedom in only one of them is sufficient.

3) No more than **30** elements can be assigned moment releases with a single command.

**SET B10:**

Title of section:

***member joint springs**

Command:

**js** ***location*** **dof** ***dof_1*** **stiffness** ***stiff_1*** **dof** ***dof_2*** **stiffness** ***stiff_2 ... element_list***

Description:

| | |
|---|---|
| **js** | keyword |
| ***location*** | = **start** |
| | = **end** |
| **dof** | keyword |
| ***dof_1*** | number identifying a degree of freedom at the ***location*** end of the element |
| **stiffness** | keyword |
| ***stiff_1*** | stiffness coefficient of the spring acting along the degree of freedom specified in ***dof_1*** |
| **dof**** | keyword |
| ***dof_2**** | number identifying a degree of freedom at the ***location*** end of the element |
| **stiffness**** | keyword |
| ***stiff_2**** | stiffness coefficient of the spring acting along the degree of freedom specified in ***dof_2*** |
| ***element_list*** | list of element numbers separated by spaces and/or<br>element number **to** element number |

** - used only if needed

Notes:

1) This command creates translational and rotational springs connecting a joint defining the end of an element to the element itself.

2) The numbers identifying the degrees of freedom in the fields ***dof_1***, ***dof_2***, etc. must be: **1** for displacement along the global X axis, **2** - displacement along the global Y axis, **3** - displacement along the global Z axis, **4** - rotation about the global X axis, **5** - rotation about the global Y axis, **6** - rotation about the global Z axis.

3) No more than **30** elements can be assigned end springs with a single command.

## LOADING INFORMATION

**SET C1:**

Title of section:

***number of load steps**

Command:

**number of load steps** ***number_of_steps***

Description:

| | |
|---|---|
| **number of load steps** | keyword |
| ***number_of_steps*** | number of load steps in **quasistatic force** or **quasistatic displacements** analysis |

**SET C2:**

Title of section:

***distributed uniform load**

Command:

**unl** ***direction load_value element_list***

Description:

| | |
|---|---|
| **unl** | keyword |
| ***direction*** | = **dx** |
| | = **dy** |
| | = **dz** |
| ***load_value*** | magnitude of load (positive, if pointing in the positive direction of the global coordinate axis identified in ***direction*** above, negative otherwise) |
| ***element_list*** | list of element numbers separated by spaces and/or<br>element number **to** element number |

Notes:

1) This command places uniform distributed load on elastic or hysteretic beam elements for use in **quasistatic force** analysis. The load acts along the global coordinate axis identified in the ***direction*** field of the command.
2) The command is not operational in this version of the program.
3) No more than **30** elements can be assigned uniform distributed load with a single command.

**SET C3:**

Title of section:

***excitation groups**

Command:

**ex file** ***file_name*** **dof** ***dof_number*** **joints** ***joint_list***

Description:

| | |
|---|---|
| **ex** | keyword |
| **file** | keyword |
| ***file_name*** | name of data file containing a singe displacement record for **dynamic displacements** analysis or a singe force record for **dynamic force** analysis, or a single number for **quasistatic displacements** analysis. |
| **dof** | keyword |
| ***dof_number*** | number (1 through 3) identifying the degree of freedom along which acts the displacement or force record applied to the joints listed in ***joint_list*** |
| **joints** | keyword |
| ***joint_list*** | list of joint numbers separated by spaces and/or<br>joint number **to** joint number |

Notes:

1) This command applies the displacement record in ***file_name*** as a boundary condition on a group of joints.

2) This command applies the force record in ***file_name*** as a nodal load on a group of joints.

3) This command applies the displacement in ***file_name*** as a boundary condition on a group of joints.

4) The data file must consist of a single column of data points with no header.

5) The number identifying the degree of freedom in field ***dof_number*** should be: **1** - displacement or force along the global X axis, **2** - displacement or force along the global Y axis, **3** - displacement or force along the global Z axis.

6) No more than **30** joints can be applied a boundary condition or a nodal load with a single command.

**SET C4:**

Title of section:

***joint load**

Command:

**pj** ***direction load_value joint_list***

Description:

| | |
|---|---|
| **pj** | keyword |
| ***direction*** | = **dx** |
| | = **dy** |
| | = **dz** |
| ***load_value*** | magnitude of load (positive, if pointing in the positive direction of the global coordinate axis identified in ***direction*** above, negative otherwise) |
| ***joint_list*** | list of joint numbers separated by spaces and/or<br>joint number **to** joint number |

Notes:

1) This command applies concentrated loads on joints in **quasistatic force** analysis. The load acts along the global coordinate axis identified in the ***direction*** field of the command.

2) No more than **30** joints can be applied a nodal load with a single command.

**SET C5:**

Title of section:

***joint weight**

Command:

**weight** ***direction weight_value joint_list***

Description:

| | |
|---|---|
| **weight** | keyword |
| ***direction*** | = **dx** |
| | = **dy** |
| | = **dz** |
| | = **all** |
| ***weight_value*** | weight of mass lumped at the joint (node) |
| ***joint_list*** | list of joint numbers separated by spaces and/or |
| | joint number **to** joint number |

Notes:

1) This command specifies nodal weights for lumped mass calculations in all types of dynamic time history and pushover analysis (thus, the need for direction input in the ***direction*** field).

2) The **all** qualifier in the ***direction*** field will assign the same weight at a joint in the three global directions. Choosing any other option effectively eliminates the inertial forces in the remaining global directions.

3) The system mass matrix contains only translational masses.

4) No more than **30** joints can be assigned nodal weights with a single command.

**SET C6:**

Title of section:

***pushover user**

Command:

**joint** ***joint_number*** **dof** ***dof_number*** **disp** ***max_disp*** **base shear** ***fraction***

Description:

| | |
|---|---|
| **joint** | keyword |
| ***joint_number*** | number of joint monitored for maximum displacement |
| **dof** | keyword |
| ***dof_number*** | number of degree of freedom at the joint (***joint_number*** field above) monitored for maximum displacement |
| **disp** | keyword |
| ***max_disp*** | maximum displacement (first stopping criterion) |
| **baseshear** | keyword |
| ***fraction_of_weght*** | fraction of total structure weight (second stopping criterion) |

Notes:

1) This command must be used if the ***input*** field of the command in the ***analysis options** section is either ***push modal*** or ***push user***.

2) This section must appear in the general input file after the commands in the ***joint weight** section.

**SET C7:**

Title of section:

***pushover rate**

Command:

**joint** ***joint_number*** **dof** ***dof_number*** **disp** ***max_disp*** **ratex** ***rate_x*** **ratez** ***rate_z***

Description:

| | |
|---|---|
| **joint** | keyword |
| ***joint_number*** | number of joint monitored for maximum displacement |
| **dof** | keyword |
| ***dof_number*** | number of degree of freedom at the joint (***joint_number*** field above) monitored for maximum displacement |
| **disp** | keyword |
| ***max_disp*** | maximum displacement (stopping criterion) |
| **ratex** | keyword |
| ***rate_x*** | rate of application of linearly increasing acceleration in the global X direction |
| **ratez** | keyword |
| ***rate_z*** | rate of application of linearly increasing acceleration in the global Z direction |

Notes:

1) This command must be used if the ***input*** field of the command in the ***analysis options** section is ***push ramp***.
2) This section must appear in the input file after the commands in the ***joint weight** section.

**SET C8:**

Title of section:

***modes number**

Command:

**number of modes** ***number_of_modes***

Description:

| | |
|---|---|
| **number of modes** | keyword |
| ***number_of_modes*** | number of modes to be extracted in **modal analysis** |

Notes:

1) This command must be used if the ***input*** field of the command in the ***analysis options** section is **modal analysis.**

2) A trial-and-error approach is recommended to request enough modes in order to satisfy the memory requirements of the modal analysis module (LANZ). If the program terminates after extracting the eigenvalues, but before relating them with the respective eigenvectors, the number of requested modes must be increased and the program rerun. Given the efficiency of the module, this is less burdening than complicating the input.

3) The mode shapes are written to file "dis_ans" for viewing in the ANSYS postprocessor (see command set E1 later).

## ANALYSIS CONTROL PARAMETERS

**SET D1:**

Title of section:

***time history analysis**

Command:

**input time step** ***input_step***
**analysis time step** ***analysis_step***
**total analysis duration** ***duration***
**damping alpha** ***alpha_value*** **beta** ***beta_value*** **gamma** ***gamma_value***
**type** ***type_of_input***
**direction of excitation** ***value***
**peak ground acceleration** ***pga_value***
**file** ***file_name***

Description:

| | |
|---|---|
| **input time step** | keyword |
| ***input_step*** | time step of input acceleration, displacement or force record |
| **analysis time step** | keyword |
| ***analysis_step*** | time step of numerical integration (substep) |
| **total analysis duration** | keyword |
| ***duration*** | duration of analysis |
| **damping** | keyword |
| **alpha** | keyword |
| ***alpha_value*** | mass-proportional damping coefficient (Rayleigh damping) |

| | |
|---|---|
| **beta** | keyword |
| ***beta_value*** | stiffness-proportional damping coefficient (Rayleigh damping) |
| **gamma** | keyword |
| ***gamma_value*** | amplitude decay factor (see section 4.2) |
| **type** | keyword |
| ***type_of_input*** | = **acceleration** |
| | = **displacements** |
| **direction of excitation** | keyword |
| ***value*** | unused field in the current version |
| **peak ground acceleration** | keyword |
| ***pga_value*** | scaling factor |
| **file** | keyword |
| ***file_name*** | name of data file containing acceleration record for **dynamic acceleration** analysis (must consist of three columns of data points of equal length with no header) |

Notes:

1) This command can be used to scale acceleration, displacement or force records. The program multiplies the input with the factor in the ***pga_value*** field. For example, if the available displacement data file is in units of [cm] but the structural geometry is already in units of [m], the user must specify a ***pga_value*** of 0.01. The record will be scaled down, so that the units are consistent.

2) The acceleration input file (***file_name*** field of the command) must consist of three columns of data points containing the components of the acceleration acting along the X, Y and Z axis of the global coordinate system. A column of zeros must be input in the appropriate place in the loading file if any of the components is zero or neglected.

## OUTPUT CONTROL PARAMETERS

The program echoes all input parameters contained in or derived from the general input file "in_file" to the general output file "out_file". The file also contains a section on damage indexes calculated for all elements of type **hysteretic beam 3d** or **hysteretic beam 3d shear**.

**SET E1:**

Title of section:

***output control**

One or more commands from the following list can be used to control the output of results by the program.

Command:

**oc displacement** ***output_type*** **dof** ***dof_number*** **joint** ***joint_list***

Description:

| | |
|---|---|
| **oc** | keyword |
| **displacement** | keyword |
| ***output_type*** | = **history** |
| | = **maximum** |
| **dof** | keyword |
| ***dof_number*** | number (1 through 6) identifying a degree of freedom |
| **joint** | keyword |
| ***joint_list*** | list of joint numbers separated by spaces and/or |
| | joint number **to** joint number |

Notes:

1) Time histories of displacements and rotations can be requested by choosing the **history** option in the ***output_type*** field. The locations in the structure were the displacements (rotations) are desired for output are identified by the joint numbers in the ***joint_list*** field along the degree of freedom in the ***dof_number*** field. Depending of the number of requests, the program creates up to 4 output files: "dis_res1", "dis_res2", "dis_res3" and "dis_res4".. Each of them consists of up to 11 columns of data points. The first column contains time, the second column - the first displacement time history, the third column - the second displacement time history, etc. For example, if only 16 displacement time histories are requested for output, all 11 columns in the file "dis_res1" and the first 7 columns in file "dis_res2" will contain information, the remaining 4 columns in "dis_res2" will be empty.

2) The number of displacement time histories is limited to 40.

3) Displacements obtained in a **dynamic acceleration** or **dynamic force** analyses are relative to the base, while **dynamic displacements** analysis produces total displacements (ground plus relative displacements).

4) The extreme response can be written to file "dis_res" by choosing the **maximum** option in the ***output_type*** field. Each line contains a joint number, a degree-of-freedom number and the maximum or minimum displacement. Sample output:

JOINT 2 DOF 1 MAX DISPLACEMENT/ROTATION/ 0.559E+02

JOINT 2 DOF 1 MIN DISPLACEMENT/ROTATION/ 0.000E+00

5) The number of displacements for maximum response output is limited to 100.

6) The displacement time histories are output only for times, which are multiples of the input time step.

7) The extreme positive and negative displacements may occur at time points, which are multiples of the analysis time step.

**SET E1 (CONTINUED):**

Command:

**oc force** ***output_type*** **element** ***element_list***

Description:

| | |
|---|---|
| **oc** | keyword |
| **force** | keyword |
| ***output_type*** | = **history** |
| | = **maximum** |
| **element** | keyword |
| ***element_list*** | list of element numbers separated by spaces and/or |
| | element number **to** element number |

Notes:

1) Time histories of forces and moments at the two ends of a member can be requested by choosing the **history** option in the ***output_type*** field. The program creates up to 6 output files: "for_res1", "for_res2", "for_res3", "for_res4", "for_res5" and "for_res6". Each consists of 13 columns of data points. Time is in column 1, element end forces at the first node of the member are in columns 2 through 7, and element end forces at the second node are in columns 8 through 13. Columns 2, 3, 4, 8, 9 and 10 contain forces along the local X, Y and Z axes, while columns 5, 6, 7, 11, 12 and 13 - moments about the local X, Y and Z axes.

2) The number of elements for output of force history is limited to 6.

3) The extreme response of a member can be obtained by choosing the **maximum** option in the ***output_type*** field. File "for_res" contains the maximum and minimum of forces and moments at both ends of each requested element. The meaning of each column was explained above.

4) The number of elements for output of maximum force response is limited to 100.

5) Force time histories are output only for time points, which are multiples of the input time step.

6) The extreme positive and negative forces may occur at time points, which are multiples of the analysis time step.

**SET E1 (CONTINUED):**

Command:

**oc displacement** ***output_type*** **dof** ***dof_number*** **joint** ***joint_1 joint_2*** **coefficient** ***coef_1 coef_2***

Description:

| | |
|---|---|
| **oc** | keyword |
| **displacement** | keyword |
| ***output_type*** | = **add history** |
| | = **add maximum** |
| **dof** | keyword |
| ***dof_number*** | number (1 through 6) identifying a degree of freedom |
| **joint** | keyword |
| ***joint_1*** | joint number |
| ***joint_2*** | joint number |
| **coefficient** | keyword |
| ***coef_1*** | multiplier |
| ***coef_2*** | multiplier |

Notes:

1) Time histories of displacements or rotations can be added by choosing the **add history** option in the ***output_type*** field. The nodal points, whose displacements are added (or, more often, subtracted), are identified by the two numbers in the ***joint_1*** and ***joint_2*** fields along with the degree-of-freedom number in the ***dof_number*** field. The coefficients in the ***coef_1*** and ***coef_2*** fields multiply the respective time history. In the current version, both multipliers must be integer numbers. This feature has utility in cases where the relative displacement of two points in

a structure is not directly available (ex. between the top and the base of a column, between the bridge deck and the ground, etc.).

2) Depending on the number of requests, the program creates up to 4 output files: "rel_dis1", "rel_dis2", "rel_dis3" and "rel_dis4". Each of them consists of up to 11 columns of data points. The first column contains time, the second column - the first added displacement time history, the third column - the second added displacement time history, etc. For example, if only 16 added displacement time histories are requested for output, all 11 columns in file "rel_dis1" and the first 7 columns in file "rel_dis2" will contain information, the remaining 4 columns in "rel_dis2" will be empty.

3) The number of time histories of added displacements is limited to 40.

4) The extreme response of time histories of added displacements can be written to file "dis_res" by choosing the **add maximum** option in the ***output_type*** field. Each line contains the joint and degree-of-freedom numbers, the respective multipliers and the maximum or minimum of the resulting displacements. Sample output:

JOINT 2 DOF 1 COEF 1 AND JOINT 1 DOF 1 COEF -1 MAX DISP 0.000E+00

JOINT 2 DOF 1 COEF 1 AND JOINT 1 DOF 1 COEF -1 MIN DISP -0.227E+01

5) The number of requests for maxima of added displacement time histories is limited to 100.

6) Added displacement time histories are output only for time points, which are multiples of the input time step.

7) The extreme positive and negative added displacements may occur at time points, which are multiples of the analysis time step.

**SET E1 (CONTINUED):**

Command:

**oc displacement shape time *list_of_times***

Description:

| | |
|---|---|
| **oc** | keyword |
| **displacement** | keyword |
| **shape** | keyword |
| **time** | keyword |
| ***list_of_times*** | list of time points for which the displaced shape of the structure is requested |

Notes:

1) The program creates two output files: "model.ansys" and "dis_ans". Importing these file in the post-processor "POST1" of the ANSYS™ computer program will enable the user to view snapshots of the displaced shape of the structure at the times in the ***list_of_times*** field. File "model.ansys" contains the geometric model and must be read first (preferably in the "PREP7" module of ANSYS™, not at the "BEGIN:" level). Both files are in ASCII format and utilize ANSYS command language to instruct the program directly.

2) In **dynamic acceleration, dynamic displacements** and **dynamic force** analyses, the displaced shape can be requested only at times, which are less than the total analysis duration.

3) In **modal analysis,** the mode shapes of the structure will be written to "dis_ans" starting with the eigenvector corresponding to the lowest natural frequency (highest period) of vibration. To display any mode shape, identify the starting line number in file "dis_ans", select the "Read Input From" submenu in the "File" menu of the ANSYS GUI (Graphical User Interface), pick "dis_ans" as input file and enter the line number in the appropriate field of the query window.

**END OF INPUT FILE**

**SET F1:**

Title of section:

***finish**

# ADDING NEW ELEMENTS TO IDARC-BRIDGE

The scope of the program can be easily extended by adding new elements or modifying those already residing in it.

## General Procedure For Programming Or Incorporating New Elements

| Subroutine | Source Code File | Status | Function |
|---|---|---|---|
| **derive_properties_array_size** | get_array_size.f | Old | Reads the number of properties of each element type - used later in array size definition and memory allocation. Action: include the new element type in the **if** statement. |
| **get_element_properties** | get_element_properties.f | Old | Calls routine **get_*element_name*_properties** for each element type encountered by the program in the **if** statement. Action: include the new element type in the **if** statement. |
| **get_*new_elem_name*_properties** | get_*new_elem_name*_properties.f | New | Reads the list of properties and attributes of the new element type from the general input file. |
| **assign_elements_types** | assign_elements_types.f | Old | Assigns a user-defined number to each element type. Action: include the new element type in the **if** statement. |

| | | | |
|---|---|---|---|
| **write_element_properties** | write_element_properties.f | Old | Calls routine **write_*element_name*_properties** for each element type encountered by the program in the **if** statement. Action: include the new element type in the **if** statement. |
| **write_*new_elem_name*_properties** | write_*new_elem_name*_properties.f | New | Writes the list of properties and attributes of the new element to the general output file. |
| **update_elements_stiffness** | update_elements_stiffness.f | Old | Calls either routine ***element_name*_stiffness,** or routine **update_*element_name*_stiffness** for each element type of given number (see **assign_elements_types** above) encountered by the program in the **if** statement. Action: include the number of the new element type in the **if** statement. |
| ***new_elem_name*_stiffness OR** | create_*new_elem_name*_stiffness.f | New | Generates the element stiffness matrix (dimension 12x12) of elements with type number corresponding to the new element type. This routine can be included in the program if the new element type has constant stiffness coefficients. |
| **update_*new_elem_name*_stiffness** | update_*new_elem_name*_stiffness.f | New | Generates and updates throughout the analysis the element stiffness matrix (dimension 12x12) |

of elements with type number corresponding to the new element type. This routine can be included in the program if the new element type has variable stiffness coefficients.

# APPENDIX B
# COMPARISON OF COMPUTATIONAL RESOURCE DEMAND

IDARC-Bridge is primarily intended for nonlinear quasi-static and dynamic analysis of bridges and an in-depth assessment of its computational efficiency must reflect this objective. However, it is difficult to adopt a general standard for evaluation of the efficiency of a nonlinear program. One possible criterion is to compare the time of execution with that of other computer codes. Unfortunately, in the context of nonlinear analysis, this measure is influenced by a variety of factors, the most notable of which are the complexity and capability of the underlying plasticity models, error tolerances, iteration schemes, etc. Furthermore, it is difficult to establish one-to-one correspondence between the response of continuum elements based on different nonlinear constitutive macro-models even if the underlying material stress-strain curves are identical. For these reasons, the authors have provided the average CPU time for dynamic analyses of the linear elastic bridge of section 6.3 for three-dimensional ground displacement input, alongside with results from an identical model analyzed by a commercial FEM package (ANSYS 5.3). All computations are performed on a Sun Ultra 5/10 workstation with Ultra SPARC-IIi 270 MHz processor and 64 MB of RAM, running Solaris operating system with Common Desktop Environment (CDE). The statistics for each process (Table B-1) are obtained from the UNIX timing utility. For more information on the User CPU, System CPU and elapsed time fields see the manual entry for the "time" command.

**Table B-1 Comparison of CPU and Real Time of Execution**

| Program | IDARC-Bridge | | | ANSYS | | |
|---|---|---|---|---|---|---|
| Run | User CPU Time [sec] | System CPU Time [sec] | Elapsed Time [min:sec] | User CPU Time [sec] | System CPU Time [sec] | Elapsed Time [min:sec] |
| 1 | 6.92 | 0.55 | 0:20.75 | 62.47 | 7.67 | 3:21.67 |
| 2 | 6.97 | 0.47 | 0:20.78 | 60.44 | 7.73 | 3:18.02 |
| 3 | 7.00 | 0.50 | 0:21.36 | 60.79 | 7.47 | 3:17.43 |
| 4 | 7.06 | 0.47 | 0:21.34 | 60.63 | 7.13 | 3:16.36 |
| 5 | 7.04 | 0.44 | 0:21.29 | 61.07 | 7.29 | 3:19.71 |
| 6 | 6.96 | 0.49 | 0:21.12 | 61.29 | 7.6 | 3:19.37 |
| 7 | 7.12 | 0.50 | 0:21.92 | 66.24 | 7.22 | 3:33.04 |
| 8 | 6.96 | 0.47 | 0:20.70 | 61.44 | 7.87 | 3:23.71 |
| 9 | 6.98 | 0.54 | 0:20.97 | 61.01 | 7.65 | 3:17.88 |
| 10 | 7.17 | 0.44 | 0:21.18 | 61.25 | 7.29 | 3:15.51 |
| **Average** | **7.02** | **0.49** | **0:21.14** | **61.66** | **7.49** | **3:20.27** |

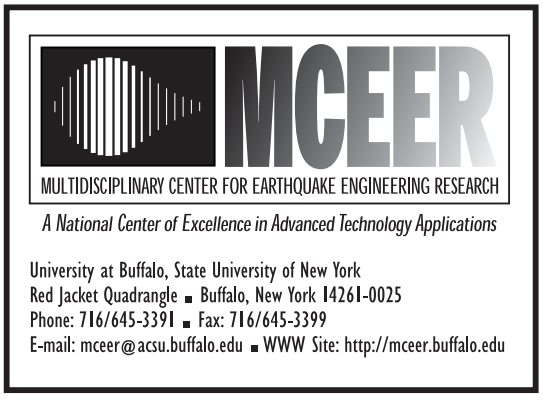


ISSN 1520-295X